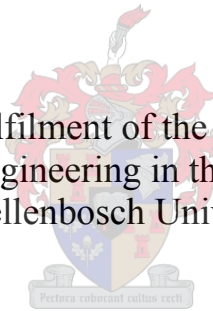# An investigation of the use of groynes as a means of riverbank erosion protection

By

Arende Daniël De Waal van den Heever

Thesis presented in partial fulfilment of the requirements for the degree of
Master of Science in Engineering in the Faculty of Engineering
at Stellenbosch University

Supervisor: Prof GR. Basson
Faculty of Engineering
Department of Civil Engineering

March 2013

By submitting this thesis electronically, I declare that the entirety of the work contained therein is my own, original work, that I am the authorship owner thereof (unless to the extent explicitly otherwise stated) and that I have not previously in its entirety or in part submitted it for obtaining any qualification.

Signature: _____   Date: _____

Synopsis

Groynes are hydraulic structures typically constructed from gabions to extend from the outer bank of a river channel into the main flow. The principal uses for groynes are as river training structures, and to protect the riverbank from erosion. This is done by deflecting the current away from the riverbanks, dissipating energy and creating lower flow velocity zones, reducing the effects of erosion. Groynes have been used extensively in the Western Cape since the early 1990s as a means to protect agricultural lands. There is, however an absence of published manuals for the design of groynes around bends as a means of riverbank protection. This study was done to better understand the flow, scour and sediment deposition patterns associated with implementing a series of groynes around a bend.

A physical model of a typical sinusoidal South African river was constructed in the Hydraulics Laboratory at the University of Stellenbosch. The model consisted of two succesive 90˚ bends to best simulate erosion patterns. Different layout designs for a series of groynes were tested to determine the optimal design for the given situation in terms of the projection lengths of the groynes, the spacing between the groynes as a factor of the projection length, and the orientation of the groynes with regard to the oncoming flow.

An integrated software package, that was developed at the National Centre for Computational Hydroscience and Engineering, at the University of Mississippi, named CCHE2D was used to simulate the physical model numerically. The model was calibrated by adjusting the Manning's n value of the sediment, and the normal tailwater depth was calculated and used for the physical and numerical models. The flow rate used during the physical model experiments was also used for the numerical model. The model was validated by comparing scour depths obtained from the physical model to the resulting depth in the hydrodynamic model.

From the results obtained from the physical and numerical models, it was found that groynes with a perpendicular orientation to the direction of the oncoming flow were optimal. Groynes with an upstream orientation resulted in excessive scour around the nose of the groynes, while recirculating flow patterns occurred at a velocity which caused bank failure. Groynes with a downstream orientation created very little recirculation of flow, resulting in less scour protection for the outer bank than found for groynes with perpendicular orientation.

Finally, the optimal design was identified as a perpendicular groyne orientation with a projection length L and a spacing of 3.5 xL. For the given design, eddy currents covered the entire area between consecutive groynes, causing low flow zones near the outer banks, promoting sediment deposition and decreasing the potential for scour.

Recommendations for further studies include the investigation of the effects of different bend radii, the sediment size, as well as various channel widths, flow rates and river slopes. The use of a three-dimensional hydrodynamic model would also be advantageous in order to better understand the flow and scour mechanics associated with different designs.

Samevatting

Groynes is hidrouliese strukture, tipies gebou uit skanskorwe in Suid Afrika, wat vanaf die buiteoewer van 'n rivier strek na die hoofkanaal. Groynes word hoofsaaklik aangewend as rigmure in riviere en om rivieroewers te beskerm teen erosie. Erosiebeskerming word geskep deur vloei weg te deflekteer van die rivieroewer en energie te dissipeer. Sodoende vorm areas met lae vloeisnelhede naby die oewer wat die potensiaal vir erosie verminder. Groynes is sedert die vroeë 1990s in die Wes-Kaap gebruik as 'n manier om landbougrond teen erosie te beskerm. Daar is egter 'n tekort aan gepubliseerde ontwerpriglyne vir die gebruik van groynes vir erosiebeskeriming in riviere. Hierdie studie is gedoen om die vloei-, uitskurings- en sediment neersettingspatrone, geassossiëer met die implementering van groynes, te ondersoek.

'n Fisiese model van 'n tipiese kronkelende Suid-Afrikaanse rivier is gebou in die Hidrouliese Laboratorium by die Universiteit van Stellenbosch. Die model bestaan uit twee opeenvolgende 90° draaiïng om die erosie-patrone te simuleer. Verskillende uitlegte vir 'n reeks groynes is getoets om die optimale ontwerp vas te stel in terme die projeksielengte van die groynes, die spasiëring tussen opeenvolgende groynes as 'n faktor van die projeksielengte en die oriëntasie van die groynes ten opsigte van die aankomende vloeirigting.

'n Geïntegreerde sagteware pakket wat ontwikkel is by die "National Centre for Computational Hydroscience and Engineering", by die Universiteit van Mississippi, genaamd CCHE2D is gebruik om die fisiese eksperimente numeries te simuleer. Die model is gekalibreer deur die Manning n waarde van die sediment aan te pas, die stroomaf waterdiepte wat bereken is, en die vloeitempo wat waargeneem is tydens die fisiese eksperimente. Die model is bekragtig deur uitskuurdieptes van die fisiese- en hidrodinamiese modelle te vergelyk.

Vanuit die resultate wat verkry is in die fisiese- en numeriese modelle, is daar gevind dat groynes met 'n loodregte oriëntasie met betrekking tot die aankomende vloei optimaal is. Daar is gevind dat groynes met 'n stroomop oriëntasie oormatige uitskuring rondom die neus van die groynes ondervind, terwyl hersirkulasie van vloei teen 'n hoë snelheid plaasvind, wat erosie van die oewer tot gevolg het. Groynes met 'n oriëntasie na die stroomaf kant het baie min hersirkulasie van vloei tot gevolg gehad, wat tot minder erosiebeskerming van die buitebank gelei het.

Die optimale ontwerp is geïdentifiseer as groynes met loodregte oriëntasie, 'n projeksielengte van 0.675 m en 'n spasiëring van 3.5 keer die projeksielengte. Vir die gegewe ontwerp is

werwelstrome gevind wat die hele area tussen opeenvolgende groynes dek, wat area van lae vloei sones veroorsaak naby die oewer, wat sediment deponering bevorder en die potensiaal vir uitskuring verminder.

Aanbeveling vir verdere studies sluit die studie van die effekte van verskillende draai radiusse en die sediment-grootte in, sowel as verskillende kanaalbreedtes, vloeie en rivierhellings. Die gebruik van 'n drie-dimensionele hidrodinamiese model sal ook voordelig wees om die betrokke vloei- en uitskuringspatrone rakende verskillende ontwerpe beter te verstaan.

Acknowledgements

The financial assistance of the National Research Foundation (NRF) towards this research is hereby acknowledged, opinions expressed and conclusion arrived at, are those of the author and are not necessarily to be attributed to the NRF.

I would also like to acknowledge the role my parents played in my upbringing, as well as affording me the opportunities needed to be able to do my master's studies.

I also acknowledge the academic help and guidance of Professor G.R. Basson, without whom the completion of this thesis would have been an impossible task.

Finally I would like to thank the following people for continued assistance throughout my master's study:

- Mr Hans King from the Department of Agriculture, Western Cape
- Mr N Combrink, Mr A Lindoor and Mr E Wanza for continued assistance in the laboratory experiments.
- Mr M.J. van Heerden for assistance in all aspects of my study.

Table of Contents

List of Figures

List of Tables

List of Symbols and Abbreviations

A   = Cosines of total load transport

π = pi (3.141592654)

δ = Bed-load zone thickness

ε_s = Diffusivity of sediment

ρ = Density of water

τ = Depth integrated Reynolds stresses

ϕ = Non-dimensional bed-load transport capacity

A   = Area

b   = Bottom width of channel

c_k = Sediment concentration

D   = Particle size of sediment

D   = Flow depth

D   = Derivation parameter

d_{50} = Mean sediment particle size

D_{bk} = Deposition flux

E   = exponential parameter

E_{bk} = Entrainment flux

f_{Cor} = Coriolis parameter

g   = Gravitational acceleration

h   = Flow depth before scoured section

H '   = Relative maximum scour

H   = Horizontal

V   = Vertical

j   = Label of a point

k_s = Absolute roughness of sediment

n   = Manning roughness coefficient

N   = Total number of points

P   = Wetted perimeter

P_{bk} = Bed material gradation

p'   = Porosity of bed material

q   = Unit discharge

Q   = Discharge

$q_{bkx/y}$ = Components of bedload transport

R   = Hydraulic radius

S   = Slope

s_j = Relative location

t(i)   = Time elapsed

V_i = Volume of scour at time t(i)

v_{ss} = Particle settling velocity

v_* = Shear velocity

v_{*c} = Critical shear velocity

w_{50} = Sediment settling velocity of median size particle

y   = Flow depth

x   = Horizontal component of side slopes

z   = Depth of scour below h

1. Introduction

"Since the beginning of time, a relationship has existed between man and water. As water has always been an integral part of human development, early civilizations and settlements were usually developed near river valleys" (Shen, 1971).

There are indications that the manipulation of rivers to obtain water for domestic and agricultural use started as early as 4000 B.C. when one of the early kings of Egypt, Menes, built a masonry dam across the Nile at Memphis (Shen, 1971).

The manipulation of rivers extends beyond only water use. Rivers have also been manipulated for centuries to protect settlements and agricultural lands from floods. This has continued to the present day, where flood protection has become a necessity to ensure sustainable development in terms of agriculture. Over the years this has prompted the development of various methods of erosion protection in rivers.

1.1   Problem statement

When considering methods for riverbank protection, the environmental impact is a challenging factor to be taken into account. The aim is to protect the riverbank from erosion (sometimes using man-made structures), while still maintaining the environmental integrity of the natural stream.

One of the techniques that has been implemented in the Western Cape since the early 1990s, is the use of "groynes". Groynes are wall-like structures that are constructed from the bank of a river to extend into the river, causing the main channel flow to shift away from the bank. This creates zones of lower flow rates close to the bank of the river, which promotes sediment deposition instead of scour (King, 2009).

The understanding of the mechanics surrounding the use of groynes as a means of riverbank protection is not complete. In other countries, groynes are used mainly as river training structures to ensure adequate depth and width for the navigation of ships. For this purpose many model studies have been done. In South Africa groynes are, however, mostly used as a means of protecting agricultural land around bends against erosion. There is a noticeable absence of model studies concerning the use of groynes around a bend to decrease erosion.

The guidelines used by the Department of Agriculture, Western Cape, for the design of groynes have been compiled from various papers and books and from experience gained over the last 10–15 years. There is, however, an absence of published design manuals for the planning of groynes (King, 2009).

1.2   Objectives

The first objective of this study is to extend the knowledge surrounding the interaction between groynes and the flow characteristics in a given river by doing and interpreting physical model experiments for a range of groyne layout designs with regard to the projection lengths, the spacing and the orientation of the groynes.

The second objective is to validate a two-dimensional hydrodynamic model in CCHE2D with a wide set of parameters and boundaries as tested in the physical experiments. A two-dimensional model is preferred to a three-dimensional model because longer simulations can be done. Large river systems can also be modelled with relative ease as a two-dimensional model is not as demanding on computer capabilities as a three-dimensional model.

The third objective is to use the results obtained from the physical model and the hydrodynamic model to determine an optimised groyne layout at river bends to limit erosion in South African rivers.

1.3   Overview of the study

The literature study (Chapter 2) commences with an in-depth study of the formation of river flow patterns. Different methods of riverbank protection are discussed, with the emphasis on the use of groynes for riverbank protection. Flow and scour patterns around groynes are discussed, as well as the design approach followed by the Department of Agriculture in the Western Cape. Finally, two case studies are discussed, referring to the farm Tradouw, on the Grootvadersbosch River and the Mullersrus farm on the Buffeljags River, where groynes were implemented as the preferred method of erosion protection.

The physical modelling chapter (Chapter 3) gives a clear overview of the design of the model that was used for this study. This includes the design of the river channel, the design of the individual groynes, as well as the layout of the groynes (spacing, orientation and projection lengths). The sediment sizes available in the hydraulics laboratory are also taken into account to ensure that sediment movement would take place. All the variables involved with the physical testing are also discussed. The methodology by which the physical experiments

were carried out is explained, and an in-depth analysis of the results obtained from these experiments is given.

Chapter 4 explains the validation of the hydrodynamic model. Here the theory that is used in the calculations of the model is discussed, as well as the calibration of the model in terms of water levels, as a result of the roughness of the sediment. The results of the hydrodynamic model are then compared to the results obtained from the physical model experiments to ascertain whether the hydrodynamic model is a good representation of the physical model. Flow patterns resulting from different layout designs are also discussed.

The conclusion (Chapter 5) gives a brief outline of the outcomes of the study for the physical model experiments and the hydrodynamic model, as well as recommendations for further studies.

2. Literature study

2.1   Introduction

This section of the thesis gives a comprehensive study of literature pertaining to the use of groynes in rivers, both for erosion protection and as river training structures for navigational purposes. The objective is to create an understanding of the mechanics surrounding the use of groynes in rivers and to outline work that has been done on this subject in the past.

2.2   River channel morphology

Flow in streams and rivers is nature's way of conveying water on the surface of the earth. Since the beginning of time, many great persons in history have contributed to the understanding of river mechanics. Greek philosophers such as Aristotle and Archimedes made a lasting impact on the development and understanding of river mechanics.

Leonardo da Vinci quoted one of the fundamental concepts in river mechanics:

"A straight river with equal width, depth and slope acquires a degree of velocity for each degree of motion. This is evident from the proportion of motion, according to which an object, the more it moves in its own natural course, the more it gathers speed, as in any other matter. The straight river, as above, although it acquires a grade of velocity for each grade of motion, nevertheless, the more obstacles it encounters on its course, the more it slows down the speed. Water has higher speed on the surface than on the bottom. This happens because water on the surface borders on air, which is of little resistance and water at the bottom touches the earth, which is of high resistance" (Shen, 1971).

A concluding remark from da Vinci is:

 "A river in each part of its length in an equal time gives passage to an equal quantity of water, whatever the width, depth, slope or the roughness" (Shen, 1971).

Other scientists such as Galileo Galilei, Bendetto Castelli and Evangelista Torricelli also contributed greatly to the understanding of hydraulic principles. The next prominent figure in the contribution to knowledge concerning river mechanics, was Domenico Guglielnini who said:

"A stream with sufficient velocity scours its bed, and with the increase in depth the slope is lessened and late in its motion, if it runs turbid, the stream will deposit sediment on the bed. Hence, I can conceive of no other reason to seek what slope would be necessary for a stream

4

than to be certain that it would not cover its bed with deposits, or, if the slope were greater than necessary, that it would scour excessively.

It is certain that a stream widens and deepens in proportion to the violence of the motion that erodes and carries away the earth that forms its sides and bottom. It is therefore necessary that the scouring force be greater than the resistance of the earth or other material that forms the bed, because otherwise, if the one were equal to the other, there would be no excavation. It is always necessary to say that in the scouring process of a stream, either the force of the water gradually decreases, or the resistance of the soil will increase until some equilibrium is found" (Shen, 1971).

2.2.2   Formation of river channel geometry

Because of the natural variability of the factors that govern the channel morphology, a natural river is never completely stable. The two main factors contributing to this are varying discharge and sediment load. A river will, however, always strive to attain a state of dynamic equilibrium by changing its cross section, slope and channel pattern to obtain optimal transport of water and sediments. Such a river is said to be in regime, meaning that it has found a long term stable configuration (Beck & Basson, 2003).

A river has at least three degrees of freedom, namely its width, depth and slope. A fourth degree could be considered as the channel pattern, which changes over longer periods of time. The main factors that affect these degrees of freedom are the discharge, sediment load and bed and bank materials (Beck & Basson, 2003).

There has been much discussion about the dominant discharge for stable alluvial channels formed by varying discharges. All natural rivers are subject to unsteady flow, but the question is: which flow is dominant? River flow varies not only with the seasons of the year, but also from year to year. Superimposed on the broad seasonal changes are floods (Ackers & Charlton, 1970).

The questions therefore remain: what flows are responsible for rapid changes in channel geometry such as depth or bed features, and what flows are responsible for longer term changes such as meander length or channel width?

2.2.2   River forms

It is widely accepted that river forms can be classified into three categories according to the sinuosity (the ratio between the lengths along the line of maximum depth to valley length) with which the river flows:

1. Straight
2. Meandering
3. Braided (multi-thread streams)

According to Chitale (1973), these three categories can be divided into stable channel forms: straight and meandering, and unstable channel forms: braided. A river is stable when no appreciable changes in bed levels occur.

1. Straight Channels

Straight channels generally occur on flat slopes with small width/depth ratios and low flow velocities. Straight channels have negligible sinuosity at bankfull stage (Beck & Basson, 2003). Although a river may have a relatively straight alignment, sand bars alternating with thalweg meanders develop at low flows. Straight channels are often regarded as a transitional form, striving to become meandering (Shen, 1971).

Leliavsky (1955), as cited by Brotherton (1979), stated that sediment deposition in straight channels may be accompanied by a reversal of twin spiral cells, giving surface flow divergence. This reduces the flow depth and therefore increases the shear stress. The river channel will remain straight, with alternating shoals.

2. Meandering Channels

Meandering channels form when the slope becomes steeper and the width/depth ratio increases, as does the velocity (Beck & Basson, 2003).

A meandering river has regular sinuous inflections along the river reach. A centrifugal force presides in the bend and causes a transverse water surface slope and helicoidal flow. These characteristics cause deep pools to be formed on the outer banks as a result of the higher flow velocities.   The transverse currents caused at the convex bank, sweep the heavier concentrations of bed load toward it, where they are deposited to form the point bar (Shen, 1971). Brotherton (1979), also attributes the formation of channel geometry to secondary currents in alluvial channels.

Many theories have been brought forth over the years speculating as to the origin of rivers meandering.   As cited by Chitale (1973), original theories have included effects of the earth's rotation and the coriolis effect by Lacey (1938), Eakin (1911) and Quarauishy(1943). Schoklitsch and Ealn (1942) attributed it to excessive slope and expending energy. Chitale (1973) cited Friedkin (1945) as considering that meandering rivers occur because of local

bank erosion and consequent overloading and deposition of heavier sediment by the river. Langbein & Leopold (1966), stated that the effect of meanders is to introduce flow resistance due to curvature in such a way that uniform utilization of energy occurs through the entire length of the river.   In this way the meandering reaches will strive more closely to equilibrium during normal flow conditions (Chitale, 1973).   According to Langbein & Leopold (1966), the meandering form of a river is the most stable form of channel geometry.

It has been considered that a river meanders in order to dissipate its excess energy. The more energy a river has, the more sinuous it should become (Yang, 1971). The main support for this hypothesis as cited by Yang (1971), observed by Shukry (1950), was that water flowing through a single bend has a higher energy loss than that flowing through a straight channel with the same discharge. This is, however, still being disputed. Figure 1 shows typical meandering river forms.
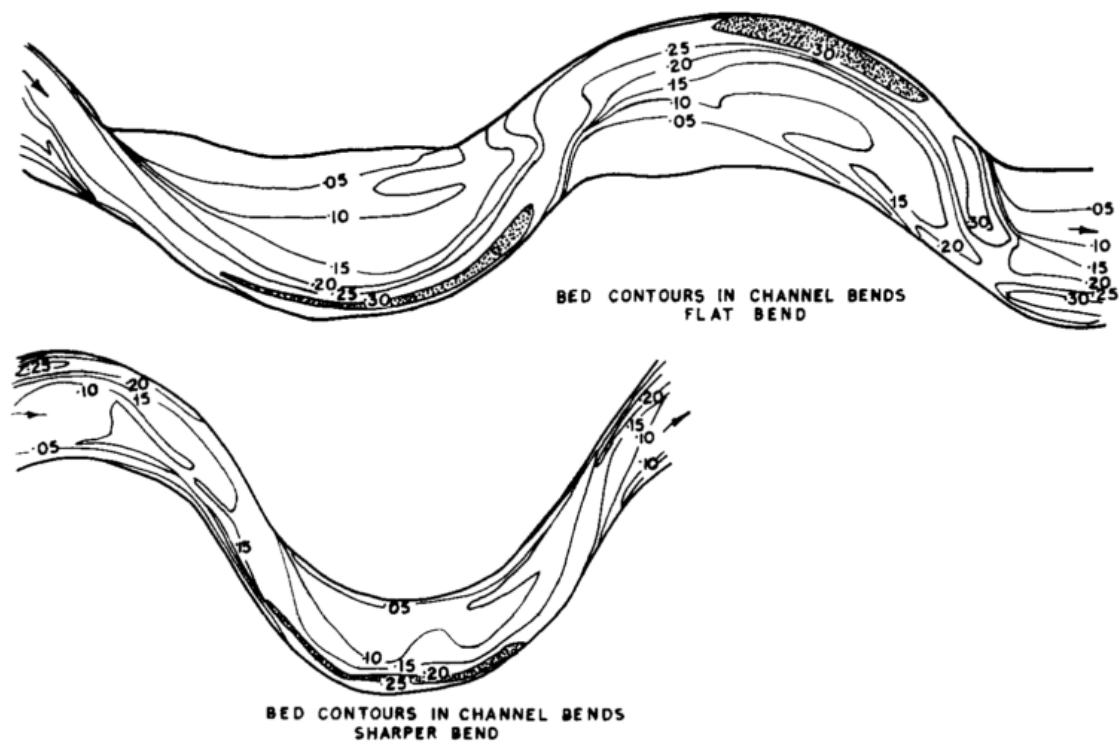
Figure 1: Meandering river forms (Chitale, 1973)

In meandering channels, shear stress on the boundary increases as bank particles are disturbed and the channel width may increase. The size of the disturbed bank material relative to the deposited sediment will influence the resulting pattern.

7

If the bank particles are smaller than those that are deposited, they may be entrained by the flow and removed from this section. If, however, this is not the case, larger particles are traded for smaller particles, whilst the total load that is carried remains more or less constant. The reduction in flow depth caused by the deposition of sediment is reversed further downstream as the amount of large particles that are carried is reduced. This deposition induces further bank erosion (Brotherton, 1979).

3. Braided Channels

On even steeper slopes than found in meandering channels, the sinuosity generally decreases and the river becomes braided. The width/depth ratio increases even more (Beck & Basson, 2003).

Braided channels are wide and the banks are unstable and poorly defined. Two or more main channels that cross one another are present, which gives the river a braided appearance at low flow. Sand bars are found between sub-channels that change in a rapid and unpredictable manner. During floods these sand bars are inundated and the river has a canal-like appearance, except that the river is much wider and has higher flow velocities (Shen, 1971).

2.3   Methods of erosion protection

Over the millennia many different techniques have been developed and used to protect riverbanks from erosion. The situations where riverbank erosion occurs are, however, extensive and many factors contribute to the choice of solution that may be implemented. The factors may include the following (King, 2009):

- The river flow velocity
- The stability of the river bed
- The location of the site relative to sources of construction material
- The priority attached to poverty alleviation projects as well as ecological considerations

Riverbank protection can be divided into two categories: Natural riverbank protection and artificial riverbank protection.

2.3.1   Natural riverbank protection
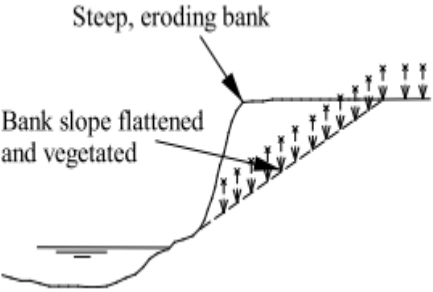
Natural riverbank protection is the most environmentally friendly way of stabilizing riverbanks. By using vegetation below the water surface, the bank is stabilized in two ways: The soil is held together by the root systems by forming a binding network. The vegetation also takes water from the soil in which it is planted, which increases the water infiltration into the soil which could improve the bank stability.

Natural riverbank protection includes the following:

- o Grass
- o Grass reinforced with synthetic materials
- o Reeds
- o Willows and other trees
- o Timberwork
- o Brushwork

Methods of applying these natural riverbank protection materials are discussed in Table 1.

Table 1: Natural riverbank protection (adapted from King, 2009)

Solution type	Sketch	Comments
Flatten side –slopes of bank and improve indigenous vegetative cover	Steep, eroding bank / Bank slope flattened and vegetated	• Ecologically desirable. • May not be sustainable where bends in rivers are relatively tight • Not practical where floods may wash away landscaped soil prior to full establishment of vegetation

2.3.2   Artificial riverbank protection

Artificial riverbank protection is used in cases where vegetation alone cannot offer the desired stability to protect the specific riverbank. Artificial riverbank protection is, however, not the most environmentally friendly method to implement when protecting a riverbank against erosion. As a result, newer and more environmentally friendly ways of protecting riverbanks by artificial means are constantly sought.
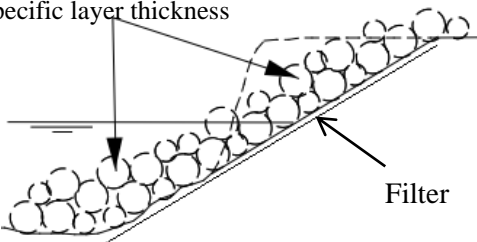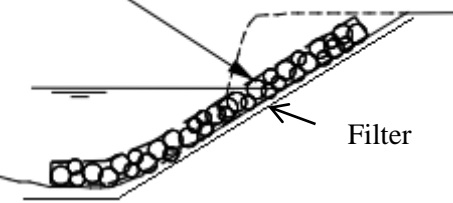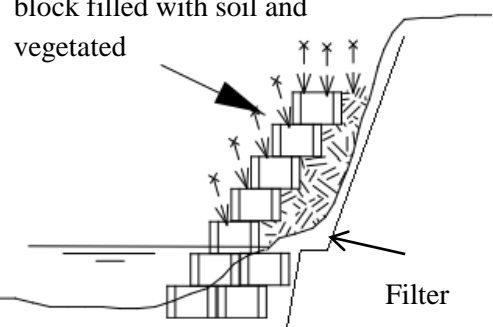
Artificial riverbank protection material includes the following:
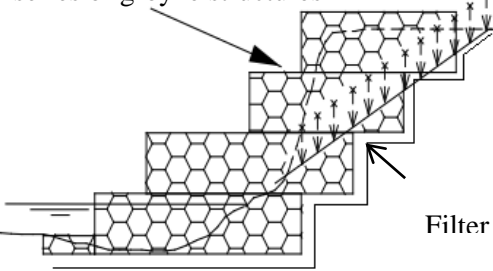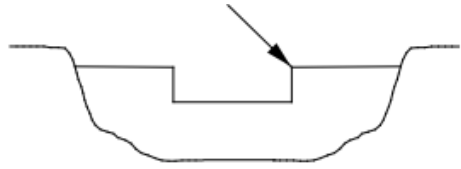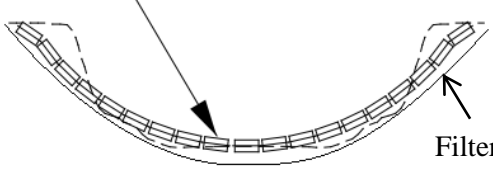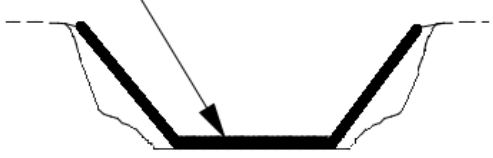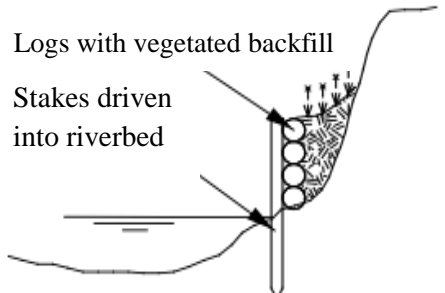
- o Steel sheet piling
- o Steel and asbestos trench sheeting
- o Gabion structures (Groynes)
- o Concrete, brick and masonry gravity walls
- o Precast units (Armorflex and Renomattress)
- o Reinforced earth structures

- o Rip Rap
- o Geotextiles and geomembranes

Methods of applying these artificial riverbank protections materials are shown in Table 2.

Table 2: Artificial riverbank protection (adapted from King, 2009)

Solution type	Sketch	Comments
Rip Rap (longitudinal protection)	Rock of specified size dumped in specific layer thickness Filter	• Can be ecologically acceptable • Expensive • Can be easier than placing gabion mattresses
Gabion mattresses (longitudinal protection)	Wire basket filled with stones placed on shaped bank Filter	• Smaller stones than Rip Rap
Pre – fabricated concrete blocks (longitudinal protection)	Hollow prefabricated concrete block filled with soil and vegetated Filter	• Many systems are available • Generally expensive • Progressive collapse due to local foundation failure at the toe can occur • Units typically too light

10

Groynes (transverse structures)	Bank shaped and vegetated, protected by a series of groyne structures Filter	• Encourages sediment deposition causing riverbank to be restored rather than eroded • Expensive • Ecologically acceptable • Damage and scour to toe area could be a problem
Weirs and sills (transverse structures)	Weir or sill lifts bed of river, flattening slope & reducing flow velocity	• Flatten the effective slope of a river reducing velocities • Can encourage river to meander • Expensive • Generally not ecologically acceptable • Energy dissipation required at weir
Full lining of channel with blocks	Shaped channel lined with system of linked concrete blocks Filter	• Quick way to stabilize a channel • Similar to concrete lining but more ecologically acceptable • Extremely expensive • Blocks typically too light during floods
Full lining of channel with concrete	Reinforced concrete lining applied to shaped channel	• Ecologically most offensive. • Can resolve problems of excessive silt movement • Extremely expensive • Hydraulically very efficient (Fr>1) and relatively small
Logging packed behind stakes, backfilled and vegetated	Logs with vegetated backfill Stakes driven into riverbed	• Can be a low cost temporary solution • Poor sustainability • Logging is not effective when it is inundated with water

2.4   Groynes

Groynes, also known by names such as groin, spur dike, retard and vane, are hydraulics structures constructed from gabions to extend from the outer bank of a channel into the main flow (Osman & Ibrahim, 2008). Groynes are principally used for river training and to protect riverbanks from erosion by deflecting the current away from the riverbank (Azinfar & Kells, 2009; Kuhnle, Alonso, & Shields, 1999). Groynes are often used in river restoration projects as this method promotes the deposition of sediment on the outer banks (Koken, 2011). It has also been found that the aquatic habitat and fish populations have improved between groynes (Azinfar & Kells, 2011).   Figure 2 shows a typical site where groynes have been constructed.

Figure 2: Groyne protection around a bend in the Gamka River, Calitzdorp (King, 2009)

A groyne roughens the bank on which it is constructed and, in doing so, creates a zone of lower flow velocity where the tendency for erosion to occur is less and that of deposition is greater. A complex three–dimensional highly turbulent flow field is found in the vicinity of groynes. Typically, eddy currents form in the groyne fields (area between consecutive groynes) where water flows upstream along the bank (King, 2009). Multiple groynes are usually employed at a given site, and act together to control the flow path of the river and the location of sediment deposits that strongly influence the overall sediment balance of a river (Yossef & Vriend, 2011).

Groynes are generally designed with a spacing between consecutive groynes as a function of the projection length of individual groynes (See Figure 3). This results in less materials required to protect a riverbank than would be needed if longitudinal protection was employed. Dissipation of energy by a series of groynes also provides some protection further downstream from where they are constructed.
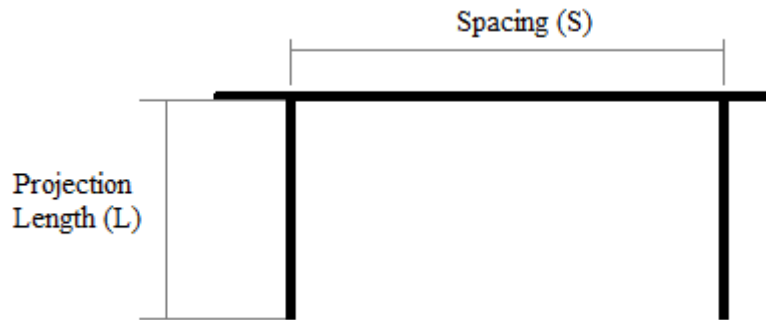
Figure 3: Projection length and spacing of groynes

Despite the usefulness of groynes, there is some concern that groynes may be responsible for increased flooding, due to the associated flow resistance. Studies show that over the past century, flood stages for given discharges along the Mississippi River have increased by 2 – 4m, which is attributed to the increase in groyne construction (Azinfar & Kells, 2011).

The basic design aspects that need to be considered when designing groynes are their shape, the orientation to the flow, the length of the groynes, the spacing between consecutive groynes, the depth of scour and the resulting flow patterns (Osman & Ibrahim, 2008).

2.4.1   Flow patterns around groynes

A number of studies have investigated the details of flow near groynes and structures similar to groynes. The hydrodynamics of the flow near groynes has been clarified, but detailed dynamics of the flow near a series of groynes remains to be fully comprehended. Present mathematical modelling capabilities have been unable to include the role of groyne fields in large–scale morphological predictions. Even smaller scale models do not fully reproduce the sedimentation/erosion behaviour of groyne fields (Yossef & Vriend, 2011).

Azinfar & Kells (2011) found that the number of groynes and the spacing between them, as well as the flow conditions, have a substantial effect on the flow resistance, and hence the backwater effect. The total drag force exerted by a groyne field increases with the number of groynes and the relative spacing between the groynes. This finding was more apparent for submerged flow conditions. The drag force of the first plate is the greatest, as it acts as a shield for the drag force experienced by the downstream groynes.

The basic method by which groynes offer riverbank protection is to confine the flow in a narrow main channel and create low flow zones characterized by eddy currents close to the banks. Submergence plays a big role when considering flow patterns around groynes as a

13

result of the flow patterns entering the groyne field. In Figure 4 typical flow patterns associated with submerged and emerged groynes are shown.
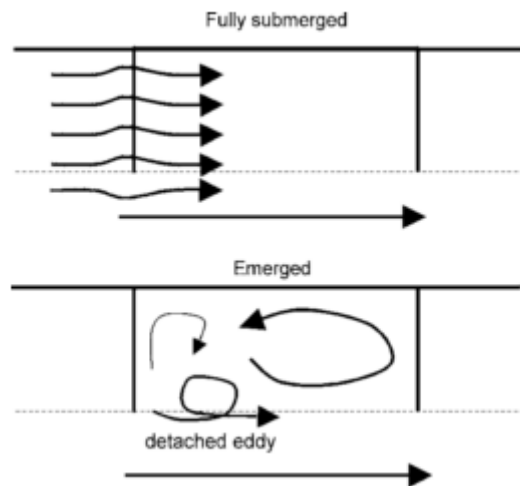
Figure 4: Emerged vs. submerged groynes (Uijttewaal, 2005)

The morphological pattern associated with different groyne layout designs correspond to the number and shape of recirculation cells between consecutive groynes. The ratio of spacing between consecutive groynes (S) and the projection length of the groynes (L) determines the number and shape of the recirculation eddies. An S/L ratio of close to 1 results in a single eddy, while an S/L ratio of 2 – 4 results in two circulations, a large primary eddy current that forms toward the downstream groyne, and a smaller secondary eddy forming close to the upstream groyne. A very large S/L ratio leads to a penetration of the main flow into the groyne field (Yossef & Vriend, 2010).

2.4.1.1 Emerged groynes

When groynes are not fully covered by water during flow, they are said to be emerged. When groynes are emerged, the flow inside the groyne fields, in the horizontal plane, shows a circulation pattern (Uijttewaal, 2005; Uijttewaal, Lehmann, & Mazijk, 2001). According to Yossef & Vriend (2011) the flow patterns are characterized by:

- A primary eddy that forms in the downstream part of the groyne field and covers nearly two thirds of its spacing (see Figure 5). The magnitude of the circulation velocity is about 30% to 40% of the main channel mean velocity
- A secondary eddy driven by the primary eddy with an opposite sense of rotation and a much smaller flow velocity (Figure 5)
- A dynamic eddy that is shed regularly from the tip of the upstream groyne. This eddy migrates in a downstream direction and merges with the primary eddy current which, in return changes in size due to the interaction with the migrating eddy (Figure 5)
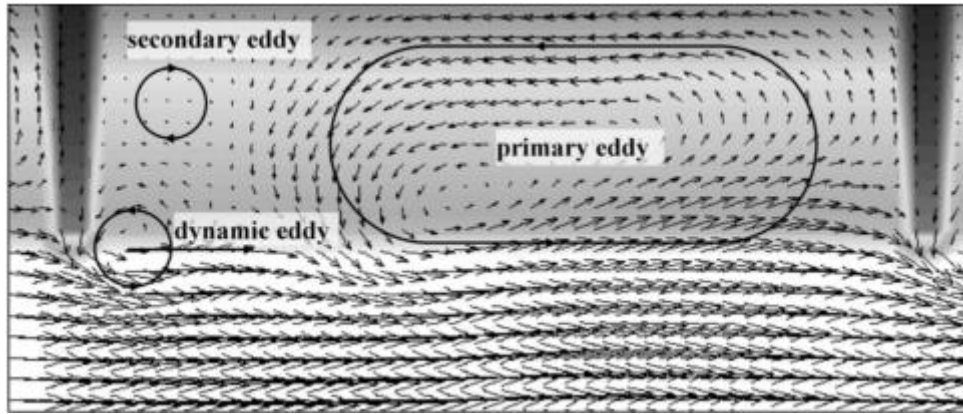
Figure 5: Flow pattern in a groyne field during emerged flow condition (Yossef & Vriend, 2011)

The whole circulation pattern is driven by the main stream via exchange of momentum through the interfacial mixing layer. The mixing layer is recognized as the gradual velocity change from the high value of flow velocity in the main channel to the almost zero value in the groyne field. The flow patterns described above, was also found in an independent study by Weitbrecht, Socolofsky, Asce, Jirka, & Asce (2008).

Abad, Rhoads, Güneralp, García, & Asce (2009) tested a three – dimensional hydrodynamic model that was used to simulate groynes constructed in the Sugar Creek in McLean County, Illinois. They found that groynes greatly reduce streamwise velocities near the outer riverbank at all cross sections. Flow was found to be weakly recirculating in the groyne fields with high velocities around the tip of the groynes. The flow patterns obtained for emerged groyne situations are shown in Figure 6.

It was found that recirculating flow in the groyne fields is largely isolated from flow in the main channel. The drag force on the middle groynes for emerged flow conditions is found to be quite small (Azinfar & Kells, 2011). Figure 6 shows the recirculation zones between two groynes for low flow conditions. The colours refers to velocity magnitude U_{mag} in m/s.
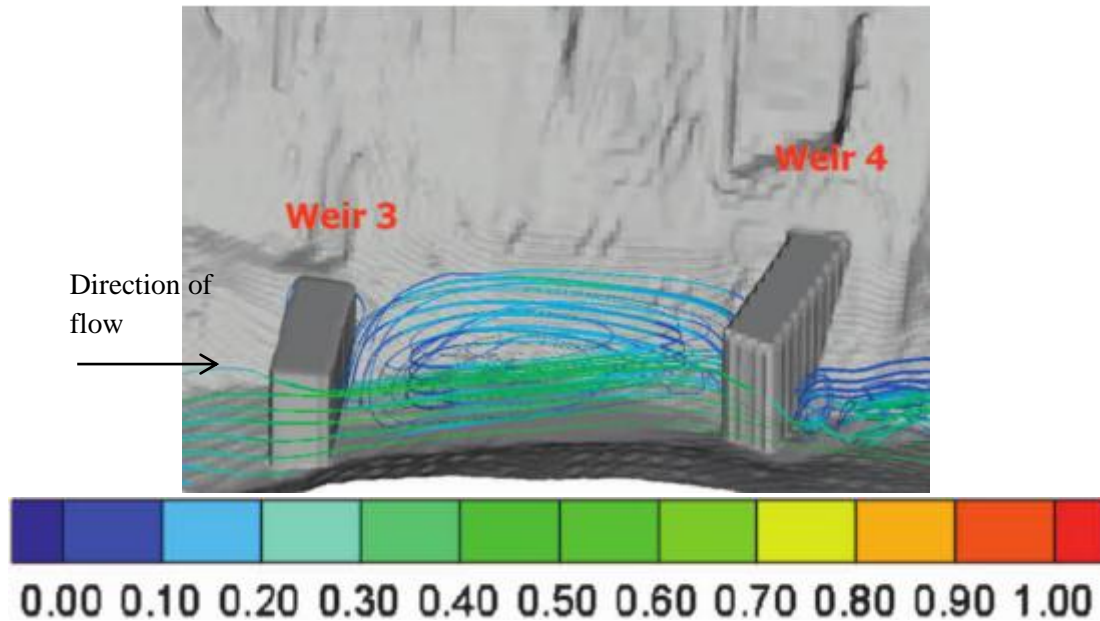
Figure 6: Three - Dimensional flow patterns for emerged groynes (Abad et al., 2009)

2.4.1.2 Submerged groynes

In practice groynes are often flooded, therefore it is important to also study the effects of submergence for different groynes. Submerged groynes do not show the horizontal circulation pattern in the groyne fields as is observed in the emerged case (Yossef & Vriend, 2011).

The groyne fields can be characterized as a low – velocity region. The momentum transfer by the water flowing over the groynes is sufficient to balance the momentum transfer through the mixing layer, that otherwise would have caused a recirculation inside the groyne field. As the groynes are submerged, the flow over the groynes hinders the horizontal recirculation, causing it to disappear after relatively low submergence. Generally the flow pattern observed in submerged cases shows an alternating accelerating and decelerating pattern between flow over and around the groynes (Yossef & Vriend, 2011).

The three – dimensional hydrodynamic model created by Abad et al. (2009) simulated submerged flow around groynes in the Sugar Creek, McLean County, Illinois, which illustrated flow patterns as shown in Figure 7.

For the submerged cases, flow was found to have a strong downward motion along the shear layer, both due to the drop after the groynes, and to well – developed secondary circulation inward of the groyne tips. As the flow approaches the downstream groyne, strong divergence was seen along the shear layer with upward fluid motion inward and outward of this layer

16

(Abad et al., 2009). The drag force on individual groynes increases as the submergence ratio increases (Azinfar & Kells, 2011).

Figure 7 shows the recirculation zones between two groynes for medium- and high-flow conditions. The colours refer to the velocity magnitude U_{mag} in m/s.
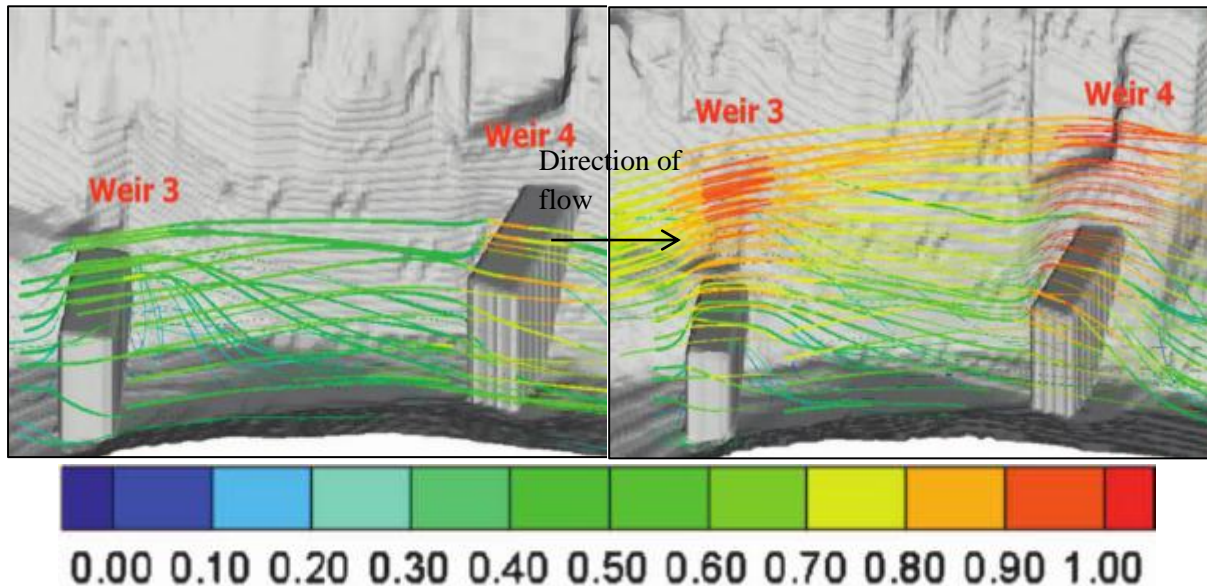
Figure 7: Three - Dimensional flow patterns for submerged groynes (Abad et al., 2009)

2.4.2   Sediment transport around groynes

In practice groynes are not always perpendicular to the flow direction, but may be oriented at different angles with respect to the approach flow (Koken, 2011). This orientation of groynes with respect to the flow direction is a very important aspect when considering the sediment movement and scour associated with groynes.

Local scour initially occurs at a very high rate, which diminishes over time, around the tips of the groynes. The bed material load increases locally downstream of the structures, due to the addition of the scoured material. The increased load results in the development of some temporary local sedimentation as bars and bed forms. Once scouring around the structure ceases, the bed further downstream eventually reaches a new equilibrium condition (Bhuiyan, Hey, & Wormleaton, 2009). The depth and volume of local scour around groynes are difficult to estimate accurately. Few studies have been done that measure the velocity distribution associated with groynes and scour holes, and the velocity distribution as scour holes evolve. As a result, most scour prediction algorithms are empirically based and only predict the maximum depth of scour (Kuhnle et al., 1999).

According to King (2009), the deposition patterns that can be expected for different groyne orientations are illustrated in Table 3.

Table 3: Sedimentation associated with groyne orientations

	Sketch	Comments
Groynes with upstream orientation		• Attracts silt upstream and downstream of structure • Pushes current away from riverbank • Has great potential for scour hole at tip
Groynes with downstream orientation		• Attracts silt only downstream of structure • Does not form much eddy currents • Has relatively low potential for scour at the tip
Groynes perpendicular to the approach flow		• Groyne attracts moderate amount of sediment upstream and downstream • Keeps current more or less parallel to the bank • Has medium potential for scour at the tip

Kuhnle et al. (1999) and Kuhnle, Alonso, & Shields (2002) conducted experiments to determine the geometry and volume of scour holes found around the tip of a groyne for angled and perpendicular orientations. They found that the volume of the scour holes increased with time in a similar fashion for all groyne orientations. The similarity of the shape of the volume vs. time relations was plotted and a power function was fit to these plotted points, giving the following relationship:

$$\frac{V_i}{V_{30}} = 0.980\left(\frac{t_i}{t_{30}}\right)^{0.653}$$

18

Where V_i is the volume of the scour hole at time i (t_i), and V_{30} and t_{30} are the volume and time at an elapsed time of 30 hours. The shape and extent of the scour holes varied for the three different angles of orientation of the groynes.

- The length of the scour holes was generally longer for the experiments with the 45º (upstream orientation) and 135º (downstream orientation) orientations as compared the 90º (perpendicular orientation) angle
- The distance from the outer channel wall was less for the 45º angle than for the 90º and 135º angles
- The upstream length and the ratio of volume of scour to volume of the groyne was higher for the 135º orientation than for the 45º and 90º orientations

According to their findings the calculated near bank bed erosion was the greatest for 45º groynes, which would be expected to lead to an increase in the bank erosion and the channel's instability. Groynes with orientation angles of 90º and 135º would therefore be expected to cause less bank, instability provided that the channel was wide enough that the scour hole would not encroach on the opposite bank (Kuhnle et al., 2002).

The depth of scour around abutments and groynes are not fully understood. The depth of scour around the tip of the groynes can be estimated by the Niell formula (King, 2009):

$$H' = \frac{2.1}{h}\left(\frac{2.5q^2}{D^{0.318}}\right)^{0.333} \text{ to } \frac{2.75}{h}\left(\frac{2.5q^2}{D^{0.318}}\right)^{0.333}$$

where $0.1 \leq D_{50} \leq 200mm$

        H′   in mm (relative maximum scoured depth) H' = (z+h)/h

        h   in mm (flow depth before scoured section)

        z   in mm (depth of scour below h)

        D   in mm (mean particle diameter to be scoured)

        q   in m^3/s/m (unit discharge)

Two other empirical formulas for the determination of the scour depth at groynes have been developed:

According to Laursen the depth of scour for groynes with a 90˚ orientation with respect to the oncoming flow can be determined according to the following equation:

$$\frac{d_s}{d_0} = 1.5K_s\left(\frac{b}{d_0}\right)^{0.5}$$

19

where:

$d_s =$ depth of scour (m)

$d_0 =$ depth of flow (m)

$b =$ effective projection length of groynes (m)

$K_s =$ 1.0 for groynes

This equation is applicable when:

$$\frac{\sqrt{gd_0s_f}}{v_{ss}} < 0.5$$

where:

$g =$ gravitational acceleration (9.81m/s^2)

$S_f =$ energy gradient (m/m)

$v_{ss}=$ particle settling velocity (m/s)

There are many relationships that have been developed to define the boundary conditions under which sediment movement will occur in streams.

From the SANRAL Drainage Manual, it is seen that Rooseboom (1983) recommends the use of settling velocities of particles in alluvial streams and the critical tractive strength of clay in cohesive materials as representative of the transportability of sediments.

The method for determining whether sediment movement will occur, is obtained from Rooseboom (1983), where the Modified Lui Diagram in Figure 8 is used. This diagram expresses the boundary between moving sediment and non–moving sediment in terms of a shear Reynolds number vs. a ratio between shear velocity and settling velocity.

$$\frac{v_{*c}}{v_{ss}} = 0.12$$

With

$$v_* = \sqrt{gDS}$$

where:

$v_* =$ shear velocity (m/s)

$v_{*c} =$ critical shear velocity (m/s)

$g =$ gravitational acceleration (9.81m/s^2)

20

D = flow depth (0.118m)

S   = energy slope (0.00333m/m)

v_{ss} = particle settling velocity (m/s)
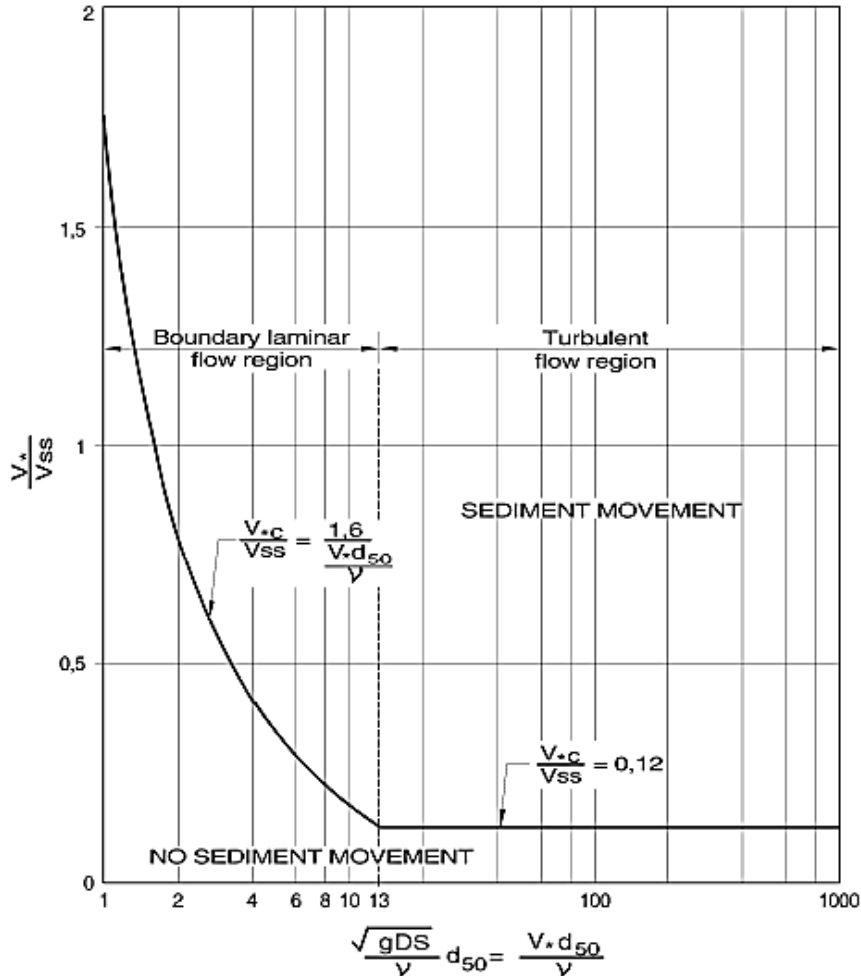
Figure 8: Modified Lui Diagram (Kruger & Gomes, 2007)

2.4.3   Design of groynes

Soils for agriculture in the Western Cape are generally shallow and irrigation is limited. The deepest and best soils are commonly found in the flood plains of rivers. Very little space is left undeveloped between the agricultural land and the low flow edge-of-water position. There is little space for rivers to meander in without the riverbanks being eroded. Because of this, some general principles have evolved for the planning of works for erosion control by means of groynes:

- When planning groynes, the structures must have a minimal impact on the river
- When planning groynes, they should not be allowed to encroach further into the river than where a riverbank can be proven to recently have been.

The following guidelines are currently used for the planning of a field of groynes according to King (2009).

- The minimum base width of the flow channel is determined using the river as surveyed, the 20–year flood and a trapezoidal section with side slopes appropriate to those found on site.
- The horizontal alignment of the river is planned by combining a collection of straight and tangential bend sections in such a way that the minimum channel fits within the existing river boundaries.
- Figure 9 shows how groynes are positioned according to the following guidelines:
    - Usually, on a bend, groynes are placed on the outer bank
    - The axis of the groynes is placed perpendicular to the approach flow direction
    - On a bend, the first groyne is positioned in line with the start of the bend
    - The nose of each groyne is placed on the outer edge of the planned rehabilitated river's main channel.
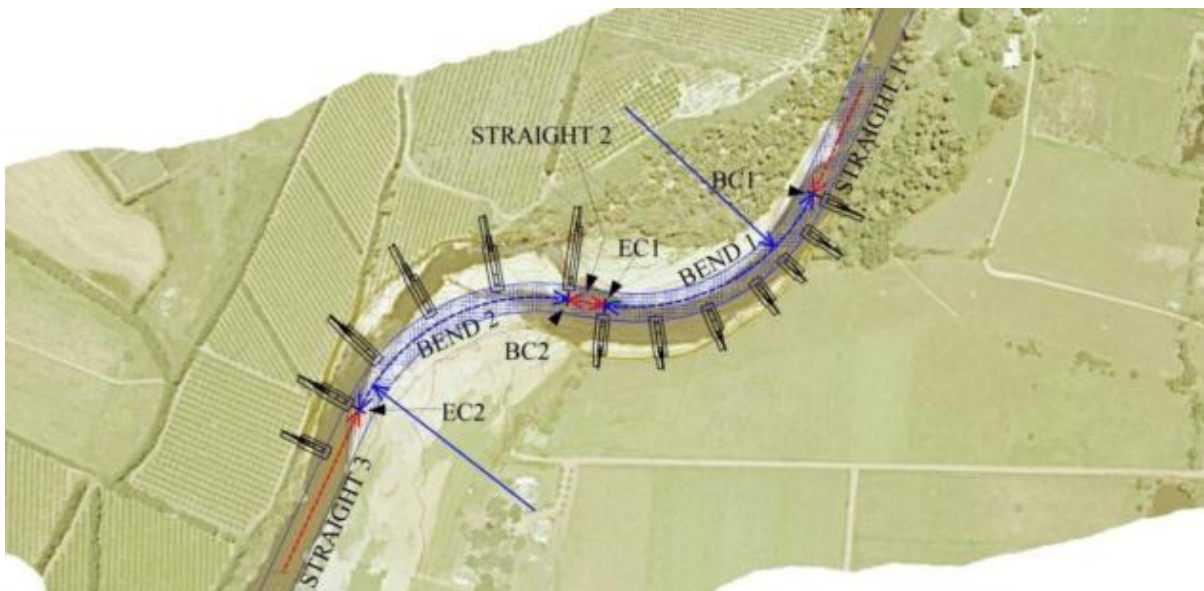
Figure 9: Typical layout of groynes with river geometry (King, 2009)

- The spacing between the groynes is determined by an empirical relationship which is based on the projection length of the groynes. The spacing of groynes varies from 3 times the projection length on the outside of bends, to 6 times the projection length on straight sections
- The vertical alignment of a field of groynes is vital to the stability of these structures. The vertical alignment is determined by the following guidelines:
    - The foundation of the structure must be placed as close as possible to the depth of the expected scour
    - Obstructions such as groynes cause the scour depth to increase locally. The estimation of this scour depth is done according to the Niell formula discussed in section 2.4.2.
- The standard long section of a groyne, as it is used by the Department of Agriculture in the Western Cape, is shown in Figure 10.
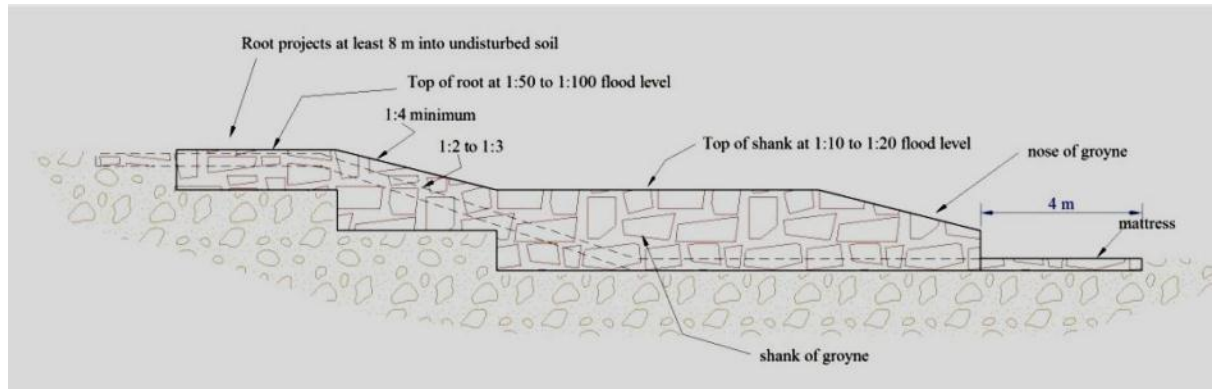
Figure 10: Standard long section of a groyne (King, 2009)

- These groynes are constructed in gabion basket form. The base of the groynes is anchored into the river bed.
- The tops of the groynes are covered by a protective layer of concrete.

It is essential to re–establish indigenous vegetation as an integral part if the riverbank rehabilitation programme.

The design guidelines used in this thesis is the same as described above. These guidelines are, however, not specific to the Western Cape, and are applicable for a wider range of rivers. These are, however, the only available guidelines according to which groynes are designed in South Africa.

2.5   Case studies

2.5.1   Tradouw

During the floods of 2006 in the Western Cape, the Grootvadersbosch River, on the farm Tradouw, started undermining the embankment on which an irrigation dam was constructed. A request was sent forth for assistance with the erosion protection and to protect the dam. A field of 8 groynes was proposed and constructed in early 2008. A few months after construction, the groynes were subjected to the 2008 flood, which has been estimated to be between a 1:50 and 1:100 year flood. The structures were inspected after the flood (King, 2009).

Figure 11 shows the design of the planned field of groynes prior to construction. Figures 12 and 13 are aerial photos taken of the site after construction in 2008, and after the flood of 2008, respectively. From Figures 12 and 13 it can be seen that no migration of the outer bank occurred during the flood, pointing to the effectiveness of the groynes.
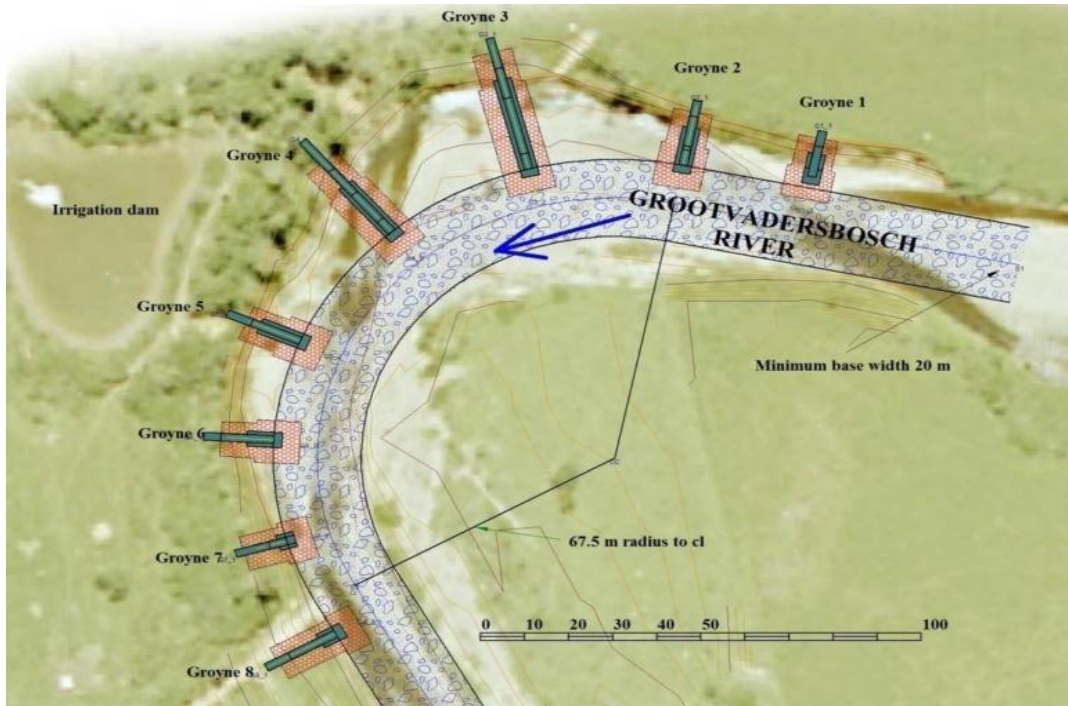
Figure 11: Tradouw project layout

Figure 12: Tradouw project after construction in 2008

Figure 13: Tradouw project after the 2008 flood

The system worked well and the embankment, on which the dam was constructed, did not suffer any damage. The flow depth over the structures at groynes 4 and 5 was 0.913 m above the level of the shank. This confirms that the flood was greatly in excess of the 1:10 and 1:20 year flood. Problems were experienced with the formation of scour holes and damage attributed to floating trees. Although some mattresses have sunk into scour holes, it is expected that, if smaller floods are encountered, these holes should fill up naturally (King, 2009).

Groyne 5 had a scour hole starting upstream of the structure, which caused the partial subsidence of the mattress. If unchecked, this will ultimately lead to the subsidence of the nose of the groyne. This is very likely due to an over–optimistic interpretation of the projection length. The result was that the groynes spacing was too wide (according to the projection length), allowing the river to meander toward the riverbank between the groynes. A 1.17 m deep scour hole was formed from just upstream of the groyne to the downstream side of the groyne. A more appropriate design would have been to move the river channel 10m further to the inner riverbank, which would have created longer projection lengths according to which a more practical groyne spacing could have been used. The disadvantage of this approach would have been a sizeable increase in constuction cost, as a result of the longer strucures to be constructed. This approach would also have been less ecologically accpetable, as the riverbank would have extended beyond where it had been recently (King, 2009).

25

The cost associated with the Tradouw project was R896 121. The division of funds was 24% for labour, 33.0% for materials and 43% for the rest.

Further images can be seen in Appendix 1.

2.5.2   Mullersrus

The Buffeljags River at the farms Mullersrus and Olivedale, has been under observation since 2002. The river forms an S–bend between the two farms, where the outside of the bend has recently experienced extensive erosion with every flood (on Olivedale the bank moved 20m during the 2004 flood and again during the 2006 flood). The growth of "Black wattles" on the inside of the bend has made erosion worse by colonising the sediment. It is also very likely that the sediment load was increased due to runaway erosion of the riverbank at upstream farms. The farm Rotterdam, for example, lost about 40 m in width of a 5 m high riverbank over a few short years, while the farm Sovereign lost 30 m of a 6 m high bank during the 2006 flood alone. Groynes were constructed with funding from the 2006 Flood Relief Scheme for both bends in early 2008. Just after construction, a severe flood (between 1:50 and 1:100 year flood) was experienced in the Buffeljags River (King, 2009).

From Figures 14 and 15 it can be seen that no migration of the outer riverbanks occurred. Some overland flow did occur on the inside of both bends, but no crops were lost.
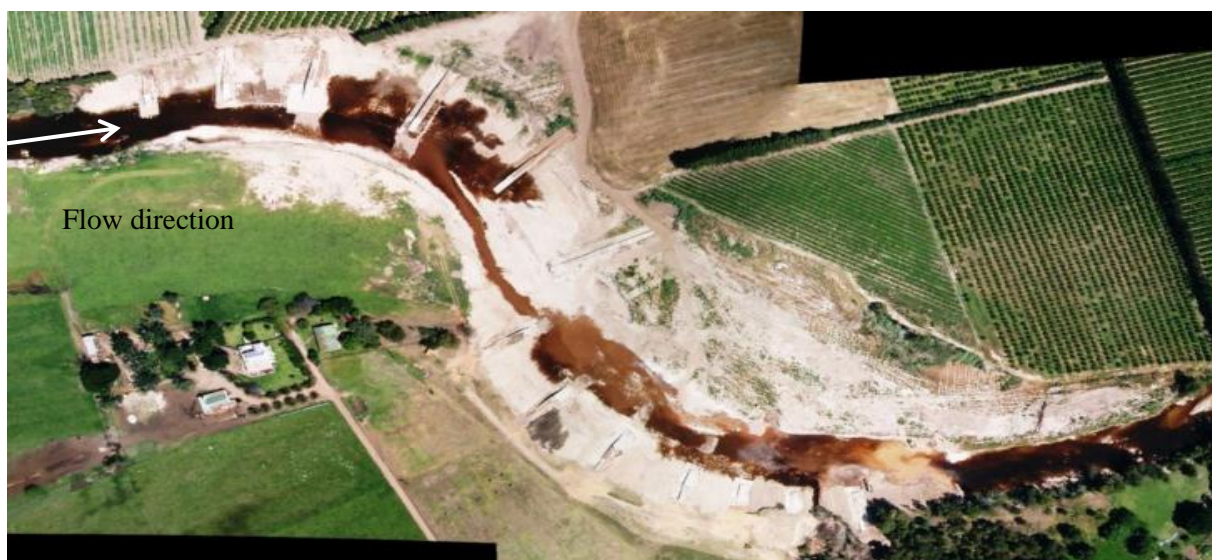
Figure 14: Aerial photo of Mullersrus and Olivedale before the 2008 flood

Figure 15: Aerial photo of Mullersrus and Olivedale after the 2008 flood

The groynes worked well in that the bank was protected from further erosion during the 2008 flood. Scour holes formed around some of the groynes. Because landscaping between the groynes had been done to a very high level, not much deposition of sediment was found. Directly downstream of the groynes, the landscaped fill was eroded by the turbulent flow over the groynes. The mattresses on the upstream side of the groynes were lifted and rolled over, despite the use of a 4 m gabion basket anchor buried under the upstream corner of the mattress. Floating branches and trees, which were found lying in the river after the flood, are suspected of hooking the mattresses and lifting them enough to enable water to lift them further. Significant damage was also done to the structures by the floating debris during the flood (King, 2009).

The costs associated with the Mullsersrus and Olivedale project were R3 058 615. The division of funds was the same as for the Tradouw project. The project also protects land further downstream by breaking the cycle of erosion and deposition.

2.5.2   Summary of case studies

From these case studies it can be seen that the implementation of groynes does assist in preventing the migration/erosion of the outer bank, if applied correctly. With 24% of the total cost of the projects going to labour, poverty alleviation is also addressed.

The main problems surrounding groynes are, local scour around the noses of the groynes resulting in the mattresses sinking into these holes and floating debris (tree trunks etc.) causing damage to the groynes as well as the surrounding mattresses.

3. Physical model

3.1   Introduction

Physical model testing is a way of determining, on a smaller scale, what will happen when the model in question is built at full scale. Physical model testing has been used for centuries for this purpose. Leonardo da Vinci was quoted in saying:

"I will treat of such a subject. But first of all I shall make a few experiments and then demonstrate why bodies are forced to act in this manner. This is the method that one has to pursue in the investigation of phenomena of nature. It is true that nature begins with reasoning and ends by experience, but nevertheless, we must take the opposite route, as I have said, we must begin with experiment and try through it to discover the reason" (Shen, 1971).

In the case of this thesis, physical model testing was used to observe flow patterns in and around groyne fields, as well as the sediment transport associated with these observed flow patterns. Finally, the main areas of deposition and scour could be determined, and assist in making an informed decision on optimising the layout design of groynes.

3.2   Objectives

The use of groynes as a means of riverbank protection has been practised extensively in the Western Cape, with the objective of poverty alleviation and the safeguarding of agricultural land. Much emphasis has been placed on model testing for the planning of groynes.

The first objective regarding the physical model was to design a river of sinusoidal shape that would typically be found in South Africa. A suitable design for the shape of the groynes had to be determined.

The main objective was to determine the optimal layout design of the groynes. The layout parameters considered for this study comprise of the following three things:

- The spacing between consecutive groynes
- The projection length of the groynes
- The orientation of the groynes (perpendicular to flow, angled upstream or downstream)

This thesis also studies the flow patterns surrounding different layout designs of groynes, as well as the sediment transport associated with the different flow patterns. The data collected from the physical model experiments is used to validate a CCHE2D model.

3.3   Model design

A physical model was designed and built in the hydraulic laboratory at the Department of Civil Engineering, University of Stellenbosch. The design of the model strived to create a likeness to typical South African rivers. As the number of rivers in South Africa is vast, the following rivers were investigated: the Berg River, the Breede River, the Buffeljags River, the Gamka River and the Grootvadersbosch River. In these particular rivers groynes have been the preferred method of erosion protection. These rivers are sinusoidal in plan where the groynes are implemented.

3.3.1   Channel layout and dimensions

As mentioned above, a sinusoidal shape was determined to be the optimum design for the given problem. It was decided to design a channel with two 90° bends, which can be seen in Figure 16, to best simulate water erosion on the banks. The second bend also allows us to see the transition of erosion vs. deposition from the outer banks to the inner banks at the change of turns.
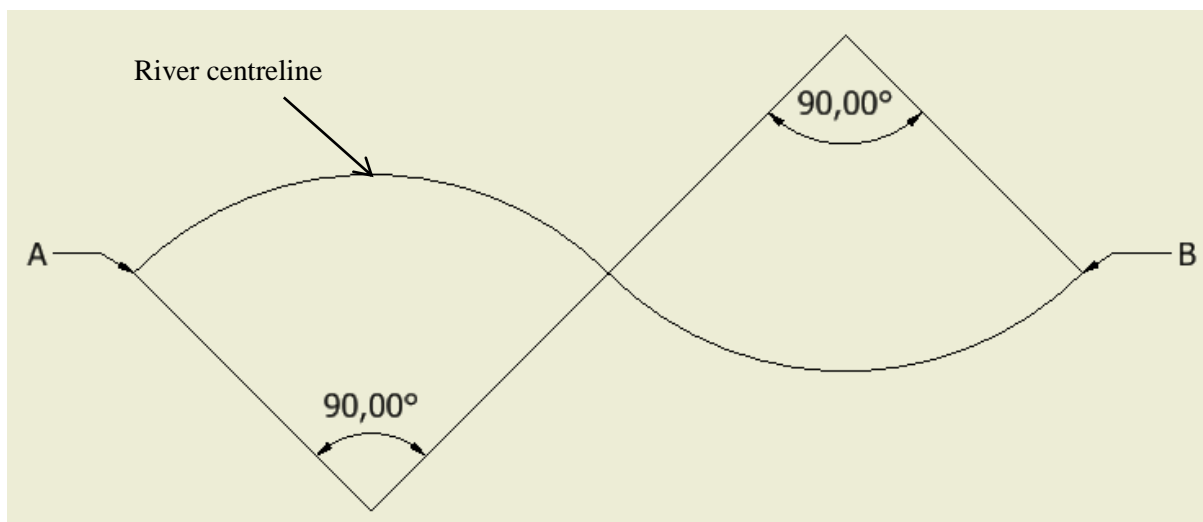
Figure 16: Channel bends

The sinuosity of a river is the ratio between the straight line distance between point A and point B (Figure 16) and the actual length along the run of the river between them. For the river to be deemed sinusoidal, the ratio needs to be at least 1:1.1. With two 90° bends and any radius the sinuosity can be calculated as follows:

- Distance along the run of the river $= \pi r$
- Straight line distance between A and B $= 2 * \sqrt{2r^2}$

Thus the ratio is given by: $\dfrac{\pi r}{2*\sqrt{2}*r}$

where the final equation after simplification is given by: $\frac{\pi}{2*\sqrt{2}} = 1.1107$

The sinuosity is therefore equal to 1.1107, which is larger than 1.1, in which case the rivers are deemed sinusoidal.

When considering current projects where groynes are implemented for the use of erosion protection of riverbanks on the Buffeljags River, the Gamka River and the Grootvadersbosch River, a mean bend radius of approximately 100 m has been determined. A width of approximately 30-35 metres has been observed. Keeping these dimensions in mind, a scale model of 1:30 was determined to have a top width of 1.2 m, a depth of 250 mm and a bend radius of 4 m to the centreline of the river.

The scouring of sediment must also be taken into account. To ensure that all the sediment will not be eroded away, (which would compromise the integrity of the tests), a sediment layer of 100 mm was used in the channel. Figure 17 shows the dimensions of the channel as well as the sediment layer.
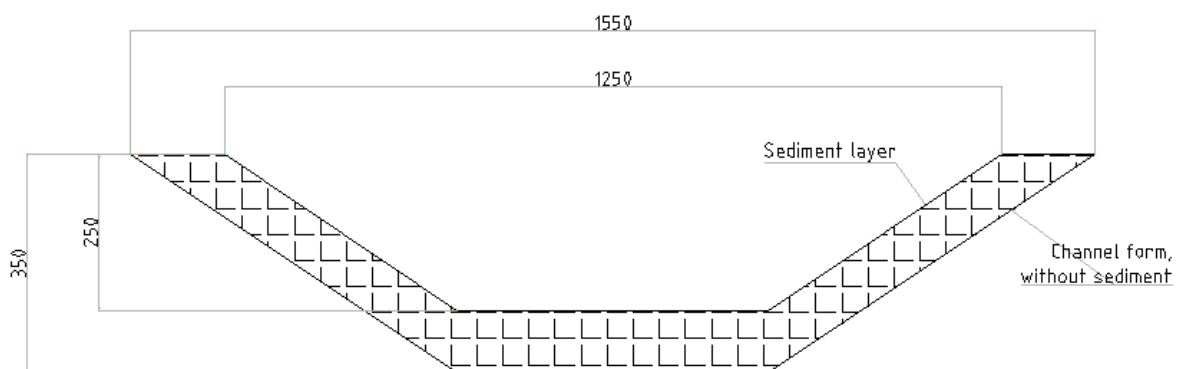
Figure 17: Channel cross section

A sediment basin with dimensions of 6m long, 3.6 m wide and a height of 450 mm was designed to allow the sediment to settle after being washed out of the channel. The sediment settling basin was designed to have a drop of 157 mm to the laboratory floor to reduce the velocity of the water, so that sediment settling would occur more readily.

An approach channel was designed to ensure a smooth transition of the inflow water at the beginning of the sediment layer. The first groyne must be positioned before the commencement of the first bend (King, 2009). To ensure that flow was fully developed at the first groyne, a 3m straight channel section was included before the first bend. Additionally a straight 1.5m section was included after the second 90° bend. This helps to determine scour effects immediately downstream of the last groyne.

A slope of 1:300 was chosen for the channel. From Beck & Basson, (2003) it was seen that this represented the average slopes for rivers like the Buffeljags River and the Gamka River. All of the above mentioned design details can be seen in Figure 18.
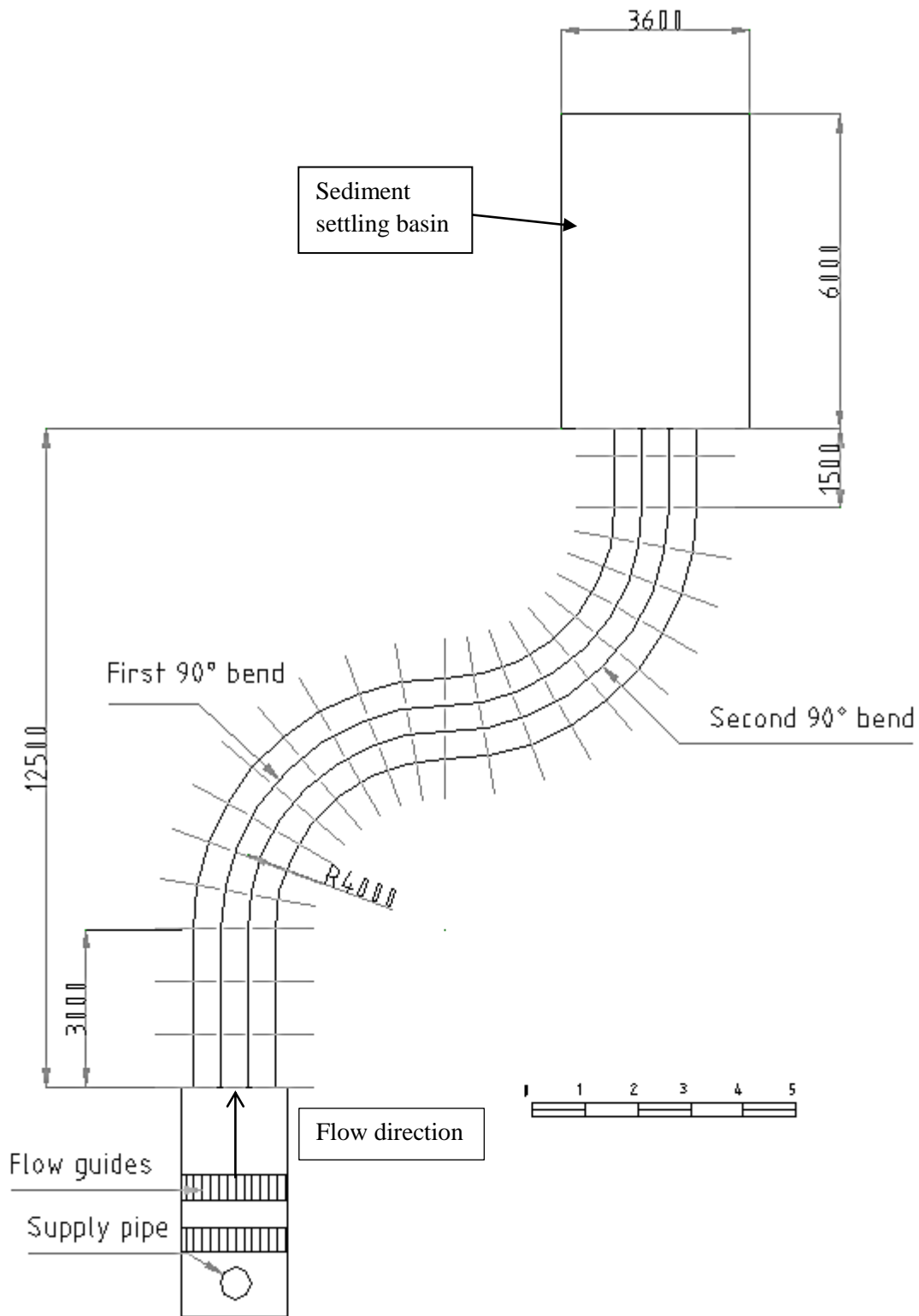
Figure 18: Channel layout

31

The scale for the above mentioned model was chosen in accordance with the availability of space in the Hydraulics laboratory, as well as taking into consideration the size of sediment that is obtainable.

As indicated in Figure 18, a sediment settling basin was incorporated into the design of the channel. The sediment settling basin was designed to allow sediment that had gone into suspension during the test run, to settle in the basin because of the decreased velocity of the water. The design of the sediment basin is discussed in section 3.3.3.

A discharge of 20 ℓ/s was chosen to simulate a 100 m^3/s prototype flow. 20 ℓ/s ensures sediment movement with a smaller possibility of bank failure occurring. Bigger flows were tested where bank failure occurred more readily. For the chosen flow rate of 20 ℓ/s, the characteristics of the channel are as follows:

Table 4: Channel characteristics

Characteristic	Equation/symbol	Value
Bottom width	b	0.5 m
Side slopes	x (H:V)	1.5
Longitudinal slope	S	0.00333 m/m
Flow depth	y	0.12 m
Area	$A = (b + xy)y$	0.082 m^2
Wetted perimeter	$P = b + 2y\sqrt{1 + x^2}$	0.933 m
Hydraulic radius	$R = \dfrac{A}{P}$	0.088 m

3.3.2 Groyne design

The design used for individual groynes was adopted from King (2009), where the design for past, current and possible future groynes is discussed. The cross sections that have been used in the past are indicated in Figure 19.
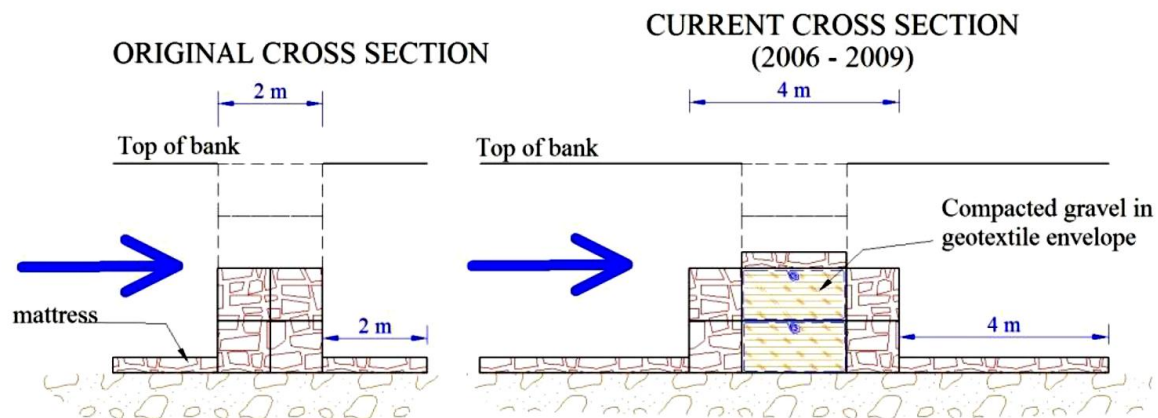
Figure 19: Cross sections of groynes (King, 2009)

32

King (2009) cited that the cross section of the shank of the groynes is to be modified with a sloping edge upstream and downstream as illustrated in Figure 20 below, to protect the groyne from tree stumps by deflecting them over the groyne.
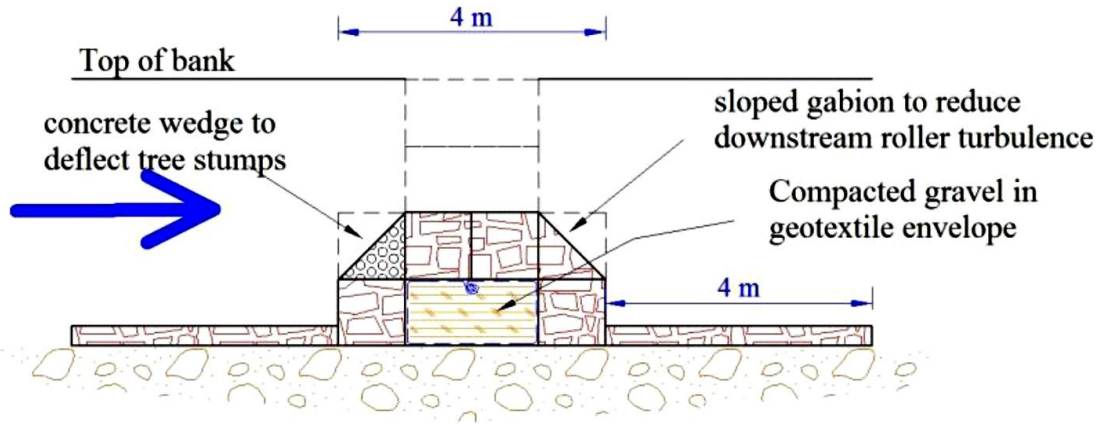
Figure 20: Proposed future design for groynes (King, 2009)

To be able to test more than one projection length, the groynes were designed to have two detachable extensions, each 100mm long, so that the projection length could vary by 200mm (see Figure 21).
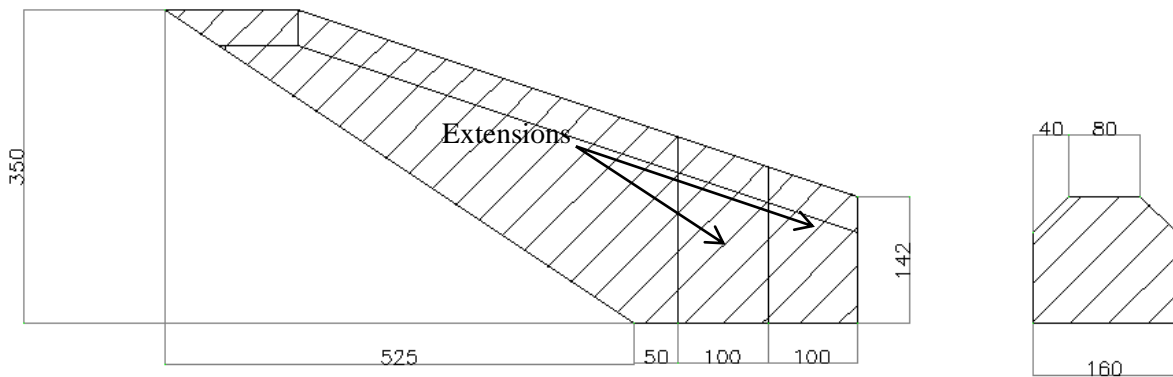
Figure 21: Individual groyne design

The projection lengths of the groynes that was used for this thesis ranged from 0.575 m to 0.775 m. With these projection lengths (0.575 m, 0.675 m and 0.775 m), groynes that stretched to the middle of the channel could be tested for the longest projection length, while the shortest projection length just extended into the channel bed, beyond the trapezoidal sides, with the 0.675 m projection extending 0.15 m past the trapezoidal sides.

33

3.3.3　Sediment

The sediment used in the experiments consisted of crushed peach pits with a relative density of 1.3. The three sediment sizes available for use in the hydraulic laboratory are:

1. $d_{50} = 0.4$ mm; $d_{90} = 0.7$ mm
2. $d_{50} = 0.7$ mm; $d_{90} = 1.6$ mm
3. $d_{50} = 1.0$ mm; $d_{90} = 2.5$ mm

The settling velocities for these different sediment sizes were determined using a settling column filled with tap water (see Figure 22). A distance of 300mm was marked on the outside of the flask. The different sizes of sediment were saturated in water and released under water. The time that elapsed for each particle to settle the 300mm that was marked, was measured. This process was followed for each of the three sediment sizes. The distance was then divided by the time that was measured to determine the settling velocities in m/s. The process was repeated 50 times with each sediment size, using randomly selected particles to be able to accurately determine the mean velocities. The mean settling velocities for each sediment size are shown in Table 5.

Table 5: Settling velocities

Sediment size (mm)	Settling velocity (m/s)	
0.4 – 0.7	$w_{50} = 0.024$	$w_{90} = 0.028$
0.7 – 1.6	$w_{50} = 0.045$	$w_{90} = 0.055$
1.0 – 2.5	$w_{50} = 0.083$	$w_{90} = 0.100$

The settling column that was used to determine the mean settling velocity is show in Figure 22.

Figure 22: Settling column used to determine settling velocities

- Sediment movement

For the physical model testing, a flow rate of 20 ℓ/s was chosen to simulate a prototype flow of approximately 100 m^3/s. The modified Lui Diagram was used to determine whether sediment movement would occur for each of the different sediment sizes available with the given flow, for both the model and the prototype.   The sediment used for the model was a mixture of two of the available sediment sizes (0.4 - 0.7 mm and 0.7 - 1.6 mm), which resulted in sediment with a mean particle sediment size, d_{50} = 0.565 mm by combining the mean size for each sediment on a log scale. A w_{50} = 0.0305 m/s was obtained by combining the already observed settling velocities for both sediment sizes.

As can be seen from Table 6**Error! Reference source not found.**, sediment movement will occur when $\frac{v_{*c}d_{50}}{v} > 13$ (This is the boundary between the laminar and turbulent flow regions) and when $\frac{v_{*c}}{v_{ss}} > 0.12$. Table 6 show the procedure followed to determine whether sediment movement would occur for the given sediment size.

Table 6: Sediment movement according to Modified Lui Diagram

Description	Model	Prototype
Flow Depth (m)	0.118	3.54
Slope (m/m)	1:300	1:300
Flow region $\left(\frac{v_{*c}d_{50}}{v}\right) > 13$	$30.51 > 13$ ($d_{50} = 0.56$ mm)	$5073 > 13$ ($d_{50} = 16.95$ mm)
Turbulent/Laminar boundary flow conditions	Turbulent	Turbulent
$\frac{v_{*c}}{v_{ss}} > 0.12$	$2.03 > 0.12$ (with $v_{ss} = 0.03$ m/s)	$2.03 > 0.12$ (with $v_{ss} = 0.168$ m/s)
Sediment movement	Yes	Yes

As mentioned earlier, a sediment settling basin with dimensions of 6 m x 3.6 m x 0.45 m, was designed to slow the velocity of the water so that the suspended sediment would settle in the basin. The following steps were followed to ensure that the design of the basin is of such a nature that the suspended sediment would settle:

From Rooseboom (1983) it is found that

$$v_c = 5.75 v_{*c} \log \frac{12R}{k_s}$$

where $v_{*c} = \sqrt{gDS}$

v_c = maximum velocity at which sediment will deposit (m/s)

R = Hydraulic Radius (A/P)

k_s = Absolute roughness of sediment (0.00056 m)

with: $\frac{v_{*c}}{v_{ss}} \leq 0.12,$ to allow sediment deposition

where: $v_{ss} = 0.0305$ m/s

then: $v_{*c} = 0.0037$ m/s

thus: $v_c = 5.75 * 0.0037 * \log \frac{12*0.2401}{0.00056}$

$v_c = 0.079$ m/s

Therefore, the velocity of the water in the sediment settling basin must be less than 0.079 m/s. This was determined as follows:

$$v = \frac{Q}{A}$$

with   A $= 3.6 * 0.277 = 0.9972$ m^2

and   Q $= 0.02$ m^3/s

Therefore the actual v $= 0.0199$ m/s, which is acceptable

3.4   Experiment methodology

As stated in section 3.2, the aim of the physical model testing is to obtain a better understanding of the interaction between groynes, sediment movement and flow patterns associated with different layout designs. By doing this, the possibility of optimising the layout design of a series of groynes can be accomplished.

A standard methodology was followed for each of the experiments, to ensure similar conditions for each run.

3.4.1   Experiment 1 (No groynes)

The first experiment was done with no structures built into the channel. The object of the first experiment was to determine the natural erosion of the channel with no riverbank protection being implemented. The results obtained from Experiment 1, were then used to compare with the results obtained when groynes were built into the channel to see the effect that the different layout designs had on the erosion and protection of the riverbanks. The areas worst affected by erosion were also made visible by this experiment.

A sediment layer of 100 mm was evenly distributed along the channel (see Figure 17). Water was dammed from the downstream sediment settling basin to the predetermined level to minimize the erosion of sediment before the desired flow depth was acquired. No additional sediment was introduced during the experiments to accentuate the scour.

The depth of flow (y) was determined using the Manning equation:

$$Q = \frac{1}{n}\frac{A^{5/3}}{P^{2/3}}\sqrt{S}$$

Q = Flow rate (m^3/s)

A = Area (m^2) (see Table 4)

P = Wetted perimeter (m) (see Table 4)

S = Longitudinal slope (m/m) (see Table 4)

n = Manning's coefficient (0.045)

This resulted in a water depth of 120 mm, which was controlled at the downstream end of the channel. The experiment ran for a duration of approximately 5 minutes, typically until the scour reached the fixed bed of the model.

Three measuring points were used for taking measurements by means of needle gauges. As can be seen from Figure 23, measuring point 1 was placed before the start of the first bend, measuring point 2 was placed at the transition from the first bend to the second bend, and measuring point 3 was placed downstream of the second bend.
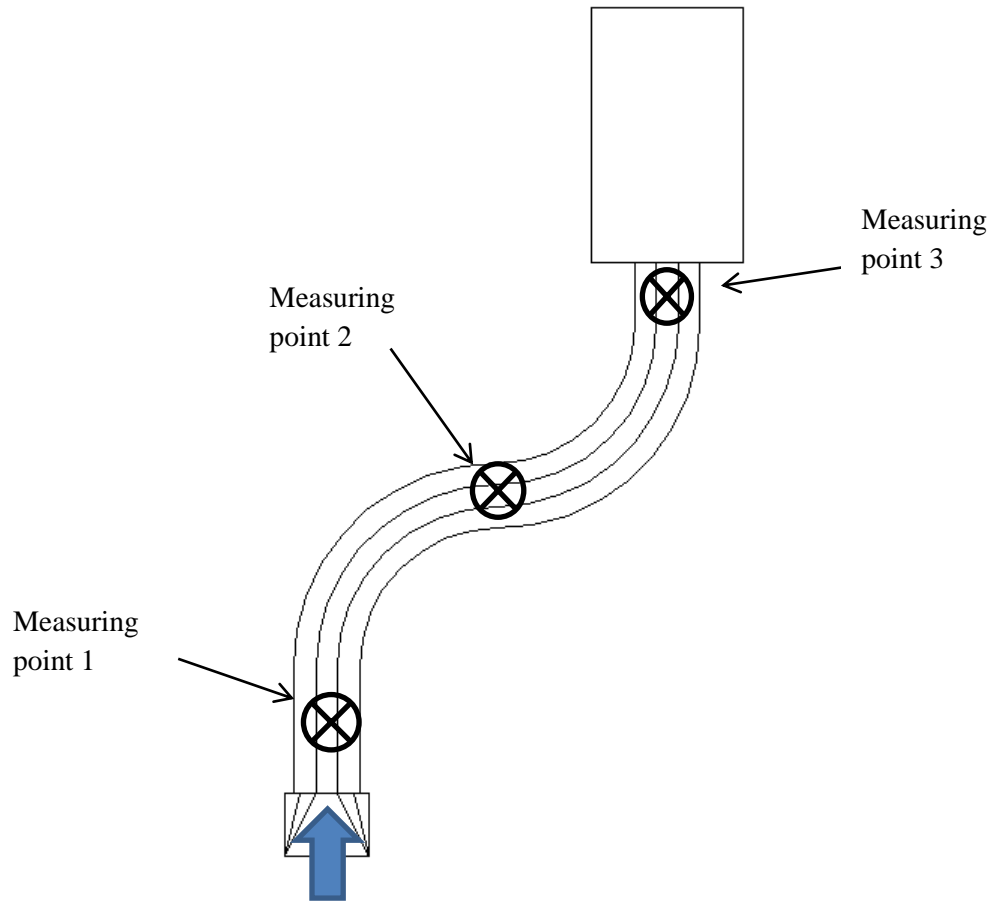
Figure 23: Experiment 1 water level measuring points

Flow- and erosion patterns were observed during the experiment. Water was drained simultaneously from the upstream and downstream sides to prevent sediment movement after the experiment was completed. A survey of the model was done with a Leica TPS 1200+ total station which provides xyz coordinates of the sediment position according to a reference point after the experiment was completed.

3.4.2   Experiments 2 to 10 (Groynes with perpendicular orientation to flow)

Experiments 2 to 10 were done with groynes inserted into the model perpendicular to the flow. Groynes were placed on the first bend only. Three different spacings between the groynes were tested, as well as three different projection lengths (0.575 m, 0.675 m and 0.775 m). The spacing between the groynes was chosen according to a ratio of the length between the groynes to the projection length of the groynes.

For experiments 2 to 4 a spacing of 1.75 m was chosen, which resulted in the following ratios for each test:

Experiment 2: Spacing 1.75 m = 2.258*projection length (0.775 m)

Experiment 3: Spacing 1.75 m = 2.593*projection length (0.675 m)

39

Experiment 4: Spacing 1.75 m = 3.044*projection length (0.575 m)

In Figure 24 the placement of the groynes can be seen as built into the channel. The measuring points are also indicated. Measuring point 1 was placed before the start of the first bend, measuring point 2 was placed between groynes 4 and 5, and measuring point 3 was downstream of the second bend.
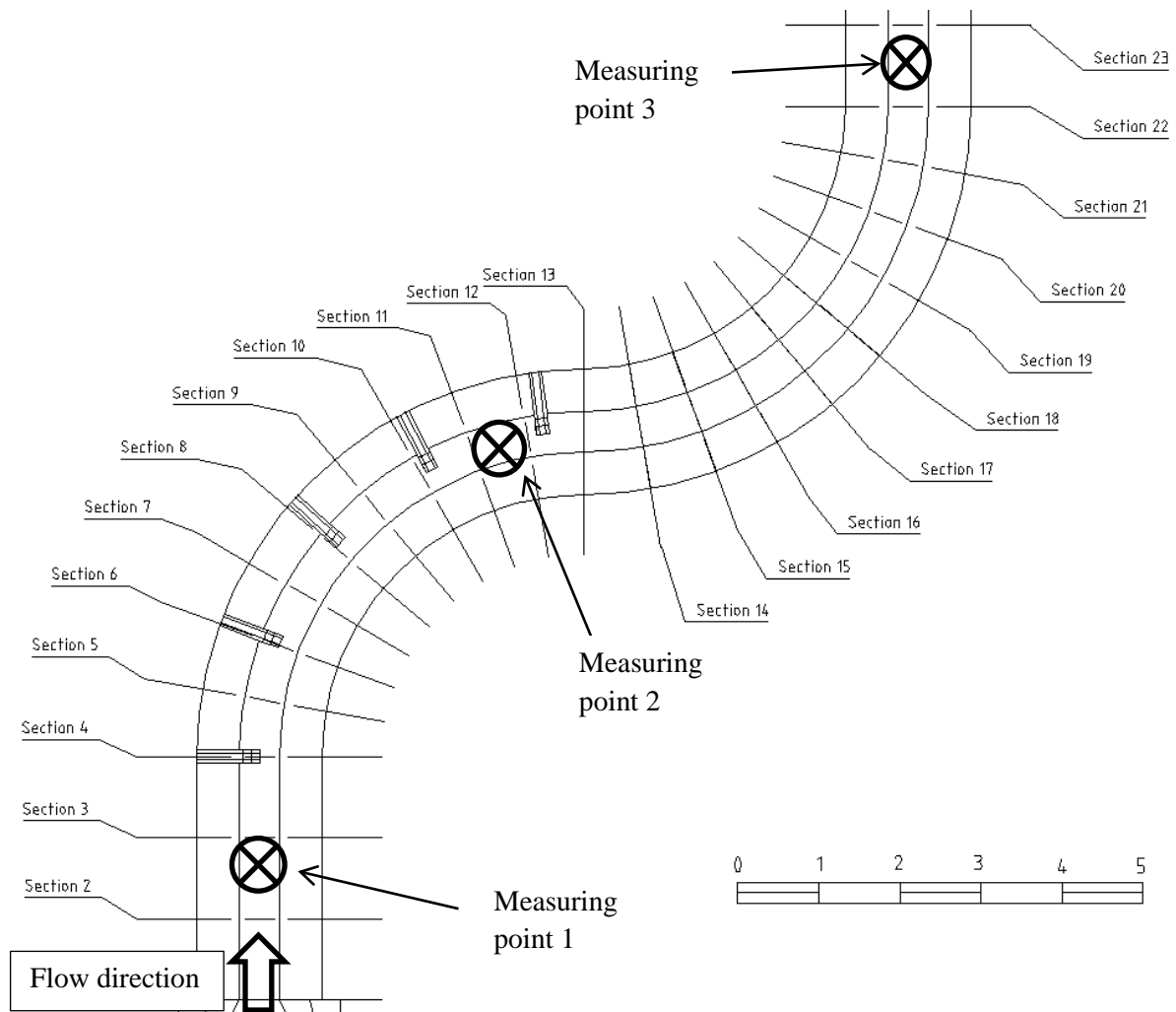
Figure 24: Experiments 2, 3 and 4 groyne placement and measuring points

For experiments 5 to 7 a spacing of 2.333 m was chosen, which resulted in the following ratios for each test:

Experiment 5: Spacing 2.333 m = 3.011*projection length (0.775 m)

Experiment 6: Spacing 2.333 m = 3.457*projection length (0.675 m)

Experiment 7: Spacing 2.333 m = 4.058*projection length (0.577 m)

40

In Figure 25 the placement of the groynes can be seen as built into the channel. The measuring points are also indicated. Measuring point 1was placed before the start of the first bend, measuring point 2 was placed after groyne 4 in between the first and second bends, and measuring point 3 was downstream of the second bend.
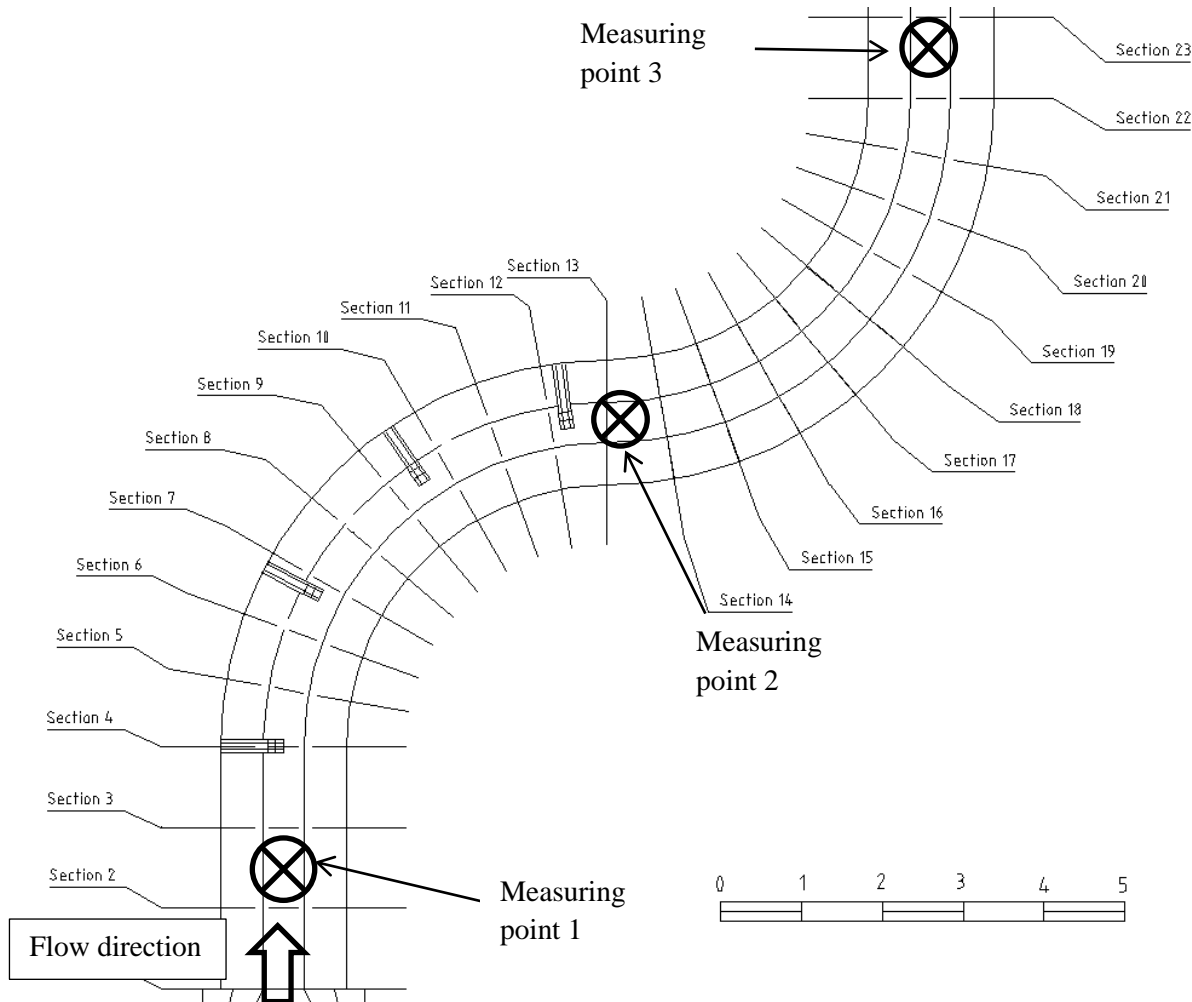
Figure 25: Experiments 5, 6 and 7 groyne placement and measuring points

For experiments 8 to 10 a spacing of 2.834 m was chosen, which resulted in the following ratios for each test:

Experiment 8: Spacing 2.834 m = 3.656*projection length (0.775 m)

Experiment 9: Spacing 2.834 m = 4.198*projection length (0.675 m)

Experiment 10: Spacing 2.834 m = 4.928*projection length (0.575 m)

In Figure 26 the placement of the groynes can be seen as built into the channel. The measuring points are also indicated. Measuring point 1was placed before the start of the first bend, measuring point 2 was placed between groynes 2 and 3, and measuring point 3 was downstream of the second bend.
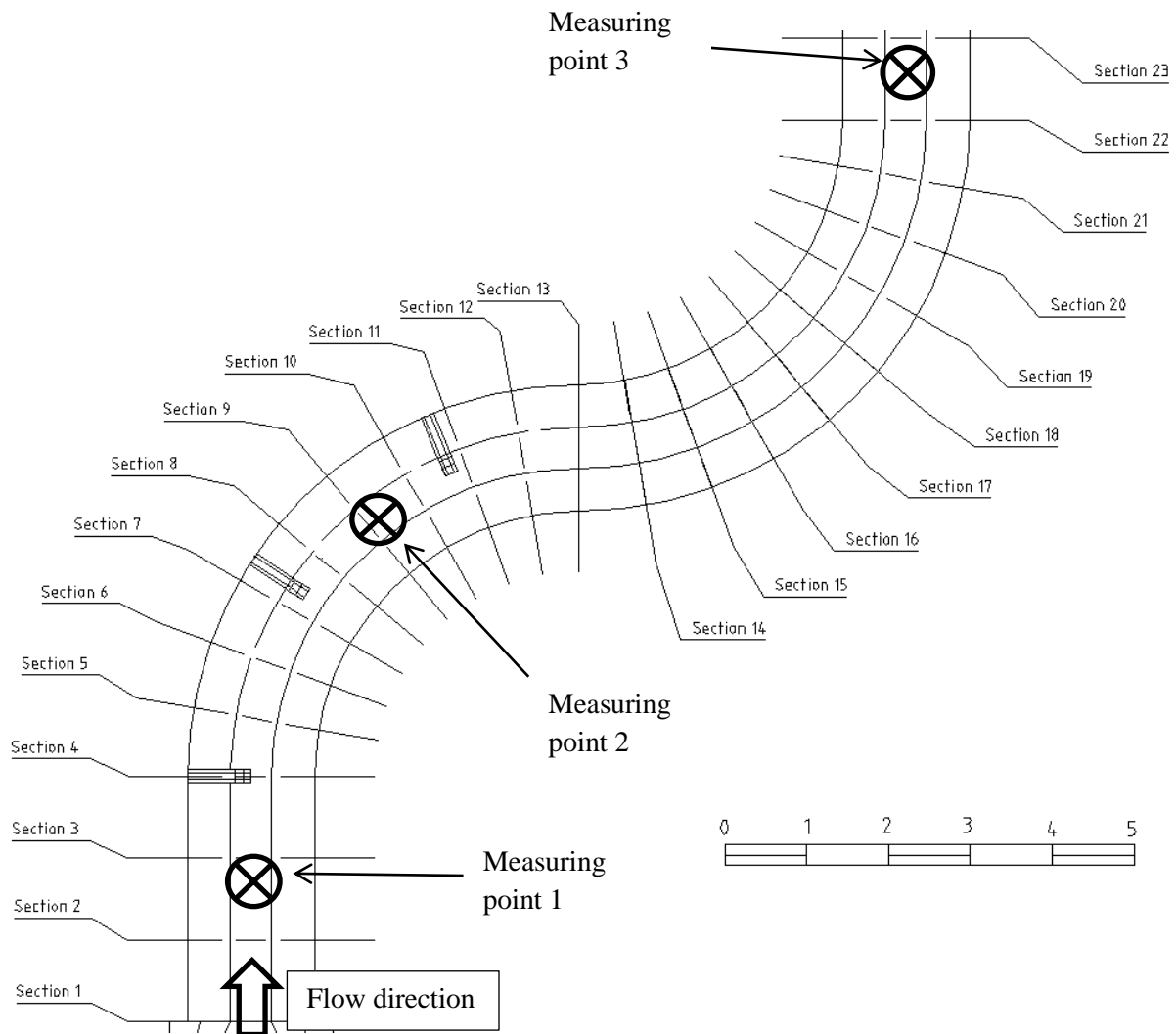
Figure 26: Experiments 8, 9 and 10 groyne placement and measuring points

3.4.3   Experiments 11 to 15 (upstream and downstream groyne orientations)

As mentioned in section 3.2, the orientation of the groynes was a variable to be tested. According to Kuhnle et al. (2002), groynes constructed at an angle of 45º to the flow direction, showed the best potential for providing improved aquatic habitats while minimizing the potential for erosion of the channel bank.

Experiments 11 to 13 were done with groynes inserted into the model at a 45º angle toward the upstream side. Groynes were placed on the first bend only. The optimal spacing (discussed in section 3.5) from tests 2 to 10 was taken as the spacing. The same projection lengths were used (0.775 m, 0.675 m and 0.575 m).

Therefore, the chosen spacing was 2.333 m, which resulted in the following ratios:

Experiment 11: Spacing 2.333 m = 3.011*projection length (0.775 m)

Experiment 12: Spacing 2.333 m = 3.457*projection length (0.675 m)

Experiment 13: Spacing 2.333 m = 4.058*projection length (0.577 m)

In Figure 27 the placement of the groynes can be seen as they were built into the channel. The measuring points are also indicated. Measuring point 1was placed before the start of the first bend, measuring point 2 was placed between groynes 3 and 4, and measuring point 3 was downstream of the second bend.
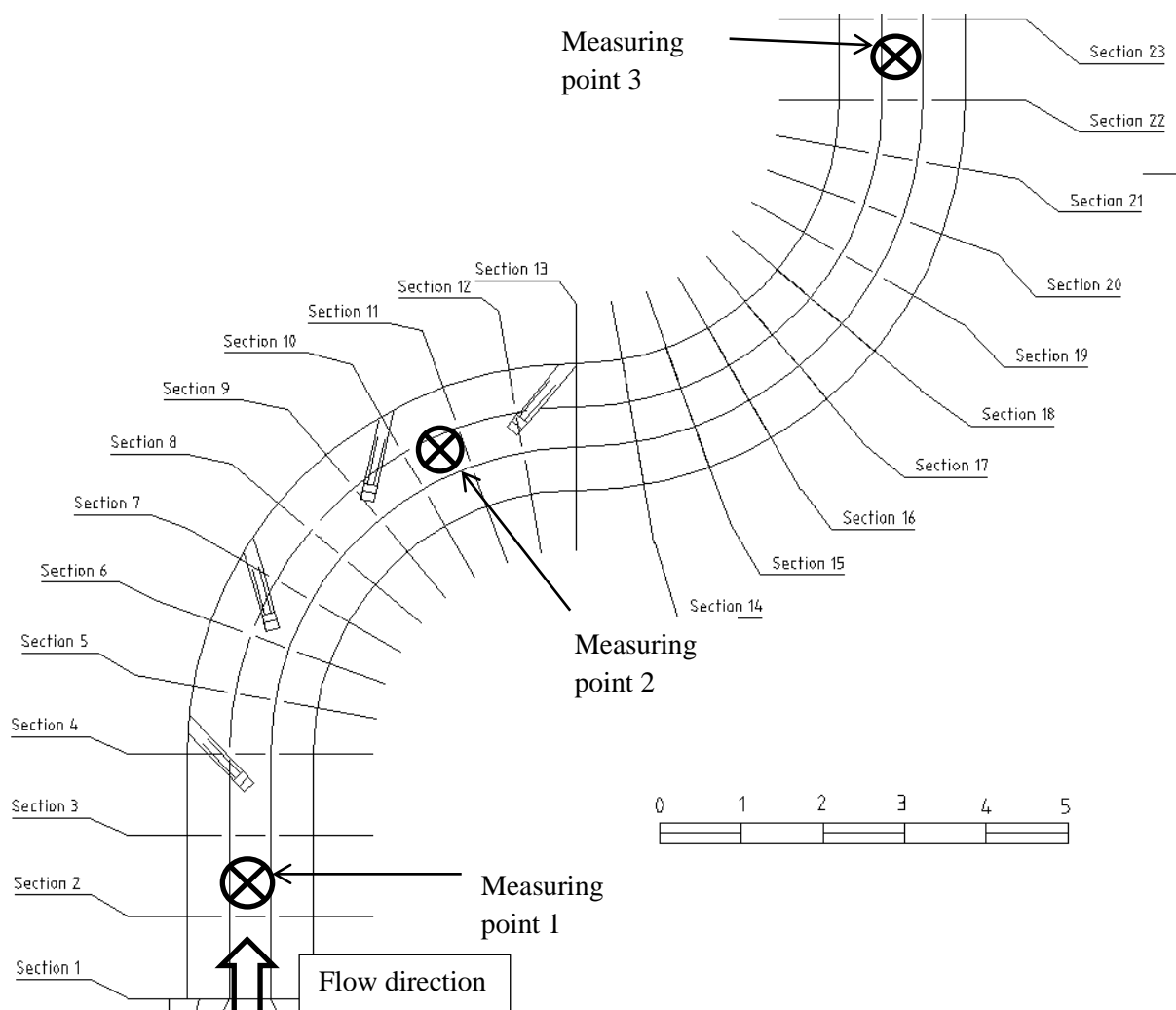
Figure 27: Experiments 11, 12 and 13 groyne placement and measuring points

Experiments 14 and 15 were done with groynes inserted into the channel at a 45° angle toward the downstream side. Groynes were placed on the first bend only. The optimal spacing (discussed in section 3.5) from tests 2 to 10 was taken as the spacing. The projection lengths used were (0.675 m and 0.575 m).

43

Therefore, the chosen spacing was 2.333 m, which resulted in the following ratios:

Test 14: Spacing 2.333m = 3.457*projection length (0.675m)

Test 15: Spacing 2.333m = 4.058*projection length (0.577m)

In Figure 28 the placement of the groynes can be seen as they were built into the channel. The measuring points are also indicated. Measuring point 1was placed before the start of the first bend, measuring point 2 was placed between groynes 3 and 4, and measuring point 3 was downstream of the second bend.
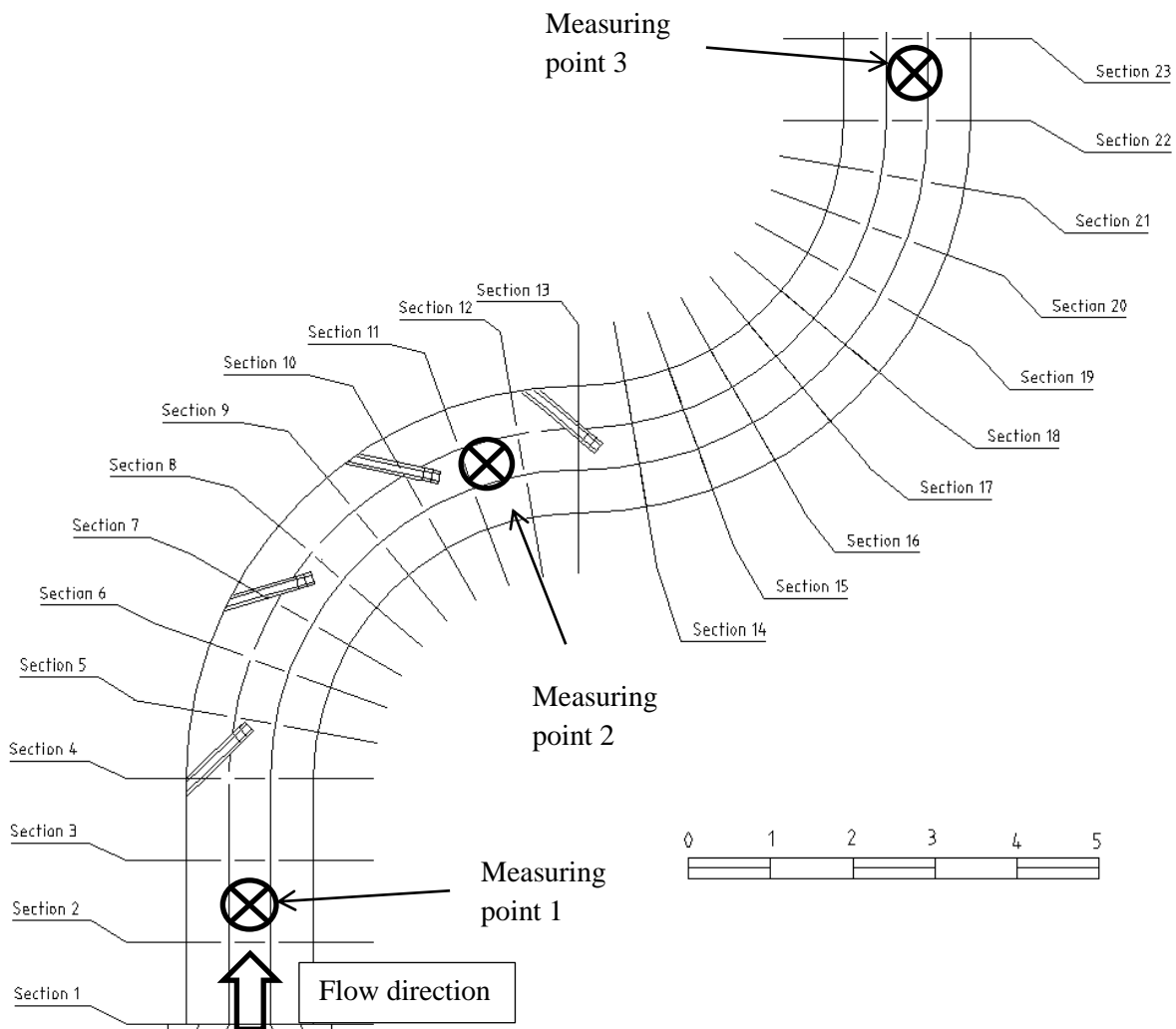
Figure 28: Experiments 14 and 15 groyne placement and measuring points

3.5   Experiment results and analysis

The following section will show the results obtained from experiments 1 through 15 as outlined in section 3.4. A thorough explanation of what was observed will be included, as well as surveys and photos of all experiments. Each experiment is individually analysed,

44

through which the optimization of the design is possible. Table 7 shows a summary of the physical model experiments.

Table 7: Summary of the variables for the physical experiments

Experiment	Duration (s)	Flow (ℓ/s)	Groyne orientation	Projection length L (m)	Spacing S (m)	S/L	Observed water levels (m) Measuring point 1	Measuring point 2	Measuring point 3
1	570	20	n/a	n/a	n/a	n/a	0.582	0.557	0.543
2	341	19	90˚	0.775	1.75	2.3	0.589	0.570	0.543
3	323	21	90˚	0.675	1.75	2.6	0.589	0.570	0.543
4	347	19	90˚	0.575	1.75	3.1	0.589	0.569	0.543
5	309	19	90˚	0.775	2.33	3.0	0.585	0.558	0.543
6	360	18	90˚	0.675	2.33	3.5	0.577	0.557	0.543
7	406	19	90˚	0.575	2.33	4.1	0.575	0.560	0.543
8	281	19	90˚	0.775	2.83	3.7	0.582	0.563	0.543
9	301	18	90˚	0.675	2.83	4.2	0.582	0.564	0.543
10	354	18	90˚	0.575	2.83	4.9	0.580	0.574	0.543
11	282	18	45˚	0.775	2.33	3.0	0.592	0.572	0.543
12	304	19	45˚	0.675	2.33	3.5	0.593	0.568	0.543
13	333	19	45˚	0.575	2.33	4.1	0.590	0.561	0.543
14	300	18	135˚	0.675	2.33	3.5	0.589	0.570	0.543
15	306	19	135˚	0.575	2.33	4.1	0.584	0.576	0.543
Optimal	298	19	90˚	0.675	2.33	3.5	0.580	0.557	0.543

3.5.1   Experiment 1 (20 ℓ/s; 9 min 30 s; no groynes)

Experiment 1 was done with no groynes built into the channel, as can be seen in Figure 29. It was done as a control experiment to which experiments 2 to 15 could be compared in order to investigate the effectiveness of different groyne layout designs.

Flow direction

Figure 29: Channel layout in lab for Experiment 1 (no groynes)

A flow rate of 20.1 ℓ/s was observed for a duration of 9 min 30 s. Sediment movement on the bed of the channel was very limited. The deposition of sediment was observed on the inner side of both bends, while clear scour patterns could be observed on the outer banks, with a maximum scour depth of 120 mm and a maximum deposition of 64 mm (Figure 31).

Figure 30 shows the survey that was done of the sediment change following Experiment 1. The scour on the outside riverbank and the deposition on the inside of the bend can be seen clearly. Figure 31 clearly shows the positions where the most scour was observed during the experiment. These results obtained from Experiment 1 clearly showed that there is a need for scour protection of the outer bend; the main areas of concern on the bend could also be identified. The deposition and scour patterns observed during this experiment indicate the migration of the main channel toward the outer bend, which would result in loss of land.
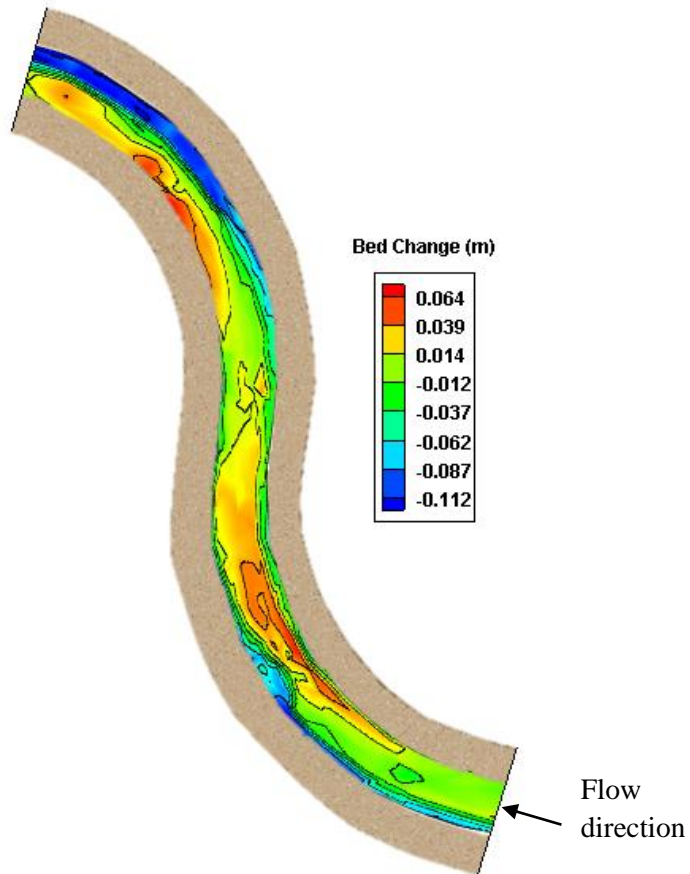
Figure 30: Experiment 1 survey (no groynes)

Figure 31: Observed scour on the upstream bend for Experiment 1 (no groynes)

48

3.5.2   Experiment 2 (19 ℓ/s; 5 min 41 s; 5 groynes; 2.3 x projection length)

Experiment 2 was done with 5 groynes installed on the first bend at a spacing of 1.75 m and a projection length of 0.775 m. The spacing between the groynes was therefore 2.3 times the projection length which can be seen in Figure 32. A flow rate of 19 ℓ/s was observed for a duration of 5 min. 41 s.

Figure 32: Layout of groynes for experiment 2 (5 groynes; 2.3 x projection length)

Flow around the noses of the groynes was observed to be very turbulent. Scour around the noses of the groynes was so accentuated that, after the time had elapsed, the 100 mm of sediment had been scoured to the bed. The scour around the nose of the groynes started at a very high rate, but slowed as the experiment progressed. A clear recirculation eddy current formed between successive groynes where sediment that was taken into suspension at the nose of the groyne, was deposited in between the groynes where the flow velocity was lower. The maximum deposition observed was 80 mm. The projection length however, seemed to be too long, as most of the suspended sediment was deposited towards the middle of the channel, causing shallower flow with high velocities to the inside of the channel.

The outer banks in between the groynes showed extensive scour, as the eddy currents that formed caused the water to recirculate at a high velocity, which caused the erosion of the outer bank. Scour was also observed just upstream of the groynes, against the bank. Failure of the inner bank across from the groyne positions could be seen where the flow channel had become narrowed.

49

Figure 33 shows the survey that was done of the sediment bed change after Experiment 2. The scour holes around the nose of the groynes can be seen clearly, as well as some sediment deposition between the groynes. Figure 34 shows the scour patterns around groyne 2.

Figure 33: Experiment 2 survey (5 groynes; 2.3 x projection length)
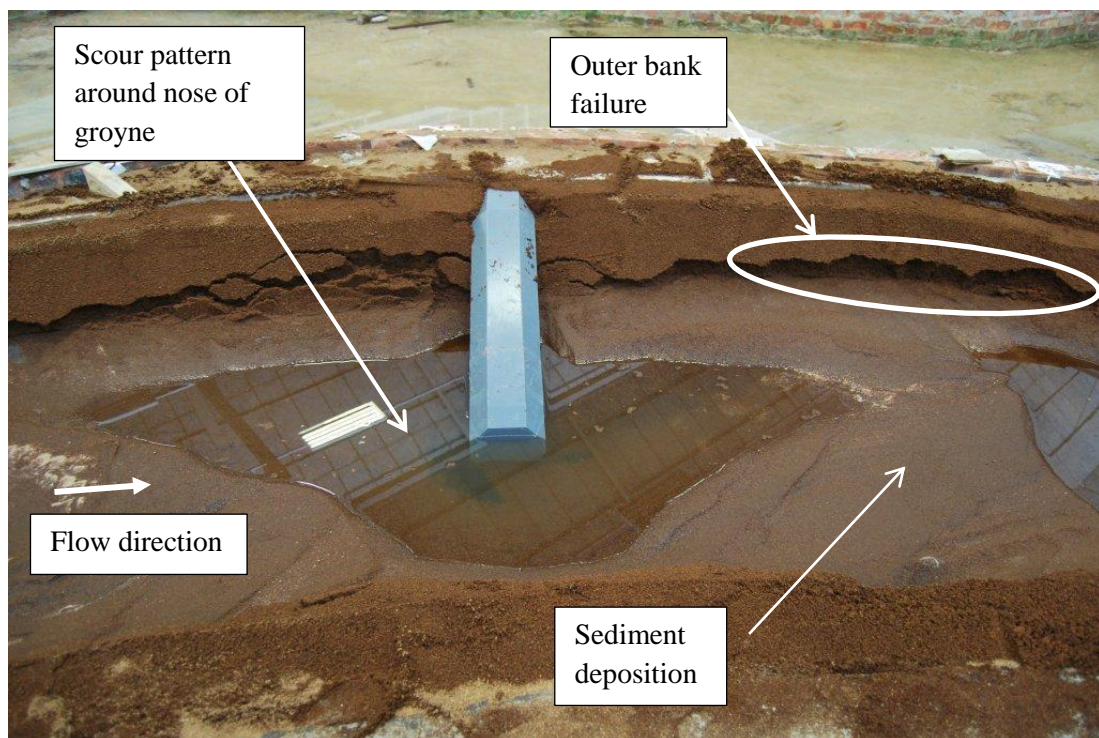
Figure 34: Scour patterns around groyne for Experiment 2 (5 groynes; 2.3 x projection length)

50

3.5.3   Experiment 3 (21 ℓ/s; 5 min 23 s; 5 groynes; 2.6 x projection length)

Experiment 3 was done with 5 groynes installed on the first bend at a spacing of 1.75 m and a projection length of 0.675 m. The spacing between the groynes was therefore 2.6 times the projection length which can be seen in Figure 35. A flow rate of 20.5 ℓ/s was observed for a duration of 5 min 23 s.

Figure 35: Layout of groynes for Experiment 3 (5 groynes; 2.6 x projection length)

Flow around the noses of the groynes was very turbulent. A maximum scour of 100 mm was observed around the noses of the groynes, the area of scour was however smaller than that of Experiment 2. The scour around the noses of the groynes started at a high rate which decreased as the experiment progressed. The recirculation eddy currents formed between successive groynes. The scoured sediment that went into suspension was deposited in between the groynes where the flow velocities were lower as a result of the eddy currents. A maximum deposition depth of 80 mm was observed.

The outer banks of the channel eroded away, resulting in deposition towards the centre of the channel, instead of on the outer bank. This caused higher flow velocities and lower flow depths, which contributes to channel instability. Sediment was scoured on the upstream side of the groynes, where a secondary eddy was formed. There was, however, also failure of the inner bank across from the groyne positions.

In Figure 36, which shows the survey of the sediment positions after Experiment 3, the scour holes around the nose of the groynes can once again be seen clearly. Some deposition can also be seen. Figure 37 shows the scour patterns observed at groyne 4.

Figure 36: Experiment 3 survey (5 groynes; 2.6 x projection length)

Figure 37: Scour patterns around groyne 4 for Experiment 3 (5 groynes; 2.6 x projection length)

3.5.4   Experiment 4 (19 ℓ/s; 5 min 47 s; 5 groynes; 3.1 x projection length)

Experiment 4 was done with 5 groynes installed at the first bend at a spacing of 1.75 m and a projection length each of 0.575 m (see Figure 38). The spacing between the groynes was therefore 3.1 times the projection length which can be seen in Figure 38. A flow rate of 18.6 ℓ/s was observed for a duration of 5 min 47 s.

Flow direction

Figure 38: Layout of groynes for Experiment 4 (5 groynes; 3.1 x projection length)

Scour around the noses and on the upstream side of the groynes were observed, a maximum scour depth of 90 mm was observed. The scoured area around the nose of the groynes is smaller than that observed during Experiments 2 and 3. The scour rate observed around the nose of the groynes slowed during the experiment. The outer banks were not protected from scour. Local scour was also seen just upstream of the groynes. The projection length of the shortest length of the groynes seemed to be insufficient.

Almost no eddy currents were formed between the groynes, as a result of the shorter projection lengths. Because of the lack of eddy currents, the flow velocity near the outer banks was not sufficiently slow, resulting in minimal scour protection between the groynes. As very little recirculation occurred, very limited sediment deposition could occur on the outer banks, as sediment could not settle, due to the high velocities. A maximum deposition depth of 63 mm was observed on the outer bend. Small eddies formed directly upstream of each of the groynes.

Figure 39 and Figure 40 show the results of Experiment 4. The scour upstream of the groynes and around the noses of the groynes can be seen clearly.
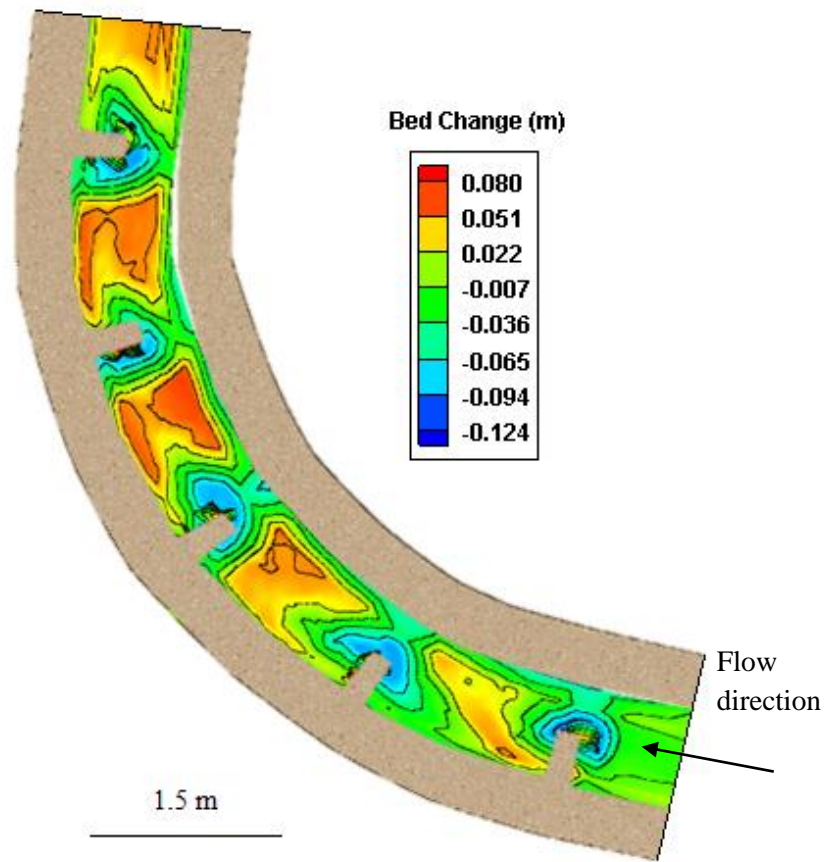

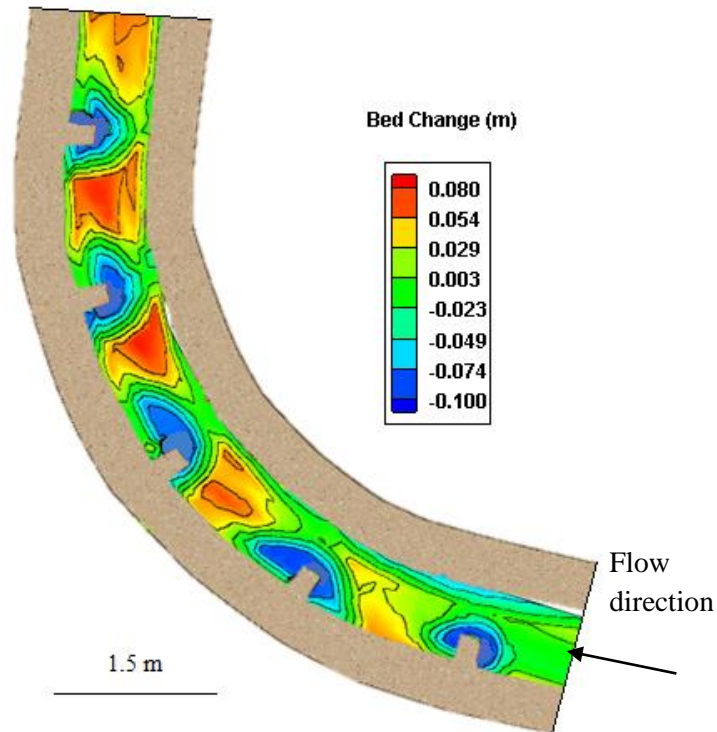**Figure 39: Experiment 4 survey (5 groynes; 3.1 x projection length)**
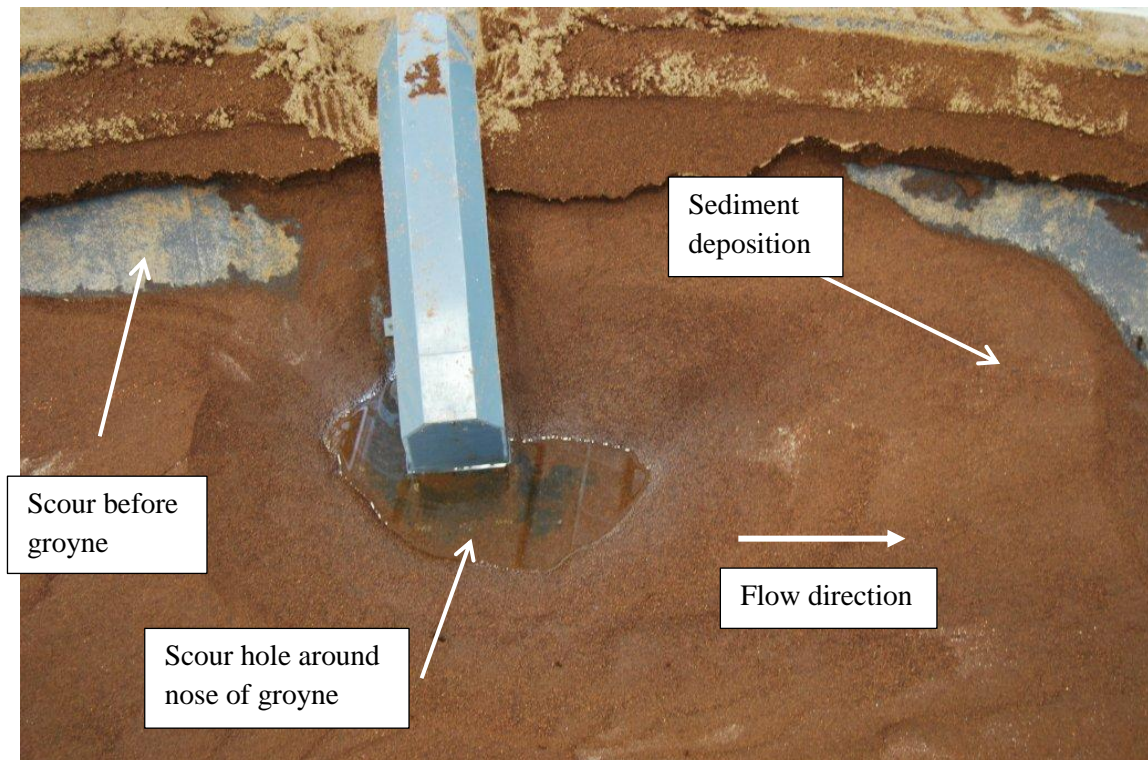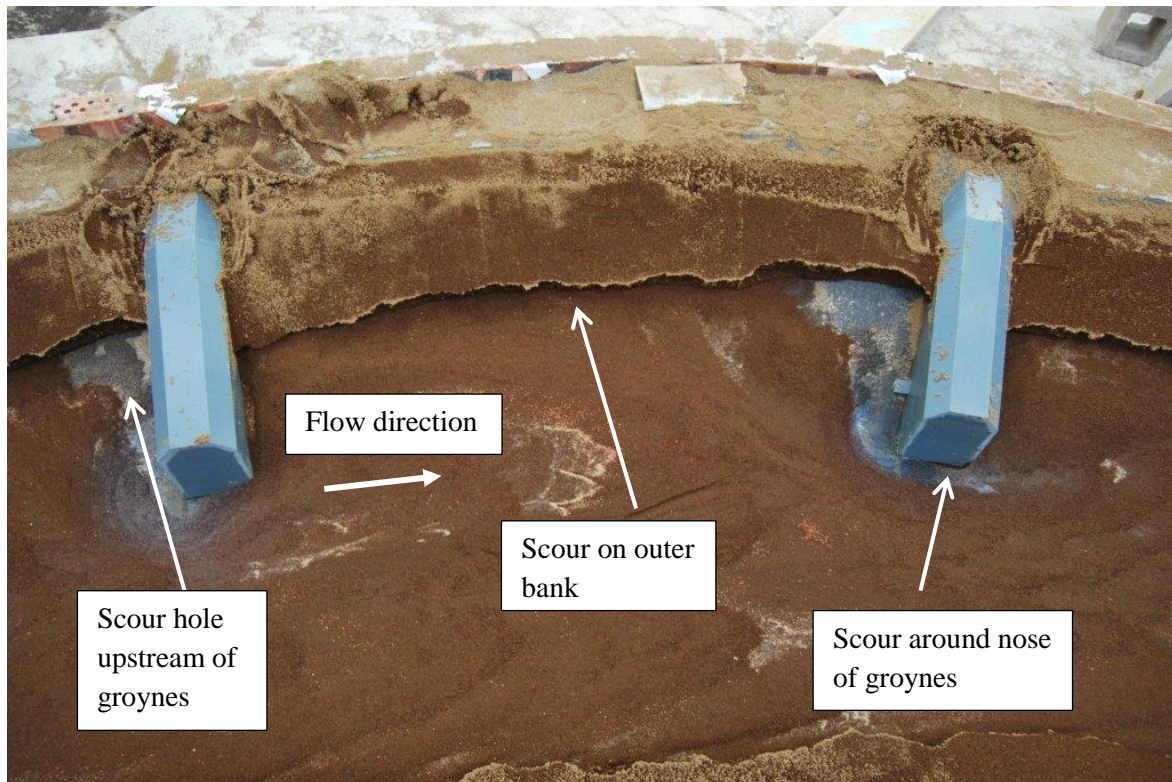

Figure 40: Scour patterns around groynes for Experiment 4 (5 groynes; 3.1 x projection length)

3.5.5   Experiment 5 (19 ℓ/s; 5 min 9 s; 4 groynes; 3.0 x projection length)

Experiment 5 was done with 4 groynes installed at the first bend at a spacing of 2.33 m and a projection length of 0.775 m. The spacing between the groynes was therefore 3.0 times the projection length which can be seen in Figure 41. A flow rate of 18.8 ℓ/s was observed for a duration of 5 min 9 s.

Flow direction

Figure 41: Layout of groynes for experiment 5 (4 groynes; 3.0 x projection length)

Local scour of 100 mm around the noses of the groynes is observed. The rate of scour around the nose of the groynes decreased as the experiment progressed and equilibrium was approached. The outer banks of the channel were better protected from scour, although some scour was still observed. Eddy currents were formed between consecutive groynes. The eddy currents that formed did not inflict as much damage as with the closer spacing. Some scour on the outer banks was, however, still visible. Sediment deposition occurred between consecutive groynes as a result of lower flow velocities, promoting sediment settling, with a maximum observed deposition depth of 70 mm on the outer bank.

The inner banks, across from the positions of the groynes, failed as a result of the higher flow velocities that were caused by the blocking of flow by the groynes at the outer bank. Sediment deposition once again was toward the middle of the channel as opposed to the outer banks.

Scour directly upstream of the groynes was much less accentuated with the wider spacing. The results of Experiment 5 can be seen in Figures 42 and 43.

Figure 42: Experiment 5 survey (4 groynes; 3.0 x projection length)
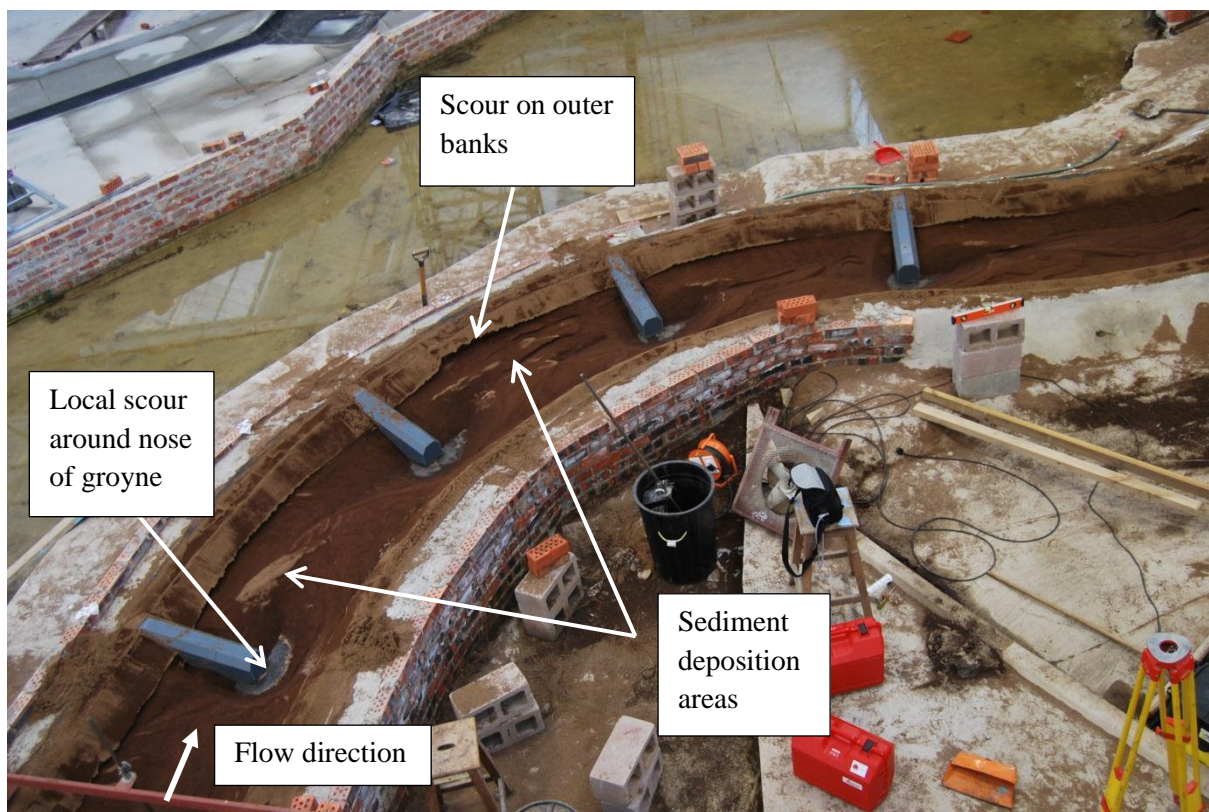
Figure 43: Scour pattern for Experiment 5 (4 groynes; 3.0 x projection length)

56

3.5.6   Experiment 6 (18 ℓ/s; 6 min 0 s; 4 groynes; 3.5 x projection length)

Experiment 6 was done with 4 groynes installed on the first bend at a spacing of 2.33 m and a projection length of 0.675 m. The spacing between the groynes was therefore 3.46 times the projection length which can be seen in Figure 44. A flow rate of 18.2 ℓ/s was observed for a duration of 6 min 0 s.

Flow direction

Figure 44: Layout of groynes for Experiment 6 (4 groynes; 3.5 x projection length)

Local scour around the noses of the groynes was quite extensive with the scour rate decreasing as equilibrium was approached. The scoured area was however much smaller than it had been for previous experiments. A maximum scour depth of 100 mm was observed. Clear sediment deposition could be seen downstream of the groynes, where eddy currents were formed and flow velocities were low enough. The sediment that was scoured from the noses of the groynes and consequently went into suspension was deposited in between the groynes. A maximum sediment deposition depth of 60 mm was observed on the outer bend.

Clear protection from scour was provided for the outside bank. From these experiments it was observed that flow velocity at the outer banks was very low, as a result of the forming of eddy currents. Compared to the results obtained from Experiment 1, a definite improvement in the outer bank could be seen, as well as some sediment deposition closer to the outer bank.

Some scour and bank failure was observed on the inner bank across from the groyne positions. This is, however, to be expected, as the flow velocity increases near the inner bank

57

because of the constriction of flow by the groynes. These results can be seen in Figure 45 and 46.
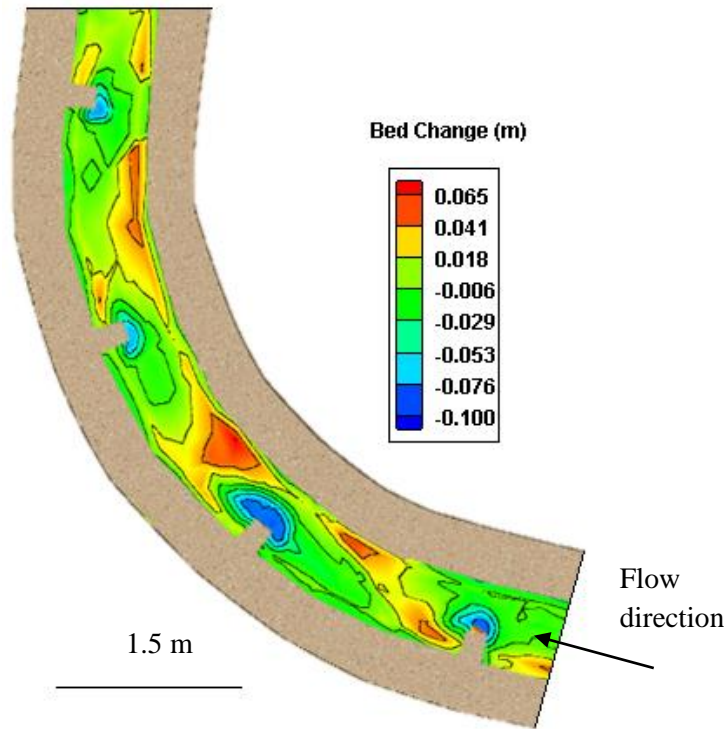
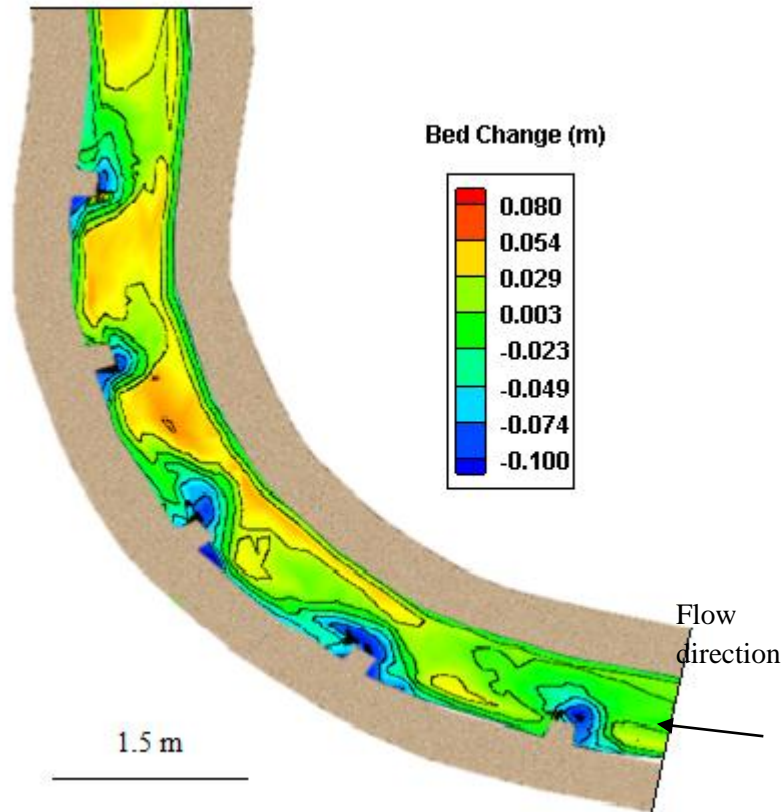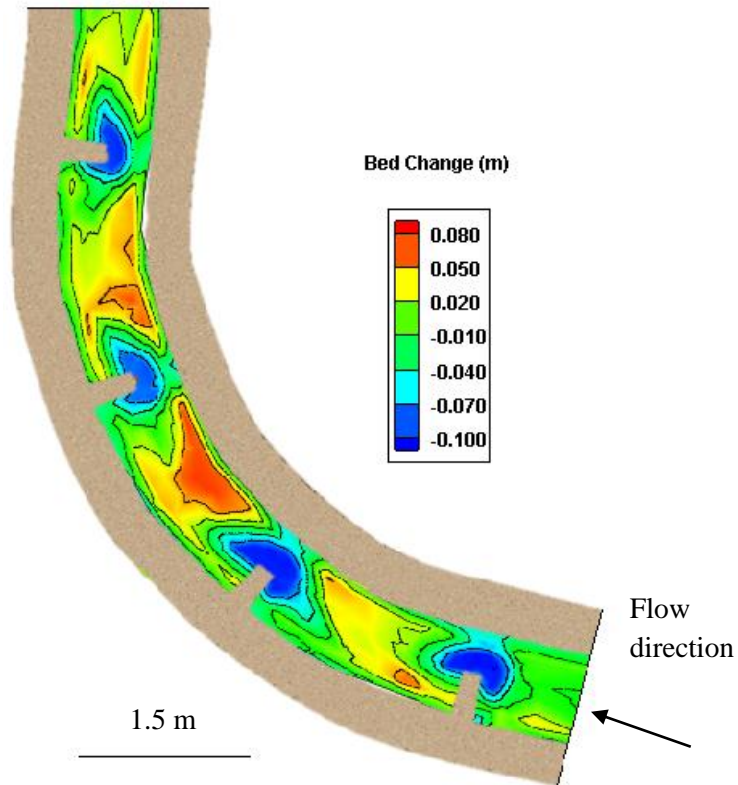**Figure 45: Experiment 6 survey (4 groynes; 3.5 x projection length)**
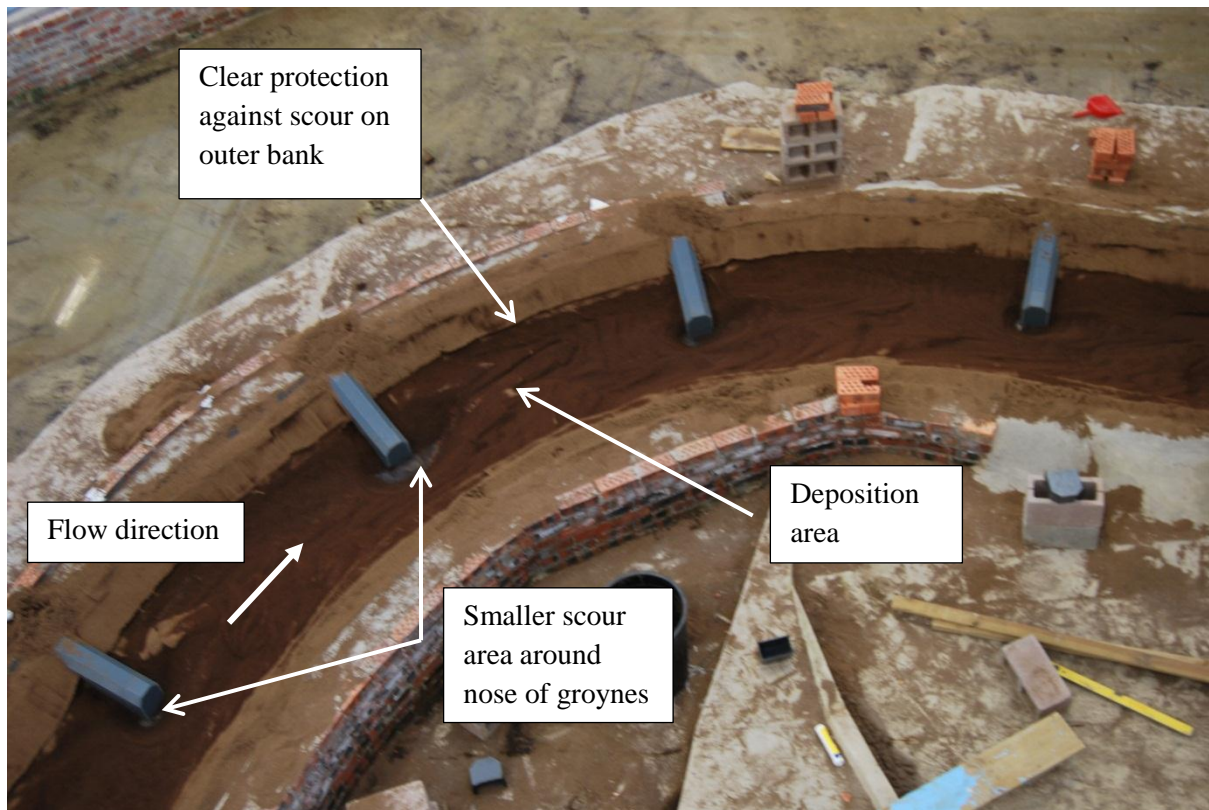
Figure 46: Scour patterns for Experiment 6 (4 groynes; 3.5 x projection length)

58

3.5.7   Experiment 7 (19 ℓ/s; 6 min; 46 s; 4 groynes; 4.1 x projection length)

Experiment 7 was done with 4 groynes installed on the first bend at a spacing of 2.33 m and a projection length of 0.575 m. The spacing between the groynes was therefore 4.1 times the projection length which can be seen in Figure 47. A flow rate of 19.44 ℓ/s was observed for a duration of 6 min 46 s.

Flow direction
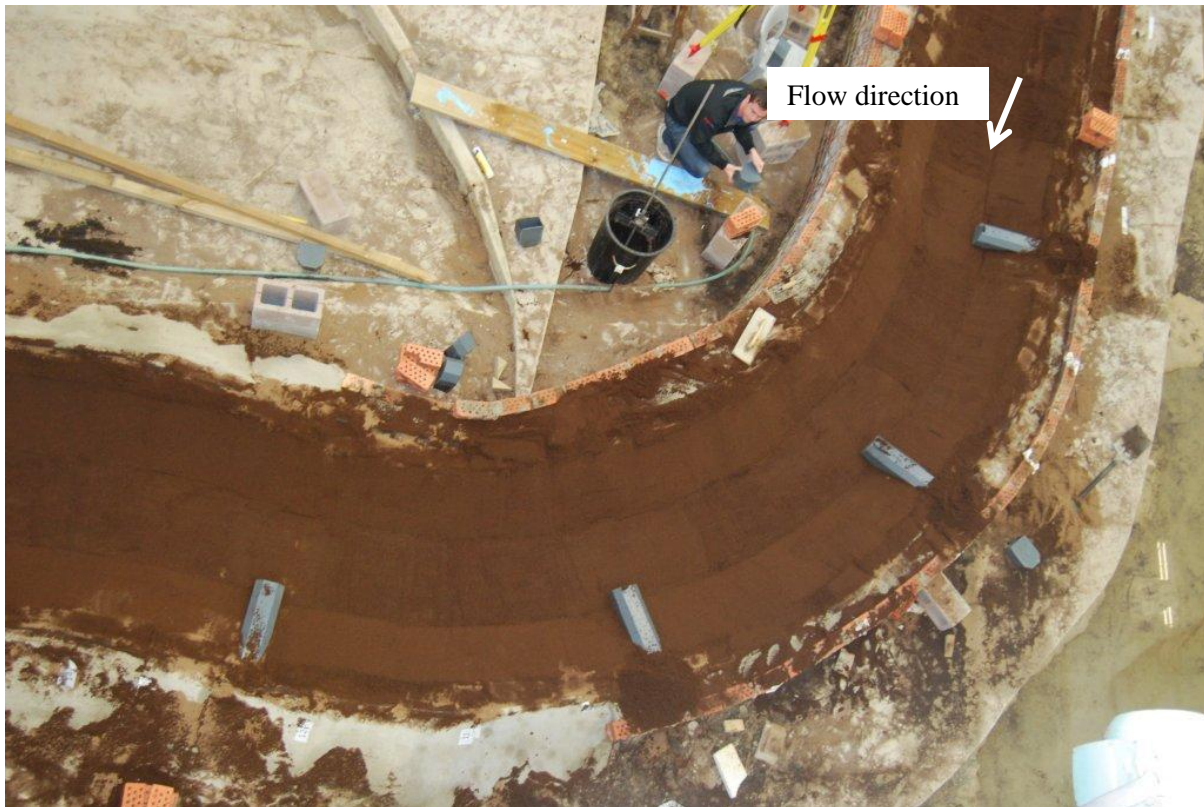
Figure 47: Layout of groynes for Experiment 7 (4 groynes; 4.1 x projection length)

Some scour was observed around the noses of the groynes. The area that was scoured, was small, relative to previous tests, the maximum depth of scour observed was 100 mm. A high rate of scour was initially observed, which slowed dramatically as the experiment progressed and equilibrium was approached. Very little sediment deposition occurred downstream of the groynes, as a result of the small amount of sediment that was taken into suspension. A maximum sediment deposition depth of 50 mm was observed on the outer bend.

Protection against the scour of the outer bank was clearly visible. Eddy currents could be seen between consecutive groynes. These eddy currents were, however, not as accentuated as they had been with longer projection lengths of the groynes, resulting in less scour protection. Some scour and bank failure also occurred on the inner bank across from the groyne positions, where the flow rate was increased as a result of the constriction of flow and subsequent higher velocities.

The results of Experiment 7 can be seen in Figures 48 and 49.
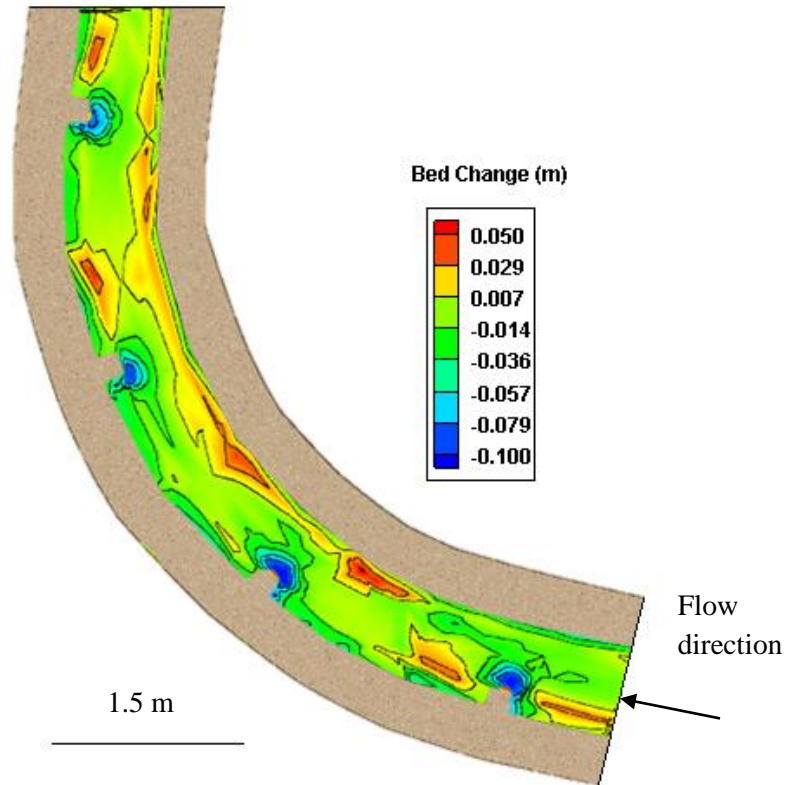
**Figure 48: Experiment 7 survey (4 groynes; 4.1 x projection length)**

Figure 49: Scour pattern around groynes for Experiment 7 (4 groynes; 4.1 x projection length)

60

3.5.8   Experiment 8 (19 ℓ/s; 4 min 41 s; 3 groynes; 3.7 x projection length)

Experiment 8 was done with 3 groynes installed on the first bend at a spacing of 2.833 m and a projection length of 0.775 m. The spacing between the groynes was therefore 3.66 times the projection length which can be seen in Figure 50. A flow rate of 18.8 ℓ/s was observed for a duration of 4 min 41 s.
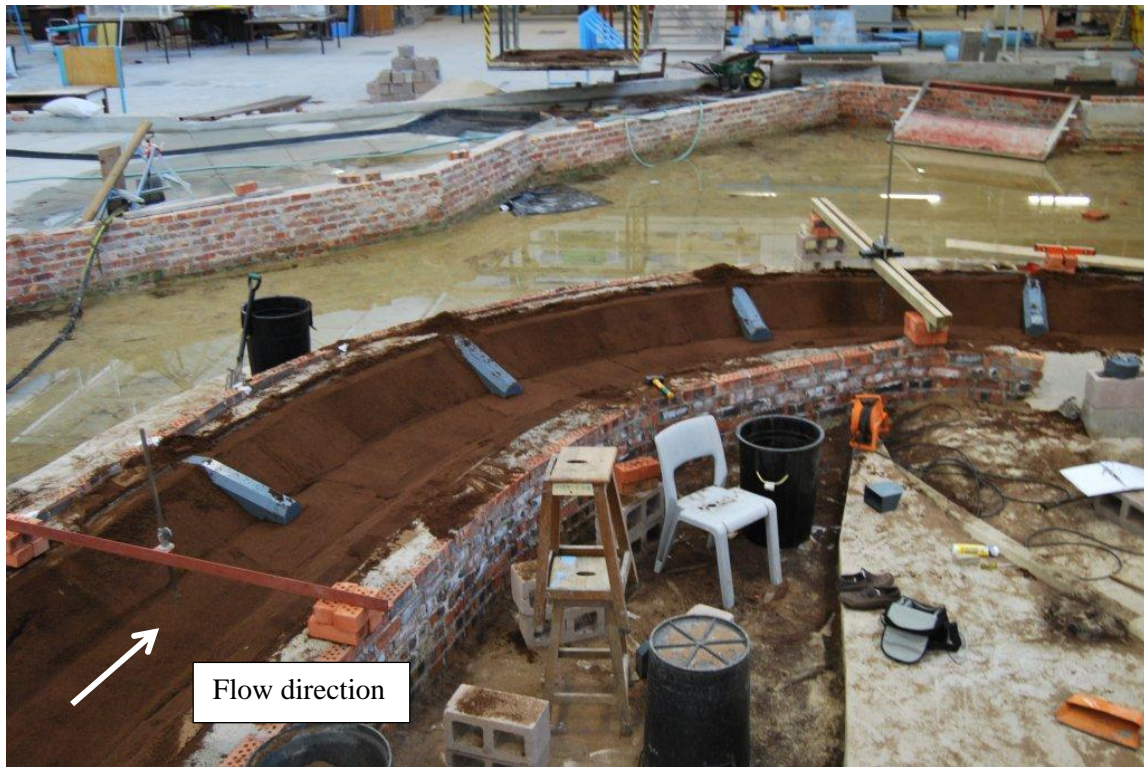

Flow direction

Figure 50: Layout of groynes for Experiment 8 (3 groynes; 3.7 x projection length)

Local scour around the noses of the groynes was extensive, with a large area having scoured through the 100 mm sediment to the bed of the channel. The rate of scour decreased as the experiment progressed and equilibrium was approached. Definite eddy currents were formed, which resulted in the deposition of sediment to the downstream side of the groynes. A maximum sediment deposition depth of 64 mm was observed on the outer bend. The longer projection length did, however, again cause the outer bank to be scoured away, as the velocity by which the recirculation of flow occurred was high when it reached the outer bank and the length between consecutive groynes was great.

Some scour and bank failure was observed on the inside bend across from the groyne positions as a result of the constriction of flow by the groynes and the resulting higher flow velocities near the inner bend. The length across which sediment is deposited on the outer bend is longer, as a result of the wider spacing. This does, however, result in the eddy

61

currents not covering the entire region between the groynes which decreases the protection that is offered to the outer bank. These results can be seen in Figures 51 and 52.

Figure 51: Experiment 8 survey (3 groynes; 3.7 x projection length)
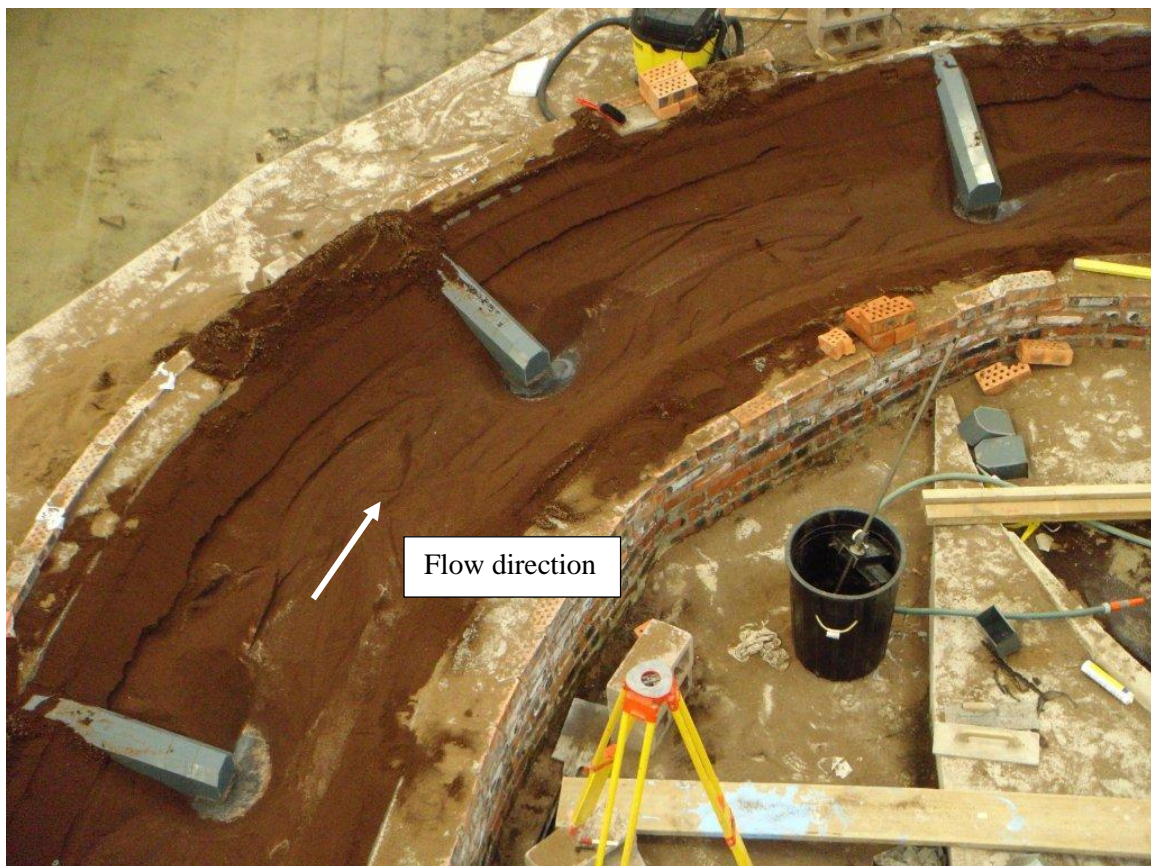
Figure 52: Scour patterns around groynes for Experiment 8 (3 groynes; 3.7 x projection length)

3.5.9 Experiment 9 (18 ℓ/s; 5 min 1 s; 3 groynes; 4.2 x projection length)

Experiment 9 was done with 3 groynes installed on the first bend at a spacing of 2.833 m and a projection length of 0.675 m. The spacing between the groynes was therefore 4.20 times the projection length which can be seen in Figure 53. A flow rate of 18 ℓ/s was observed for a duration of 5 min 1 s.


Flow direction

Figure 53: Layout of groynes for Experiment 9 (3 groynes; 4.2 x projection length)

Scour around the noses of the groynes was observed, the rate of scour decreased as the experiment progressed and equilibrium was approached. A maximum scour depth of 100 mm was observed. Eddy currents formed, but did not cover the entire area between the groynes, indicating that the spacing between the groynes is too great. Therefore, the protection of the outer bank is limited and the flow profile forms an S–shape as the water flows in and out between the groynes (see Figure 55).

A maximum sediment deposition depth of 59 mm was observed on the outer bank. Sediment that was scoured from around the nose of the groynes and went into suspension, was deposited downstream of the groynes, where the flow velocities were smaller. Some scour was also observed on the inner bank across from the groyne positions, where higher velocities were encountered. These results can be seen in Figure 55 and 55.
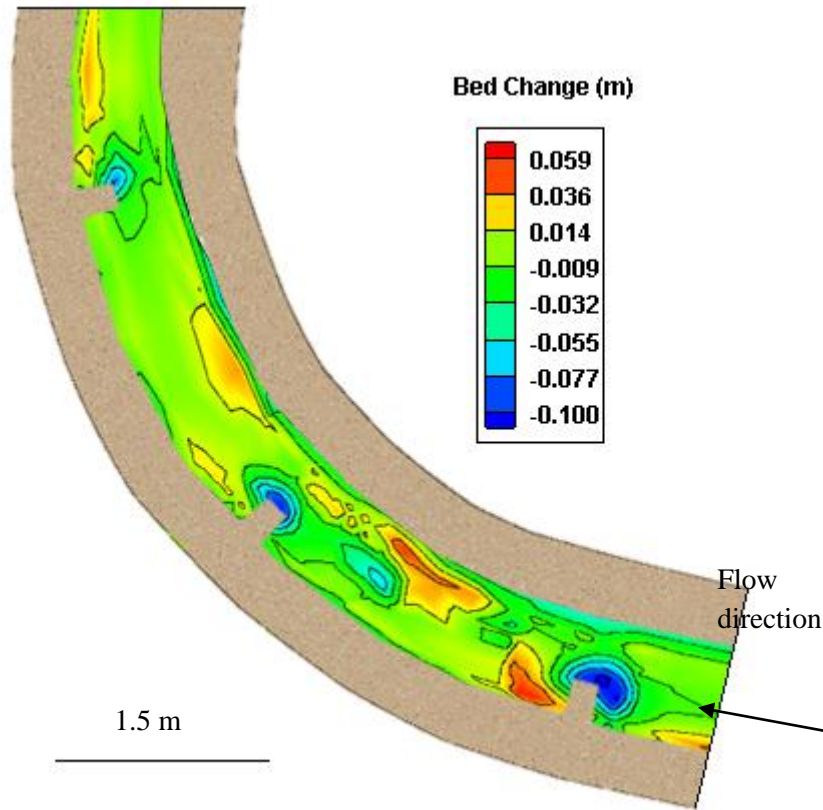
Figure 54: Experiment 9 survey (3 groynes; 4.2 x projection length)
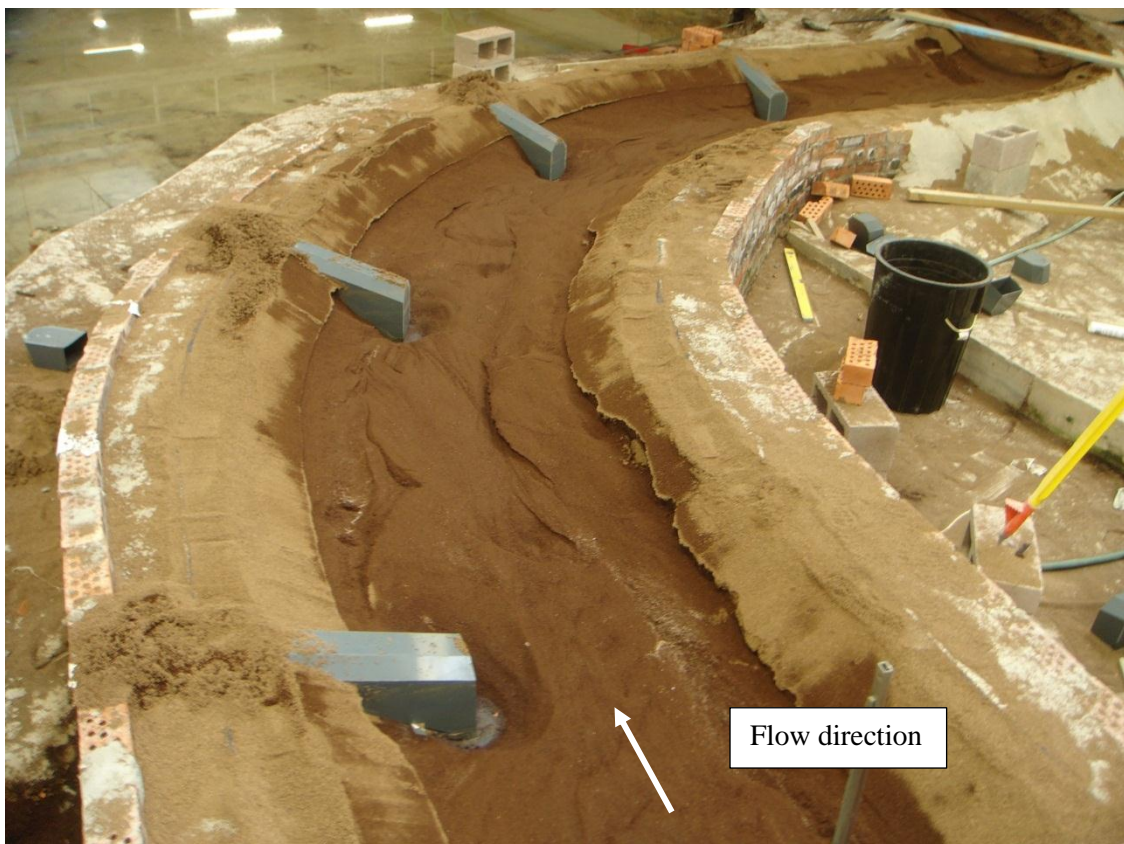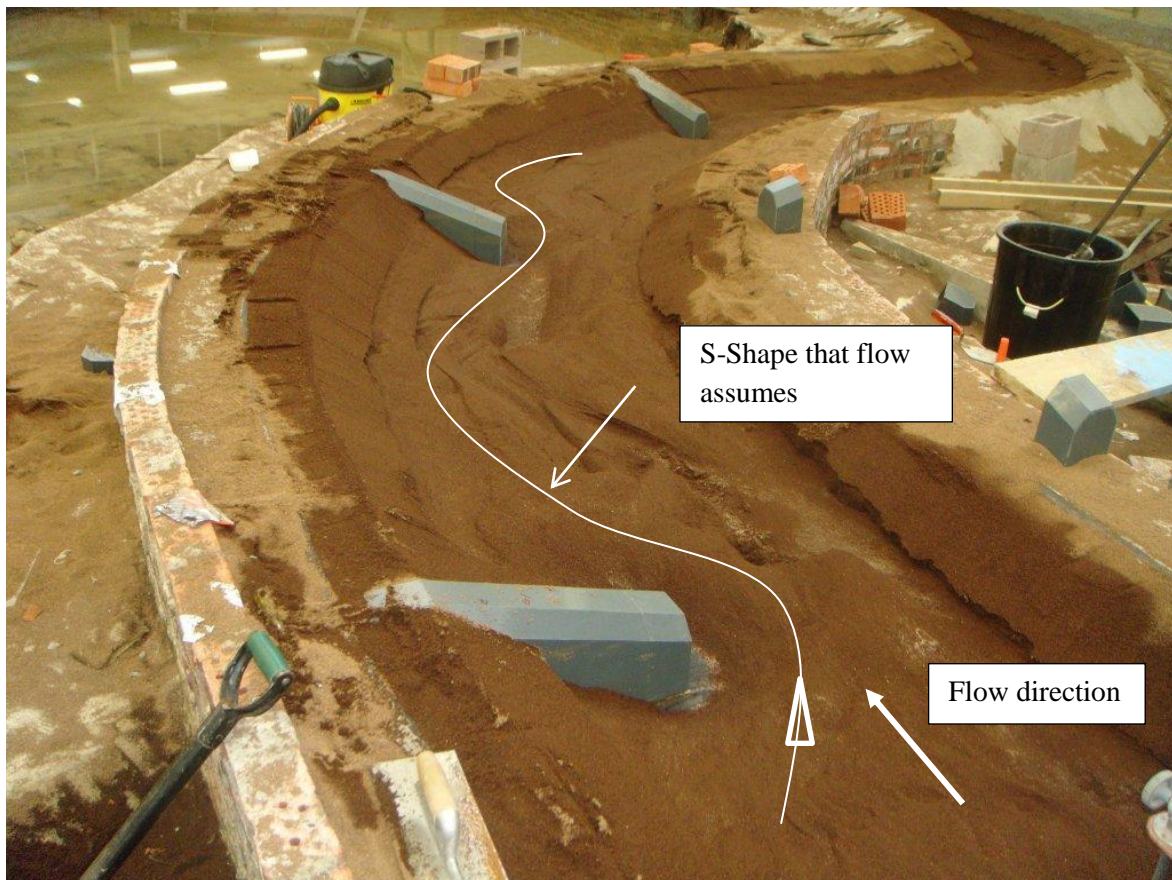

Figure 55: Scour pattern around groynes for Experiment 9 (3 groynes; 4.2 x projection length)

3.5.10   Experiment 10 (18 ℓ/s; 5 min 54 s; 3 groynes; 4.9 x projection length)

Experiment 10 was done with 3 groynes installed on the first bend at a spacing of 2.833 m and a projection length of 0.575 m. The spacing between the groynes was therefore 4.92 times the projection length which can be seen in Figure 56. A flow rate of 17.8 ℓ/s was observed for a duration of 5 min 54 s.

Figure 56: Layout of groynes for Experiment 10 (3 groynes; 4.9 x projection length)

A maximum scour depth of 100 mm around the noses of the groynes was observed. The rate of scour around the noses of the groynes also decreased as equilibrium was approached during the experiment.   Some scour was observed directly upstream of the groynes. Scour protection was created for the outer bank, but the flow profile that was observed indicated that with bigger flow, the scour protection would be negated. The eddy currents that formed between the groynes were, however, very small as a result of the shorter projection lengths of the groynes. The spacing between the groynes was therefore too great and the projection length of the groynes too short.

Because of the small amount of scour around the noses of the groynes and the lack of eddy currents, very small areas of deposition were observed. A maximum sediment deposition depth of 45 mm was observed. These results can be seen in Figure 58 and 58.
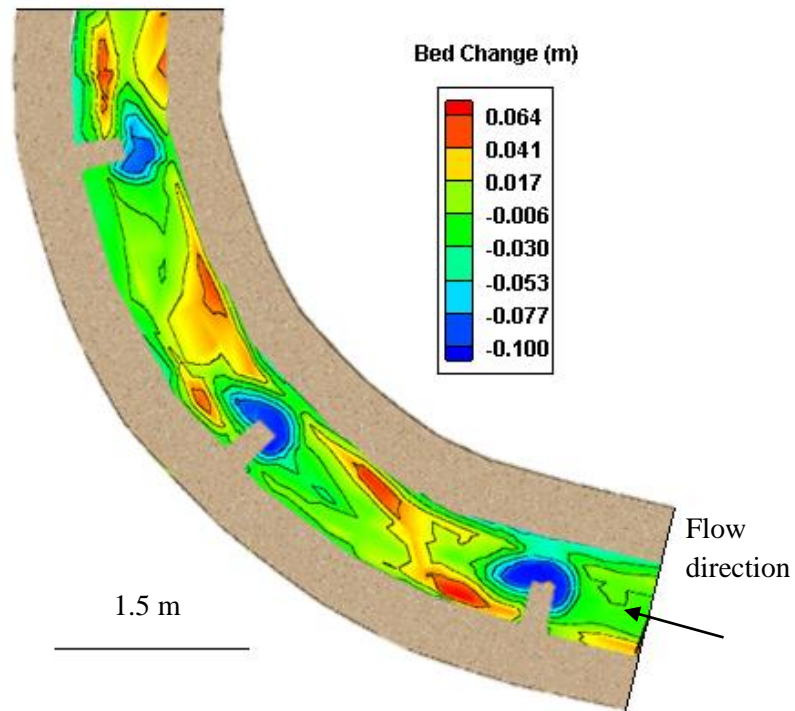
**Figure 57: Experiment 10 survey (3 groynes; 4.9 x projection length)**

Figure 58: Scour patterns around groynes for Experiment 10 (3 groynes; 4.9x projection length)

3.5.11   Experiment 11 (18 ℓ/s; 4 min 42s; upstream orientation)

Experiments 11, 12 and 13 were done with groynes installed at an angle of 45˚ with regard to the flow direction. The spacing between the groynes was taken as the optimal spacing from experiments 2 to 10, which was 2.33 m (see Figure 27). A spacing of 2.33m created the most riverbank protection for the given projection lengths, with eddy currents covering the entire groyne fields in between consecutive groynes. Figure 59 shows the orientation of the groynes with respect to the oncoming flow.

Figure 59: Orientation of groynes

Experiment 11 was done with 4 groynes installed on the first bend at a spacing of 2.33 m and a projection length of 0.775m. The spacing between the groynes was therefore 3.01 times the projection length which can be seen in Figure 60. A flow rate of 18.16 ℓ/s was observed for a duration of 4 min 42 s.
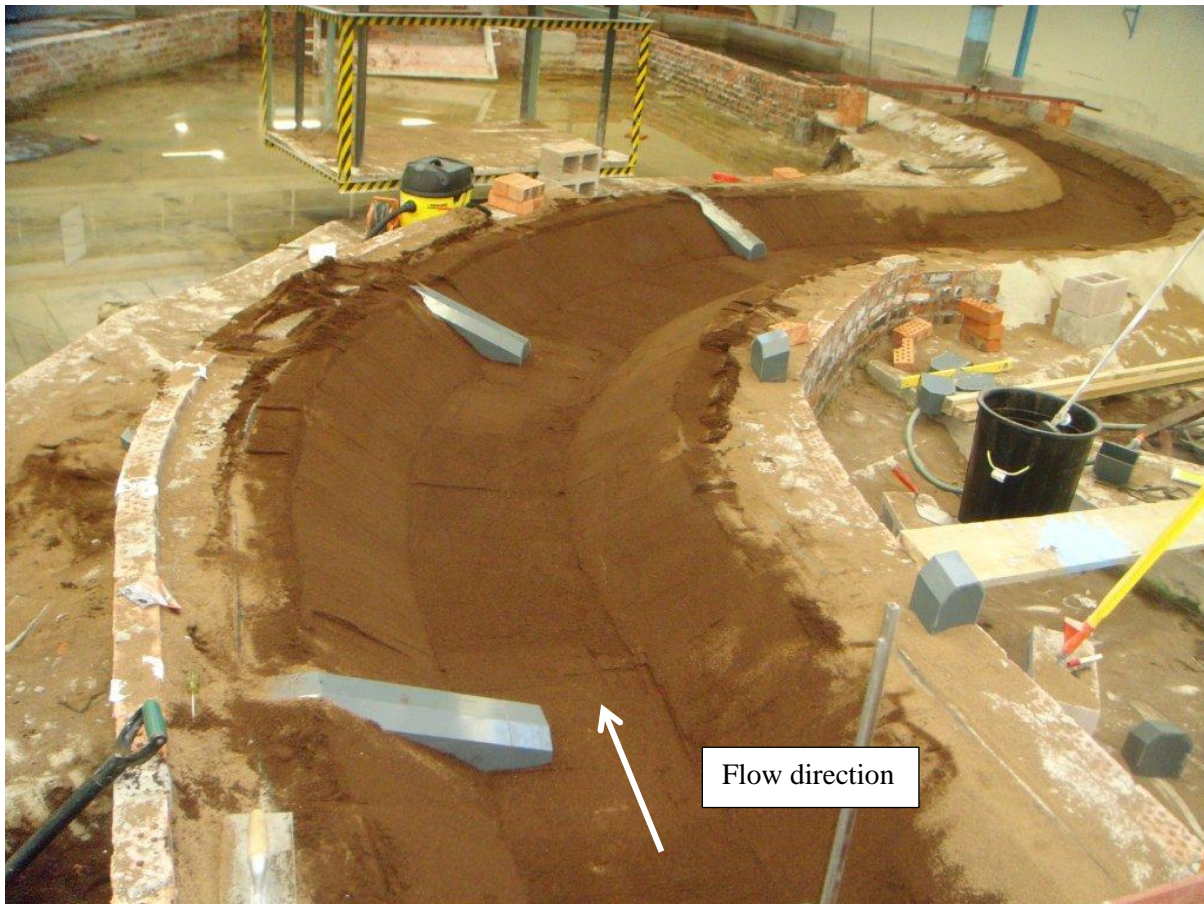
Figure 60: Layout of groynes for Experiment 11 (4 groynes; 3.0 x projection length)

Local scour around the noses of the groynes was observed to be more extensive than for cases with perpendicular groyne orientation. The scour rate decreased as equilibrium was approached during the run of the experiment. A maximum scour depth of 100 mm was observed. A lot of sediment was taken into suspension and deposited just downstream of the groynes, where the formation of eddy currents slowed the flow velocities. The water velocity with which the eddy currents hit the outer bank caused some scour. Bank failure could be seen on the inner bend at positions just downstream of the groyne placements as a result of higher velocities created by die constriction of flow by the groynes. A large portion of the sediment did not deposit in the groyne field, but more toward the main channel as a result of secondary currents forming around the bend and close to noses of the groynes. This caused shallow flow with higher velocities to the inside of the groyne fields, which is detrimental to channel stability. A maximum sediment deposition depth of 90 mm was observed.

Still standing pools formed just upstream of the groyne positions, which almost eradicated all scour prior to the groynes. The results from Experiment 11 shows more deposition, but also much more scour around the noses of the groynes, as well as on the outer bank, when compared to experiments where groynes with perpendicular orientation were used. The above mentioned results can be seen in Figures 61 and 62.

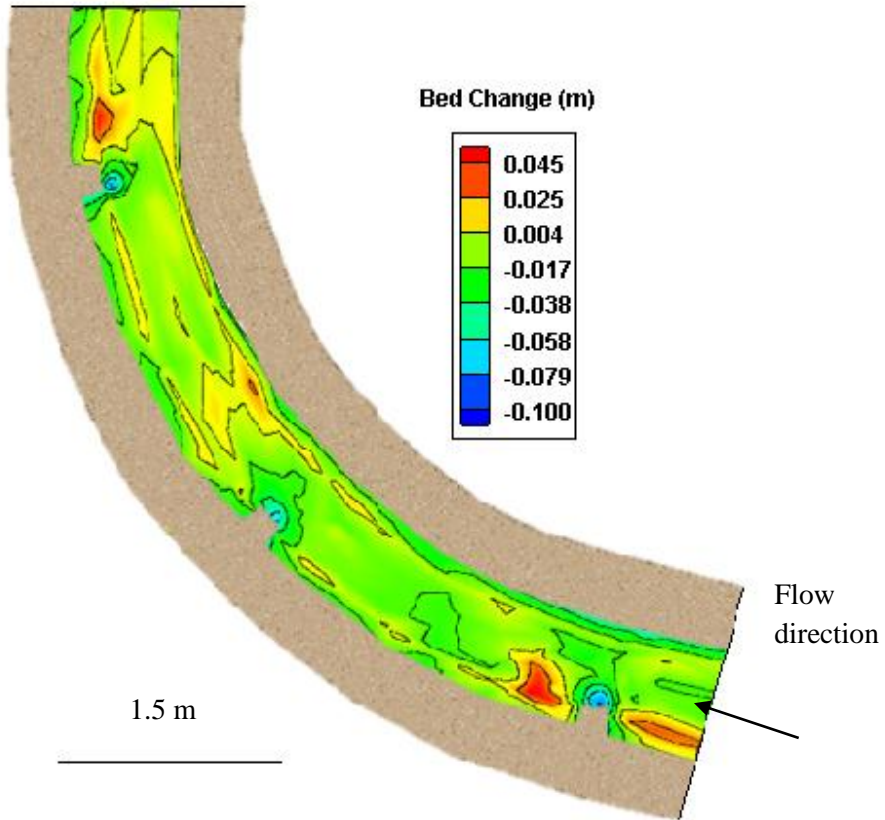**Figure 61: Experiment 11 survey (4 groynes; 3.0 x projection length)**

Figure 62: Scour patterns around groynes for Experiment 11 (4 groynes; 3.0x projection length)

3.5.12   Experiment 12 (19 ℓ/s; 5 min 04 s; upstream orientation)

Experiment 12 was done with 4 groynes installed on the first bend at a spacing of 2.33 m and a projection length of 0.675 m. The spacing between the groynes was therefore 3.5 times the projection length which can be seen in Figure 63. A flow rate of 18.8 ℓ/s was observed for a duration of 5 min 04 s.

Flow direction

Figure 63: layout of groynes for Experiment 12 (4 groynes; 3.5 x projection length)

Local scour around the noses of the groynes was again very evident. The rate at which scour occurred around the noses of the groynes decreased as equilibrium was approached. A maximum scour depth of 100 mm was observed. The velocity at which recirculation occurred was higher than with groynes that had a perpendicular orientation to the flow, causing some scour of the outer bank. Scour of the inner bend could also be seen at positions just downstream of the groyne placements. Scour on the inner bend occurred due to the increase in velocity as a result of the groynes causing a narrowing of the channel.

Large scour areas around the noses of the groynes resulted in large amounts of sediment deposition in between individual groynes near to the outer bank with a maximum deposition depth 70 mm. The outer bank did, however, undergo some scour at the water level as a result of the velocity of flow in the eddy currents. Still standing pools formed just upstream of the groynes and provided protection from erosion.

The above mentioned results can be seen in Figures 64 and 65 below.

70

Figure 64: Experiment 12 survey (4 groynes; 3.5 x projection length)

Figure 65: Scour patterns around groynes for Experiment 12 (4 groynes; 3.5x projection length)
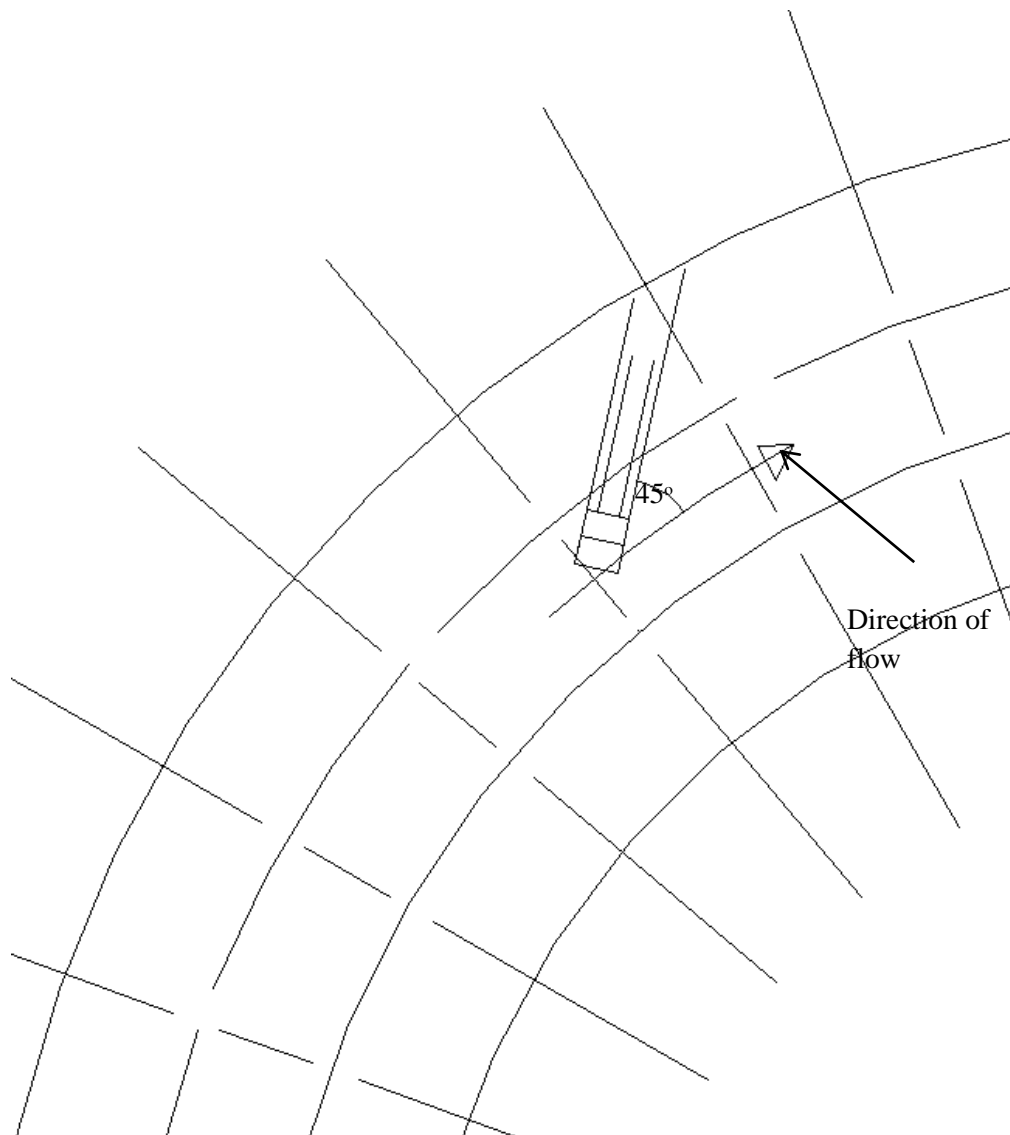
3.5.13 Experiment 13 (19 ℓ/s; 5 min 33 s; upstream orientation)

Experiment 13 was done with 4 groynes installed on the first bend at a spacing of 2.33 m and a projection length of 0.575 m. The spacing between the groynes was therefore 4.1 times the projection length which can be seen in Figure 66. A flow rate of 18.8 ℓ/s was observed for a duration of 5 min 33 s.
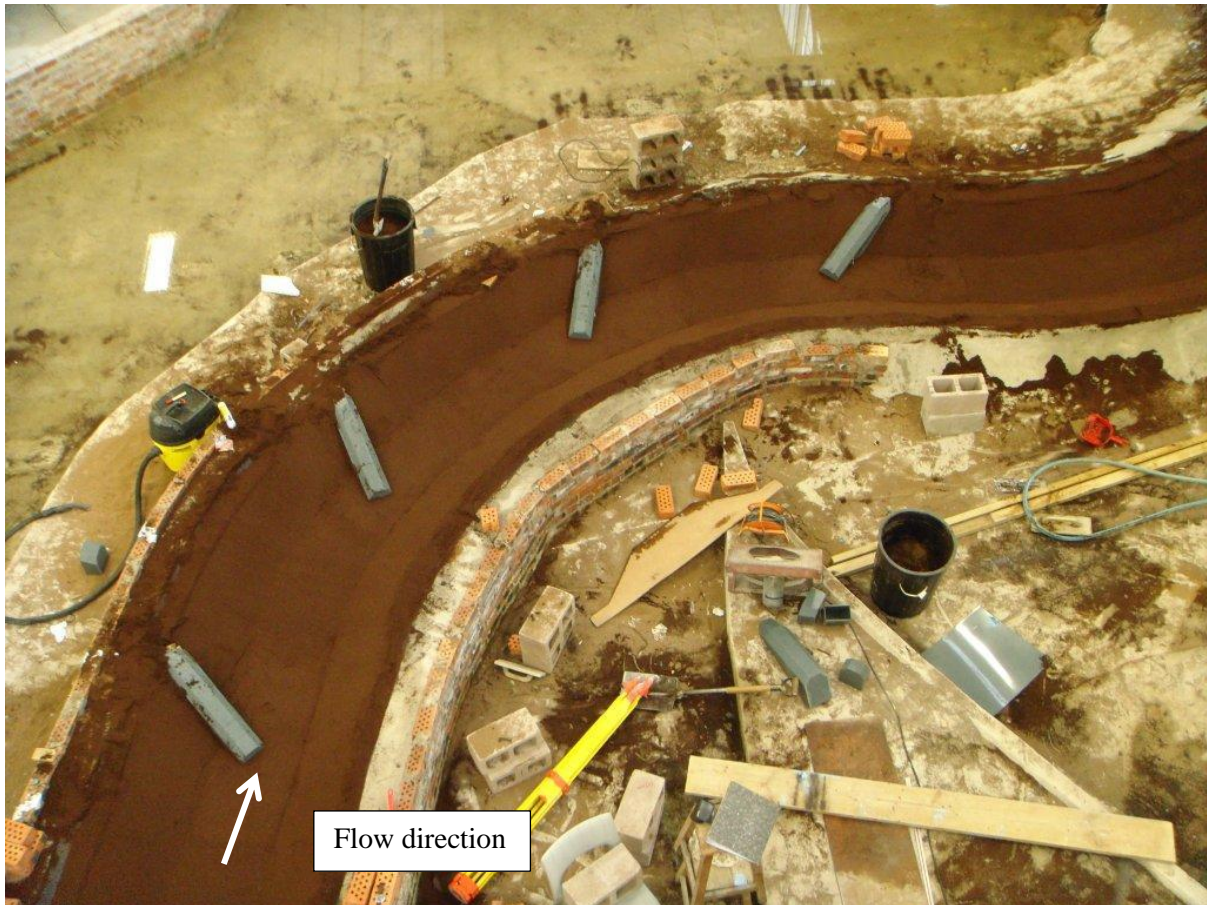

Flow direction

Figure 66: Layout of groynes for Experiment 13 (4 groynes; 4.1 x projection length)

Local scour around the noses of the groynes was not as accentuated as was observed for experiments 11 and 12. The rate of scour decreased as equilibrium was approached during the run of the experiment. A maximum scour depth of 100 mm was observed. The shorter projection length caused less constriction of the flow. Deposition downstream of the groynes could be seen to a maximum depth of 70 mm. The shorter projection length, however, did not offer as much scour protection to the outer bend, with the eddy currents not covering the entire area between consecutive groynes.

Scour could be seen on both the inner and outer bends. Failure of the inner bend was observed just downstream of the groyne placements. Scour on the outer banks was seen in between the groynes, except just upstream of the groynes, where still standing pools formed during the experiment. These results can be seen in Figures 67 and 68.
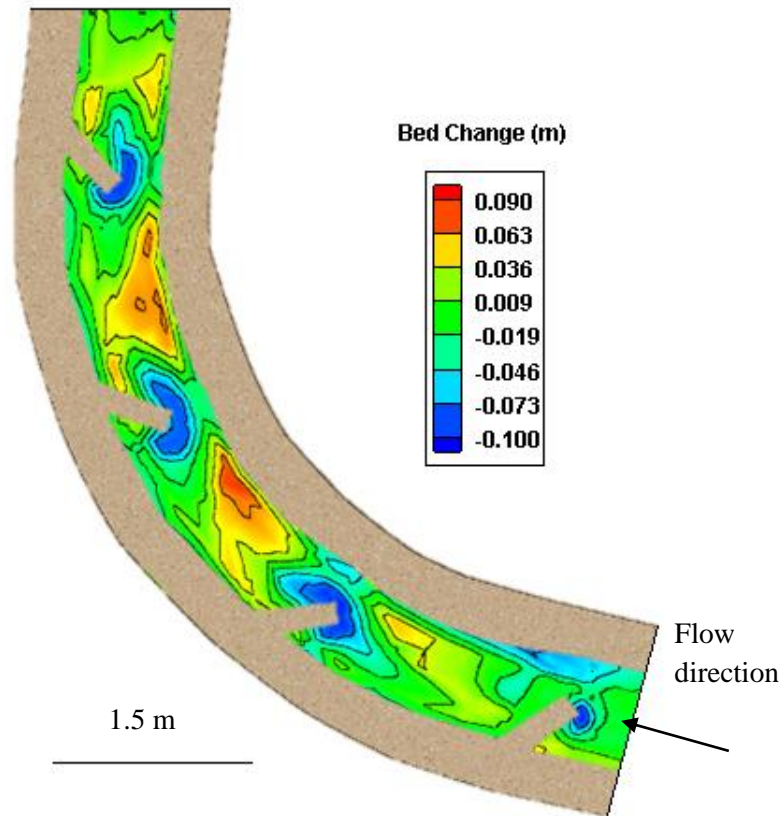
Figure 67: Experiment 13 survey (4 groynes; 4.1 x projection length)

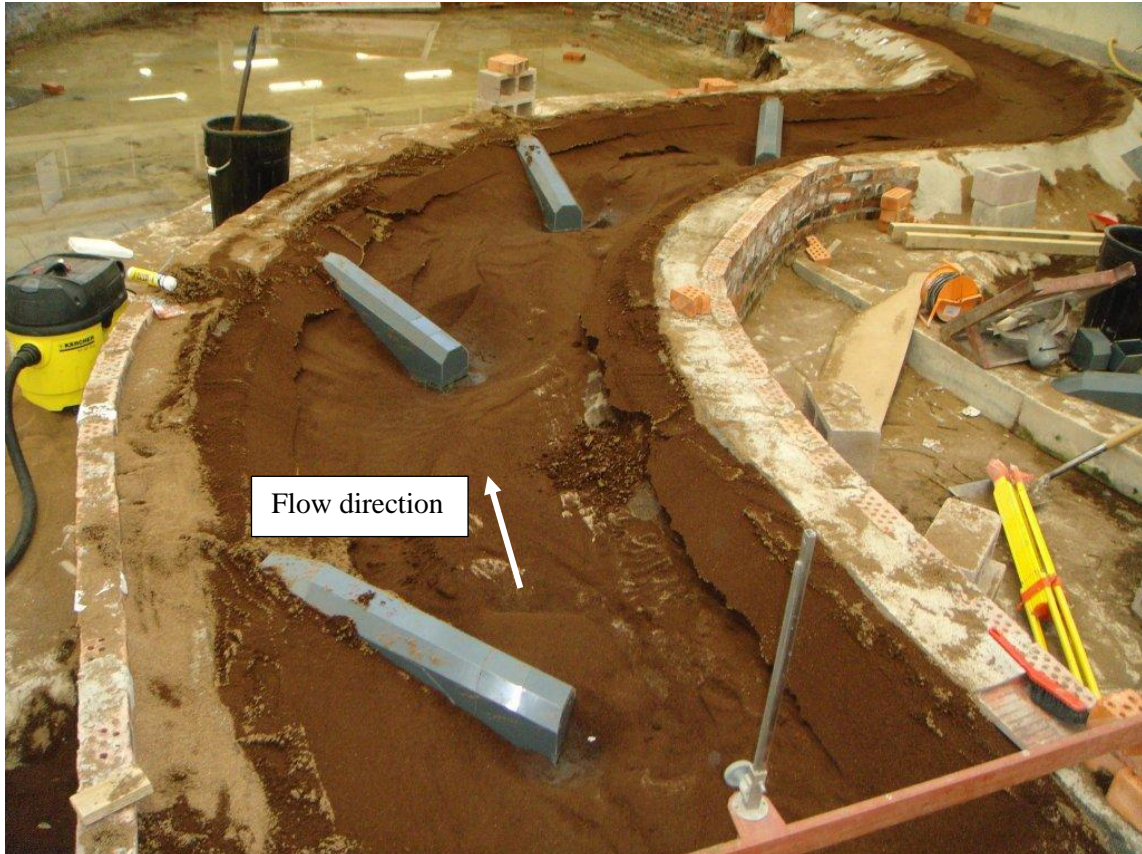**Figure 68: Scour patterns around groynes for Experiment 13 (4 groynes; 4.1x projection length)**

73

3.5.14   Experiment 14 (19 ℓ/s; 5 min 0 s; downstream orientation)

Experiments 14 and 15 were done with groynes installed at an angle of 135° with regard to the flow direction. The spacing between the groynes was taken as the optimal spacing from experiments 2 to 10, which was 2.33 m (see Figure 28). Figure 69 shows the orientation of the groynes with respect to the oncoming flow.
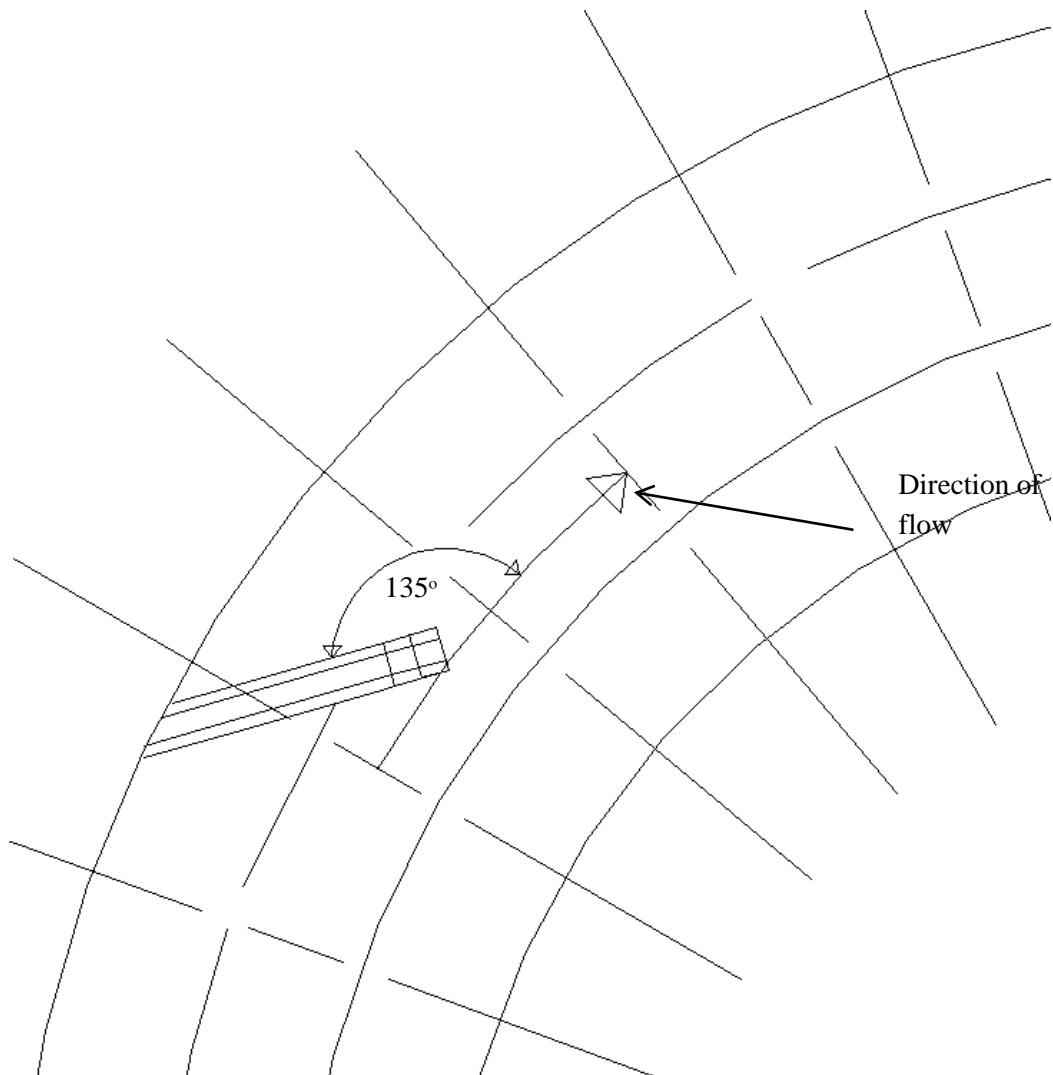
Figure 69: Orientation of groynes

Experiment 14 was done with 4 groynes installed on the first bend at a spacing of 2.33 m and a projection length of 0.675 m. The spacing between the groynes was therefore 3.46 times the projection length which can be seen in Figure 70. A flow rate of 18.16 ℓ/s was observed for a duration of 5 min 0 s.
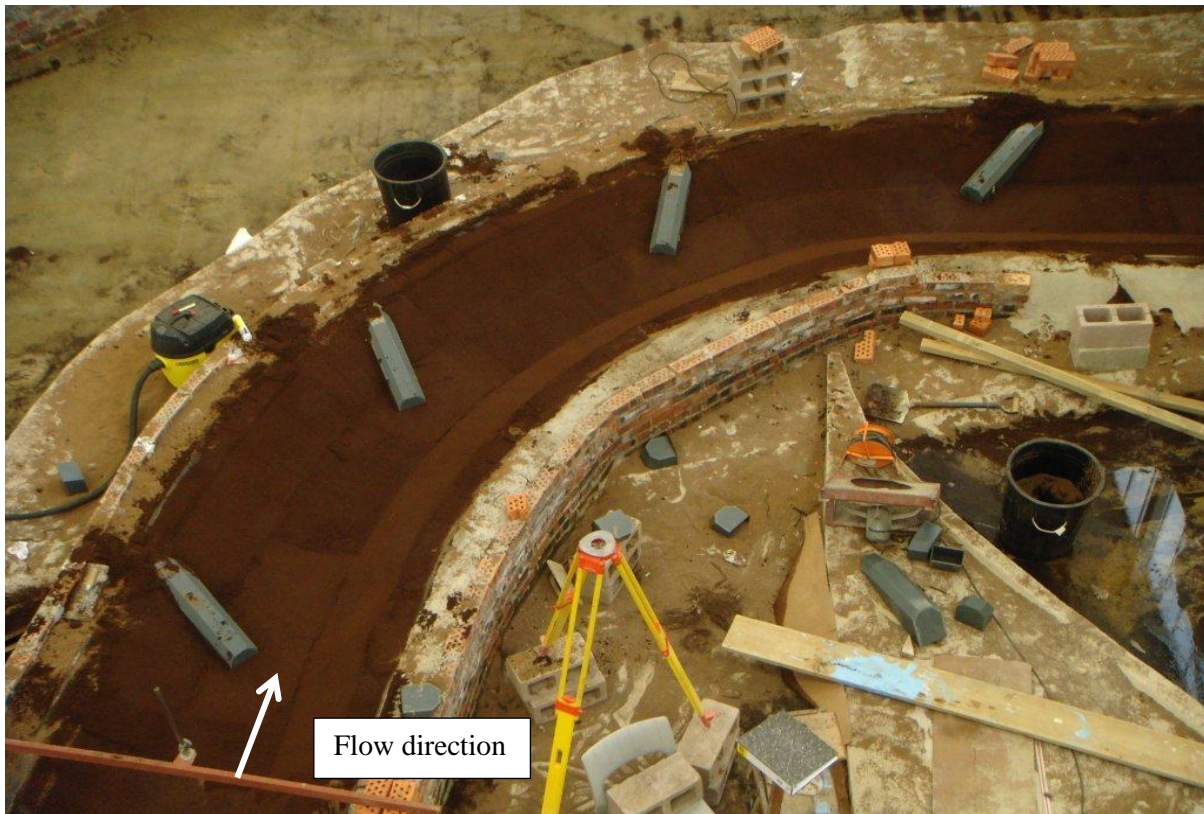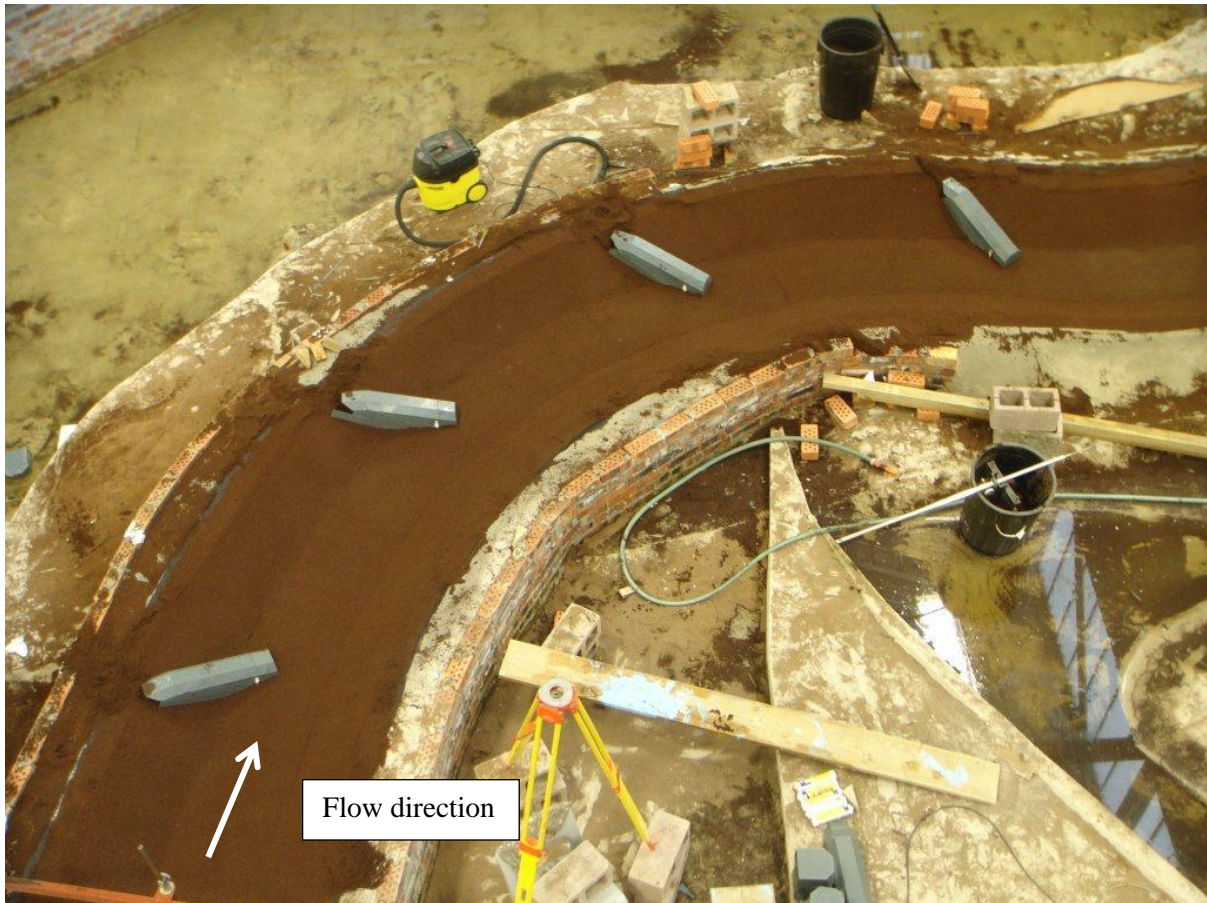
Figure 70: Layout of groynes for Experiment 14 (4 groynes; 3.5 x projection length)

Local scour around the noses of the groynes was observed. The scour rate observed around the noses of the groynes decreased during the run of the test as equilibrium was reached. The area that was scoured was the largest that occurred in all the designs. A maximum scour depth of 100 mm was observed. Very good scour protection was, however, provided for the outer banks of the channel, as limited scour occurred. Very limited scour was observed directly upstream of the groynes, which was a problem area for the design where groynes were placed perpendicular to the flow.

The inner banks opposite the groyne positions failed, as a result of higher flow velocities caused by the constriction and deflection of flow. Deposition occurred directly downstream of each of the groynes, as the sediment that was taken into suspension is deposited as a result of the lower flow velocities caused by the eddy currents that formed between consecutive groynes. A maximum sediment deposition depth of 52 mm was observed at the outer riverbank.

This appears to be a very conservative design, as the eddy currents that were formed had very low flow velocities. The flow pattern does, however, form an S – shape between the groynes, which could have a detrimental effect with bigger flows. These results can be seen in Figures 71 and 72.
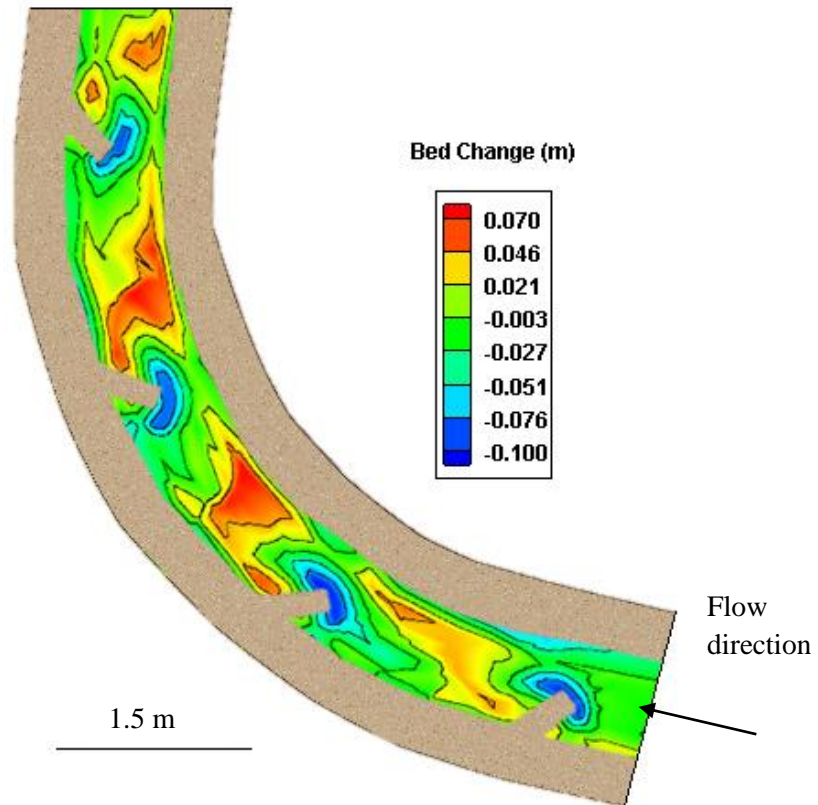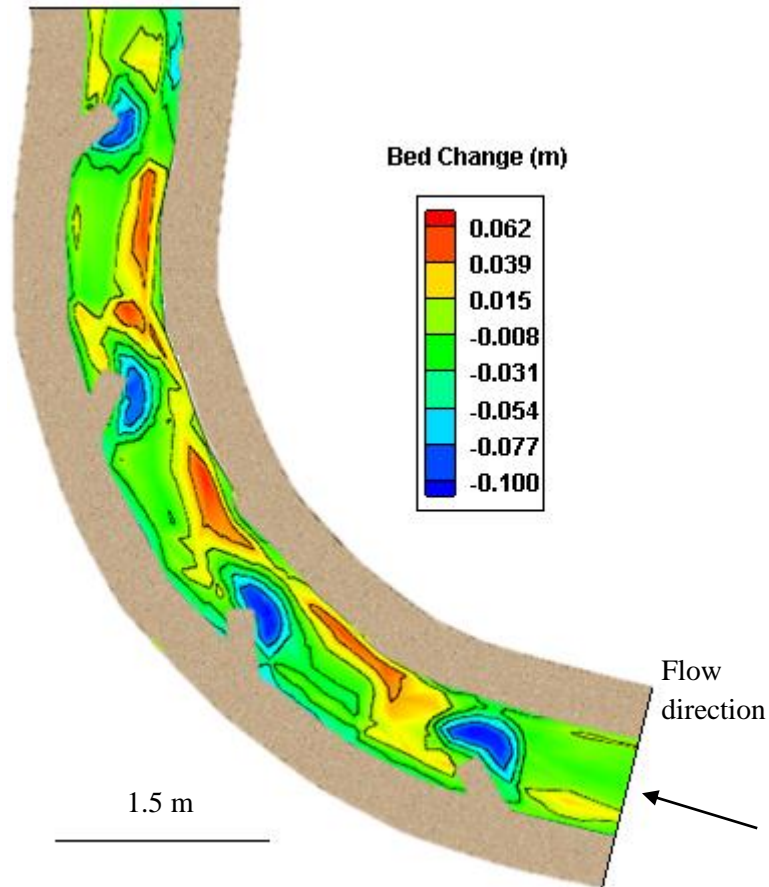
Figure 71: Experiment 14 survey (4 groynes; 3.5 x projection length)
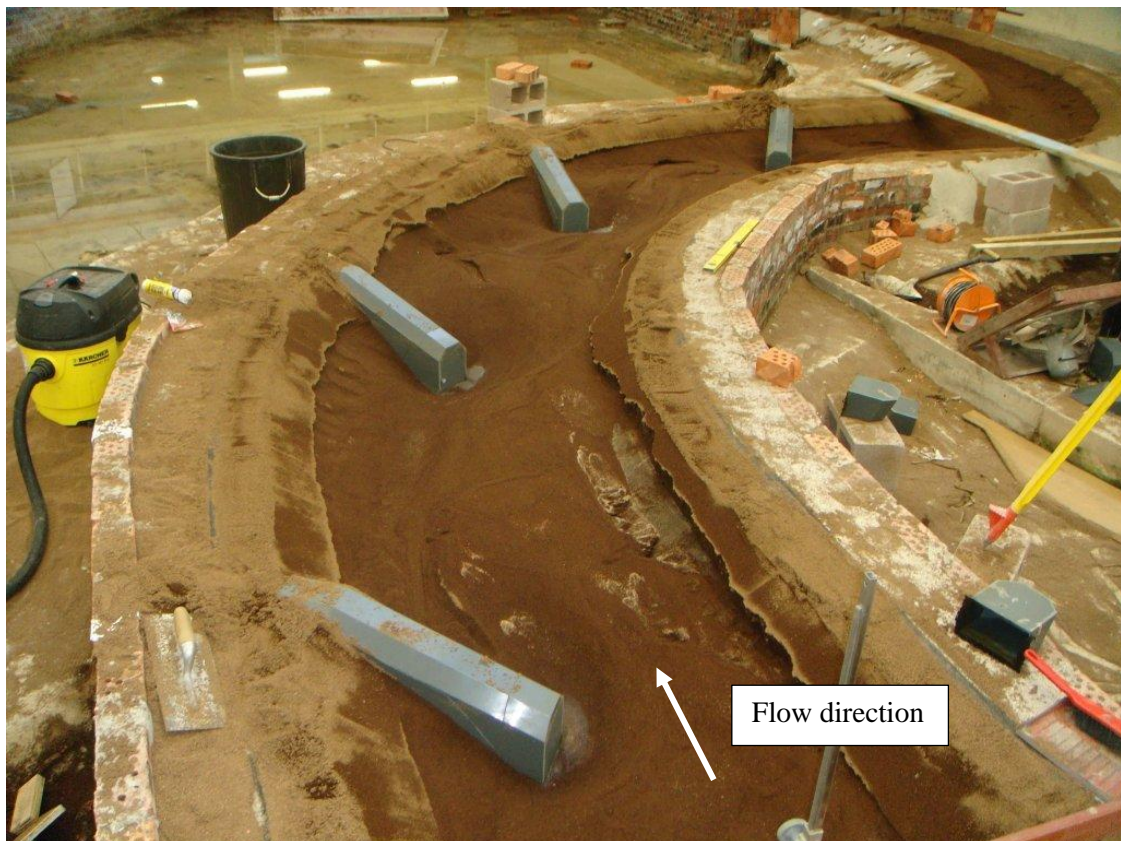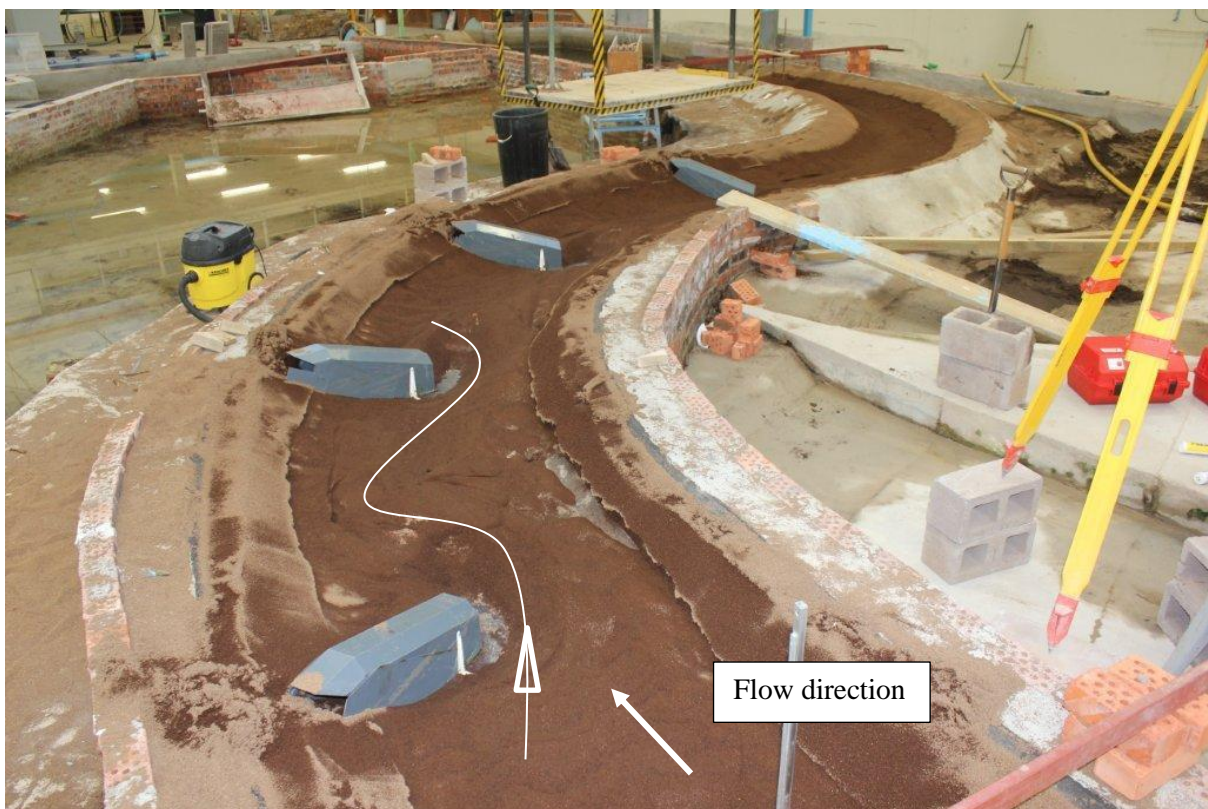

Figure 72: Scour patterns around groynes for Experiment 14 (4 groynes; 3.5x projection length)

76

3.5.15   Experiment 15 (19.12 ℓ/s; 5 min 6 s; downstream orientation)

Experiment 15 was done with 4 groynes installed on the first bend at a spacing of 2.33 m and a projection length of 0.575 m. The spacing between the groynes was therefore 4.06 times the projection length which can be seen in Figure 73. A flow rate of 19.12 ℓ/s was observed for a duration of 5 min 06 s.

Figure 73: Layout of groynes for experiment 15 (4 groynes; 4.1 x projection length)

Some local scour was observed around the noses of the groynes. As equilibrium was approached, the scour rate around the nose of the groynes decreased. A maximum scour depth of 100 mm was observed. Although some scour protection was provided for the outer banks, some signs of erosion could still be seen at the water level. Minimal recirculation of flow (eddy currents) was seen as the projection length of the groynes was too short. The eddy currents that formed were localised to the upstream and downstream sides of the groynes.

Some deposition was seen downstream of the groyne positions. The area of deposition was, however, very small as a result of the localised eddy currents, with a maximum sediment deposition depth of 59 mm at the outer riverbank. Scour was also observed on the inner banks across from the groyne positions where constricting flow resulted in higher velocities. The abovementioned results can be seen in Figures 74 and 75.
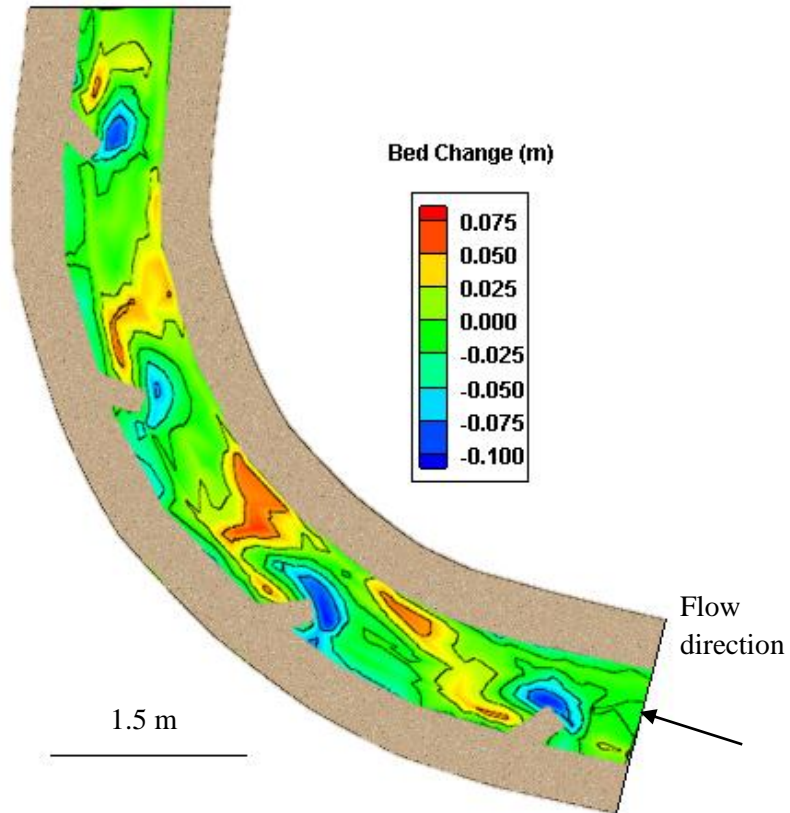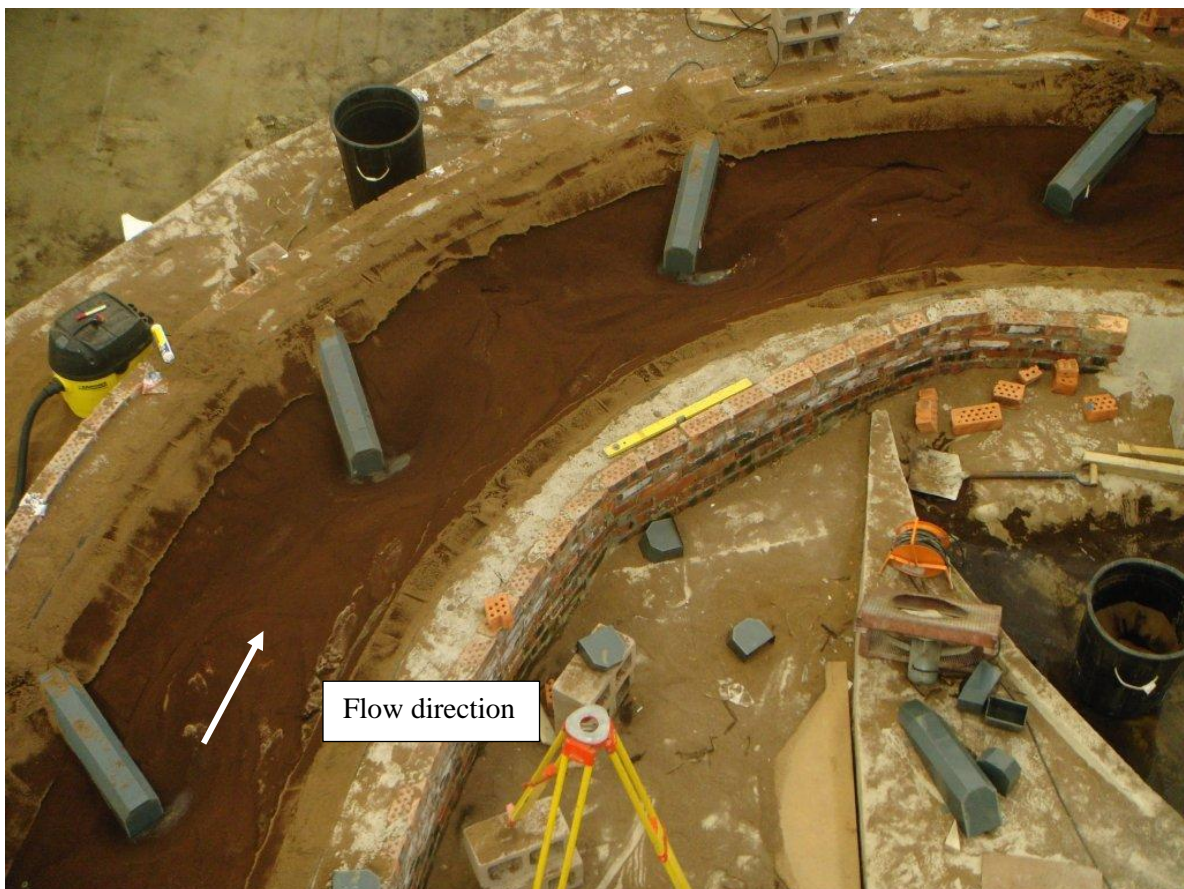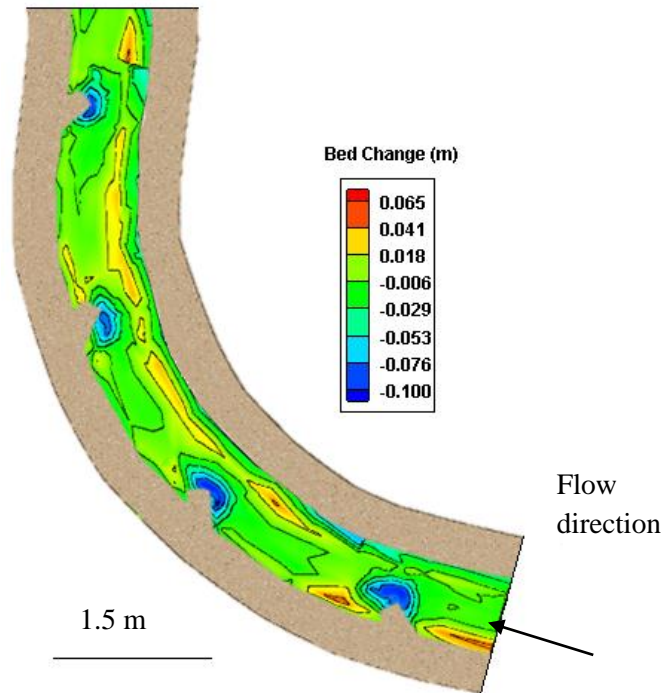
Figure 74: Experiment 15 survey (4 groynes; 4.1 x projection length)
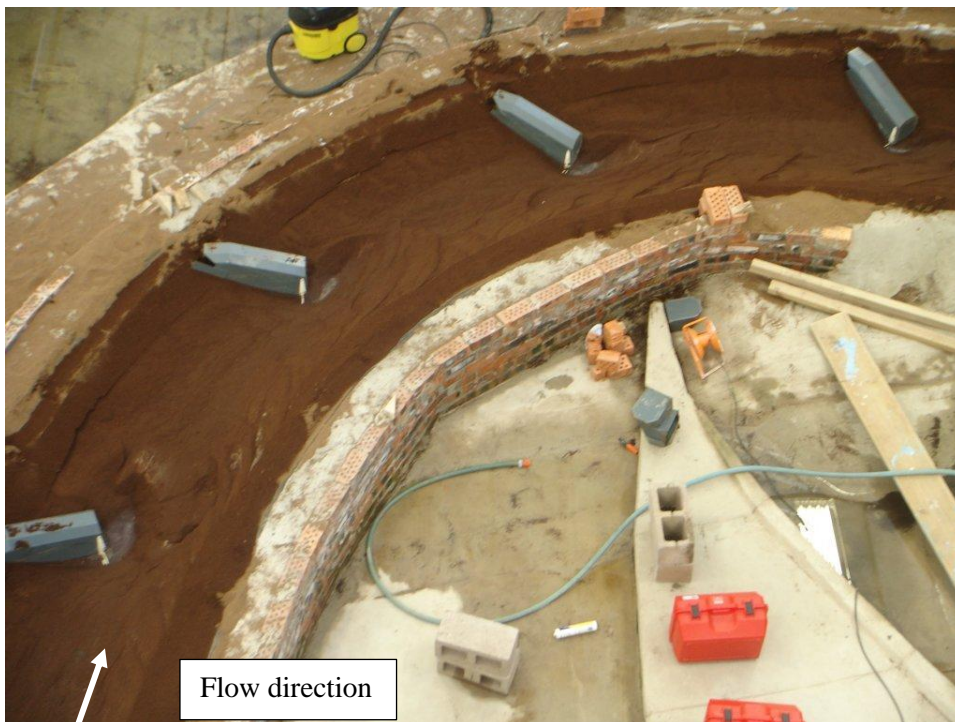
Figure 75: Scour patterns around groynes for Experiment 15 (4 groynes; 4.1x projection length)

3.5.16   Summary of experiment surveys

Table 8 shows a summary of all the surveys for the different experiments with the same legend. From Table 8 the difference in scour and deposition patterns for the different designs can be seen.

Table 8: Summary of experiment surveys

0.070 0.046 0.021 -0.003 -0.027 -0.051 -0.076 -0.100	**Experiment 2** Q = 19 ℓ/s; S = 1.75m L = 0.775m	**Experiment 3** Q = 21 ℓ/s; S = 1.75m L = 0.675m
Experiment 4 Q = 19 ℓ/s; S = 1.75m L = 0.575m	**Experiment 5** Q = 19 ℓ/s; S = 2.33m L = 0.775m	**Experiment 6** Q = 18 ℓ/s; S = 2.33m L = 0.675m
Experiment 7 Q = 19 ℓ/s; S = 2.33m L = 0.575m	**Experiment 8** Q = 19 ℓ/s; S = 2.83m L = 0.775m	**Experiment 9** Q = 18 ℓ/s; S = 2.83m L = 0.675m
Experiment 10 Q = 18 ℓ/s; S = 2.83m L = 0.575m	**Experiment 11** Q = 18 ℓ/s; S = 2.33m L = 0.775m	**Experiment 12** Q = 19 ℓ/s; S = 2.33m L = 0.675m
Experiment 13 Q = 19 ℓ/s; S = 2.33m L = 0.575m	**Experiment 14** Q = 18 ℓ/s; S = 2.33m L = 0.675m	**Experiment 15** Q = 19 ℓ/s; S = 2.33m L = 0.575m

3.6 Optimal design

From Experiment 1 it was determined that there was a definite need for scour protection of the outer banks. The three aspects that were considered to determine the optimal layout design of the groynes for the channel were:

1. The spacing between the groynes
2. The projection length of the groynes and
3. The orientation of the groynes

The combination of scour and sediment deposition was taken into account, which directly correlates to the resulting flow patterns in the channel. An ideal design would see eddy currents form and cover the entire groyne field, resulting in low flow velocities near the riverbank, decreasing the potential for erosion and promoting sediment deposition.

From the physical model experiments it was found that the optimal projection length was 0.675 m with a perpendicular orientation. Three experiments were performed with this projection length with spacings of 2.6, 3.5 and 4.2 times the projection length. A spacing of 2.33 m (3.5 times the projection length) was found to offer the best results in terms of eddy formations, scour protection and sediment deposition (as discussed in Section 3.5).

The third aspect considered in the design was the orientation of the groynes with regard to the approach flow direction. The spacing obtained as discussed above was used to determine the variation in scour protection offered to the outer bank for groyne orientations of 45° and 135° with respect to the flow (90° had already been tested).

Refer to Tables 9, 10 and 11 for the positive and negative aspects of each groyne orientation.

Table 9: Positive and negative aspects of perpendicular orientation

Positive aspects	Negative aspects
1. The deposition area was found to be the biggest 2. Local scour around the noses of the groynes was found to cover the smallest area 3. The scour around the noses of the groynes was not as deep as for other orientations 4. Very good protection was offered to the outer bank	1. Some scour was observed just upstream of the groynes 2. The deposition depth was less than experienced with other orientations

Table 10: Positive and negative aspects of 45º orientation (upstream)

Positive aspects	Negative aspects
1. More deposition occurs 2. Still pools form upstream of groynes, which has ecological advantages as well as preventing scour	1. Local scour around the noses of the groynes is larger and deeper than for all other orientations 2. The deposition area is smaller than that observed for perpendicular orientation 3. Scour of the outer bank still occurs 4. Scour of the inner bank is also a problem

Table 11: Positive and negative aspects of 135º orientation (downstream)

Positive aspects	Negative aspects
1. Average amount of local scour encountered around the noses of the groynes 2. Very conservative design (i.e. less scour and less deposition of sediment) 3. Scour just upstream of the groynes is minimal	1. Limited sediment deposition is seen 2. Deposition depth is less than for other designs 3. Scour of the outer river bank still occurs

From these results it can be seen that the optimal design in terms of scour protection and sediment deposition will be achieved by a perpendicular orientation of the groynes. The optimal design therefore is deemed to be that of Experiment 6, where groynes were placed perpendicular to the flow at a spacing of 2.33 m (3.5 times the projection length), with a projection length of 0.675 m.

For Experiment 6, the area of sediment deposition was the largest, while the scoured area around the noses of the groynes was the smallest. Very good scour protection was created for the outer banks around the bend.

3.6.1   Optimal experiment (7 groynes; 19ℓ/s; 3.5 x projection length)

The optimal experiment was done with 7 groynes installed on both bends at a spacing of 2.33 m and a projection length of 0.675 m which is the same as for Experiment 6, but with both bends being tested. The spacing between the groynes was therefore 3.5 times the projection length which can be seen in Figure 76. A flow rate of 19.4 ℓ/s was observed for a duration of 4 min 58 s.
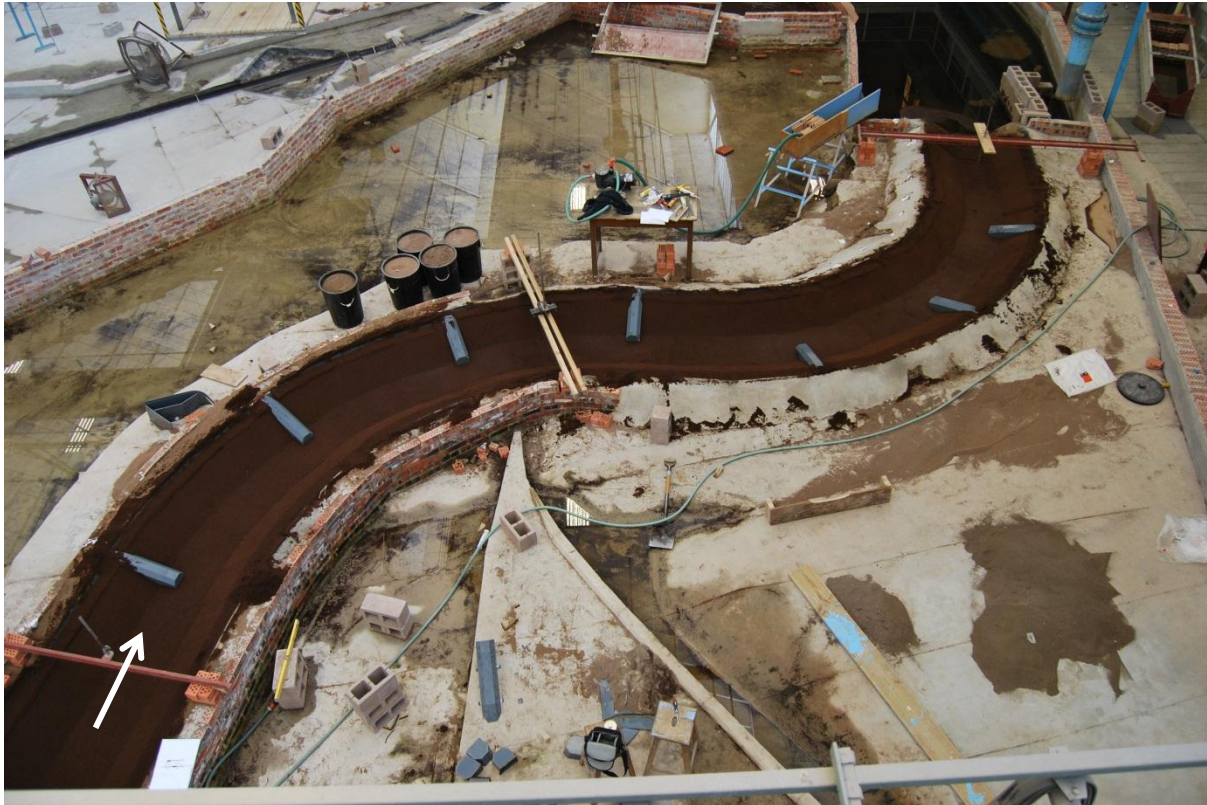
Figure 76: layout of groynes for optimal experiment (7 groynes; 3.5 x projection length)

Local scour around the noses of the groynes started at a very high rate which decreased as equilibrium was approached. Scour around groynes decreases with each consecutive groyne, as energy is dissipated by each groyne. A maximum scour depth of 100 mm was observed. As a result of bank failure on the first bend, less scour is observed on the second bend in the physical model experiment. Scour around the first bend showed a clear correlation to the results obtained from Experiment 6.

Clear eddy currents could be seen between all groynes, resulting in very low flow velocities close to the outer banks. Very good scour protection was created for the outer banks, as almost no scour was visible after the run of the experiment.

The transition from the first bend to the second bend resulted in some sediment deposition in the middle of the channel between groynes 4 and 5, where the velocity profile changed according to the change in the channel alignment. Sediment deposition could also be seen downstream of all groynes, where flow velocities were lower due to eddy formation, as a result of the sediment that was taken into suspension around the noses of the groynes. The maximum deposition depth observed for the experiment was 44 mm. These results can be seen in Figures 77 and 78.
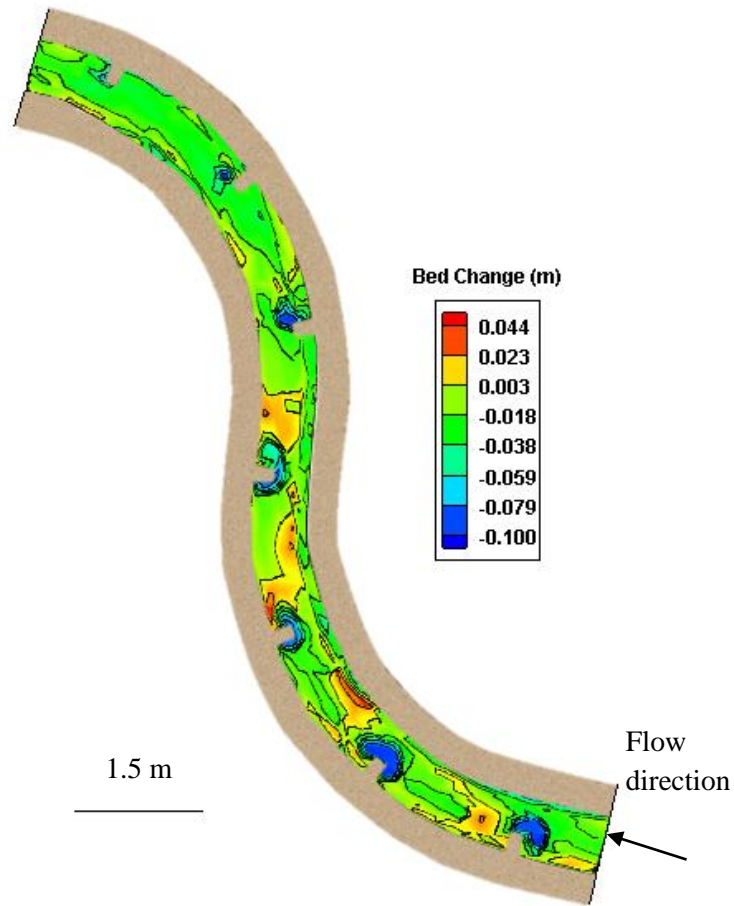
Figure 77: Survey of optimal experiment (7 groynes; 3.5 x projection length)

Figure 78: Scour patterns around groyne for optimal design (7 groynes; 3.5 x projection length)

3.7 Summary of physical model results

Different layout designs of groynes were tested to determine the optimal design for this case. The design aspects considered were: The spacing between consecutive groynes, the projection length of the groynes and the orientation of the groynes with regard to the oncoming flow. Results in terms of scour around the noses of the groynes and deposition depth at the outer bank are indicated in Table 12 below.

Table 12: Scour and deposition depth for physical model experiments

Experiment	Orientation	Projection length, L (m)	Spacing S (m)	S/L	Discharge (ℓ/s)	Maximum scour (mm)	Maximum deposition (mm)
1	n/a	n/a	n/a	n/a	20	120	64
2	90	0.775	1.75	2.3	19	100	80
3	90	0.675	1.75	2.6	21	100	80
4	90	0.575	1.75	3.1	19	90	63
5	90	0.775	2.33	3.0	19	100	70
6	90	0.675	2.33	3.5	18	100	60
7	90	0.575	2.33	4.1	19	100	50
8	90	0.775	2.83	3.7	19	100	64
9	90	0.675	2.83	4.2	18	100	59
10	90	0.575	2.83	4.9	18	100	45
11	45	0.775	2.33	3.0	18	100	90
12	45	0.675	2.33	3.5	19	100	70
13	45	0.575	2.33	4.1	19	100	70
14	135	0.675	2.33	3.5	19	100	52
15	135	0.575	2.33	4.1	19	100	50
Optimal	90	0.675	2.33	3.5	19	100	44
					Average deposition =		63.2 mm

The greatest deposition depth was observed for an upstream groyne orientation (Experiment 11) as a result of more scour around the noses of the groynes. A perpendicular groyne orientation resulted in the smallest scour area around the noses of the groynes, while larger area of deposition was observed when compared to the upstream and downstream groyne orientations. As the spacing between the groynes increases, the scour area around the noses of the groynes decreases, and the deposition depth also decreases as a result of less sediment being taken into suspension.

Flow patterns obtained from the physical model results coincides with what was found in literature, with two eddy currents forming between consecutive groynes. Some correlation was found between observed scour/deposition patterns and the patterns proposed by (King, 2009). Deposition areas downstream of individual groynes are similar. According to (King,

2009), sediment deposition occurs directly upstream of groynes for both perpendicular and upstream groyne orientations. In the physical model experiments it was found that scour occurs upstream of groynes with perpendicular orientation. Very limited bed change was observed upstream of groynes with upstream and downstream orientations.

A perpendicular groyne orientation was found to result in the best combination of erosion protection and deposition on the outer riverbank. An optimal projection length of 0.675 m was determined with a spacing of 2.33 m (3.5 times the projection length).

The above mentioned design was implemented on both bends of the physical model. Clear protection of the outer riverbank could be seen on both bends when compared to experiments done with no groynes installed in the model.

Further images of physical model results can be seen in Appendix 2.

Data obtained from the physical model experiments was used in Chapter 4 to simulate a 2-dimensional numerical model in CCHE2D.

4. Hydrodynamic modelling of groyne sedimentation patterns

4.1 Introduction

A two–dimensional hydrodynamic model was used for a series of numerical simulations in an attempt to validate the model against the results obtained from the physical model test results. Achieving corresponding results between the hydrodynamic model and the physical model tests will give researchers the opportunity to obtain dependable results through numerical modelling for different design scenarios.

4.2 CCHE – 2D

The National Center for Computational Hydroscience and Engineering (NCCHE) at the University of Mississippi developed an integrated software package. It is a general model for two–dimensional simulation and analysis of river flows, dam break flows, non-uniform sediment transport, morphologic processes, coastal processes, pollutant transport and water quality. These processes are solved with the depth integrated Reynolds equations, mass transport equations, sediment sorting equation, bed load and bed deformation equations. The model is based on the Efficient Element Method, a collocation approach of the Weighted Residual Method. CCHE – MESH 3.0 and CCHE – GUI 3.26 were used for the simulation process (National Center for Computational Hydroscience and Engineering, 1999)

4.2.1 CCHE mesh generator

Computational Fluid Dynamics (CFD) is based on solving a set of non-linear Partial Differential Equations (PDEs) on a physical domain, which is usually discretised and represented by a computational mesh. The success of solving these PDEs depends largely on the mesh quality (Zhang & Jia, 2009).

Two types of mesh are used in CFD: the structured and the unstructured. For this report a structured mesh was implemented. A structured mesh consists of families of mesh lines with the property that members of a single family do not cross each other, and cross a member of another family only once. The advantage is that one has clearly defined nodal points in the mesh (Zhang & Jia, 2009).

The algebraic mesh generator was used, which interpolates between the interior mesh nodes directly from the boundary. The two-boundary method, combined with a multi–block scheme, was used for algebraic mesh generation. Basically three steps are involved in the two–boundary algebraic mesh generation, which can be seen in Figure 79.

- The inner and outer boundaries are defined by placing boundary control points
- An equal number of boundary points are distributed along the top and bottom boundaries (j–direction). Each pair of boundaries forms a control line

- The internal mesh nodes (I–direction) along the control lines are distributed
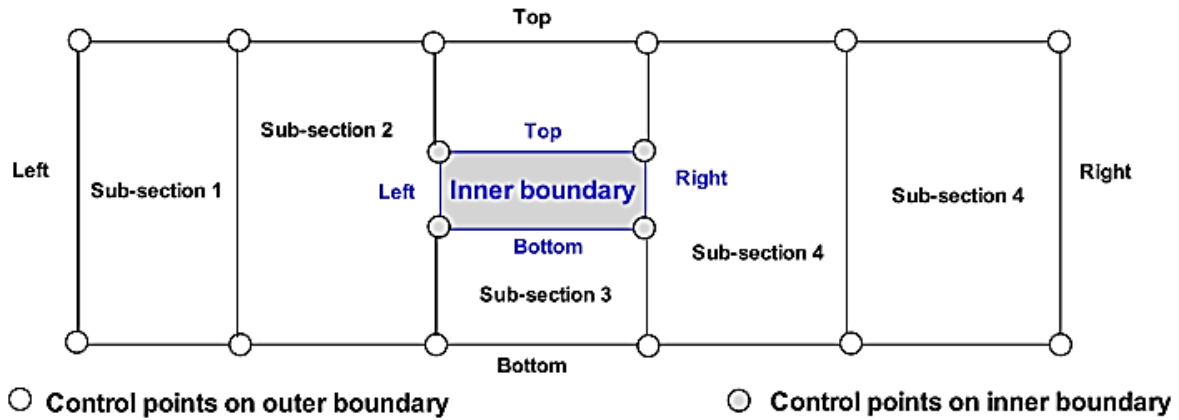

Figure 79: Mesh domain (Zhang & Jia, 2009)

In CCHE – MESH a flexible and powerful two-direction stretching function EDS is used to control the nodal distribution.

$$s_j = \sum_1^{j-1} \left| \frac{2}{\exp(\phi) + \exp(\phi)} \right|^E \bigg/ \sum_1^{N-1} \left| \frac{2}{\exp(\phi) + \exp(\phi)} \right|^E$$

$$\emptyset = \left[\frac{j-1}{N} - D \right] \times S$$

where s_j is the relative location, j is the label of one point; N is the total number of points along a mesh line, E (=-1, 0, 1) is the exponential parameter, D ($0 \le D \le 1$) is the derivation parameter, S (>0) is the parameter used to control the degree of stretching, called the scale parameter (Zhang & Jia, 2009).

The nodal distribution was controlled by an RL (Ryskin and Leal) system with a smoothness function. A planar interpolation method that was on a triangle plane was used to interpolate between nodes. Using the equations below, the bed elevation at grid point G (Figure 80) can be obtained.

$$a = y_1 \cdot (z_2 - z_3) + y_2 \cdot (z_3 - z_1) + y_3 \cdot (z_1 - z_2)$$

$$b = z_1 \cdot (x - x_3) + z_2 \cdot (x_3 - x_1) + z_3 \cdot (x_1 - x_2)$$

$$c = x_1 \cdot (y_2 - y_3) + x_2 \cdot (y_3 - y_1) + x_3 \cdot (y_1 - y_2)$$

$$d = -x_1 \cdot (y_2 z_3 - y_3 z_2) - x_2 \cdot (y_3 z_1 - y_1 z_3) - x_3 \cdot (y_1 z_2 - y_2 z_1)$$

$$Z_G = -\frac{(a \cdot x_G + b \cdot y_G + d)}{c} \text{ (if } c \ne 0)$$

87

where x_i, y_i and z_i are the x, y and z coordinates of the respective points surrounding G (see Figure 80)
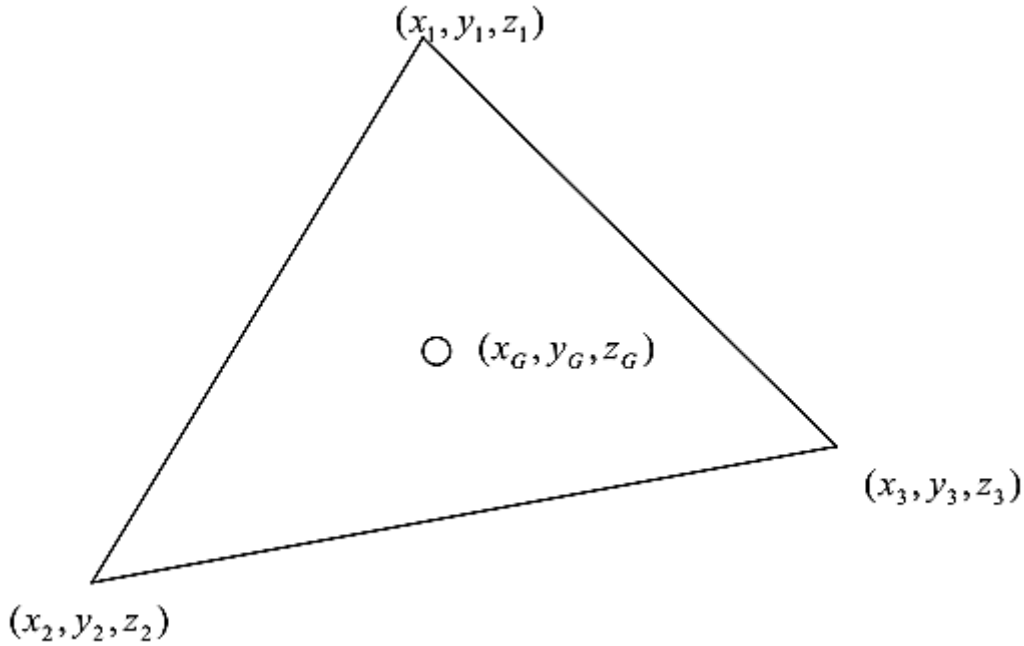

Figure 80: A triangle plane (Zhang & Jia, 2009)

4.2.2   Sediment transport model

4.2.2.1 Governing equations

The depth integrated two-dimensional equations that are used in the CCHE2D model are:

Continuity equation:

$$\frac{\partial Z}{\partial t} + \frac{\partial (hu)}{\partial x} + \frac{\partial (hv)}{\partial y} = 0$$

Momentum equations:

$$\frac{\partial u}{\partial t} + u\frac{\partial u}{\partial x} + v\frac{\partial u}{\partial y} = -g\frac{\partial Z}{\partial x} + \frac{1}{h}\left[\frac{\partial (h\,\tau_{xx})}{\partial x} + \frac{\partial (h\,\tau_{xy})}{\partial y}\right] - \frac{\tau_{bx}}{\rho\,h} + f_{Cor}v$$

$$\frac{\partial v}{\partial t} + u\frac{\partial v}{\partial x} + v\frac{\partial v}{\partial y} = -g\frac{\partial Z}{\partial y} + \frac{1}{h}\left[\frac{\partial (h\,\tau_{yx})}{\partial x} + \frac{\partial (h\,\tau_{yy})}{\partial y}\right] - \frac{\tau_{by}}{\rho\,h} + f_{Cor}u$$

Where u and v are the depth-integrated velocity components in the x and y directions respectively, g is the gravitational acceleration, Z is the water surface elevation, ρ is water density, h is the local water depth, f_{Cor} is the Coriolis parameter, τ_{xx}, τ_{xy}, τ_{yx} and τ_{yy} are the depth integrated Reynolds stresses, and τ_{bx} and τ_{by} are shear stresses at the bed surface (Zhang, 2006).

88

4.2.2.2 Total sediment load

According to convention, moving sediment is divided into suspended load and bed load, where bed load is the part of the sediment that moves near the bed by rolling, saltation or sliding. Suspended load consists of sediment that was taken into suspension and occupies the flow depth above the bed layer (Wu, 2001).

4.2.2.3 Depth averaged sediment transport equations

As mentioned in above, the full water depth is divided into two zones: the suspended-load zone and the bed-load zone. The thickness of the bed-load zone, δ, is assumed to be twice the sediment diameter. Therefore the bed-load zone (z_b) is set from z_b to $z_b + δ$, and the suspended–load zone from $z_b + δ$ to z_s, where $δ = 2d$, and d is the diameter of the sediment (Wu, 2001).

In the case of non-uniform sediment transport, the sediment mixture can be divided into several size classes. For each size class, the three–dimensional convection–diffusion equation of sediment transport is:

$$\frac{\partial c_k}{\partial t} + \frac{\partial (uc_k)}{\partial x} + \frac{\partial (vc_k)}{\partial y} + \frac{\partial (wc_k)}{\partial z} - \frac{\partial (\omega_{sk} c_k)}{\partial z} = \frac{\partial}{\partial x}\left(\varepsilon_s \frac{\partial c_k}{\partial x}\right) + \frac{\partial}{\partial y}\left(\varepsilon_s \frac{\partial c_k}{\partial y}\right) + \frac{\partial}{\partial z}\left(\varepsilon_s \frac{\partial c_k}{\partial z}\right)$$

where c_k is the concentration of the k-th size class of sediment, u, v and w are the velocity component in the x-, y-, and z-directions, ω_{sk} is the settling velocity and ε_s is the eddy diffusivity of sediment. The integration of the abovementioned equation over the bed–load zone leads to the continuity equation of bed - load:

$$(1 - p')\frac{\partial z_{bk}}{\partial t} + \frac{\partial (\delta\, c_{bk})}{\partial t} + \frac{\partial q_{bkx}}{\partial x} + \frac{\partial q_{bky}}{\partial y} = -E_{bk} + D_{bk}$$

where p' is the porosity of the bed material, c_{bk} is the average concentration of bed-load at the bed–load zone, q_{bkx} and q_{bky} are the components of bed load transport rate in the x- and y–directions, q_{bk} is the bed-load transport rate which results from the sediment exchange between the sediment and the bed material. E_{bk} and D_{bk} are the entrainment (upward) and deposition (downward) fluxes of the sediment at the interface between the suspended – load zone and the bed–load zone (Wu, 2001).

4.2.2.4 Channel morphological change

When the equilibrium transport model is adopted for the bed–load, the bed change can be calculated from either the bed–load continuity equation, or the overall mass balance equation for sediment transport:

$$(1 - p') \frac{\partial z_{bk}}{\partial t} + \frac{\partial (hC_{tk})}{\partial t} + \frac{\partial (q_{bkx} + q_{skx})}{\partial x} + \frac{\partial (q_{bky} + q_{sky})}{\partial y} = 0$$

where q_{skx} and q_{sky} are the suspended load transport rates in the x- and y – directions and C_{tk} is the transport capacity of the total load. Usually the diffusion terms in q_{skx} and q_{sky} are neglected (Wu, 2001).

4.2.2.5 Bed material sorting

Because bed material gradation usually varies in a vertical direction, the bed material above the non–erodible layer is divided into layers. The top layer is the mixing layer, and the second layer is the sub-surface layer. The variation of bed material gradation in the mixing layer is determined by (Wu, 1991, and Wu and Li, 1992) (Wu, 2001):

$$\frac{\partial (\delta_m p_{bk})}{\partial t} = \frac{\partial z_{bk}}{\partial t} + p_{bk}^* \left(\frac{\partial \delta_m}{\partial t} - \frac{\partial z_b}{\partial t} \right)$$

where p_{bk} is the bed material gradation in the mixing layer, δ_m is the thickness of the mixing layer, which is related to the flow and sediment conditions, as well as the bed deformation, $\frac{\partial z_b}{\partial t}$ is the total bed deformation rate, $\frac{\partial z_b}{\partial t} = \sum_{k=1}^{N} \frac{\partial z_b}{\partial t}$, with N being the total number of size classes and p_{bk}^* is the bed material gradation in the sub–surface layer. The bed material gradations in the layers under the mixing layer are determined by using the mass conservation law (Wu, 2001).

4.2.2.6 Bed load type model

CCHE2D adopts 3 models for non-uniform sediment transport modelling. The bed-load type model simulates bed-load transport only, without considering the diffusion of suspended-load, which is the approach adopted for this study. The governing equation for this model is:

$$\frac{\partial (hC_{tk})}{\partial t} + \frac{\partial (\alpha_{tx} q_{tk})}{\partial x} + \frac{\partial (\alpha_{ty} q_{tk})}{\partial y} + \frac{1}{L_t} (q_{tk} - q_{t*k}) = 0$$

where α_{tx} and α_{ty} are direction cosines of total load transport, q_{tk} and q_{t*k} are the actual transport rate and transport capacity of the bed material. C_{tk} is the suspended-load concentration, L_t is the adaptation length of bed material load and h is the flow depth. The bed deformation is then determined by:

$$(1 - p') \frac{\partial z_{bk}}{\partial t} = (q_{tk} - q_{t*k})/L_t$$

where p′ is the porosity of the bed material. The bed deformation can also be calculated by the continuity equation of bed-load given in section 4.2.2.3 (Wu, 2001).

4.2.2.7 Boundary conditions

The inflow of sediment must be given at each inlet boundary. In the case of non–uniform sediment transport, the size distribution of the inflow sediment is needed. A fractional discharge of each sediment size class can be allocated. Once the fractional sediment discharge Q_{bk} is given for the whole cross–section, the CCHE2D model distributes it along the inlet cross-section by:

$$q_{bk} = \frac{Q_{bk}q^{m_b}}{\int_0^B q^{m_b}dy}; \qquad q_{sk} = \frac{Q_{sk}q^{m_s}}{\int_0^B q^{m_s}dy}$$

where q is the specific flow discharge at each node and m_b and m_s are empirical coefficients. On any kind of fixed boundaries, the bed-load transport rate is set to zero and the gradient of suspended–load concentration on the normal direction is set to zero (Wu, 2001).

4.2.2.8 Numerical methods

The flow and sediment calculations are separately conducted. The flow calculation is based on the CCHE2D flow model. The whole calculation procedure for flow and sediment transport is as follows:

1. Initialize parameters
2. Calculate the flow field using the CCHE2D flow model
3. Calculate q_{b*k}^{n+1} and/or C_{*k}^{n+1}
4. Calculate the actual concentration of suspended-load C_k^{n+1}
5. Calculate the actual transport rate of bed–load q_{bk}^{n+1}
6. Determine the bed deformations Δz_{bk}^{n+1} and Δz_b^{n+1} and adjust the bed elevation
7. Calculate the bed material gradation p_{bk}^{n+1}
8. Return to step 2 for the next time step until a specified time is reached. (Wu, 2001)

4.2.2.9 Empirical formulas of non – cohesive sediment transport

The CCHE2D employs four formulas from dozens of available formulas. These were selected by considering the evaluation of many investigators and the capability of accounting for the hiding and exposure effect, as well as by testing with many experimental and field data. The four formulas in use are (Wu, 2001):

1. Modified Ackers and White's formula (by Proffit and Sutherland, 1983)
2. SEDTRA module (by Garbrecht, Kuhnle and Alonso, 1995)
3. Wu, Wang and Jia's formula (2000)
4. Modified Engelund and Hansen's formula (1967)

The modified Ackers and White's formula, and the modified Engelund and Hansen formula have mostly been adopted for single–size (uniform or quasi–uniform) sediment transport. SEDTRA module and Wu et al. formula can both accommodate multiple sediment sizes. Wu

et al. was, however, calibrated using four sets of laboratory data, as well as five sets of field data from natural rivers (Wu, 2001) which made it the logical choice to simulate the sediment transport. The Wu et al. formula is also the default formula applied by the CCHE2D model.

The formula for determining the fractional bed–load transport capacity proposed by Wu, Wang and Jia (2000) is

$$\phi_{bk} = 0.0053 \left[\left(\frac{n'}{n} \right)^{3/2} \frac{\tau_b}{\tau_{ck}} - 1 \right]^{2.2}$$

where $\boldsymbol{\phi}_{bk}$ is a non–dimensional bed–load transport capacity, $\phi_{bk} = q_{b*k} / \left[p_{bk} \sqrt{(\gamma_s / \gamma - 1) g d_k^3} \right]$, q_{b*k} is the equilibrium transport rate of the k-th size class of bed-load per unit width (m^2/s), p_{bk} is the bed material gradation, n is the Manning's roughness coefficient for the channel bed, and n' is the Manning's coefficient corresponding to the grain roughness, $n' = d_{50}^{1/6} / 20$, τ_b is the shear stress and τ_{ck} is the critical shear stress (Wu, 2001).

4.3   Hydrodynamic model setup

The hydrodynamic model was tested against data obtained from the physical model experiments with the aim of validating the model. This section will explain the steps taken to set up the numerical model as well as the input values that are needed to perform the sediment transport procedure as outlined in section 4.2.

A survey of the initial channel bed sediment conditions in the laboratory was done with the Leica TPS 1200+ total station to provide the xyz–coordinates of the bathymetry. These xyz-coordinates were converted to a *.mesh_xyz text file format which is compatible with CCHE2D. A mesh was generated with 200 points across the channel (i-direction) and 600 along the direction of the channel (j-direction). The generated bathymetry is shown in Figure 81 below.
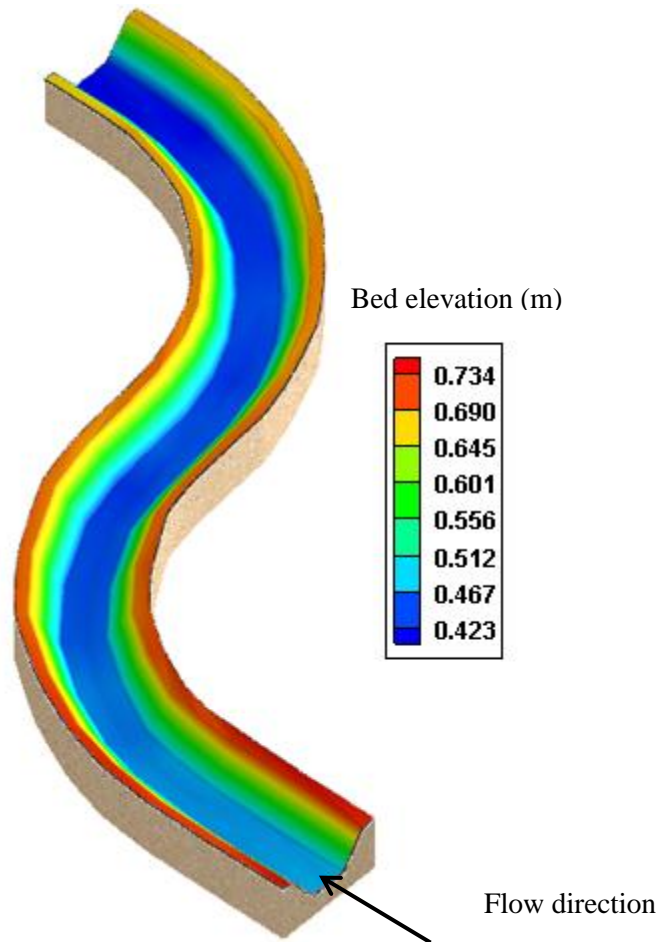
Bed elevation (m)

	0.734
	0.690
	0.645
	0.601
	0.556
	0.512
	0.467
	0.423

Flow direction

Figure 81: Bathymetry of model

Similarly a groyne field mesh (200 points in i-direction and 600 points in j-direction) was generated for the base bathymetry of the model. The coordinates of the groynes for the various layout designs could be obtained from AutoCAD drawings. By doing this the groyne positions could be overlaid onto the base bathymetry. The bathymetry of the channel with a groyne field is shown in Figure 82 below.
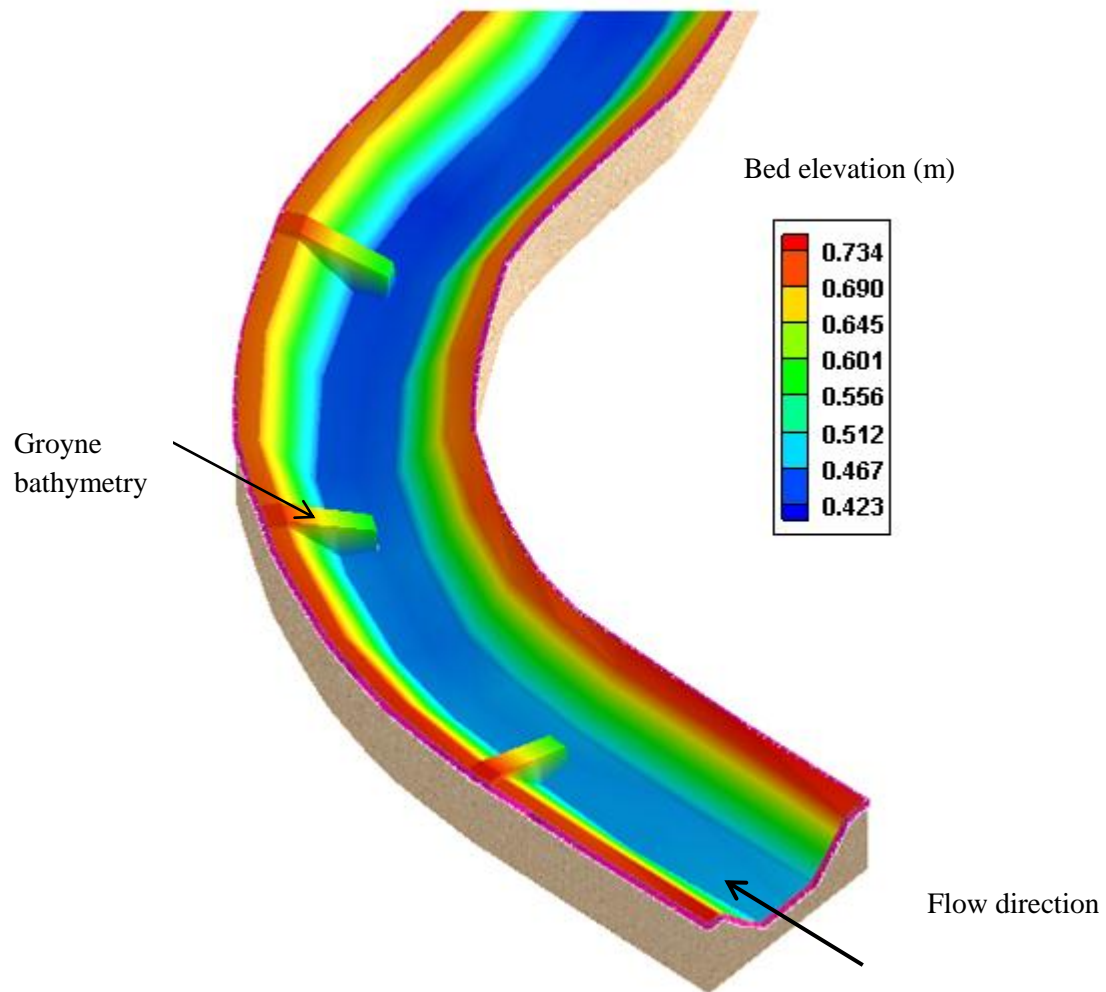
Figure 82: Bathymetry with groyne field

The groynes were then made non–erodible to ensure that they remained unchanged during the course of the simulation.

Table 13 shows the input values for the CCHE2D model that was used for all simulations to create likeness to the laboratory data.

Table 13: Input for all numerical models

Input	Description	Value
Manning's n	Calibrated roughness parameter of channel	0.045
Water level	Outlet boundary condition	120 mm
Discharge	Inlet boundary condition	as in Table 4
Sediment size classes	Range	0.4 mm and 0.8 mm
Sediment specific gravity		1300 kg/m^3
Time step	Time elapsed per iteration	0.1 s
Transport mode		Total load as bed-load
Transport capacity formula		Wu et al. formula

4.3.1   Model calibration

The numerical model was calibrated to correspond with the physical model by adjusting the Manning roughness and the corresponding normal flow depth.

- Manning's n

An initial Manning's n value of 0.035 was assumed for the hydraulic roughness. During the physical model testing it was, however, found that bedforms developed which increased the Manning value. A Manning's n value of 0.045 was therefore calibrated for the numerical model

- Outlet boundary water level

With a Manning's n value of 0.045, the Manning equation was used to determine the theoretical normal flow depth in the channel. The theoretical normal flow depth obtained with the channel characteristics and inlet discharge of 20 ℓ/s was 120 mm. The outlet boundary in the physical and numerical models was therefore set to 120 mm, from where water levels further upstream were calculated by the program. These values were then

compared to the flow depths observed during the physical testing to evaluate the model calibration accuracy in terms of the water levels.

- Inlet boundary

The inlet boundary condition is given by the inflow of water into the model. This was set to the flow rates observed for each of the physical model experiments. These values can be seen in Table 7.

4.3.2   Model validation

The four non cohesive – sediment transport capacity formulas were tested against 1859 sets of uniform bed – material load data chosen from Brownlie's (1981) data. These data have been observed over many decades by many investigators and covers flow discharges of $0.00094 – 297 m^3/s$, flow depths of $0.01 – 2.56$m, flow velocities of $0.086 – 2.88$ m/s, surface slopes of $0.0000735 – 0.0367$ m/m and sediment sizes of $0.088 – 28.7$mm. From Table 14 the error ranges r, with r = (numerical model) / (physical model) can be seen (Wu, 2001).

Table 14: Comparison of calculated versus measured transport rates of uniform bed-material load using Brownlie's data (Wu, 2001)

Error ranges	Percentage (%) of calculated transport rates in error				
	Ackers & White	Yang	Engelund & Hansen	SEDTRA	Wu et al.
$0.8 \leq r \leq 1.25$	37.3	33.4	33.6	36.6	40.4
$0.667 \leq r \leq 1.5$	57.9	56.6	55.4	59.1	62.7
$0.5 \leq r \leq 2$	82.4	76.6	77	78.1	81.3

4.4   Numerical model sediment dynamics simulation results

The following section describes the results obtained from the numerical model as outlined above. The results from the numerical model are compared to the results obtained from the physical model to determine the correlation between the two sets of data.

Table 15 shows the results obtained from both the physical and numerical models. Water levels of both models are compared to determine the accuracy of the numerical model. The water levels in Table 15 are according to a datum level chosen as the floor of the Hydraulics Laboratory. A maximum water level deviation of 10% was seen between the physical and numerical models.

Measuring point 1 found in Table 15 is the upstream water level, with measuring point 2 as the water level in the middle of the channel (Refer to Figures 22–25). Measuring point 3 is omitted as all levels for the physical- and numerical models are at 0.543 m above the chosen datum, where the downstream water level was regulated.

Very good correlation was found between the water levels in the physical and numerical models with a standard deviation of 5.40%.

Table 15: Physical model results vs numerical model results

| Experiment | Flow | Water levels (m) | | | | Percentage error | |
| | | Measuring point 1 | | Measuring point 2 | | | |
		Physical model	Numerical model	Physical model	Numerical model	Measuring point 1	Measuring point 2
1	20	0.582	0.584	0.557	0.562	2.04%	4.76%
2	19	0.589	0.591	0.570	0.574	1.74%	3.25%
3	21	0.589	0.582	0.570	0.557	-6.09%	-10.57%
4	19	0.589	0.583	0.569	0.568	-5.22%	-0.82%
5	19	0.585	0.585	0.558	0.555	0.00%	-2.54%
6	18	0.577	0.567	0.557	0.55	-9.71%	-6.09%
7	19	0.575	0.585	0.560	0.564	9.90%	3.39%
8	19	0.582	0.575	0.563	0.567	-6.48%	3.57%
9	18	0.582	0.583	0.564	0.572	0.93%	7.14%
10	18	0.580	0.581	0.574	0.570	0.94%	-3.25%
11	18	0.592	0.599	0.572	0.576	5.93%	3.23%
12	19	0.593	0.593	0.568	0.574	0.00%	5.00%
13	19	0.590	0.588	0.561	0.571	-1.72%	8.85%
14	18	0.589	0.592	0.570	0.574	2.61%	4.03%
15	19	0.584	0.588	0.576	0.573	3.64%	-2.31%
Optimal	19	0.580	0.59	0.557	0.569	9.43%	10.43%

4.4.1   Numerical model of Experiment 1 (20 ℓ/s, no groynes)

Simulation 1 was done with no groynes to offer scour protection at the riverbanks. A discharge of 20 ℓ/s was simulated for a duration of 5min 31s, as was observed during the physical model test. Water depths during the simulation for measuring points 1, 2, and 3 were, 100 mm, 110 mm and 120 mm, respectively. These water depths correlate very well with the observed water depths during the physical experiment, which were 98 mm, 105 mm and 120 mm, respectively.

Typical scour of the bed could be seen from the results obtained from the numerical model. The similarity between the bed change of the physical model and the numerical model is very good, with similar scour and deposition patterns that can be seen. Sediment deposition was seen on the inner bank, and scour on the outer bank can be seen on the bed change of both the numerical- and physical models. More deposition can be seen in the numerical model, with a larger area of scour in the physical model. These results can be seen in Figures 83 and 84.

Figure 83: Numerical results of Experiment 1

Figure 84: Physical results of Experiment 1
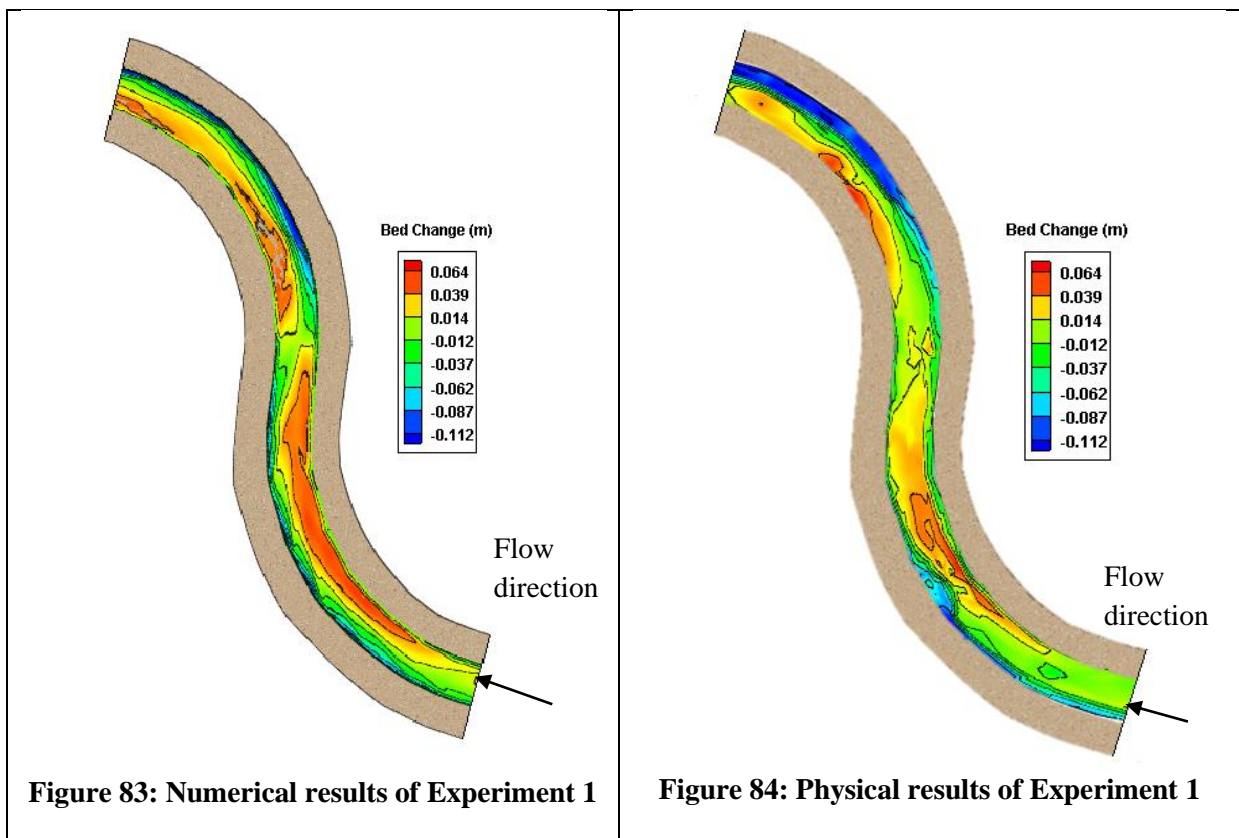
The velocity profile obtained from the numerical model, which can be seen in Figure 85, is as expected, with higher velocities near the outer banks, where scour occurred and lower flow velocities near the inner bank where deposition occurred.
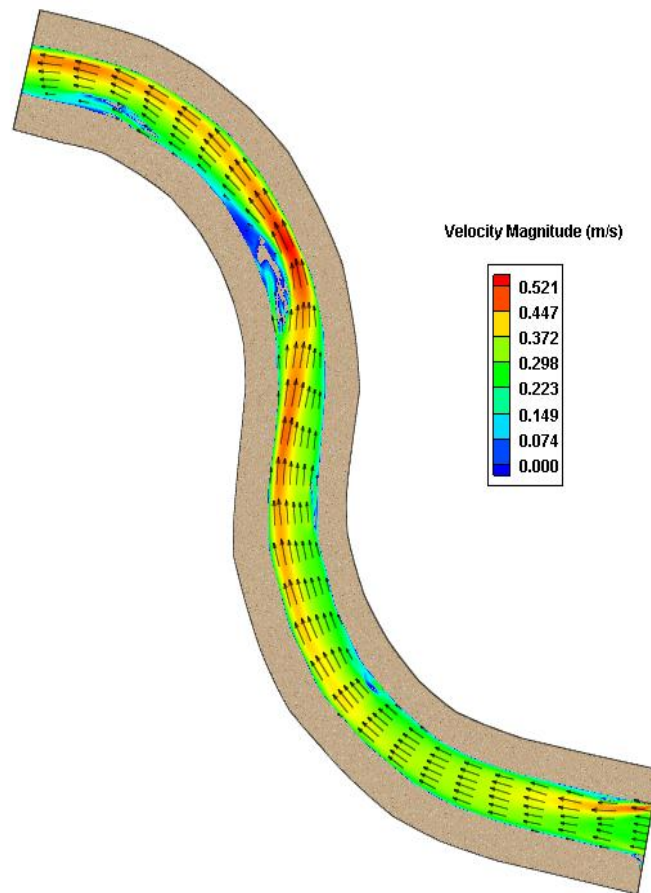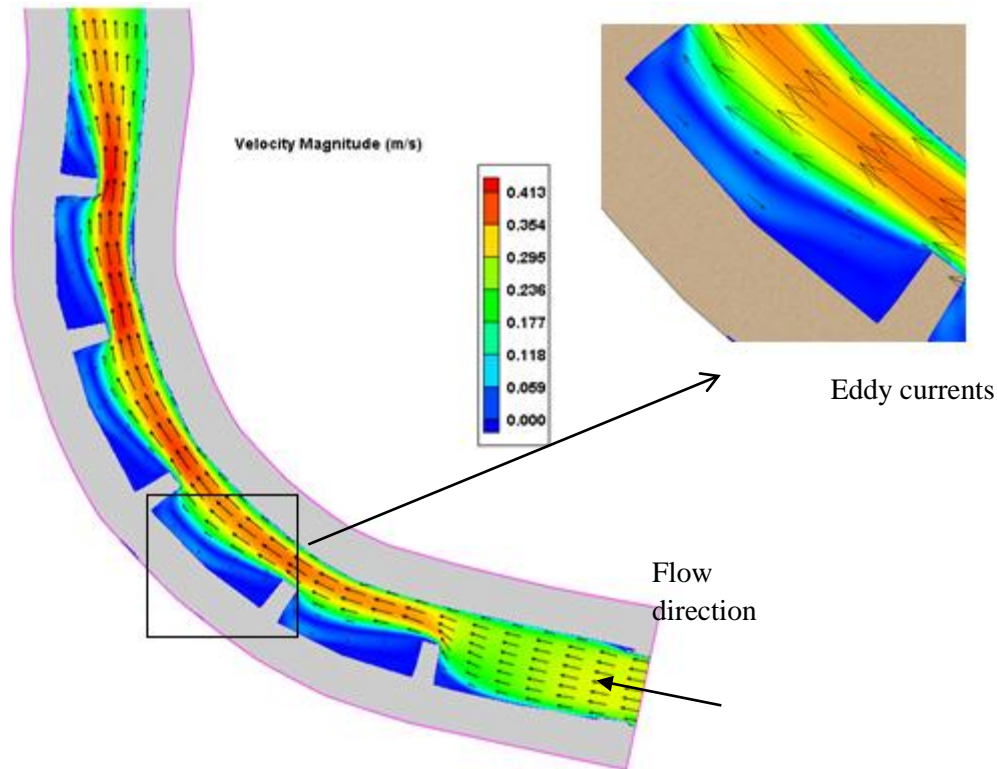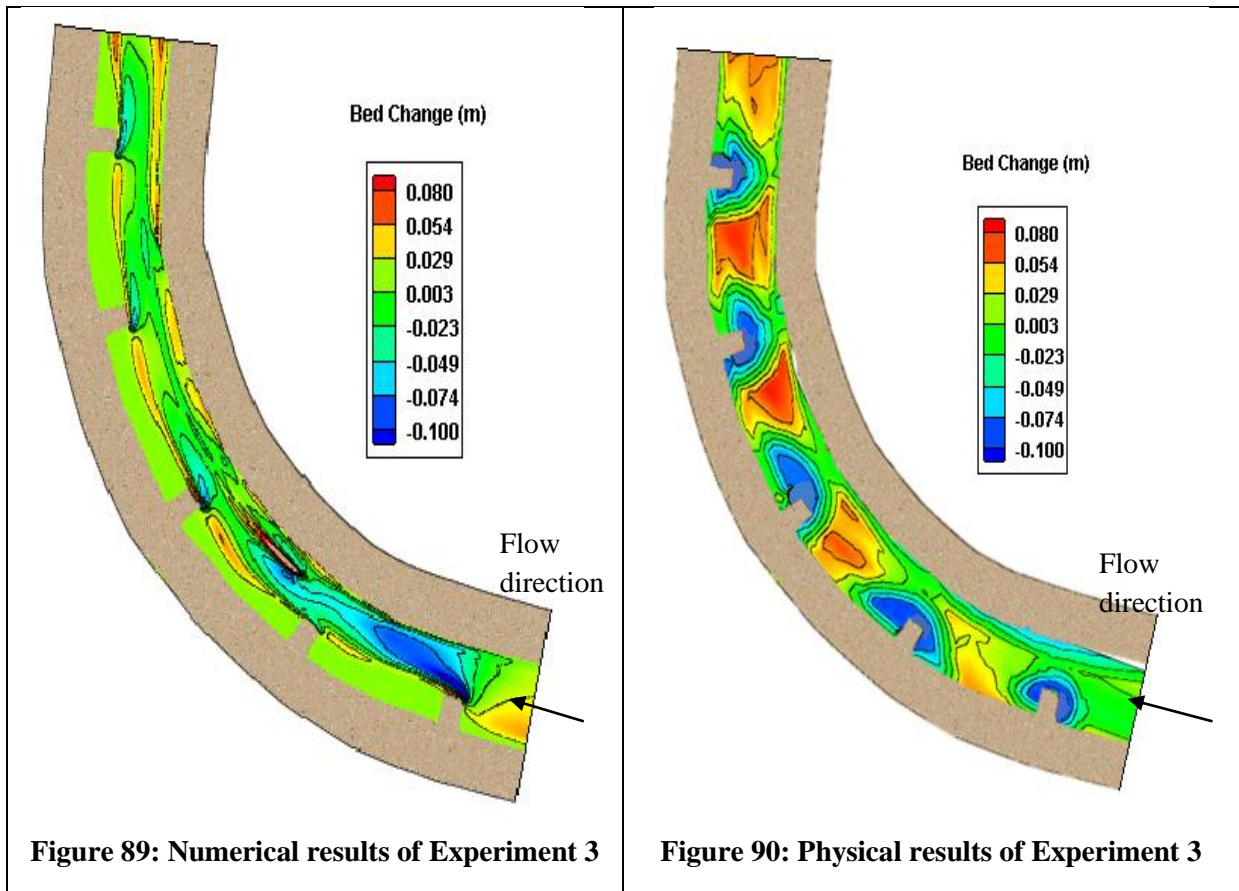
Figure 85: Velocity profile for Experiment 1

4.4.2   Numerical model of Experiment 2 (19 ℓ/s, 5 groynes, 2.3 x projection length)

Simulation 2 was done with 5 groynes installed on the first bend at a spacing of 1.75 m and a projection length of 0.775 m. The spacing between the groynes was therefore 2.3 times the projection length. A discharge of 19 ℓ/s was simulated for a duration of 5 min 41 s, as was observed during the physical model test.   Water depths during the numerical model simulation for measuring points 1, 2, and 3 were 117 mm, 127 mm and 120 mm, respectively. These water depths correlated very well with the observed water depths during the physical experiment which were 115 mm, 123 mm and 120 mm, respectively.

Clear scour holes around the noses of the groynes are visible in both the numerical and physical models. Some deposition can also be seen in the bed elevation of the numerical model on the downstream side of the groynes. The velocity profile seen in the numerical model clearly shows the lower velocities in between the groynes. Slight eddy currents have formed where deposition has occurred. The velocity around the noses of the groynes is seen to be much higher than in the rest of the channel, causing the accentuated scour.

A significant difference in bed change can be seen between the physical and numerical models. The difference can be attributed to the CCHE2D model not simulating secondary streams around the bend, causing deposition to occur almost exclusively on the outer bend downstream of the groyne positions. Bank failure, of both the inner and outer banks, was seen during the physical model experiment, which is not modelled by CCHE2D contributing to a larger area of deposition in the physical model results, with deposition occurring across the entire bed of the river between consecutive groynes. Secondary flow patterns developing around the noses of the groynes, not taken into account in the numerical model also assists in the larger deposition area toward the inner bank for the physical model.

The depth of scour observed during the physical model experiment was 100 mm, therefore the scour was to the bed of the channel. The maximum scour observed for the numerical model was 120 mm, which is more than for the physical model. These results can be seen in Figures 86 and 87.

Figure 86: Numerical results of Experiment 2 | **Figure 87: Physical results of Experiment 2**
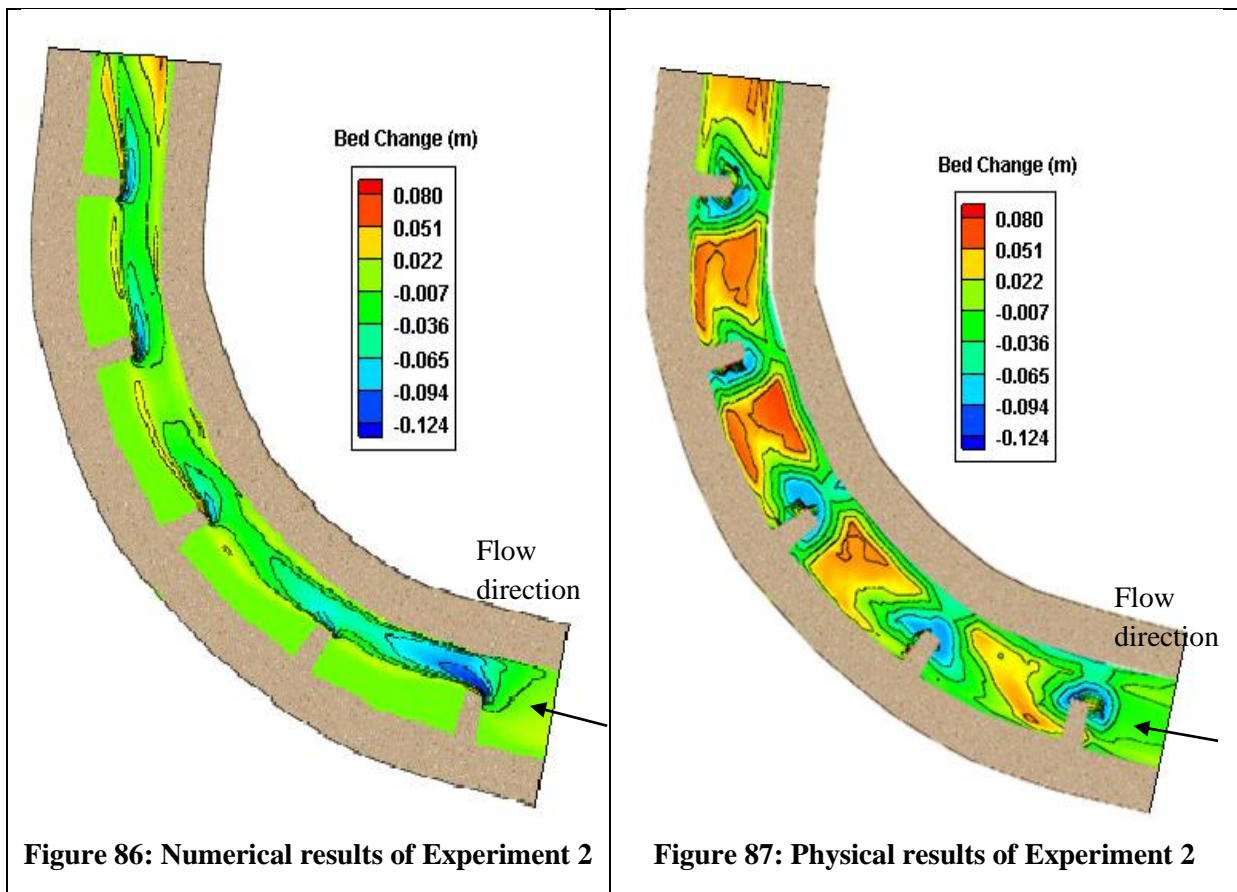
Figure 88 shows the velocity profile obtained through CCHE2D. Low flow zones can be seen near the outer bend between consecutive groynes, as opposed to the high velocities seen for Experiment 1.
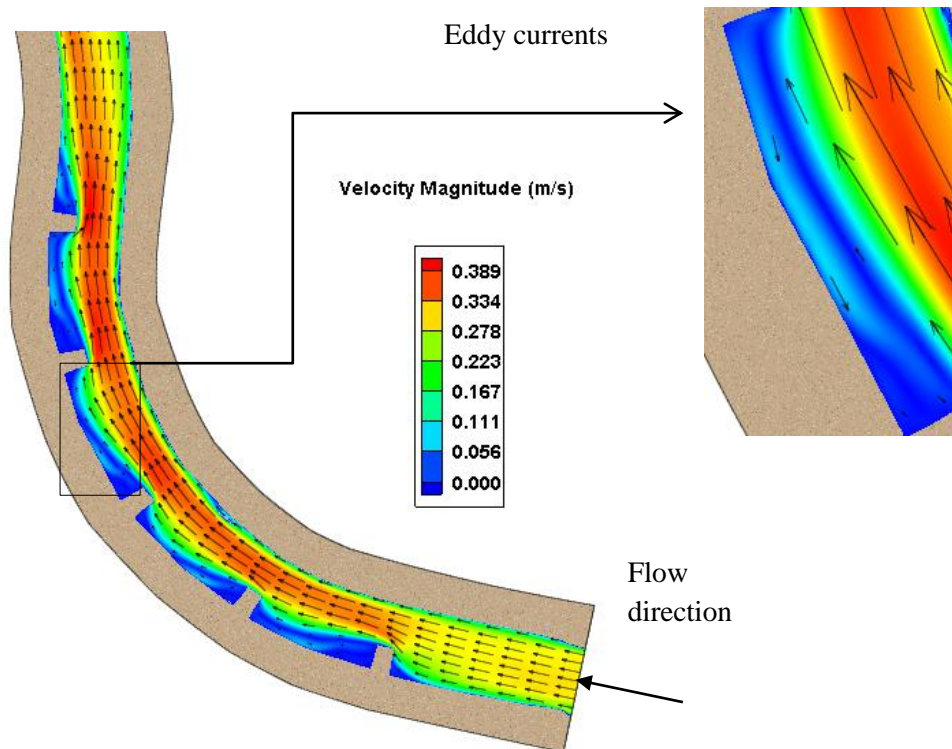
101

Figure 88: Velocity profile for Simulation 2

4.4.3 Numerical model of Experiment 3 (21 ℓ/s, 5 groynes, 2.6 x projection length)

Simulation 3 was done with 5 groynes installed on the first bend at a spacing of 1.75 m and a projection length of 0.675 m. The spacing between the groynes was therefore 2.6 times the projection length. A discharge of 20.5 ℓ/s was simulated for a duration of 5 min 23 s as was observed during the physical model test. Water depths during the numerical model simulation for measuring points 1, 2, and 3 were 108 mm, 110 mm and 120 mm respectively. These water depths are within 10% of the observed water depths during the physical experiment which were 115 mm, 123 mm and 120 mm respectively

Local scour holes around the nose of the groynes were observed in both the numerical- and physical model results. The shape and positioning of the scour holes are similar. Some deposition can be seen downstream of the groyne positions on the outer bank. A scour depth of 100 mm was observed during the physical model experiment compared to the maximum scour depth of 97 mm obtained through the numerical modelling.

A significant difference in bed change can be seen between the physical- and numerical models. The difference can be attributed to the CCHE2D model not simulating secondary streams around the bend and the noses of the groynes. Bank failure experienced for the physical model experiments and the secondary flows resulted in large deposition areas across

the entire river bed. CCHE2D do not account for these aspects, reducing the area of deposition. These results can be seen in Figures 89 and 90.
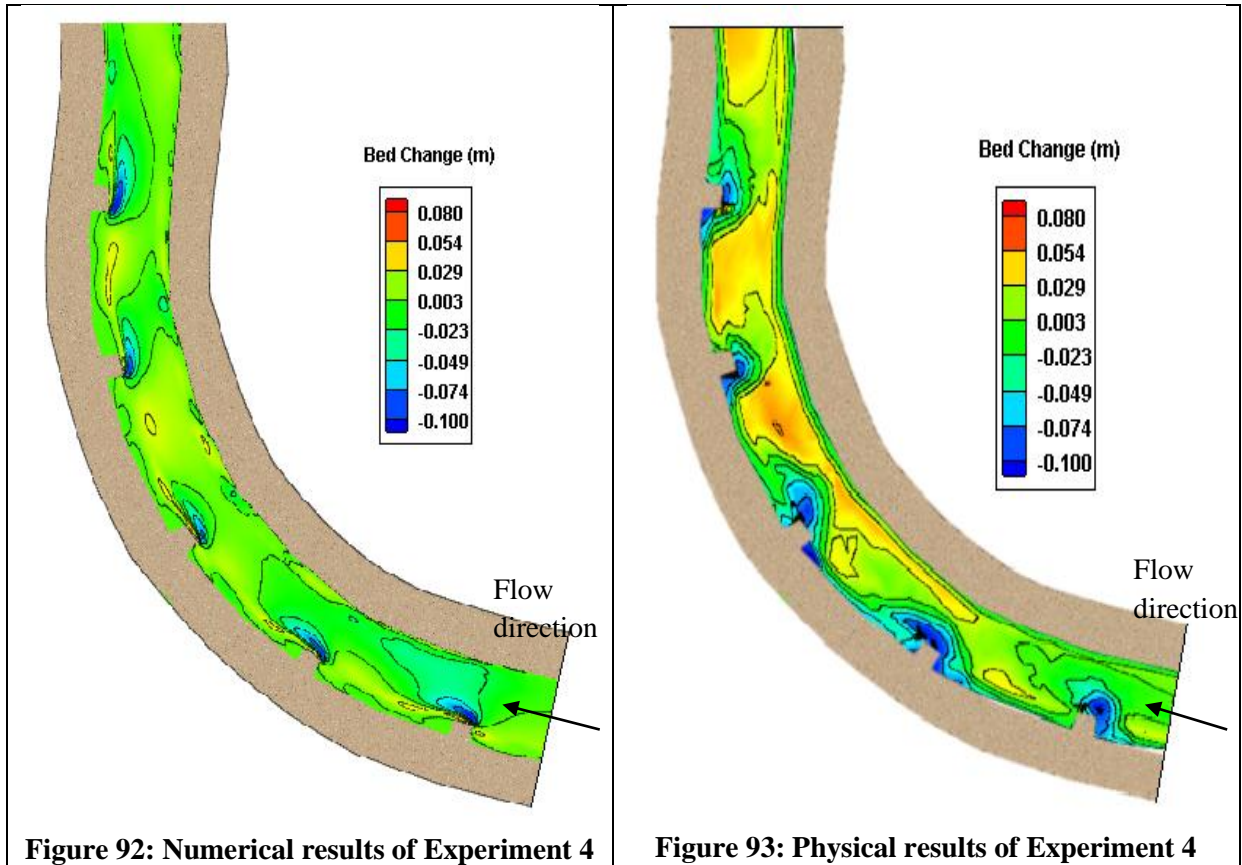

| Figure 89: Numerical results of Experiment 3 | Figure 90: Physical results of Experiment 3 |

From the velocity profile in Figure 91, obtained from the numerical model, it can be seen that eddy currents form in between consecutive groynes. The flow velocity near the outer bank was also much lower than in the main channel, which reduces the potential for scouring to occur on the outer bank.

Figure 91: Velocity profile for Simulation 3

4.4.4   Numerical model of Experiment 4 (19 ℓ/s, 5 groynes, 3.1 x projection length)

Simulation 3 was done with 5 groynes installed on the first bend at a spacing of 1.75 m and a projection length of 0.575 m. The spacing between the groynes was therefore 3.1 times the projection length. A discharge of 18.6 ℓ/s was simulated for a duration of 5 min 47 s, as was observed during the physical model test. Water depths during the simulation for measuring points 1, 2, and 3 were, 109 mm, 121 mm and 120 mm, respectively. These water depths are within 10% of the observed water depths during the physical experiment, which were 115 mm, 122 mm and 120 mm, respectively.

Similar scour holes can be seen around the noses of the groynes in the numerical and physical models. Some deposition close to the outer bank can be seen on both the numerical and physical models. Larger areas experienced sediment deposition in the physical model experiments, as a result of bank failure and secondary flow patterns around the noses of the groynes. CCHE2D does not account for bank failure, which resulted in the smaller areas of deposition, as well as smaller deposition depths.

The depth of scour observed during the physical model experiment was 90 mm. The maximum scour observed for the numerical model was 66 mm, which is less than for the physical model. The above mentioned results can be seen in Figures 92 and 93.

Figure 92: Numerical results of Experiment 4

Figure 93: Physical results of Experiment 4

From the velocity profile in Figure 94 obtained from the numerical model, it can be seen that the effects of the groynes on the flow patterns are very small. The projection length is too small to create enough flow blockages near the outer bank to slow the velocities and prevent scour.
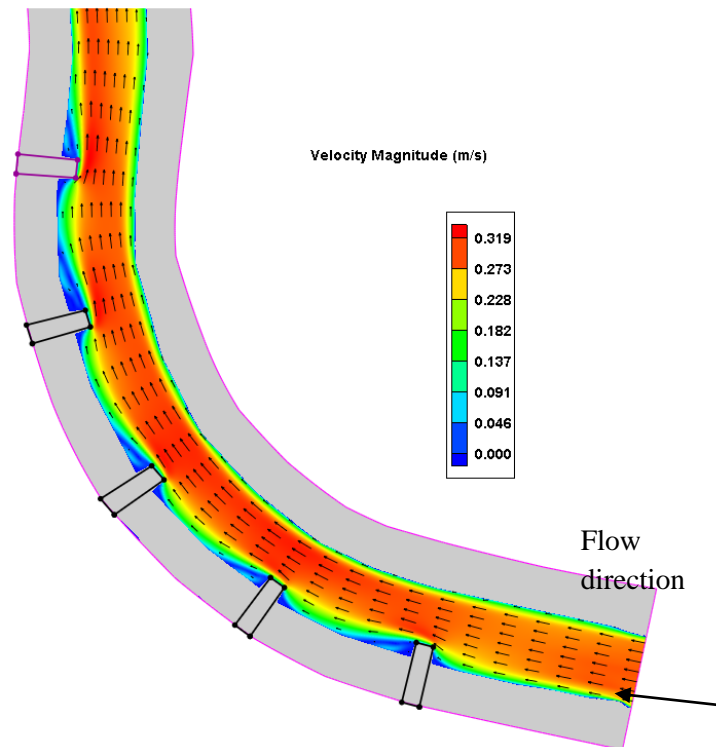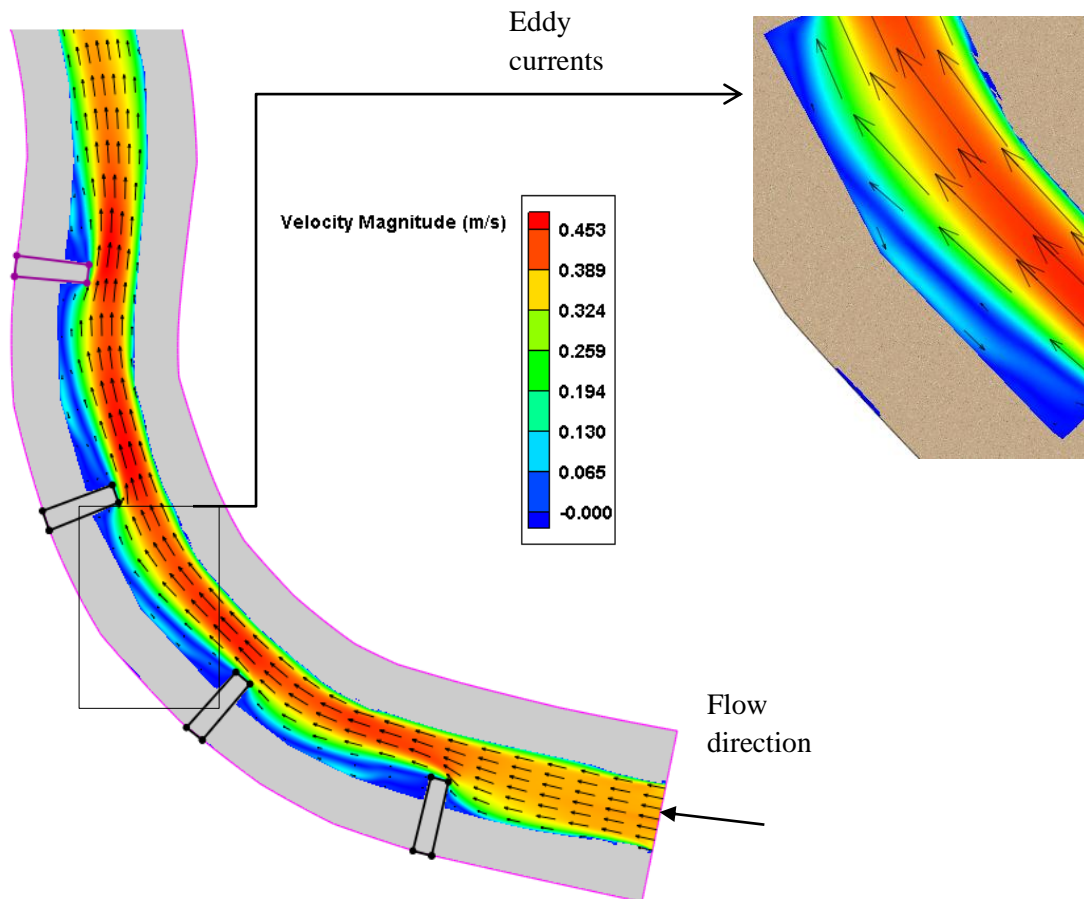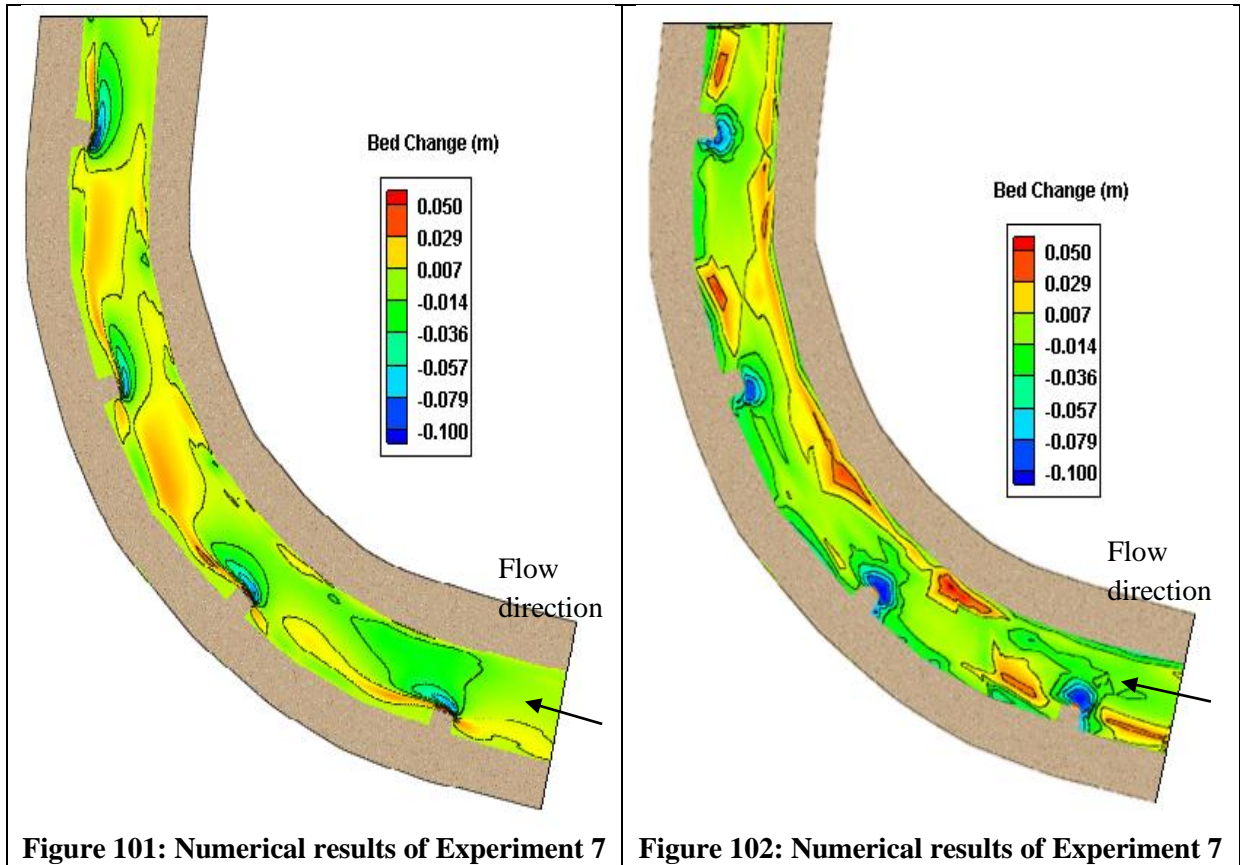
Figure 94: Velocity profile for Simulation 4

4.4.5   Numerical model of Experiment 5 (19 ℓ/s; 4 groynes; 3.0 x projection length)

Simulation 5 was done with 4 groynes installed on the first bend at a spacing of 2.33 m and a projection length of 0.775 m. The spacing between the groynes was therefore 3.0 times the projection length. A discharge of 19 ℓ/s was simulated for a duration of 5 min 9 s, as was observed during the physical model test. Water depths during the simulation for measuring points 1, 2, and 3 were 101 mm, 115 mm and 120 mm, respectively. These water depths are within 10% of the observed water depths during the physical experiment which were 101 mm, 118 mm and 120 mm, respectively.

Clear scour holes can again be seen around the noses of the groynes with a similar shape to the results obtained from the physical experiment. A larger area was scoured in the physical model experiment. Deposition patterns between the numerical and physical models are not consistent. Deposition can be seen downstream of the groynes on the outer banks in both the numerical and physical models. Deposition can be seen on the inner bank of the physical model, which is a result of failure of the inner bank and secondary flow patterns arising from around the noses of the groynes, which CCHE2D does not account for. The maximum depth of scour observed during the physical experiment was 100 mm, as the sediment was scoured to the channel bed. The maximum scour observed for the numerical model was 138 mm, which was more than the physical model.

These results can be seen in Figures 95 and 96.

Figure 95: Numerical results of Experiment 5

Figure 96: Physical results of Experiment 5
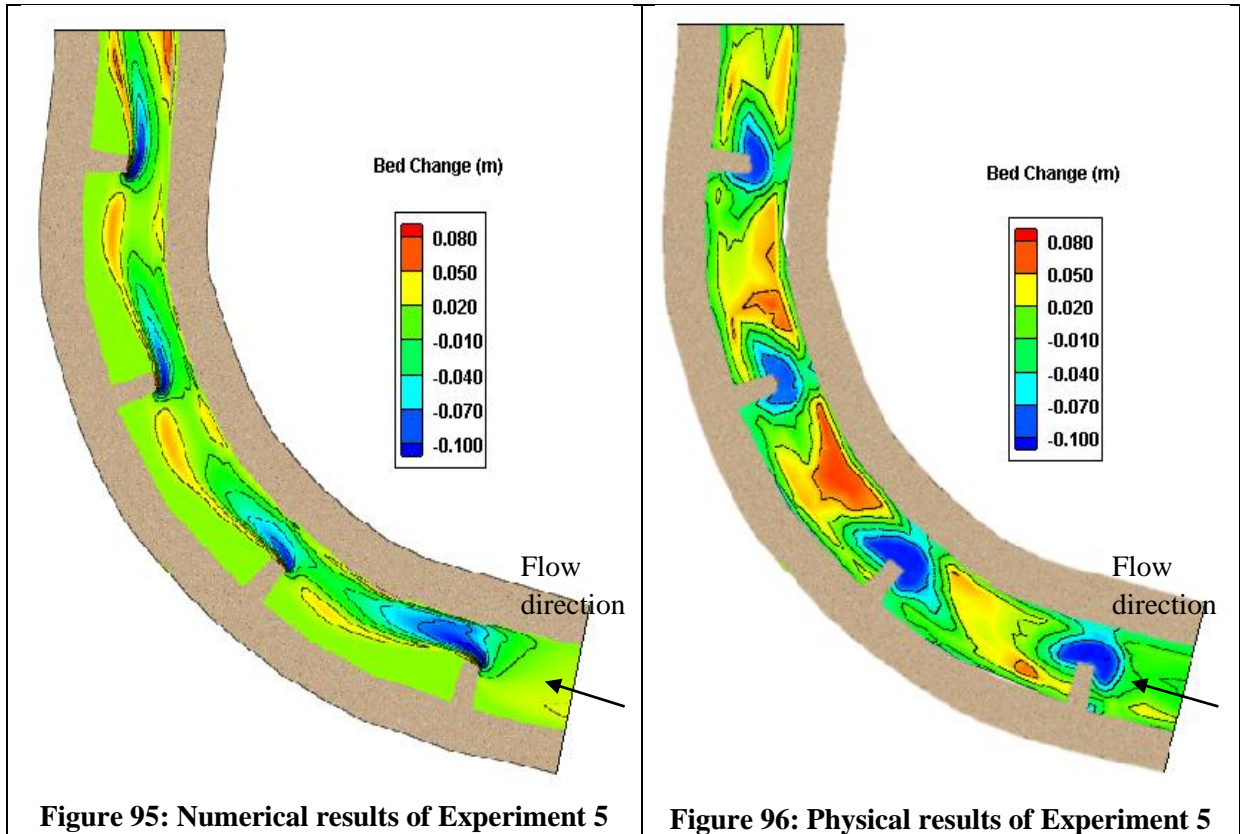
Figure 97 shows the velocity profile obtained from the numerical model. Low flow zones are observed near the outer riverbank, where recirculation of flow occurs due to the effect of the groynes on the patterns. This is in comparison with Experiment 1, where no groynes were present and high flow velocities were observed close to the outer riverbank.
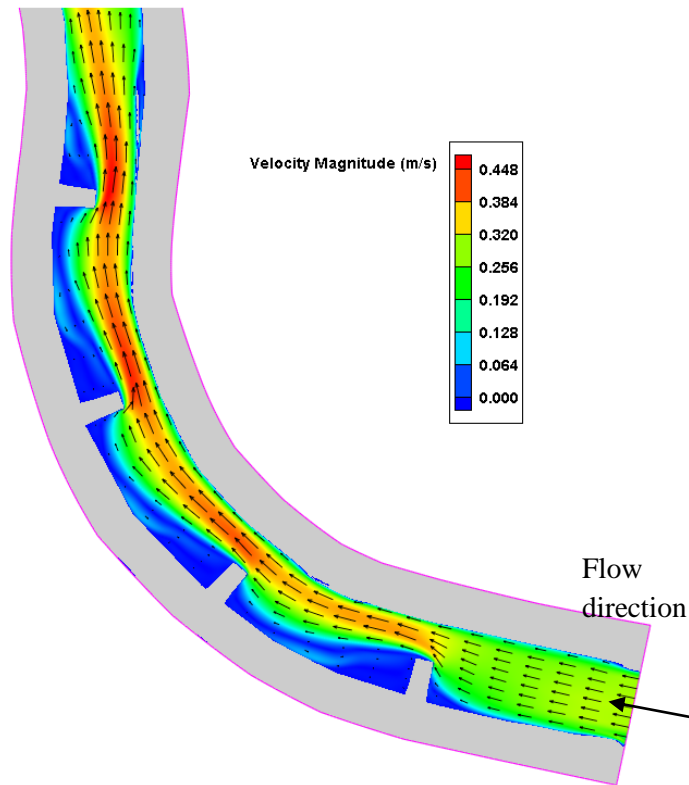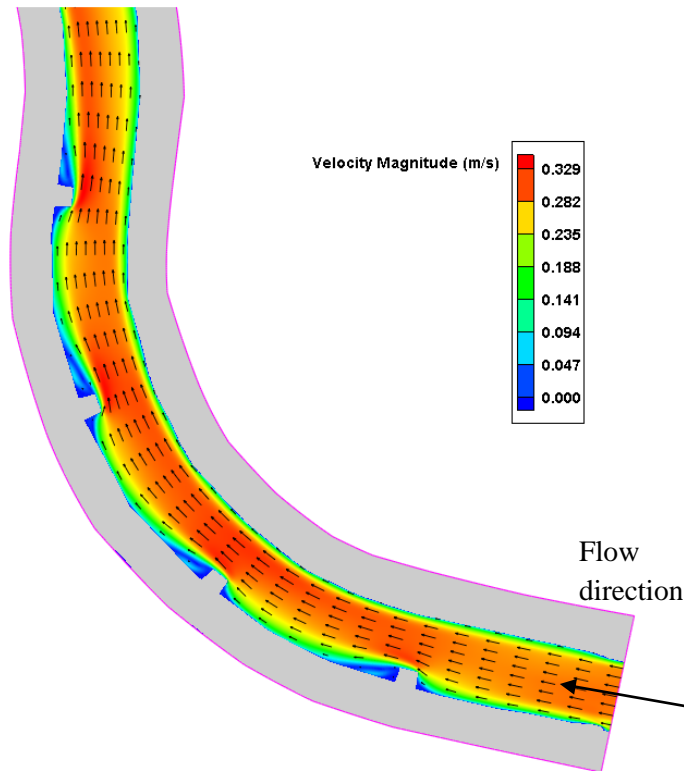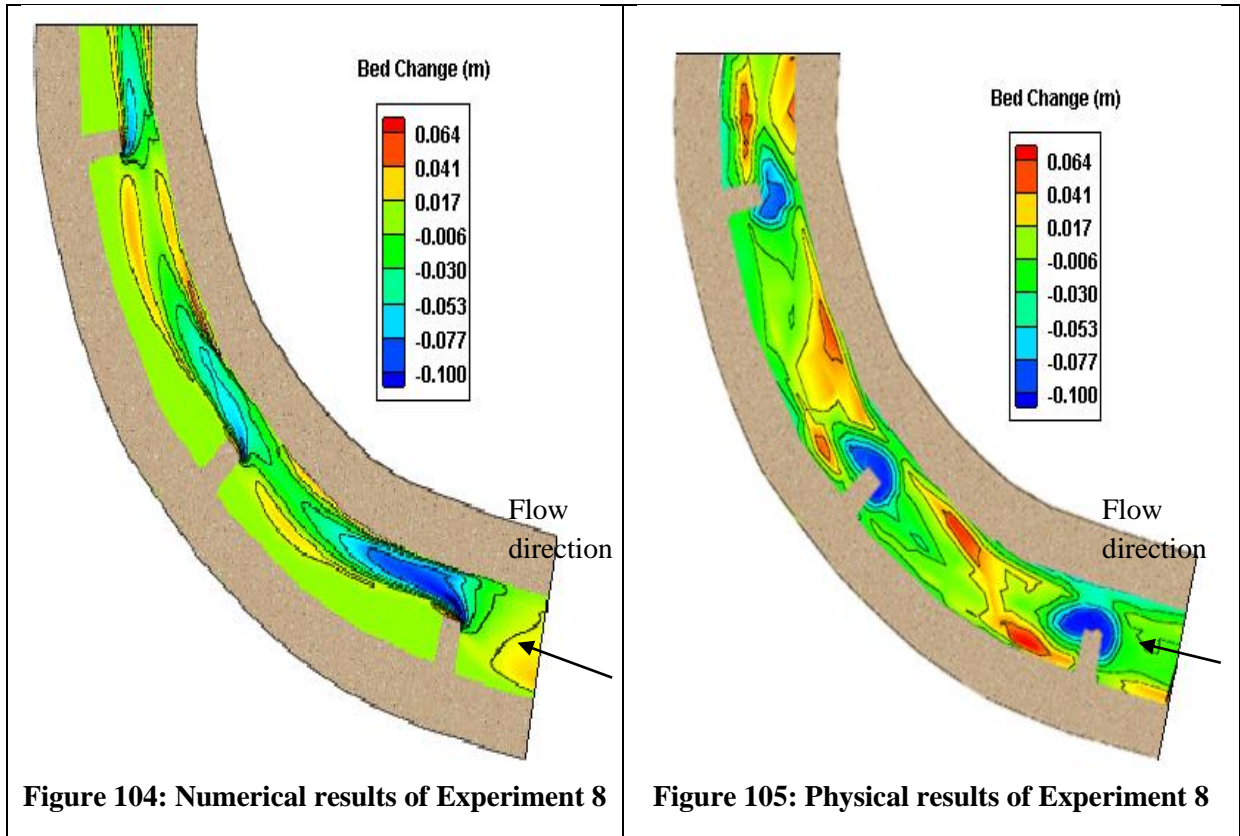
Figure 97: Velocity profile for Simulation 5

4.4.6   Numerical model of Experiment 6 (18 ℓ/s; 4 groynes; 3.5 x projection length)

Simulation 6 was done with 4 groynes installed on the first bend at a spacing of 2.33 m and a projection length of 0.675 m. The spacing between the groynes was therefore 3.5 times the projection length. A discharge of 18.2 ℓ/s was simulated for a duration of 6 min 0 s, as was observed during the physical model test. Water depths during the simulation for measuring points 1, 2, and 3 were 93mm, 108 mm and 120mm, respectively. These water depths are within 10% of the observed water depths during the physical experiment which were 103 mm, 115 mm and 120 mm, respectively.

Scour patterns around the noses of the groynes are similar in both the numerical and physical models. Some deposition was seen on the outer banks, just downstream of the groynes' positions. Limited bank failure was observed on the inner bend for the physical model testing, resulting in deposition on the inner bend. CCHE2D does not account for bank failure or the development of secondary flow patterns around the noses of the groynes, resulting in the lack of deposition on the inner bend of the numerical model. The depth of scour during the physical experiment was 100 mm onto the channel bed. The maximum scour obtained from the numerical model was 85 mm. These results can be seen in Figures 98 and 99.

| Figure 98: Numerical results of Experiment 6 | Figure 99: Physical results of Experiment 6 |
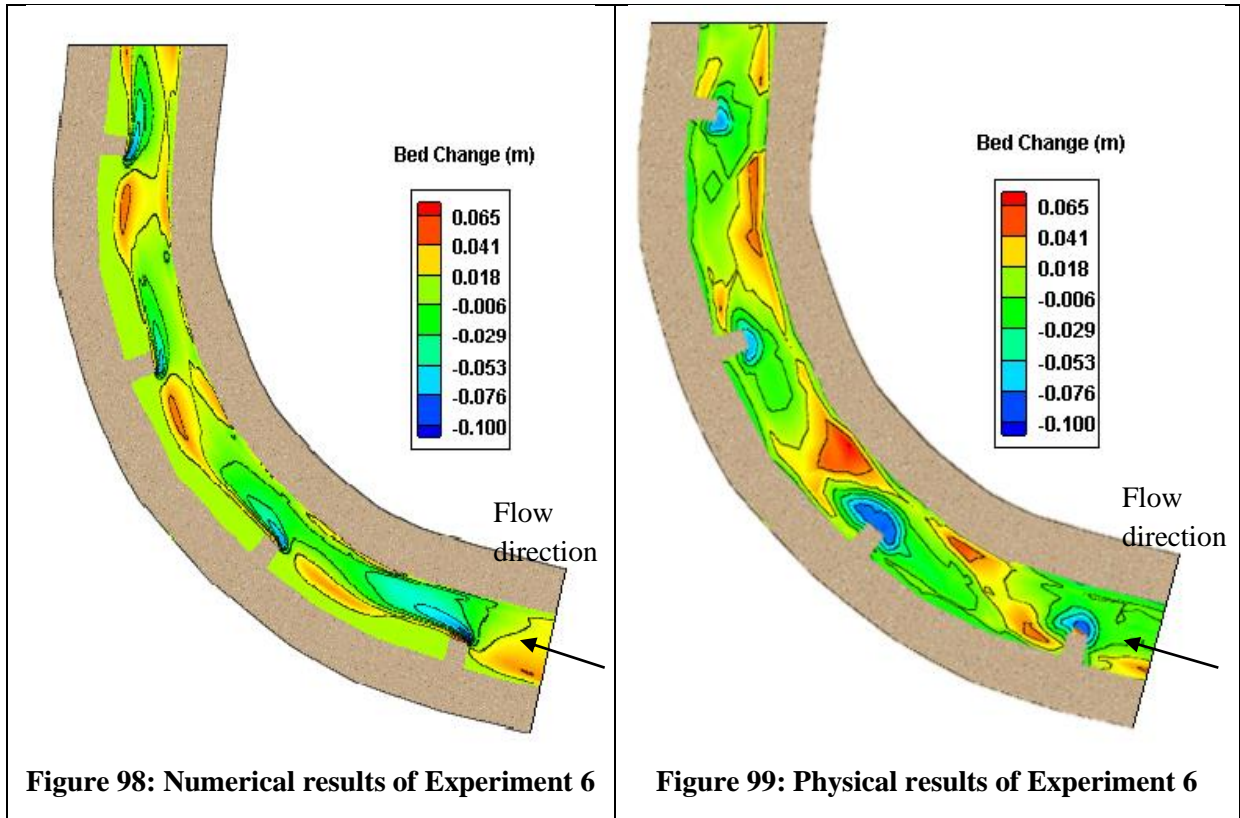
Areas with low flow velocities near the outer banks can be seen from the velocity profile for Experiment 6, obtained from the numerical model, in Figure 100.   The effect of the groynes on the flow patterns reduces the potential for scour to occur on the outer bend, and promotes sediment deposition. These flow patterns are consistent with observed flow patterns for the physical experiment.
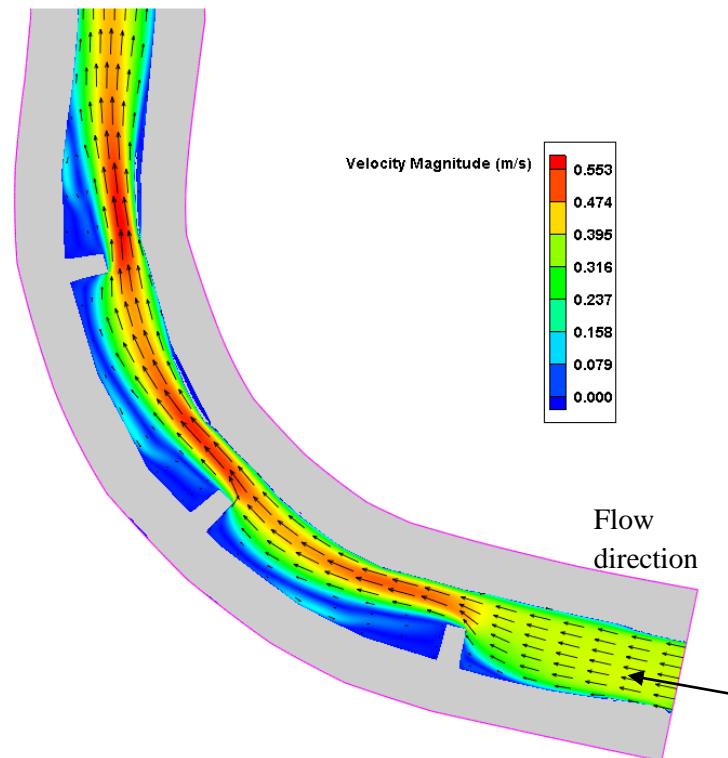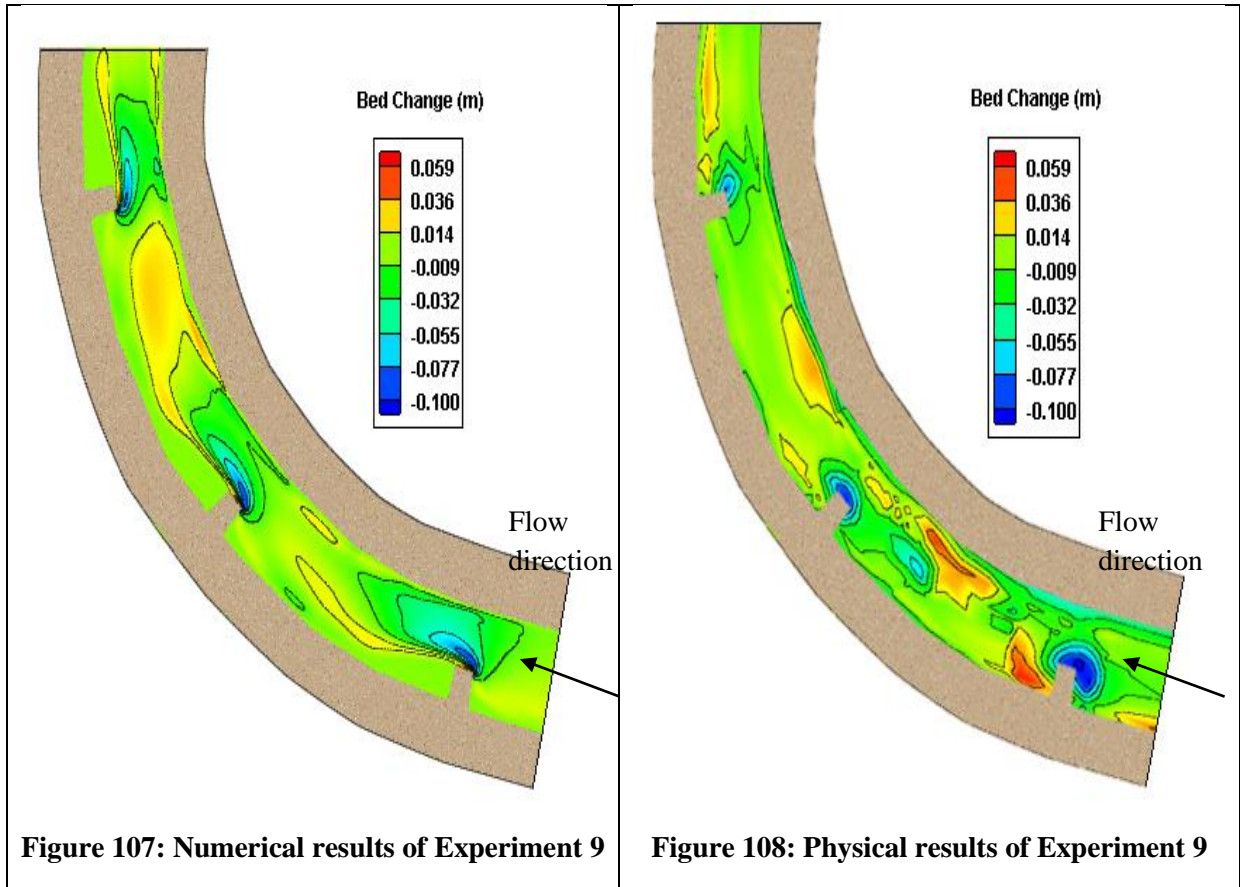
Figure 100: Velocity profile for Simulation 6

4.4.7 Numerical model of Experiment 7 (19 ℓ/s; 4 groynes; 2.3 x projection length)

Simulation 7 was done with 4 groynes installed on the first bend at a spacing of 2.33 m and a projection length of 0.575 m. The spacing between the groynes was therefore 4.1 times the projection length. A discharge of 19.4 ℓ/s was simulated for a duration of 6 min 46 s, as was observed during the physical model test. Water depths during the simulation for measuring points 1, 2, and 3 were 111 mm, 122 mm and 120 mm, respectively. These water depths are within 10% of the observed water depths during the physical experiment which were 101 mm, 118 mm and 120 mm, respectively.

Similar local scour around the noses of the groynes can be seen in both the numerical and physical models. Some deposition can be seen downstream of the groynes, the deposition is however very small. As bank failure decreases in the physical model, the correlation between results from the numerical and physical models increases. During the physical experiment a scour depth of 100 mm was observed. The maximum scour obtained from the numerical model test was 80 mm. These results can be seen in Figures 101 and 102.

Figure 101: Numerical results of Experiment 7 | **Figure 102: Numerical results of Experiment 7**

From the velocity profile in Figure 103 it is observed that the projection lengths of the groynes are too short. The groynes offer limited protection in terms of slowing the flow rate near the outer banks, compared to longer projection lengths. Flow velocities observed near the outer bank are lower than those observed for Experiment 1.

Velocity Magnitude (m/s)
0.329
0.282
0.235
0.188
0.141
0.094
0.047
0.000

Flow direction

Figure 103: Velocity profile for Simulation 7

4.4.8   Numerical model of Experiment 8 (19 ℓ/s; 3 groynes; 2.8 x projection length)

Simulation 8 was done with 3 groynes installed on the first bend at a spacing of 2.83 m and a projection length of 0.775 m. The spacing between the groynes was therefore 3.7 times the projection length. A discharge of 18.8 ℓ/s was simulated for a duration of 4 min 41 s, as was observed during the physical model test. Water depths during the simulation for measuring points 1, 2, and 3 were 101 mm, 116 mm and 120 mm, respectively. These water depths are within 10% of the observed water depths during the physical experiment which were 108 mm, 112 mm and 120 mm, respectively.

Local scour holes around the noses of the groynes were seen in both the numerical and physical models. Longer scour patterns was observed for the numerical model, with smaller area of deposition. Deposition on the inner bend of the physical model was observed as a result of failure of the inner bank and the development of secondary flow patterns around the noses of the groynes, which is not simulated in CCHE2D. Deposition could be seen downstream of the groynes close to the outer bank in both models. A maximum scour depth of 100 mm was observed during the physical model experiment, compared to a maximum scour depth of 102 mm observed in the numerical model. These results can be seen in Figure 104 and 105.
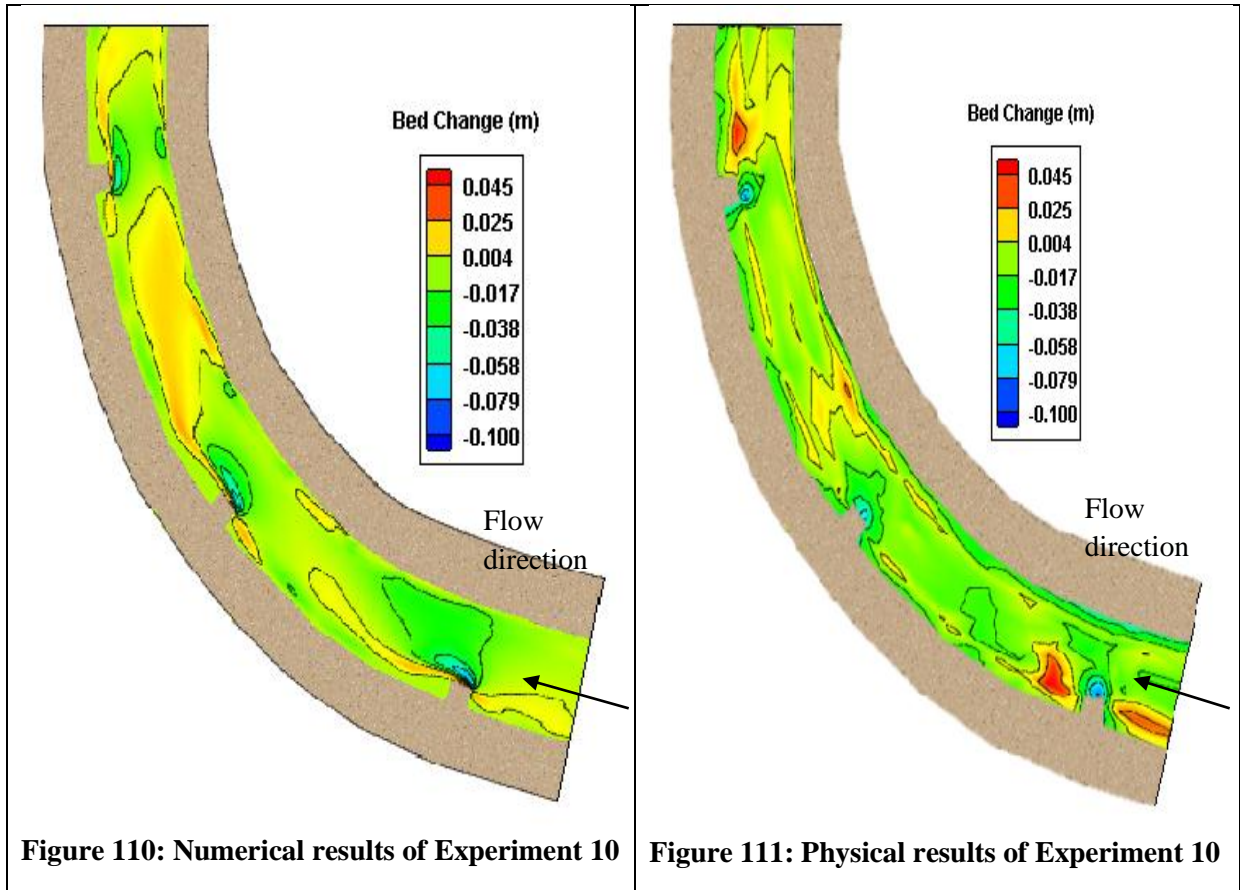
| **Figure 104: Numerical results of Experiment 8** | **Figure 105: Physical results of Experiment 8** |

From Figure 106 the velocity profile shows that eddy currents do form between consecutive groynes. The formation of an S-shaped velocity profile between consecutive groynes can be seen as a result of the flow resuming normal flow conditions due to greater spacing between the groynes.
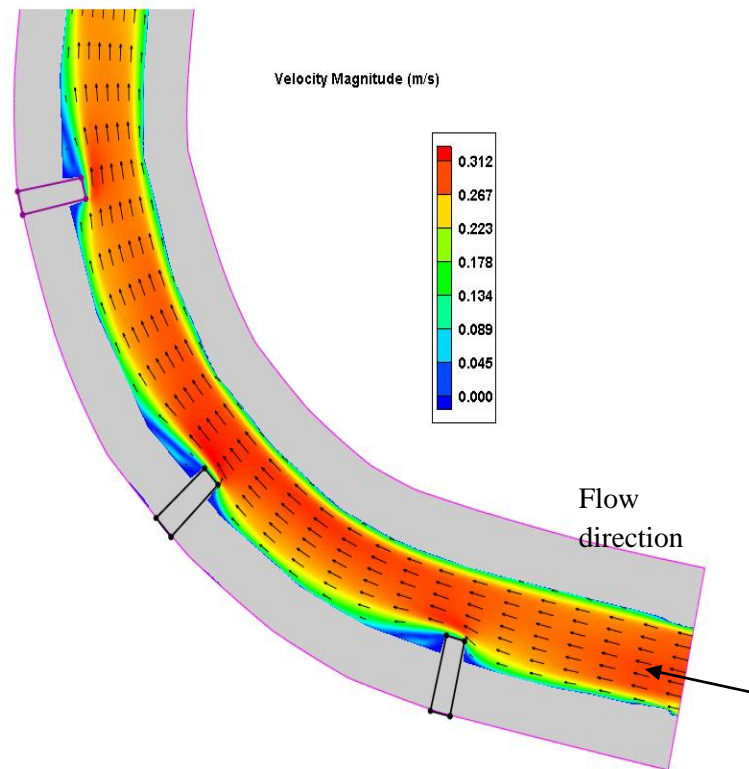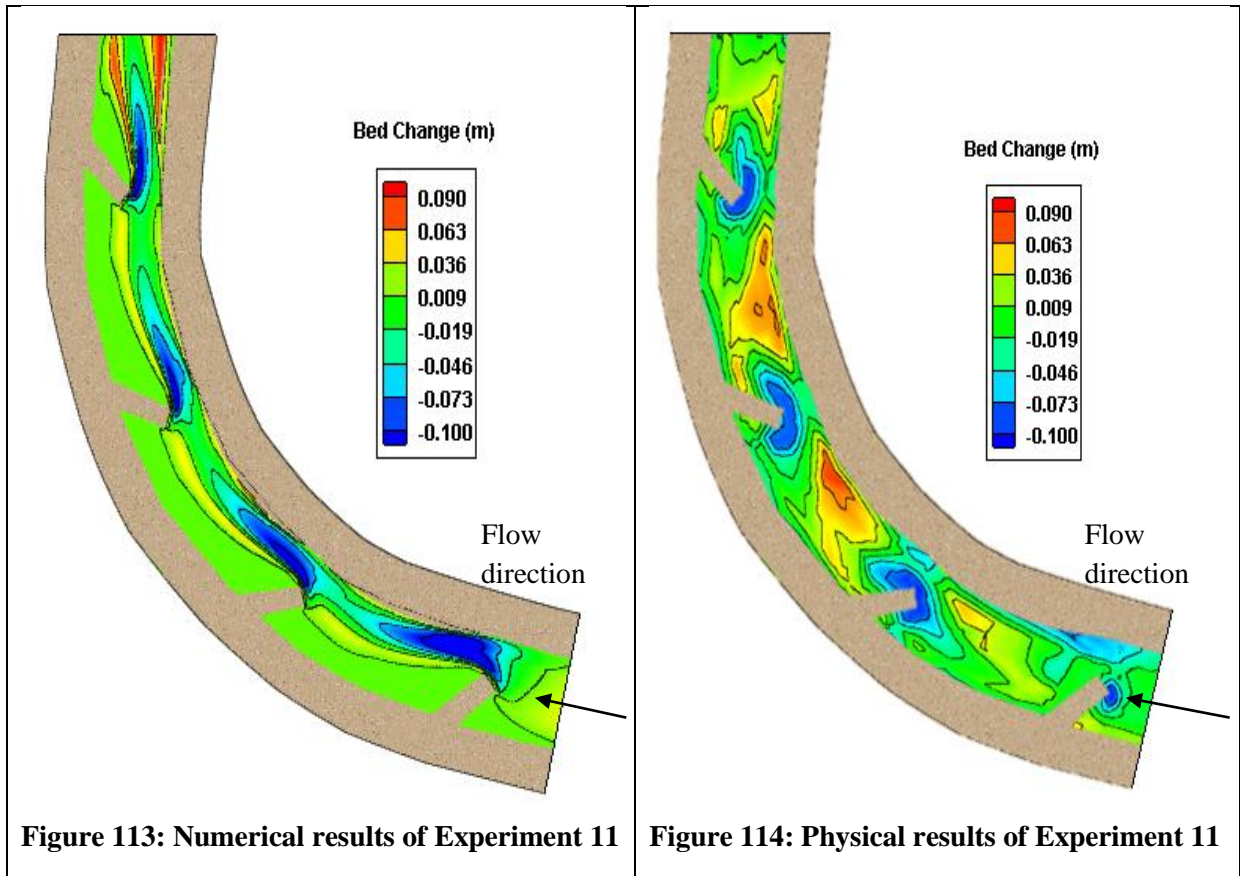
Figure 106: Velocity profile for Simulation 8

4.4.9   Numerical model of Experiment 9 (18 ℓ/s; 3 groynes; 4.2 x projection length)

Simulation 9 was done with 3 groynes installed on the first bend at a spacing of 2.83 m and a projection length of 0.675 m. The spacing between the groynes was therefore 4.2 times the projection length. A discharge of 17.5 ℓ/s was simulated for a duration of 5,min 1,s, as was observed during the physical model test. Water depths during the simulation for measuring points 1, 2, and 3 were 109 mm, 120 mm and 120 mm, respectively. These water depths are within 10% of the observed water depths during the physical experiment which were 108 mm, 112 mm and 120 mm, respectively.

Local scour patterns around the noses of the groynes are consistent for the numerical and the physical model results. Some deposition of sediment can be seen downstream of the groynes. Bank failure occurred on the inner bend across from the groyne positions, causing more deposition in the physical model than in the numerical model. The maximum scour depth observed during the physical model experiment was 100 mm compared to the maximum scour depth obtained from the numerical model which was 93 mm. These results can be seen in Figures 107 and 108.

Figure 107: Numerical results of Experiment 9 | **Figure 108: Physical results of Experiment 9**

From Figure 109, the velocity profile shows that the spacing between the groynes is too great for the given projection length. Only one small eddy current is seen directly downstream of the groynes, after which the velocity at the outer banks increases, causing a reduction in scour protection.
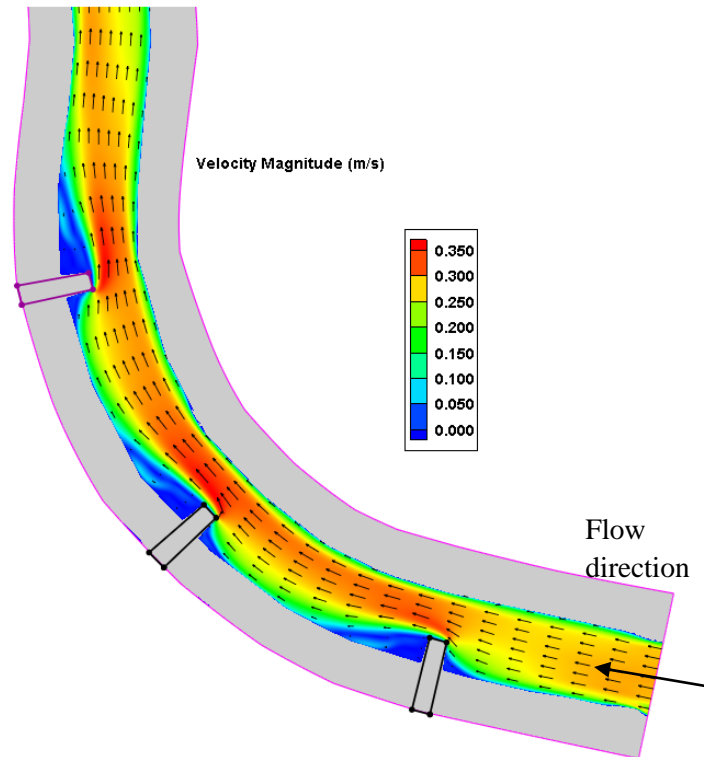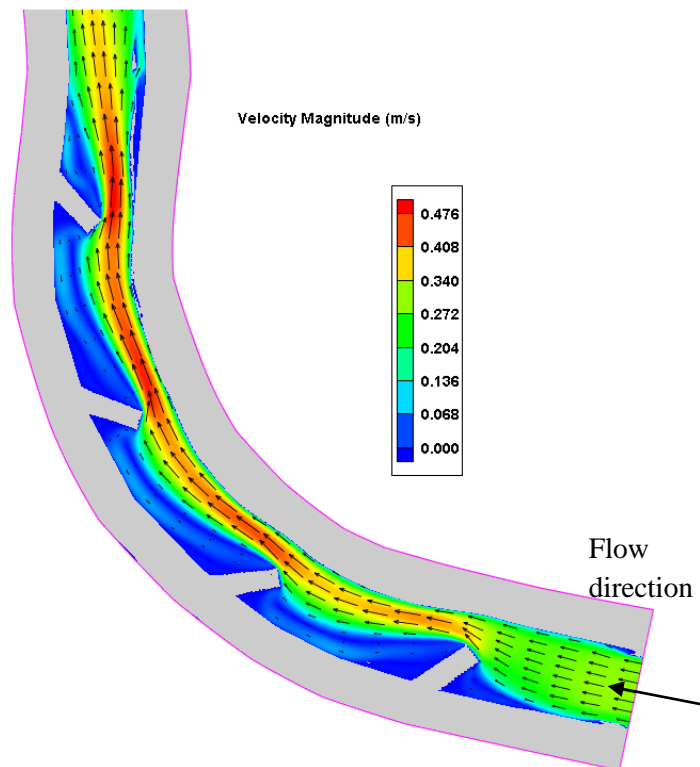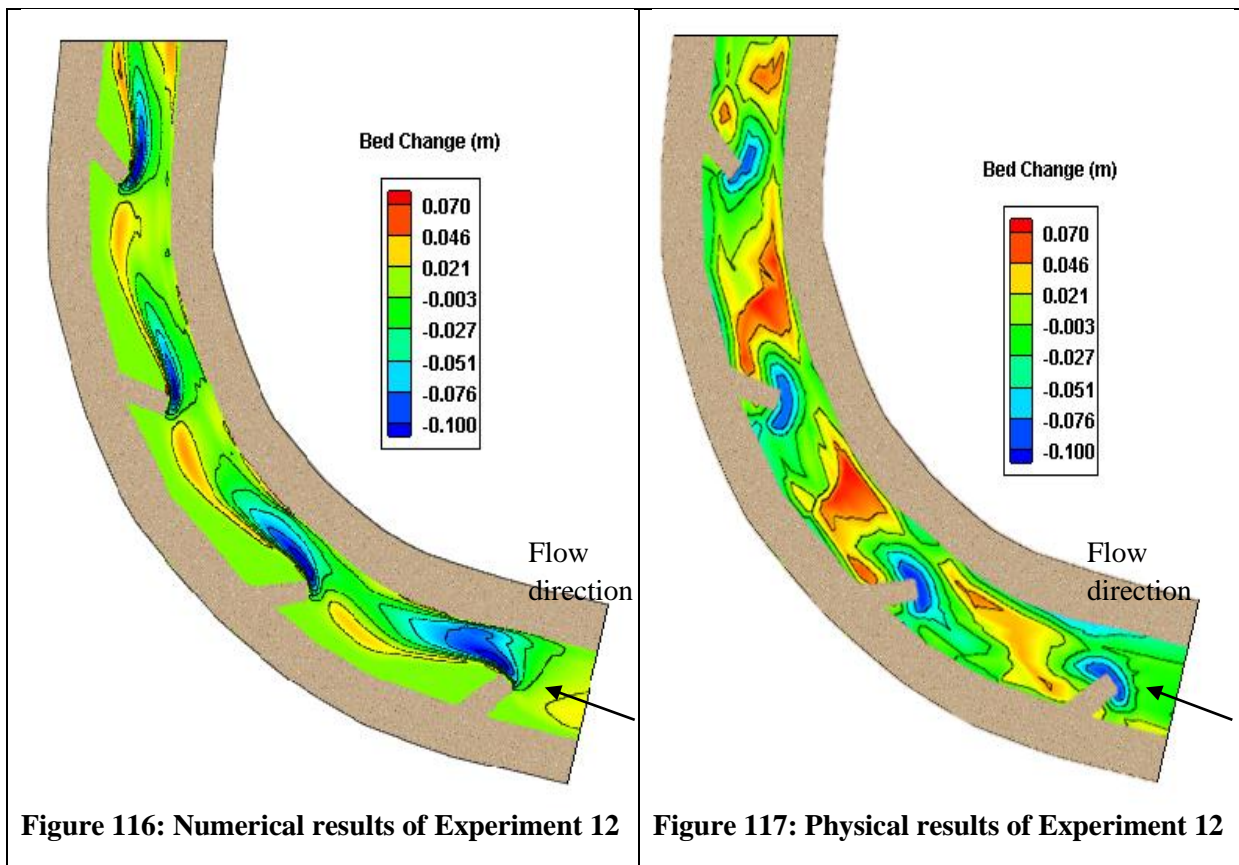
Figure 109: Velocity profile for Simulation 9

4.4.10 Numerical model of Experiment 10 (18 ℓ/s; 3 groynes; 4.9 x projection length)

Simulation 10 was done with 3 groynes installed on the first bend at a spacing of 2.83 m and a projection length of 0.575 m. The spacing between the groynes was therefore 4.9 times the projection length. A discharge of 18 ℓ/s was simulated for a duration of 5 min 54 s, as was observed during the physical model test. Water depths during the simulation for measuring points 1, 2, and 3 were 107 mm, 119 mm and 120 mm, respectively. These water depths are within 10% of the observed water depths during the physical experiment which were 106 mm, 123mm and 120 mm, respectively.

Local scour holes around the noses of the groynes were observed in both the numerical and physical models. A very good correlation is found between the bed change of the both models. Very little sediment deposition is found downstream of the groynes in both models. Longer deposition patterns are observed in the numerical model results, when compared to the physical model. The scour depth observed during the physical model experiment was 80 mm, compared to the maximum scour depth of 66 mm in the numerical model. These results can be seen in Figures 110 and 111.

Figure 110: Numerical results of Experiment 10 | **Figure 111: Physical results of Experiment 10**

In Figure 112, the velocity profile shows that the groynes have a limited effect on slowing the flow velocity close to the outer bank. Small areas of low flow velocity are observed just downstream of the groynes as a result of the groynes. The projection length is, however, too short to provide comprehensive scour protection at this spacing.
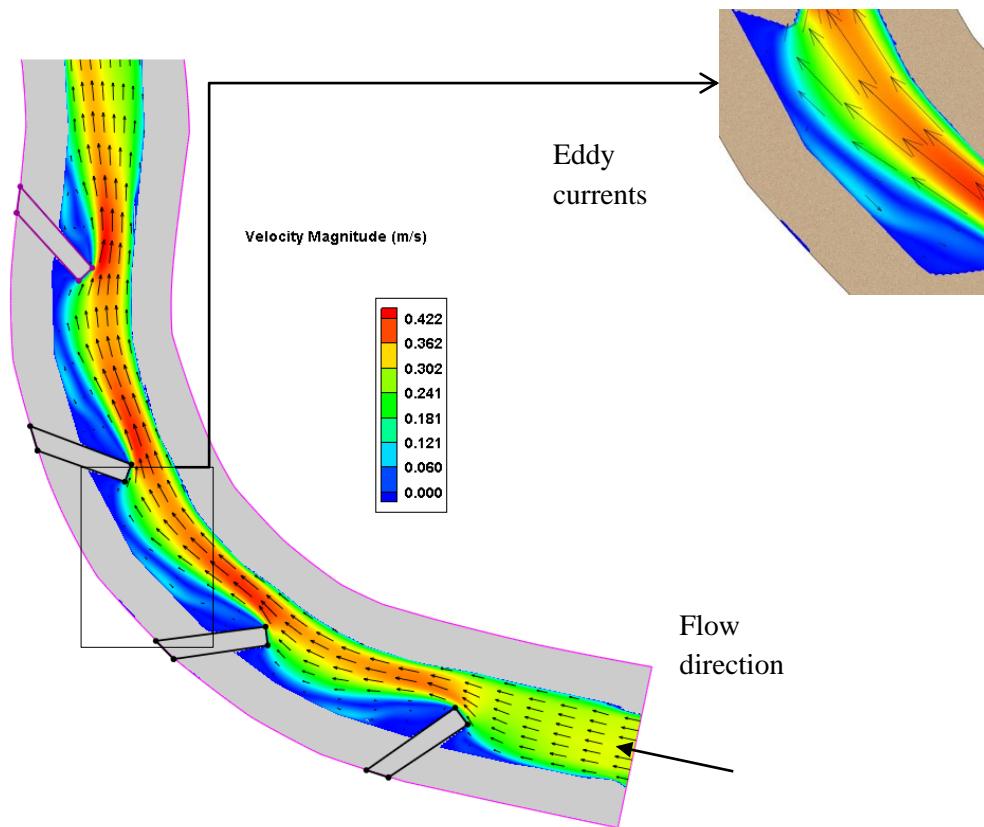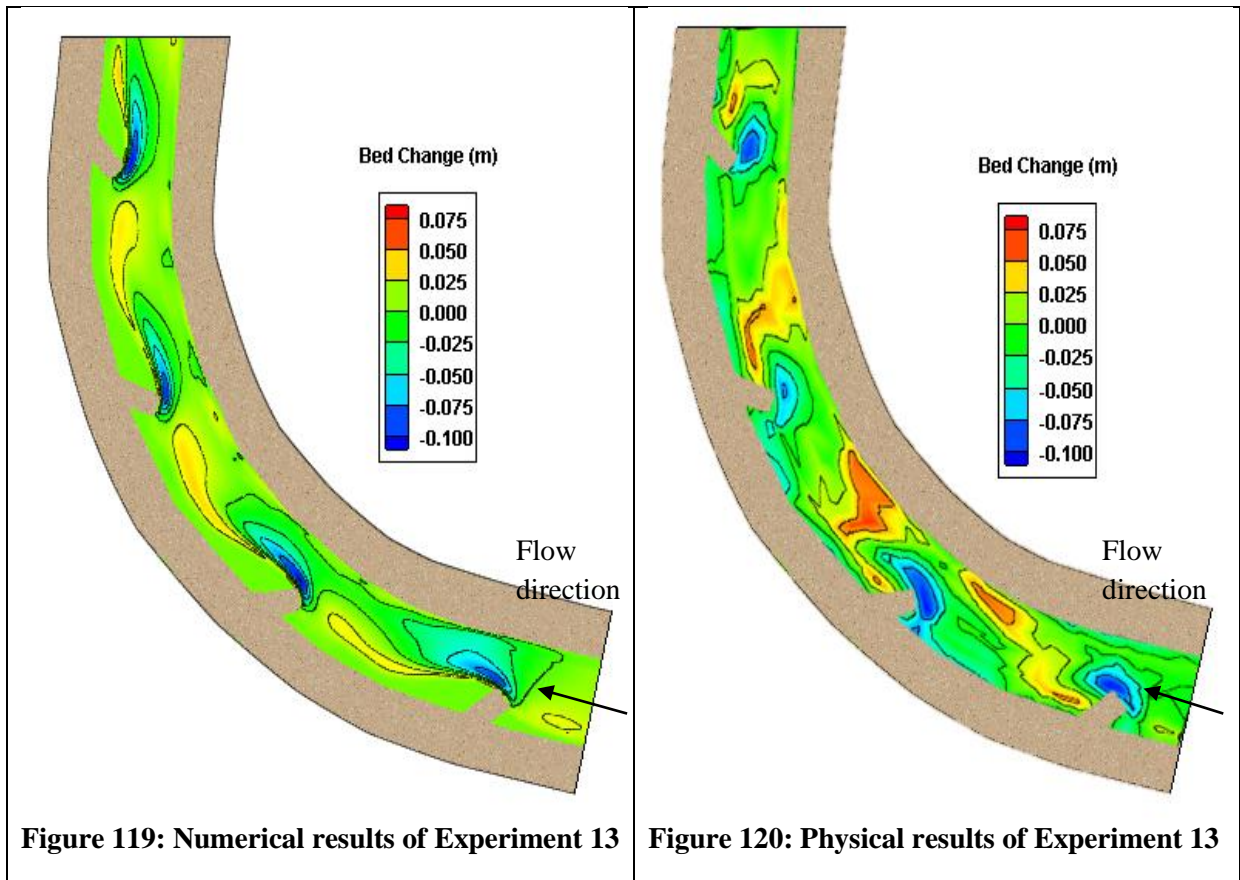
117

Figure 112: Velocity profile for Simulation 10

4.4.11 Numerical model of Experiment 11 (18 ℓ/s; 4 groynes; 3.0 x projection length)

Simulation 11 was done with 4 groynes installed at an angle of 45° with regards to the flow direction on the first bend with a spacing of 2.33 m and a projection length of 0.775 m. The spacing between the groynes was therefore 3.0 times the projection length. A discharge of 18.2 ℓ/s was simulated for a duration of 4min 42s, as was observed during the physical model test. Water depths during the simulation for measuring points 1, 2, and 3 were 125 mm, 128 mm and 120 mm, respectively. These water depths are within 10% of the observed water depths during the physical experiment which were 118 mm, 124 mm and 120 mm, respectively.

Local scour around the noses of the groynes was observed for both the numerical- and the physical models. The numerical model showed a more elongated scour profile when compared to the physical model. Deposition areas could be seen downstream of the groynes. Bank failure occurred on the inner bend during the physical model experiment, as well as the development of secondary flow patterns from around the noses of the groynes resulting in sediment deposition toward the inner bank between consecutive groynes. Deposition on the inner bend is not seen in the numerical model, as CCHE2D does not take for bank failure or secondary flow patterns into account. A maximum scour depth of 130 mm was found in the numerical model compared to the 100 mm of scour observed during the physical model experiment.

These results can be seen in Figures 113 and 114.

Figure 113: Numerical results of Experiment 11 | **Figure 114: Physical results of Experiment 11**

In Figure 115, the velocity profile shows clear eddy currents that formed between consecutive groynes, causing lower flow velocities close to the outer bank. Recirculation did, however, occur at a higher velocity than observed for experiments with perpendicular groyne orientation, explaining the scour observed at the outer bank during the physical model experiment.
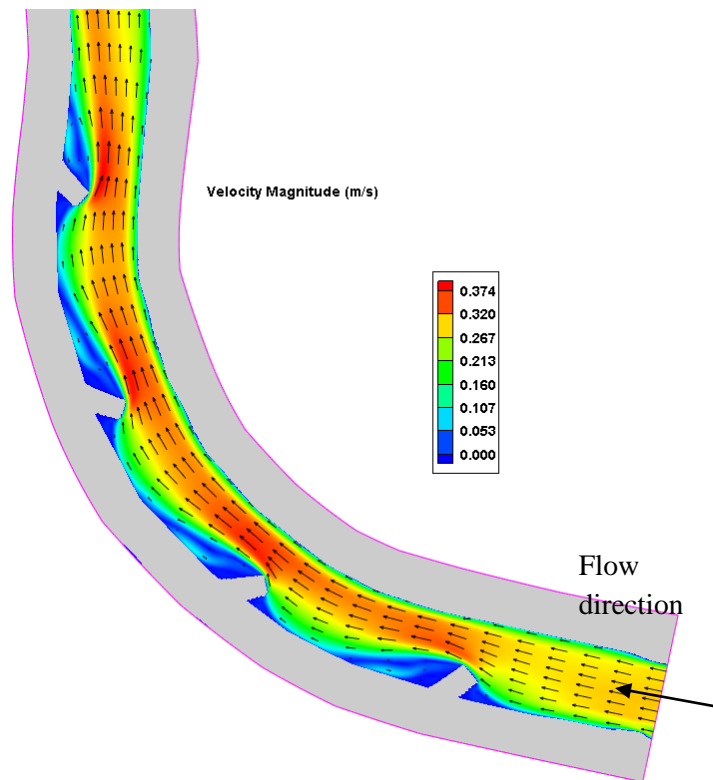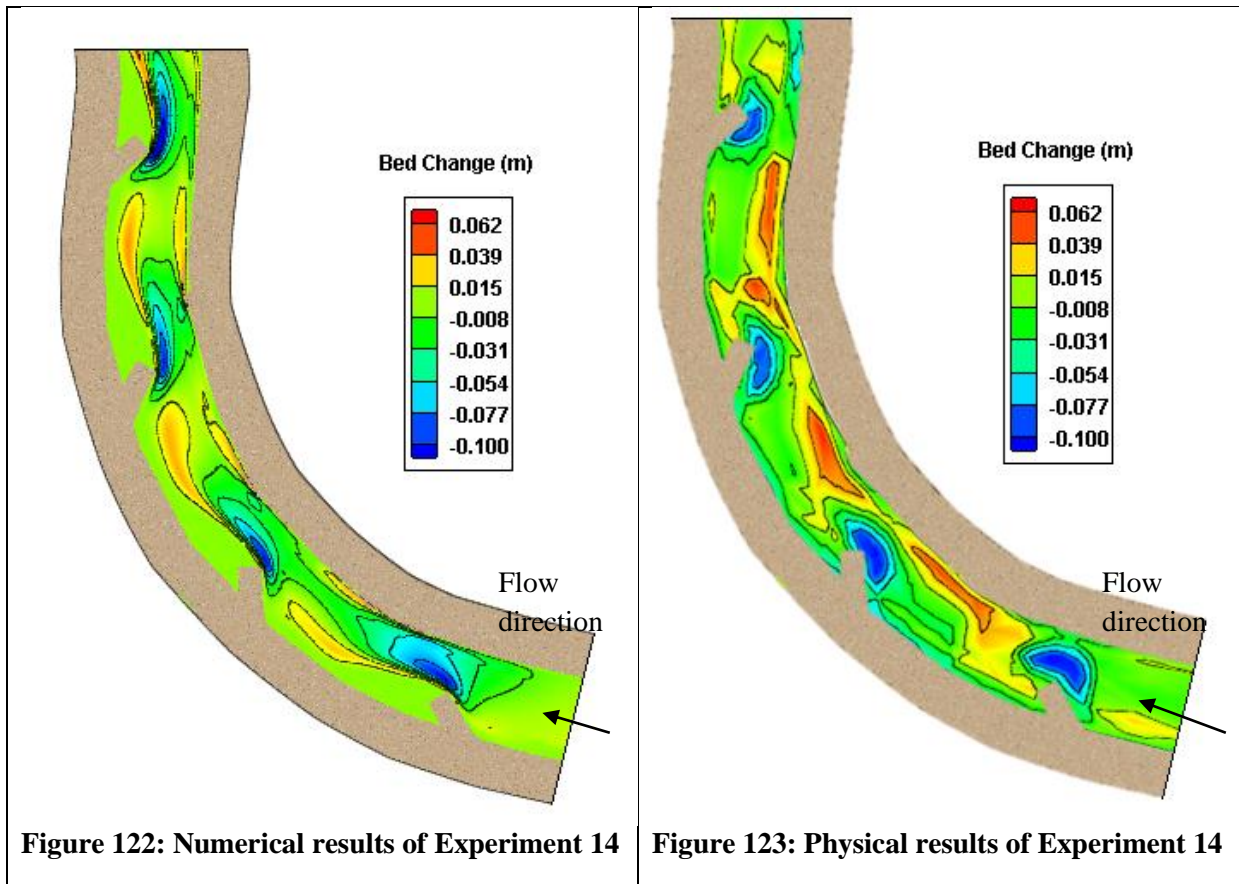
Figure 115: Velocity profile for Simulation 11

4.4.12   Numerical model of Experiment 12 (19 ℓ/s; 3 groynes; 3.5 x projection length)

Simulation 12 was done with 4 groynes installed at an angle of 45° with regards to the flow direction on the first bend with a spacing of 2.33 m and a projection length of 0.675 m. The spacing between the groynes was therefore 3.5 times the projection length. A discharge of 18.8 ℓ/s was simulated for a duration of 5min 4s as, was observed during the physical model test. Water depths during the simulation for measuring points 1, 2, and 3 were 119 mm, 126 mm and 120 mm, respectively. These water depths are within 10% of the observed water depths during the physical experiment which were 119 mm, 120 mm and 120 mm, respectively.

Local scour around the noses of the groynes shows some similarities in the shape and size of the scour holes between the numerical and the physical models. Some sediment deposition can be seen on the outer bank between consecutive groynes. A more elongated deposition profile can be seen for the numerical model, when compared to the physical model. Bank failure occurred on the inner bend, as well as the development of secondary flow patterns around the noses of the groynes, during the physical model experiment, resulting in deposition close to the bank which is not seen in the numerical model. A maximum scour depth of 119 mm was found in the numerical model, compared to a scour depth of 100 mm in the physical model, where scour continued onto the channel bed, causing the difference between scour depths.

These results can be seen in Figures 116 and 117.

Figure 116: Numerical results of Experiment 12 | **Figure 117: Physical results of Experiment 12**

In Figure 118 eddy currents can be seen between consecutive groynes, slowing the flow velocities near the outer bank. This provides some scour protection. The formation of an S-shape in the velocity profile is observed, resulting in higher flow velocities near the outer bank than were observed for perpendicular groyne orientation.
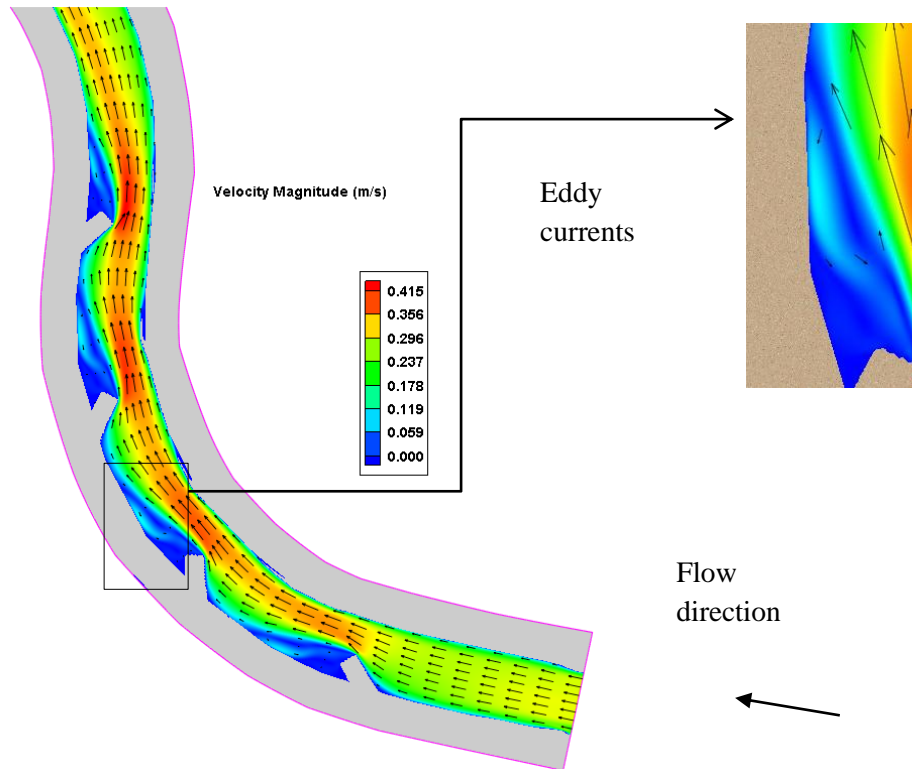
Figure 118: Velocity profile for Simulation 12

4.4.13 Numerical model of Experiment 13 (19 ℓ/s; 4 groynes; 4.1 x projection length)

Simulation 13 was done with 4 groynes installed at an angle of 45° with regards to the flow direction on the first bend with a spacing of 2.33m and a projection length of 0.775 m. The spacing between the groynes was therefore 4.1 times the projection length. A discharge of 18.8 ℓ/s was simulated for a duration of 5 min 33 s, as was observed during the physical model test. Water depths during the simulation for measuring points 1, 2, and 3 were 114 mm, 123 mm and 120mm, respectively. These water depths are within 10% of the observed water depths during the physical experiment which were 116 mm, 113 mm and 120 mm, respectively.

Local scour was observed around the noses of the groynes for both the numerical and physical models. Some similarities between the size and the shape of the scour holes can be seen. The correlation of the sediment deposition that occurred was not good. Some deposition could be seen near the outer bank for the physical model, although a longer deposition pattern was seen in the numerical model. Deposition can also be seen on the inner bend of the physical model, where bank failure occurred, and secondary flow patterns developed around the noses of the groynes, which are not modelled in CCHE2D. A maximum scour depth of 101 mm was obtained through the numerical model, compared to the 100 mm that was found during the physical model experiment.

122

These results can be seen in Figures 119 and 120.

| **Figure 119: Numerical results of Experiment 13** | **Figure 120: Physical results of Experiment 13** |

From the velocity profile in Figure 121 it can be seen that small eddy currents form directly downstream from the groynes, but do not cover the entire area between consecutive groynes because of the shorter projection length of the groynes. Optimal scour protection is therefore not created for the entire outer bank.

Figure 121: Velocity profile for Simulation 13

4.4.14   Numerical model of Experiment 14 (18 ℓ/s; 4 groynes; 3.5 x projection length)

Simulation 14 was done with 4 groynes installed at an angle of 135° with regards to the flow direction on the first bend with a spacing of 2.33 m and a projection length of 0.675 m. The spacing between the groynes was therefore 3.5 times the projection length. A discharge of 18.2 ℓ/s was simulated for a duration of 5 min 0 s, was observed during the physical model test. Water depths during the simulation for measuring points 1, 2, and 3 were 118 mm, 129 mm and 120 mm, respectively. These water depths are within 10% of the observed water depths during the physical experiment which were 115 mm, 124 mm and 120 mm, respectively.

Local scour around the noses of the groynes is similar in shape and size for the numerical and physical models. Some deposition could be seen downstream of individual groynes on the outer bank with the numerical model, resulting in longer deposition areas. Some deposition can also be seen in both models at the inner bank. The deposition at the inner bank for the physical model is larger, as a result of bank failure, and the development of secondary flow pattern around the noses of the groynes which is not modelled in CCHE2D. A maximum scour depth of 120 mm was observed for the numerical model, compared to the 100 mm of scour seen during the physical model experiment.

These results can be seen in Figures 122 and 123.

| **Figure 122: Numerical results of Experiment 14** | **Figure 123: Physical results of Experiment 14** |

From the velocity profile in Figure 124 it can be seen that some eddy currents do form, but they do not cover the entire area between consecutive groynes, which indicates that scour protection is not provided for the entire outer bank.

125

Figure 124: Velocity profile for Simulation 14

4.4.15 Numerical model of Experiment 15 (19 ℓ/s; 4 groynes; 4.1 x projection length)

Simulation 15 was done with 4 groynes installed at an angle of 135° with regards to the flow direction on the first bend with a spacing of 2.33m and a projection length of 0.575 m. The spacing between the groynes was therefore 4.1 times the projection length. A discharge of 19.1 ℓ/s was simulated for a duration of 5 min 6 s, was observed during the physical model test. Water depths during the simulation for measuring points 1, 2, and 3 were 114 mm, 127 mm and 120 mm, respectively. These water depths are within 10% of the observed water depths during the physical experiment which were 110 mm, 130 mm and 120 mm, respectively.

Local scour holes in the numerical and physical models are of similar shape and size. Sediment deposition can be seen downstream of individual groynes at the outer bank in both models, with some deposition also observed at the inner bank for both models. Higher correlation can be seen between the numerical and physical models as a result of less bank failure during the physical experiment. A maximum scour depth of 100 mm was seen in both the numerical and the physical models.

These results can be seen in Figures 125 and 126.

126

Figure 125: Numerical results of Experiment 15

Figure 126: Physical results of Experiment 15
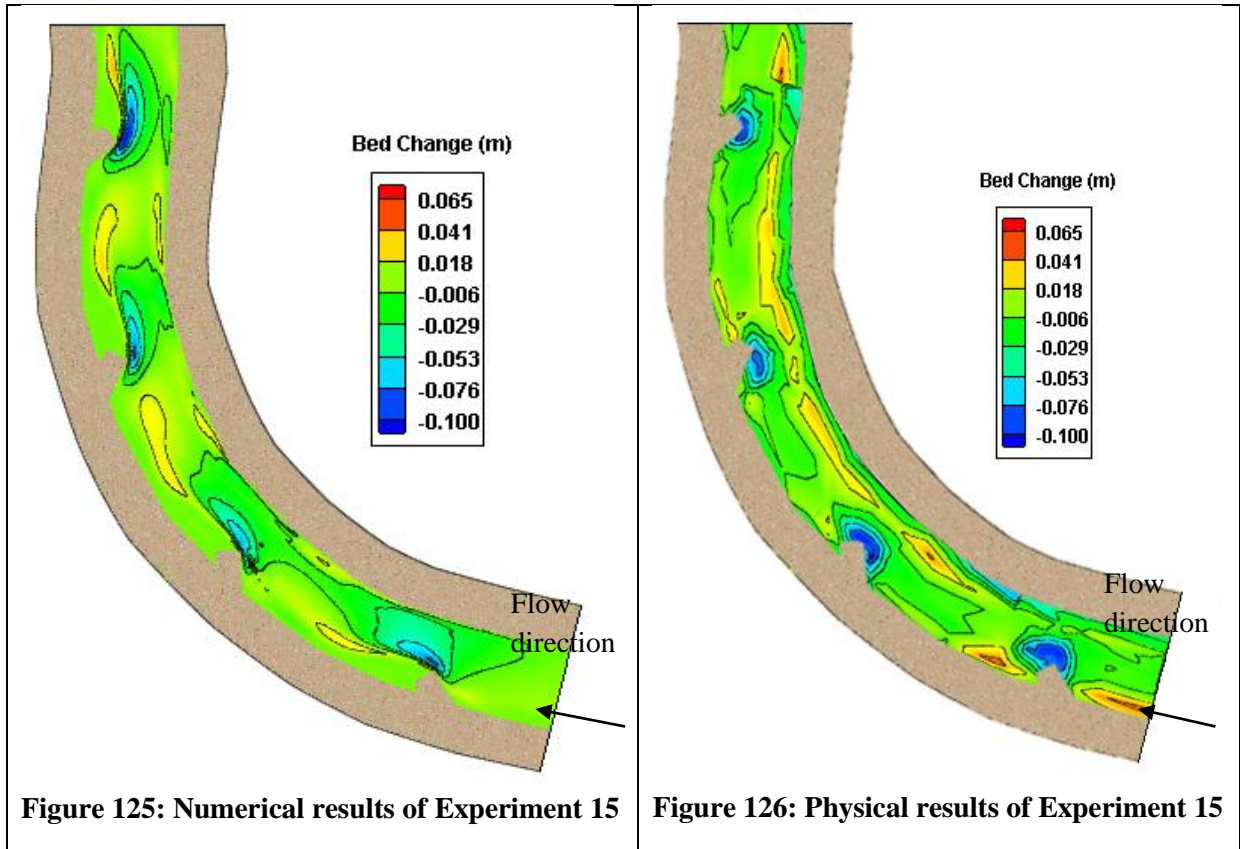
The velocity profile in Figure 127 shows small eddy currents forming just downstream of each of the groynes. The lower flow velocities do not cover the entire area between consecutive groynes, therefore scour protection is not created for the entire outer bank.
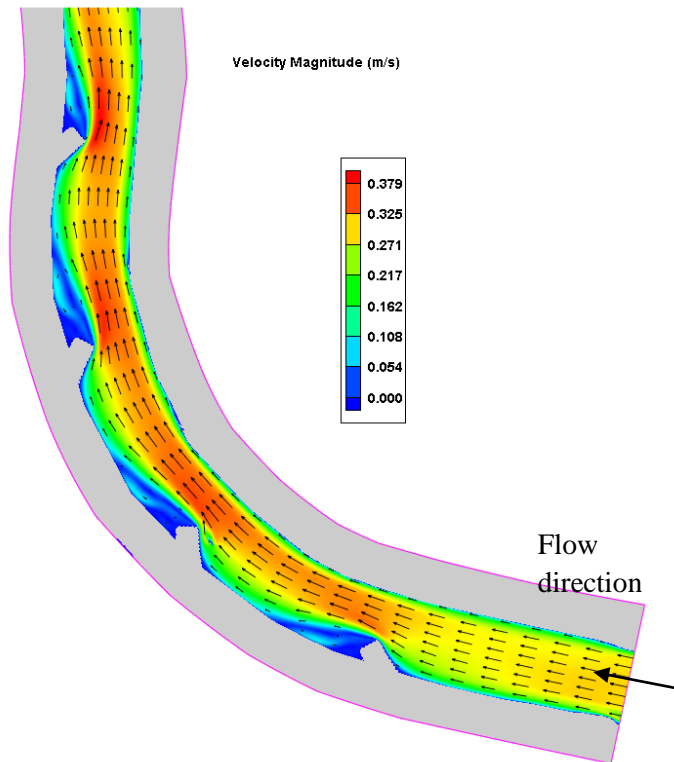
Figure 127: Velocity profile for Simulation 15

4.4.16 Numerical model of optimal design (19 ℓ/s; 7 groynes; 3.5 x projection length)

The optimal design simulation was done with 7 groynes installed on both bends at a spacing of 2.33 m and a projection length of 0.675 m. The spacing between the groynes was therefore 3.5 times the projection length. A discharge of 19.4 ℓ/s was simulated for a duration of 4 min 48 s, as was observed during the physical model test. Water depths during the simulation for measuring points 1, 2, and 3 were, 116mm, 127 mm and 120 mm, respectively. These water depths are within 15% of the observed water depths during the physical experiment which were 106 mm, 115 mm and 120 mm, respectively.

Scour patterns around the noses of the groynes are similar in both the numerical and physical models. Some deposition was seen on the outer banks, just downstream of the groynes' positions. As a result of bank failure on the first bend, less scour is observed on the second bend in the physical model experiment. The depth of scour during the physical experiment was 100 mm onto the channel bed. The maximum scour obtained from the numerical model was 101 mm.

These results can be seen in Figures 128 and 129.

Figure 128: Numerical results of optimal design

Figure 129: Physical results of optimal design
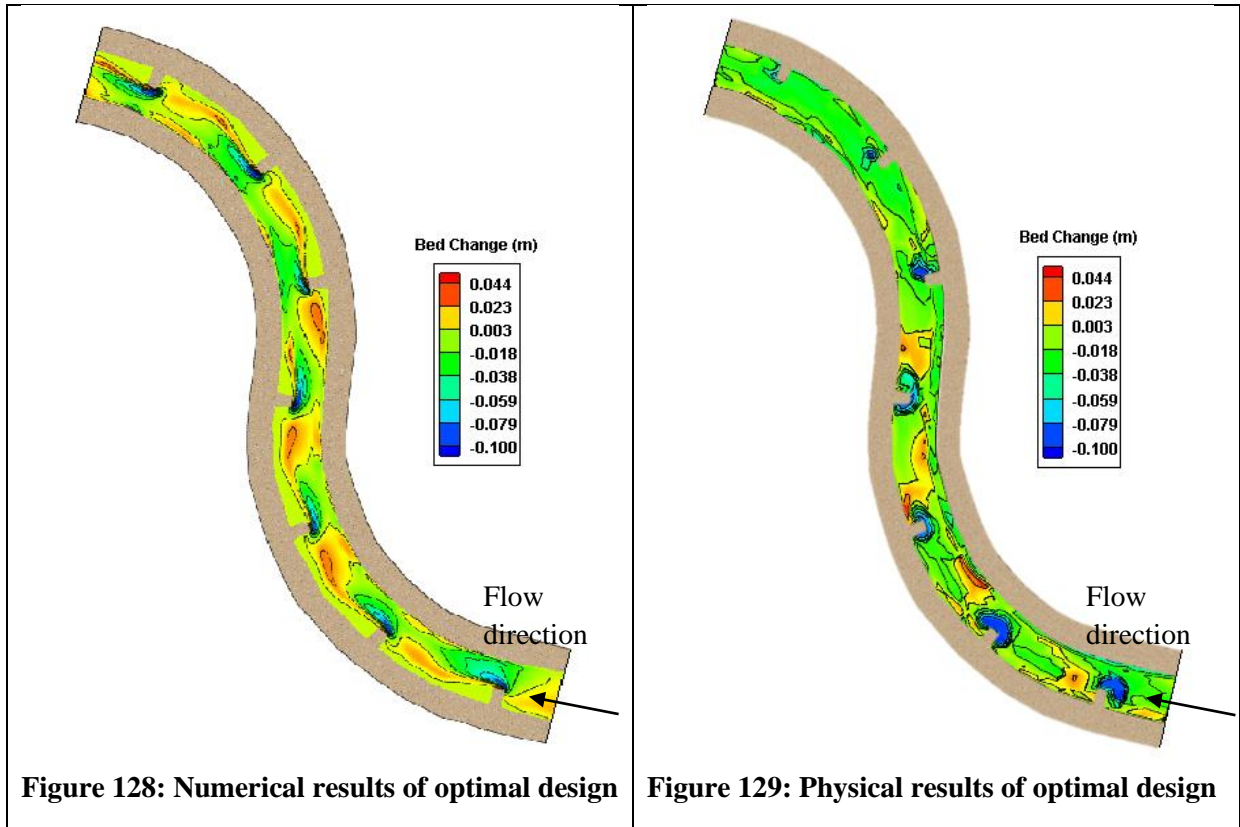
In Figure 130 the formation of eddy currents between consecutive groynes can be seen. Flow velocities in between the groynes are very low, causing little to no scour on the outer bank.
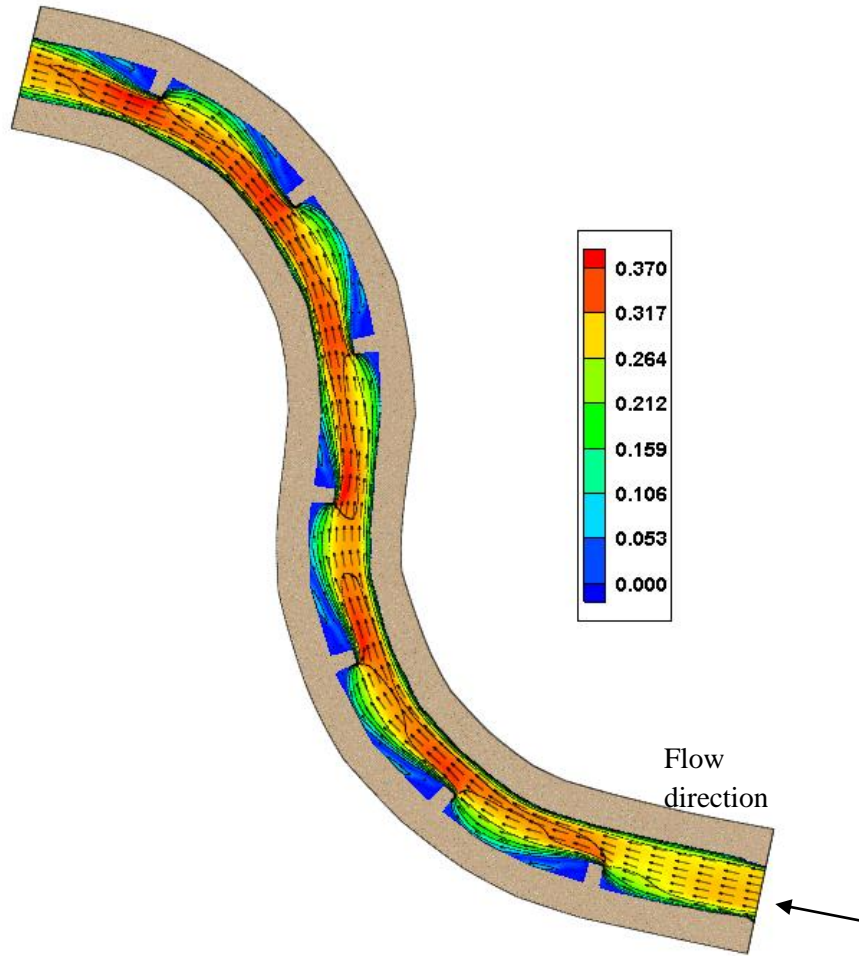
Figure 130: Velocity magnitude for optimal design

4.5 Summary of numerical model results

From the numerical model results it can be seen that conditions where bank failure occurs cannot be accurately simulated in CCHE2D. For groyne layout designs where bank failure did not occur, scour and deposition patterns were modelled with a good degree of accuracy.

From the velocity profiles obtained from CCHE2D, a definite correlation could be seen between flow patterns between consecutive groynes of the physical and numerical models. Recirculation of flow occurred in the form of eddy currents, creating zones of low flow velocity between consecutive groynes, resulting in scour protection for the outer bank, while also promoting sediment deposition.

CCHE2D does, however, not incorporate secondary flows that occur as a result of the curvature of the channel and the presence of groynes. As a result, very limited sediment

deposition is seen on the inner bend for the numerical model. During physical model testing, secondary currents developed, resulting in more deposition in that direction.

Table 16 shows the maximum scour and deposition depths obtained from the physical- and numerical models to determine the accuracy of the sediment transport for the numerical model.

Table 16: Maximum scour and deposition depths for physical and numerical experiments

Experiment	Flow (ℓ/s)	Maximum scour depth (m)		Maximum deposition depth (m)		Percentage error (scour)	Percentage error (deposition)
		Physical model	Numerical model	Physical model	Numerical model		
1	20	0.120	0.112	0.064	0.061	-6.67%	-4.69%
2	19	0.100	0.120	0.080	0.067	20.00%	-16.25%
3	21	0.100	0.097	0.074	0.051	-3.00%	-31.08%
4	19	0.090	0.066	0.065	0.035	-26.67%	-46.15%
5	19	0.100	0.138	0.082	0.069	38.00%	-15.85%
6	18	0.100	0.085	0.065	0.040	-15.00%	-38.46%
7	19	0.100	0.080	0.050	0.043	-20.00%	-14.00%
8	19	0.100	0.102	0.064	0.055	2.00%	-14.06%
9	18	0.100	0.093	0.059	0.042	-7.00%	-28.81%
10	18	0.100	0.066	0.045	0.036	-34.00%	-20.00%
11	18	0.100	0.130	0.085	0.070	30.00%	-17.65%
12	19	0.100	0.119	0.070	0.059	19.00%	-15.71%
13	19	0.100	0.101	0.069	0.049	1.00%	-28.99%
14	18	0.100	0.120	0.062	0.051	20.00%	-17.74%
15	19	0.100	0.100	0.059	0.041	0.00%	-30.51%
Optimal	19	0.100	0.101	0.044	0.042	1.00%	-4.55%

The average r calculated for the model applied for this study is $0.799 \leq r \leq 1.201$, with a maximum value of $r = 1.38$. Therefore this model, using the Wu et al. Formula, falls in an error range of 62.7% according to Table 14.

Considering the results shown in Table 16 and the comparison of bed change between the physical and numerical models, it is seen that, because CCHE2D does not account for secondary flows in the model, some results obtained from the numerical model did not result in a good representation of the physical model.

The positions where deposition was found in the numerical model was mainly on the outer bend where lower flow velocity was observed. For the physical model, large areas of deposition could be seen toward the inner bank as a result of secondary flow arising from

around the noses of the groynes. The correlation between physical and numerical models in terms of the scoured area and depth was also found to be inconsistent.

Considering the shortcomings of the CCHE2D model, it is necessary to employ a three-dimensional numerical model to accurately simulate the physical results.

5   Conclusions and recommendations

The use of groynes as a means of riverbank erosion protection has been employed over the last few decades to protect agricultural land to good effect.

The objectives of this study were to investigate the flow and scour patterns associated with various groyne layout designs by means of a physical model. A hydrodynamic model was also used in an attempt to accurately reproduce the results obtained from the physical model experiments. The variations in design considered for this study were: the spacing between groynes, the projection length of groynes and the orientation of groynes relative to the approach flow direction.

5.1   Flow and sediment transport pattern for physical model

The flow patterns observed during the physical model experiments showed definite eddy currents forming between consecutive groynes. This caused low flow zones near the outer riverbanks, promoting sediment deposition and decreasing the potential for scour to occur. The results obtained from the hydrodynamic model confirmed these findings, which coincides with the literature on flow patterns surrounding groynes.

As a result of the constriction of flow by the groynes, a zone of higher flow velocity was formed toward the inside bank of the groyne fields. This resulted in the main channel of the river moving toward the inner bends, limiting local scour of the outer bend of the river. Very turbulent flow was, however, encountered around the noses of the groynes, causing local scour.

It was found that for shorter projection lengths, in this case 0.575 m, the velocity found at the outer bends tended to be closer to normal conditions as not enough flow was being blocked to cause effective recirculation. For this study a projection length of 0.775 m was found to constrict flow too much causing scour and failure of the inner bank. The outer banks also sustained some damage, as the velocity at which recirculation of flow occurred was very high, causing the velocity at the outer banks to be high. For the given model, a projection length of 0.675 m was found to be optimal to maintain a balance between constricting flow while protecting both the inner and outer banks.

The spacing between the groynes is a function of the projection lengths. Spacings that ranged from 2.26 times the projection length to 4.92 times the projection length was tested. For the given projection lengths and the model that was used, it was found that the optimal spacing between consecutive groynes was 3.5 times the projection length.

The orientation of the groynes with regard to the oncoming flow greatly affected the resulting flow patterns. The orientations chosen for this study were 45° (angled upstream), 90°

(perpendicular to flow) and 135° (angled downstream). From all the results obtained from both the physical and hydrodynamic models, it was found that groynes with a perpendicular orientation to the oncoming flow were optimal. Eddy currents associated with other orientations were found to create less scour protection for the outer banks.

The main area where scour was found was around the noses of the groynes, where very turbulent flow was observed. The sediment that was taken into suspension as a result of the high flow velocity was transported to the areas where the eddy currents formed in the groyne fields and sediment deposited. As a result of secondary flows around the noses of the groynes, some sediment was transported toward the inner bank and deposited. Most of the deposited sediment was found just downstream of each groyne.

Scour around the noses of the groynes was found to be much more extensive, both in area and volume, for groynes angled at 45° and 135° than for groynes with perpendicular orientation.

5.2   Accuracy of the numerical model

As a result of the numerical model not accounting for the development of secondary flows around the bend and around the noses of the groynes, the correlation between the physical and numerical models was not as desired.

Scour patterns for the numerical model was found to be more elongated in shape when compared to the physical model. Sediment deposition also, to a large extent, occurred only on the outer bend in the numerical model, in comparison to the deposition that found toward the inner bank during the physical model experiments.

Considering these aspects, a two-dimensional numerical model cannot accurately simulate too complex flow and sediment patterns arising from the use of groynes.

5.3   Recommendations for further studies

After the completion of this study it is clear that further testing is needed to determine the effect of variables not tested for in this study.

Variables that were not considered for this study, but that definitely will have an effect on optimising designs for different situations are:

1. The radius of the bend

2. The size of the sediment
3. The width of the river
4. The flow depth associated with different flood events
5. The slope of the river

It is therefore recommended that these variables be tested in combination with different spacing and projection lengths, to obtain a solution which can incorporate all the variables associated with the design of a series of groynes for riverbank protection.

A three–dimensional hydrodynamic model will also help to create a better understanding of the exact flow patterns associated with different designs. A validated model can then also be used to simulate designs in the field, to ensure that optimised design will be obtainable for all projects.

References

Abad, J. D., Rhoads, B. L., Güneralp, İ., García, M. H., & Asce, M. (2009). Flow structure at different stages in a meander-bend with bendway weirs. *Journal of Hydraulic Engineering*, *134*(8), 1052-1063.

Ackers, P., & Charlton, F. G. (1970). Meander geometry arising from varying flows. *Journal of Hydrology*, *11*, 230-252.

Azinfar, H., & Kells, J. A. (2009). Flow resistance due to a single spur dike in an open channel. *Journal of Hydraulic Research*, *47*(6), 755-763. doi:10.3826/jhr.2009.3327

Azinfar, H., & Kells, J. A. (2011). Drag force and associated backwater effect due to an open channel spur dike field. *Journal Of Hydraulic Research*, *49*(2), 248-256. doi:10.1080/00221686.2011.552470

Beck, J., & Basson, G. R. (2003). The hydraulics of the impacts of dam development on the river morphology. *Water Research Comission*.

Bhuiyan, F., Hey, R. D., & Wormleaton, P. R. (2009). Effects of vanes and w-weir on sediment transport in meandering channels. *Journal of Hydraulic Engineering*, *135*(May), 339-349. doi:10.1061/(ASCE)0733-9429(2009)135:5(339)

Brotherton, D. I. (1979). On the origin of and characteristics of river channel patterns. *Journal of Hydrology*, *44*, 211-230.

Chitale, S. V. (1973). Theories and relationships of river channel patterns. *Journal of Hydrology*, *19*, 285-308.

King, H. (2009). *The use of groynes for riverbank erosion protection*. Western Cape.

Koken, M. (2011). Coherent structures around isolated spur dikes at various approach flow angles. *Journal of Hydraulic Research*, *49*(6), 736-743.

Kruger, E., & Gomes, N. (Eds.). (2007). *SANRAL Drainage Manual* (5th ed.). The South African National Roads Agency Ltd.

Kuhnle, R. A., Alonso, C. V., & Shields, F. D. (1999). Geometry of scour holes associated with 90 spur dikes. *Journal of Hydraulic Engineering*, (September), 972-978.

Kuhnle, R. A., Alonso, C. V., & Shields, F. D. (2002). Local scour associated with angled spur dikes. *Journal of Hydraulic Engineering*, (December), 1087-1093.

Langbein, W., & Leopold, L. (1966). River meanders - theory of minimum variance. *Geological survey professional paper*, *422-H*, 1-15.

National Center for Computational Hydroscience and Engineering. (1999). Retrieved May 5, 2012, from www.ncche.olemiss.edu/sw_download

Osman, M. A., & Ibrahim, A. A. A. (2008). Empirical assessment of local ccour at the head of groynes. *Nile Basin Water Engineering Scientific Magazine*, *1*, 54-64.

Rooseboom, A. (1983). *National Transport Commission road drainage manual*.

Shen, H. W. (1971). *River Mechanics*. (H. W. Shen, Ed.). Michigan: Shen.

Uijttewaal, W. S. J. (2005). Effects of groyne layout on the flow in groyne fields. *Journal of Hydraulic Engineering*, *131*(September), 782-791.

Uijttewaal, W. S. J., Lehmann, D., & Mazijk, A. V. (2001). Exchange processes between a river and its groynes fields: model experiments. *Journal of Hydraulic Engineering*, (November), 928-936.

Weitbrecht, V., Socolofsky, S. A., & Jirka, G. H. (2008). Experiments on mass exchange between groin fields and main stream in rivers. *Journal of Hydraulic Engineering*, (February), 173-183.

Wu, W. (2001). *CCHE2D Sediment Transport Model* (pp. 1-43).

Yang, C. T. (1971). On river meanders. *Journal of Hydrology*, *13*, 231-253.

Yossef, M. F. M., & Vriend, H. J. D. (2010). Sediment Exchange between a River and Its Groyne Fields : Mobile-Bed Experiment. *Journal of Hydraulic Engineering*, (September), 610-625.

Yossef, M. F. M., & Vriend, H. J. D. (2011). Flow details near river groynes : experimental investigation. *Journal of Hydraulic Engineering*, (May), 504-516. doi:10.1061/(ASCE)HY.1943-7900

Zhang, Y. (2006). *NCCHE-GUI – Graphical Users Interface for NCCHE model user ' s manual – Version 3 . 0*.

Zhang, Y., & Jia, Y. (2009). NCCHE 2D Structured Mesh Generator User's Manual -Version 3 . x.

Appendices

Appendix 1: Tradouw and Mullersrus case studies

Figure 131: Debris found on groynes after flood (Tradouw)
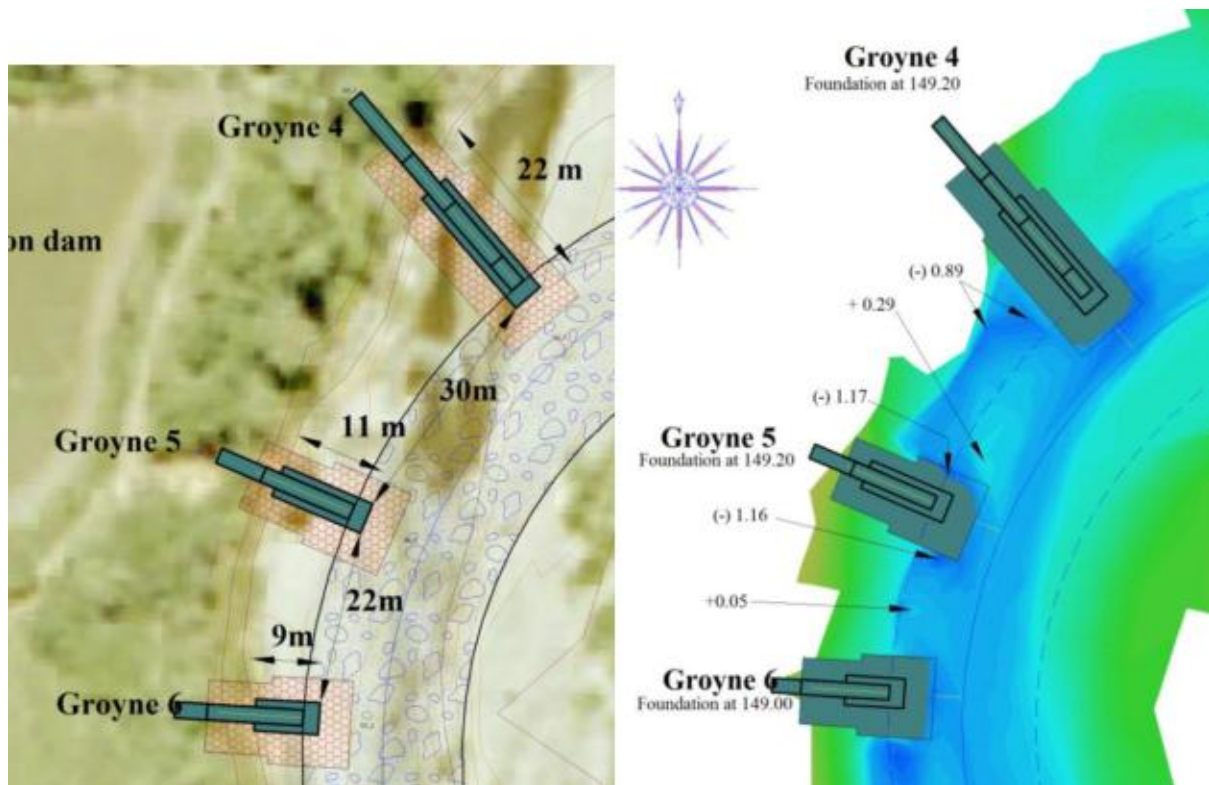
Figure 132: Aerial view of groynes 4 to 6

Figure 133: Mullersrus prior to 2008 flood

Figure 134: Mullersrus during 2008 flood

Figure 135: Mullersrus after 2008 flood

Appendix 2: Physical experiment photos

Figure 136: Experiment 1 results

Figure 137: Experiment 2 groyne 1
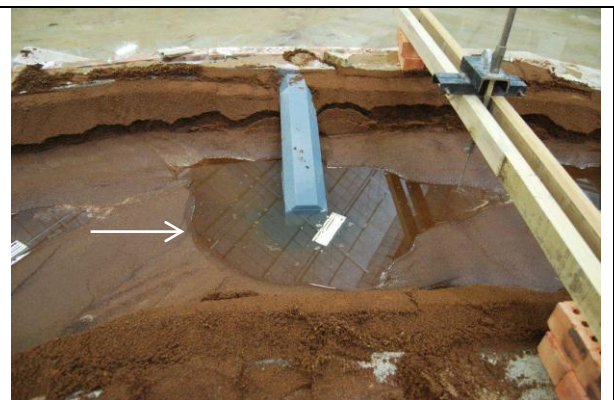
Figure 138: Experiment 2 groyne 3

Figure 139: Experiment 2 groyne 4

Figure 140: Experiment 2 groyne 5

141
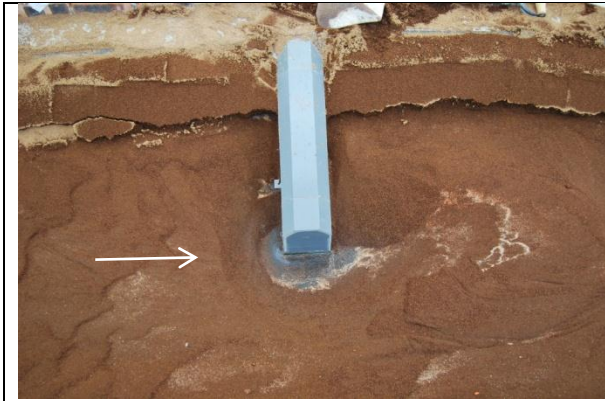
Figure 141: Experiment 3 groyne 1
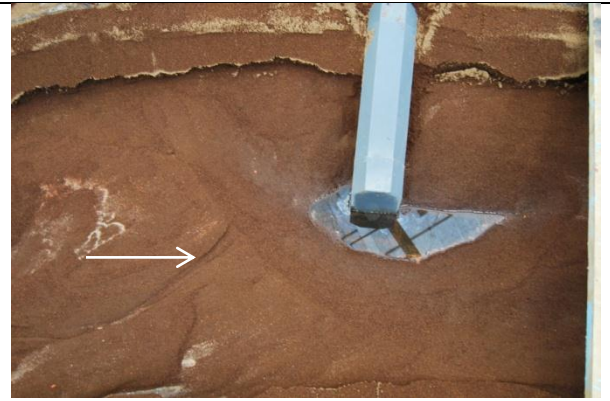
Figure 142: Experiment 3 groyne 2
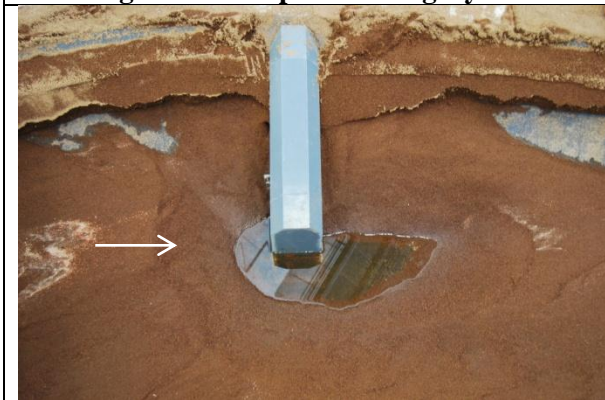
Figure 143: Experiment 3 groyne 3
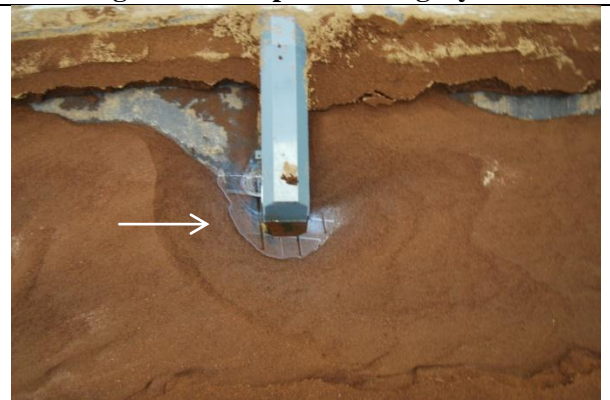
Figure 144: Experiment 3 groyne 5
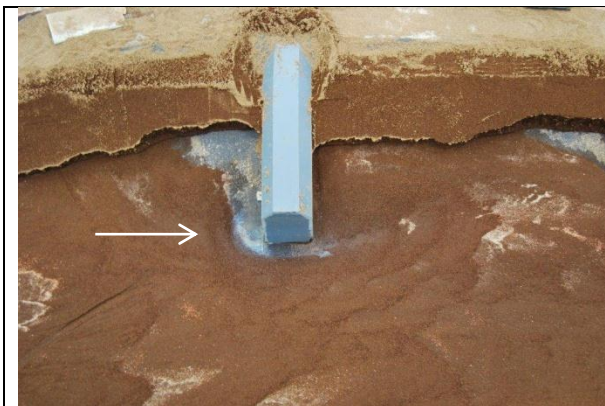
Figure 145: Experiment 4 groyne 2
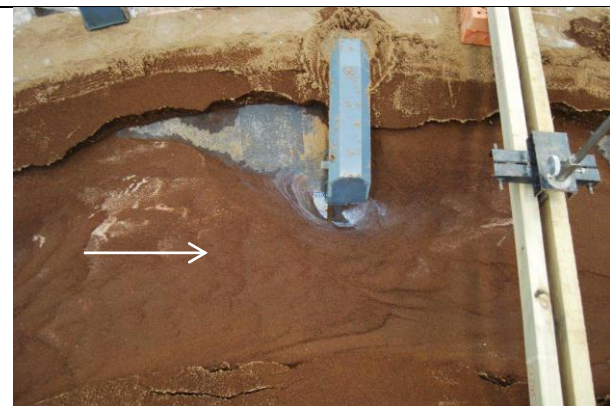
Figure 146: Experiment 4 groyne 3
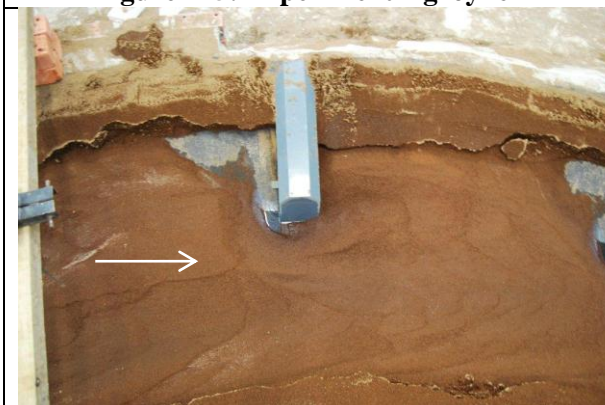
Figure 147: Experiment 4 groyne 4
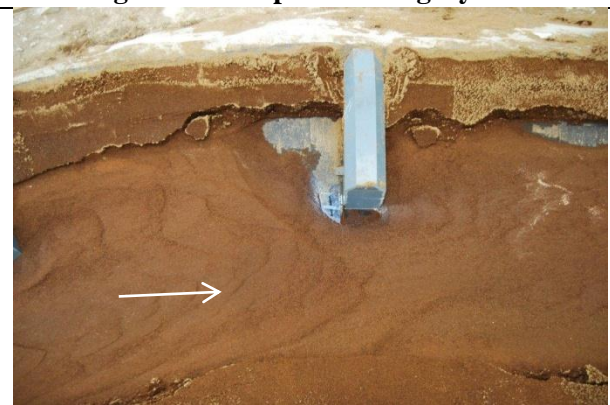
Figure 148: Experiment 4 groyne 5
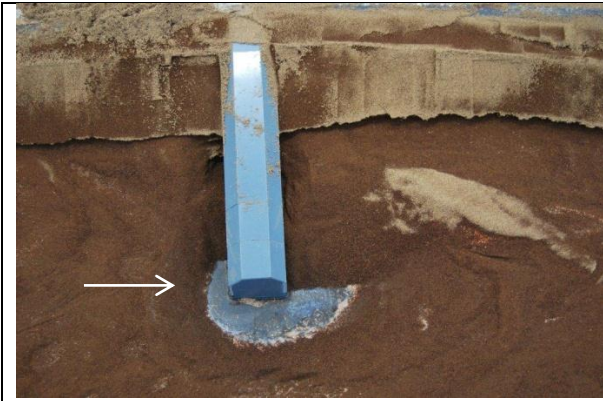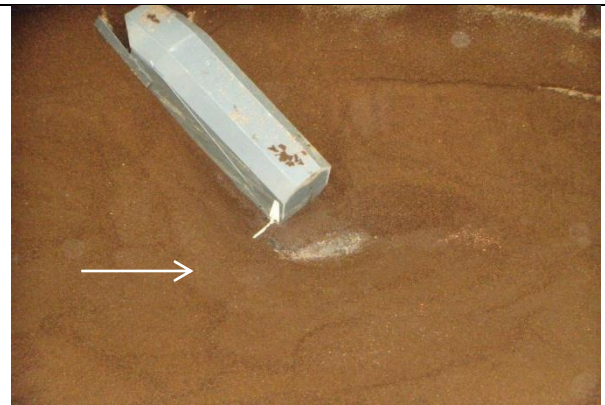
Figure 149: Experiment 5 groyne 1

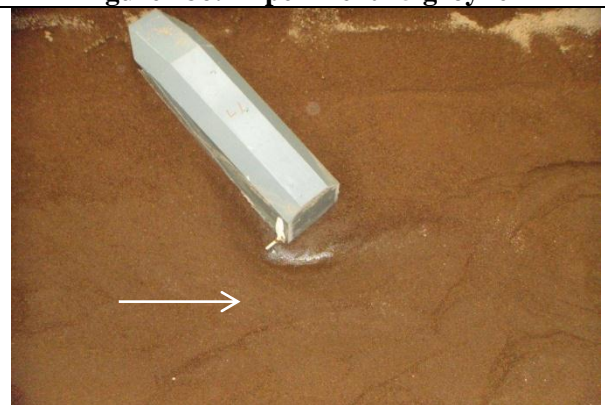**Figure 150: Experiment 5 groyne 2**
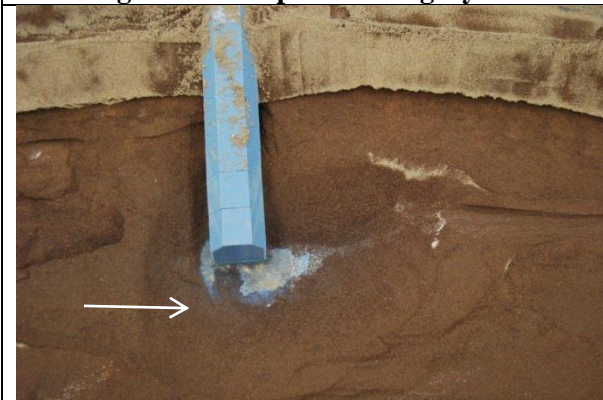
Figure 151: Experiment 5 groyne 3
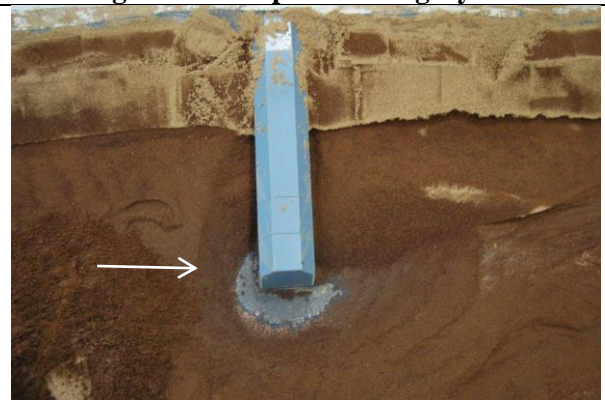
Figure 152: Experiment 5 groyne 4
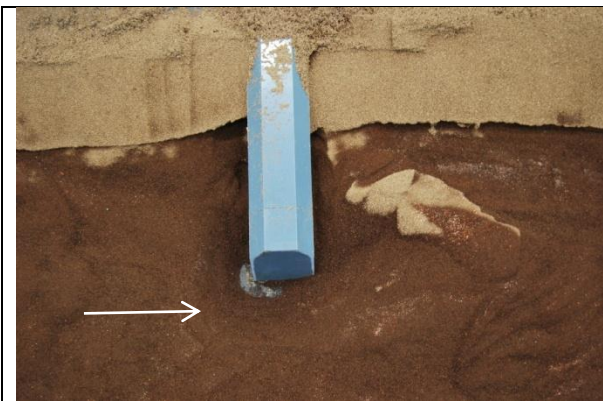
Figure 153: Experiment 6 groyne 1
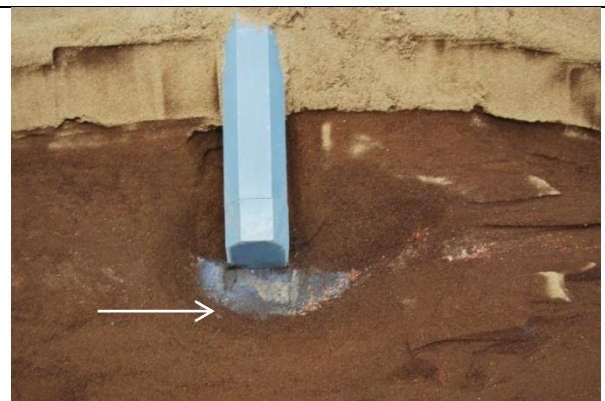
Figure 154: Experiment 5 groyne 2
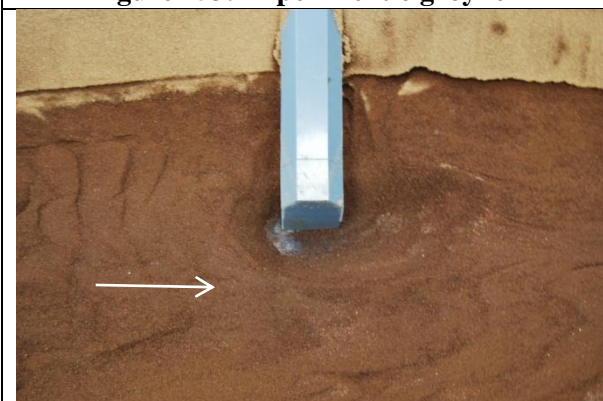
Figure 155: Experiment 6 groyne 3

Figure 156: Experiment 6 groyne 4

143
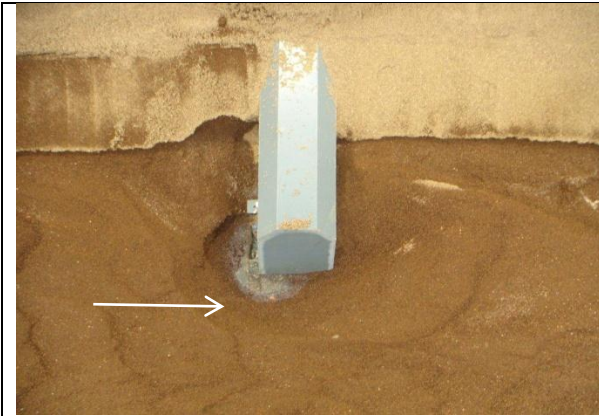
Figure 157: Experiment 7 groyne 1
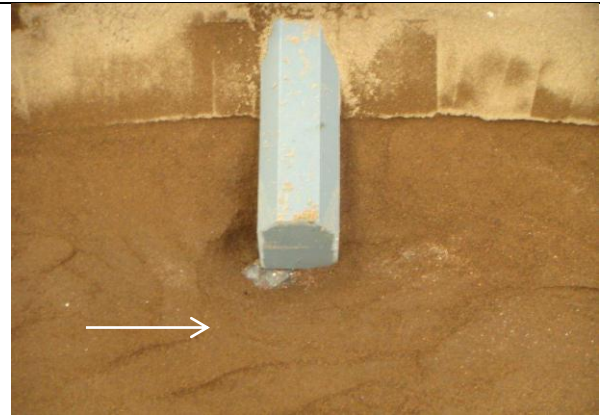
Figure 158: Experiment 7 groyne 2
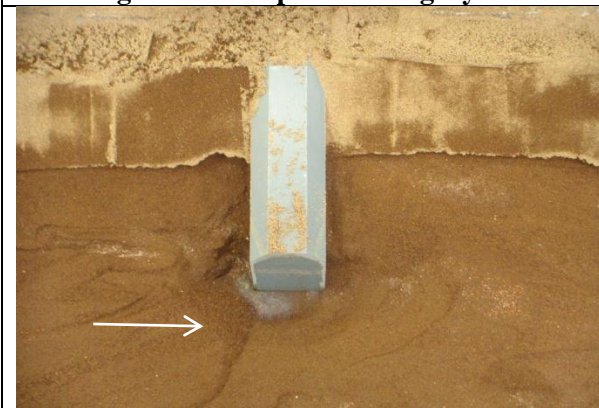
Figure 159: Experiment 7 groyne 3
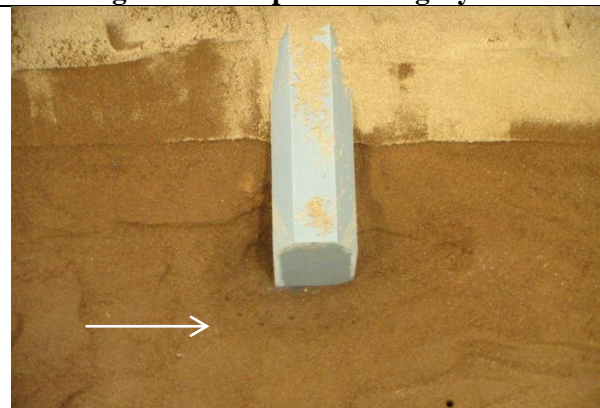
Figure 160: Experiment 7 groyne 4
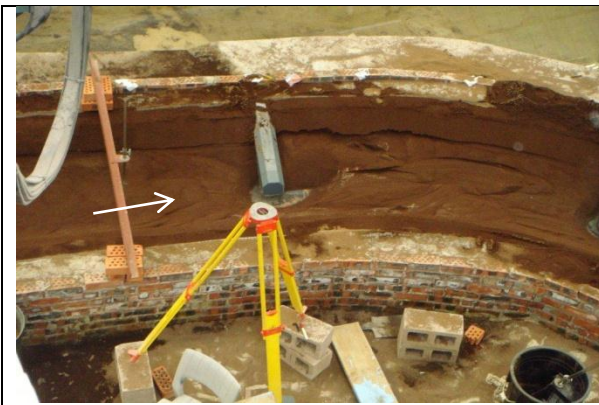
Figure 161: Experiment 8 groyne 1

Figure 162: Experiment 8 groyne 2

Figure 163: Experiment 8 groyne 3

Figure 164: Experiment 8 groyne 1 to 3
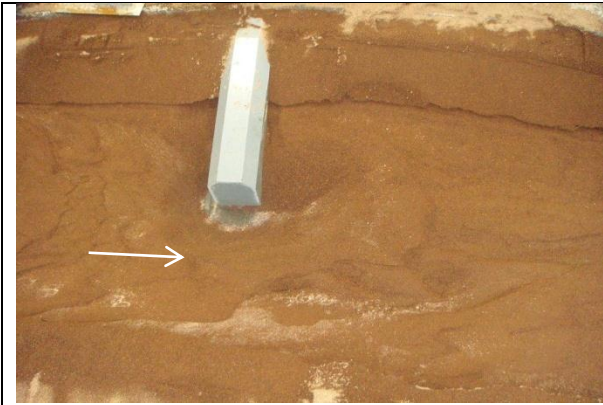
Figure 165: Experiment 9 groyne 1

Figure 166: Experiment 9 groyne 2
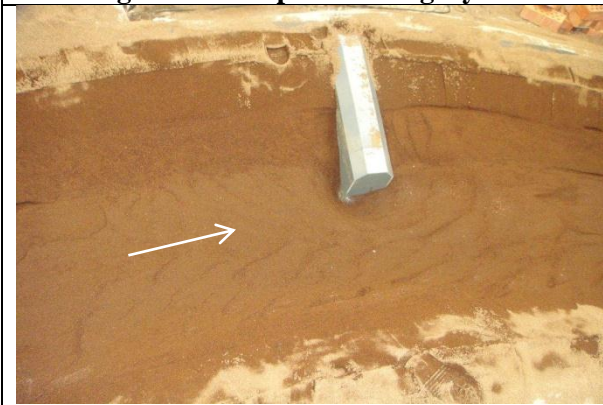
Figure 167: Experiment 9 groyne 3

Figure 168: Experiment 9 groyne 1 to 3
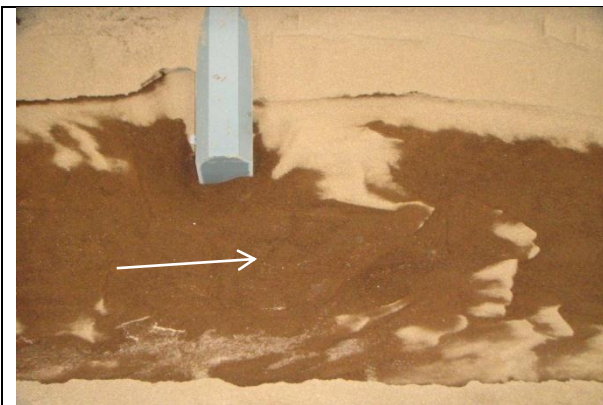
Figure 169: Experiment 10 groyne 1
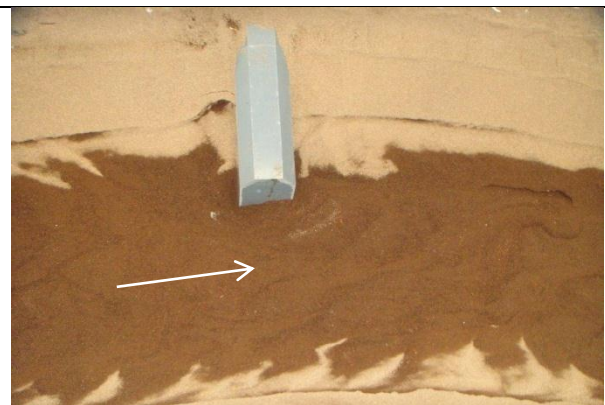
Figure 170: Experiment 10 groyne 2
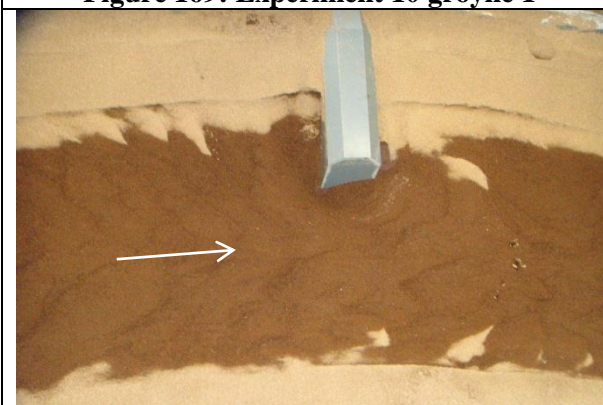
Figure 171: Experiment 10 groyne 3
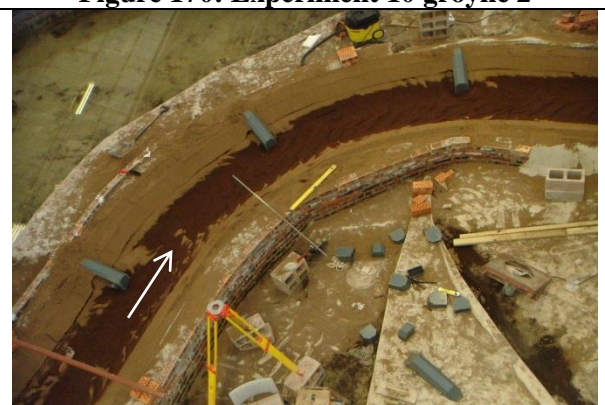
Figure 172: Experiment 10 groynes 1 to 3

145
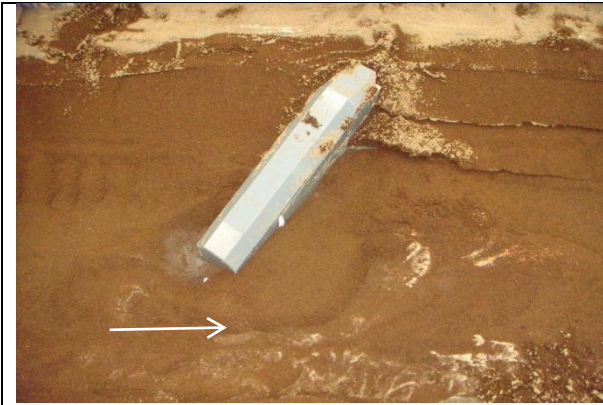
Figure 173: Experiment 11 groyne 1
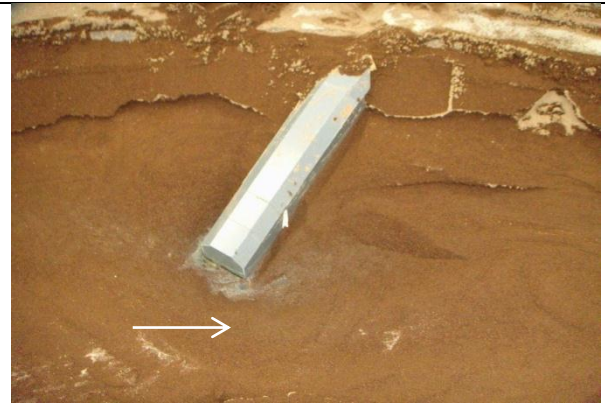
Figure 174: Experiment 11 groyne 2
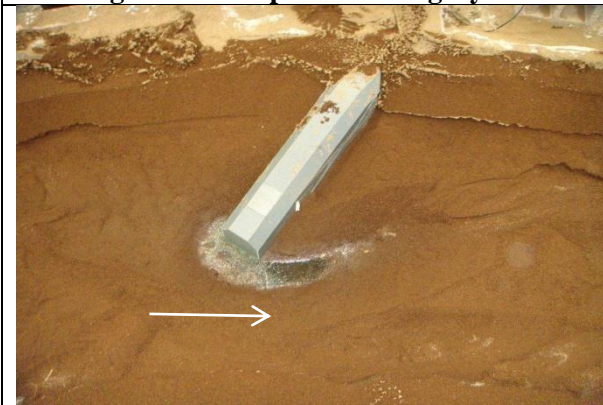
Figure 175: Experiment 11 groyne 3

Figure 176: Experiment 11 groyne 4
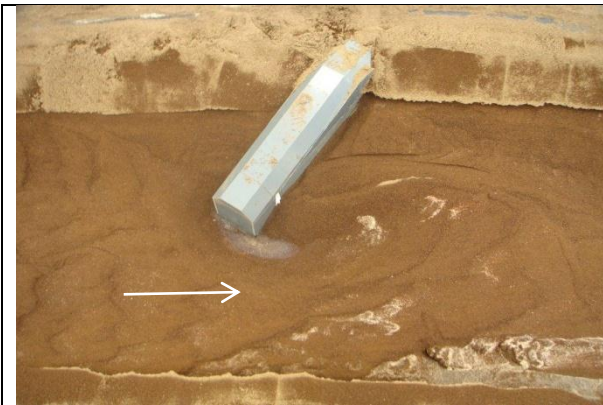
Figure 177: Experiment 12 groyne 1
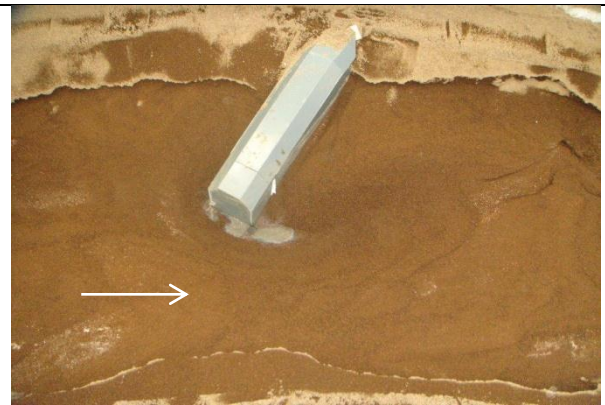
Figure 178: Experiment 12 groyne 2
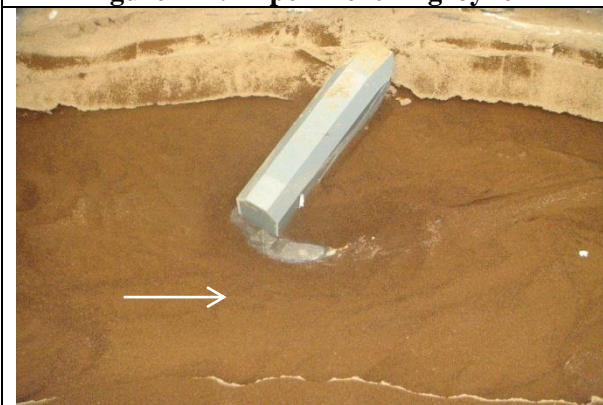
Figure 179: Experiment 12 groyne 3
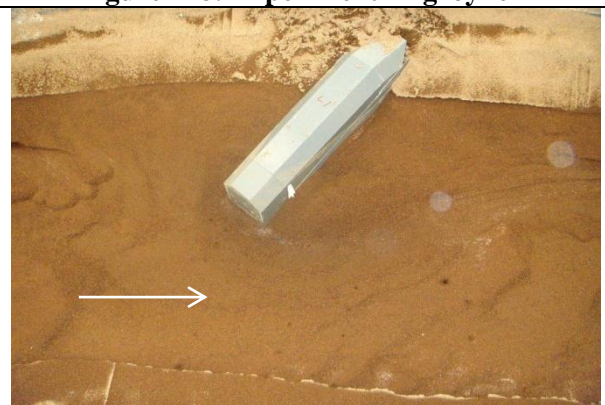
Figure 180: Experiment 12 groyne 4
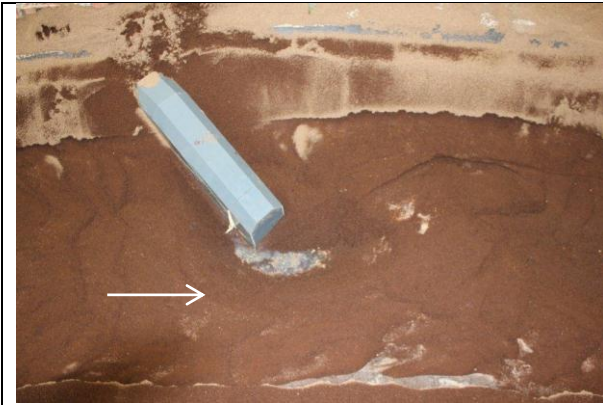
Figure 181: Experiment 14 groyne 1
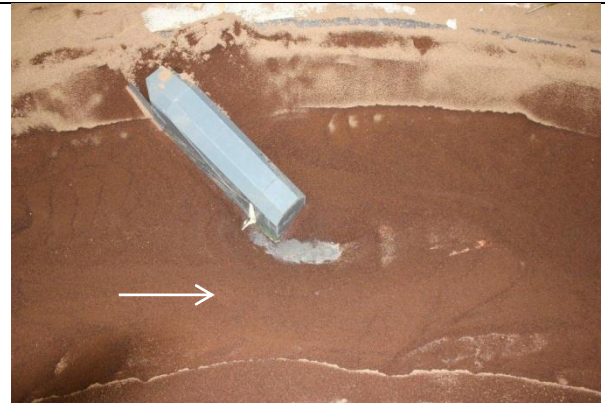
Figure 182: Experiment 14 groyne 2

Figure 183: Experiment 14 groyne 3
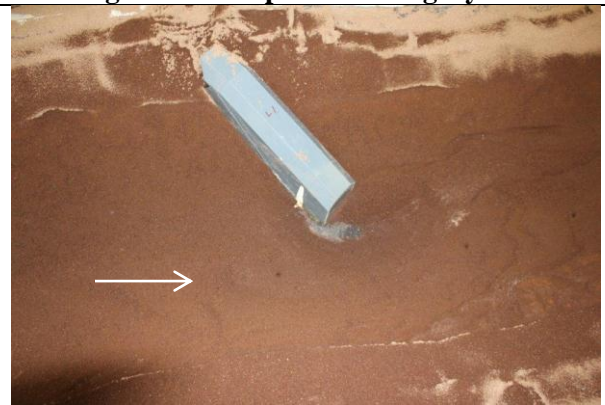
Figure 184: Experiment 14 groyne 4

Figure 185: Experiment 15 groyne 1

Figure 186: Experiment 15 groyne 2
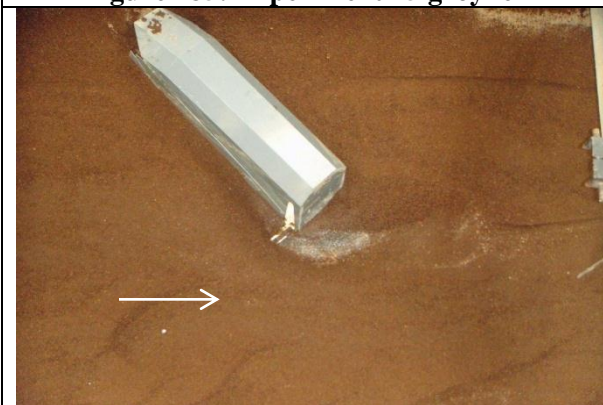
Figure 187: Experiment 15 groyne 3

Figure 188: Experiment 15 groyne 4
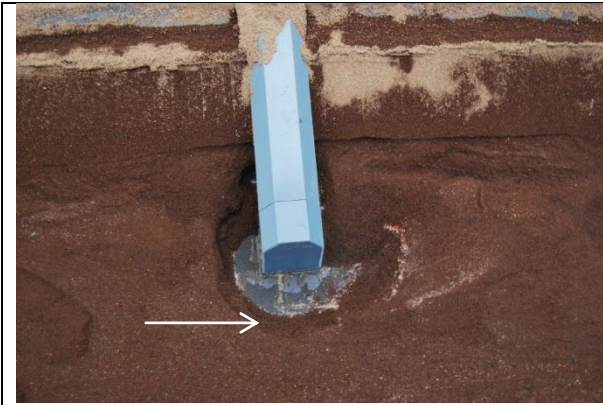
Figure 189: Optimal design groyne 1
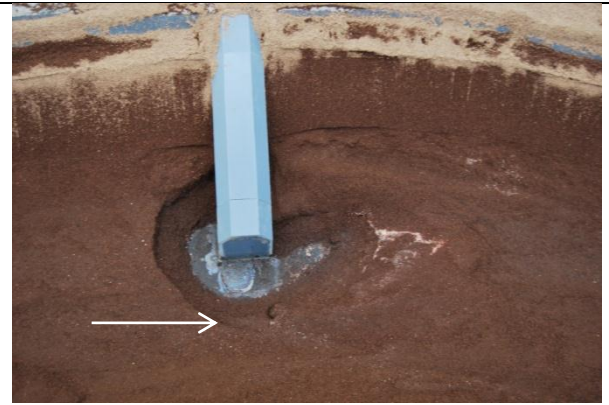
Figure 190: Optimal design groyne 2
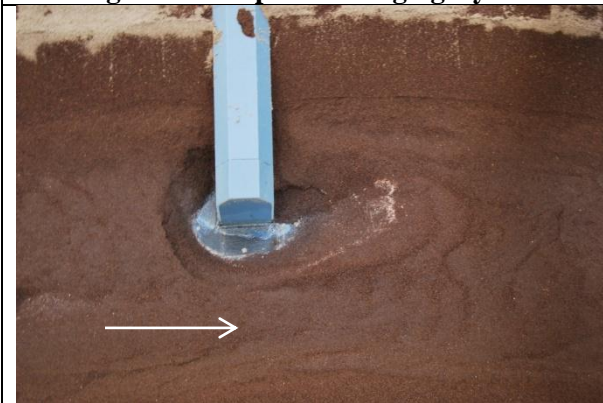
Figure 191: Optimal design groyne 3
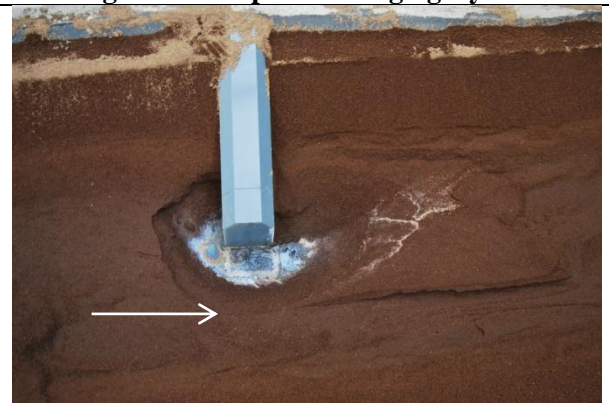
Figure 192: Optimal design groyne 4
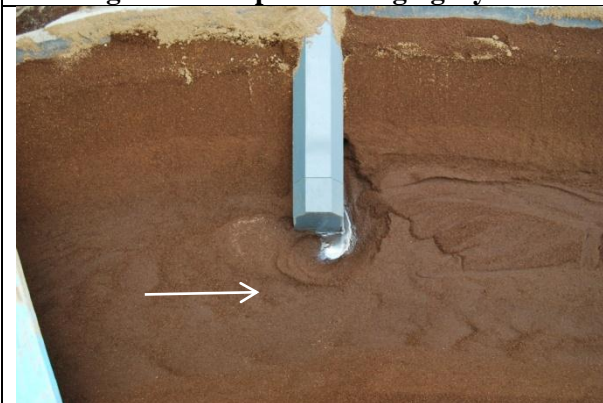
Figure 193: Optimal design groyne 5
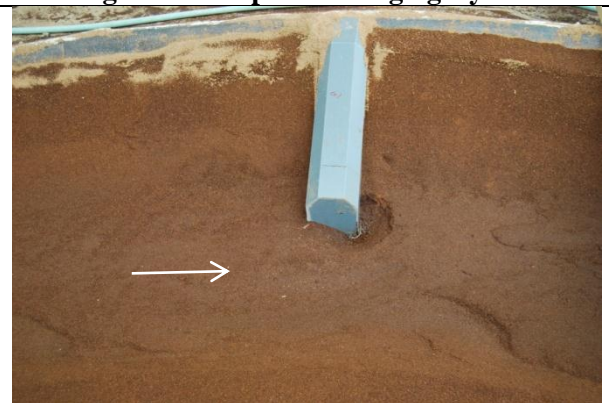
Figure 194: Optimal design groyne 6
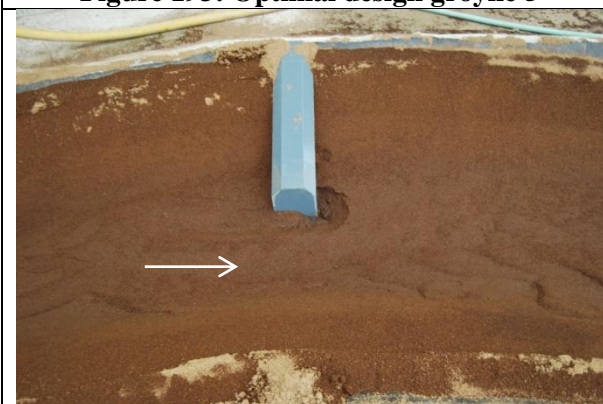
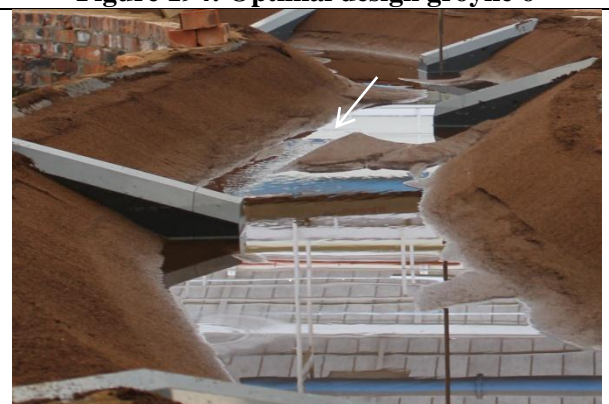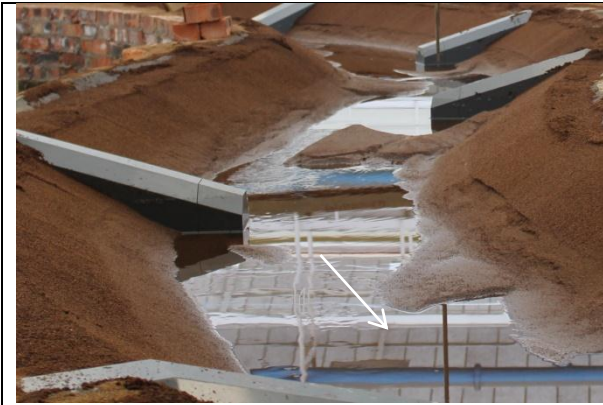**Figure 195: Optimal design groyne 7**

Figure 196: River draining t = 0 min

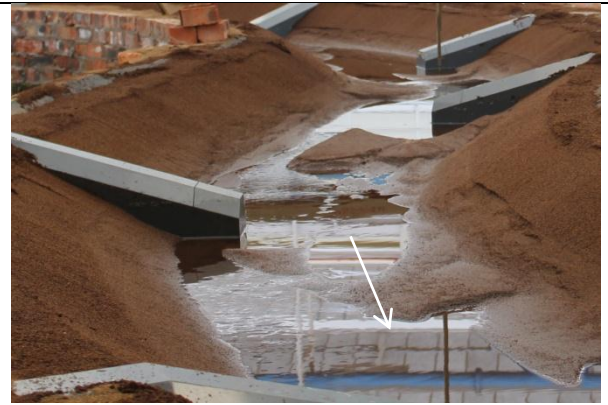**Figure 197: River draining t = 1 min**

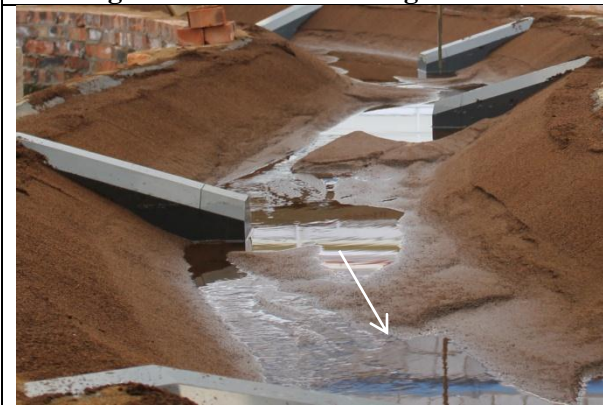**Figure 198: River draining t = 2 min**

Figure 199: River draining t = 4 min

Figure 200: River draining t = 5 min